

Biodegradation of plastics

Edited by

Zhanyong Wang, Fan Li, Aamer Ali Shah,
Ken'ichiro Matsumoto and Martin Koller

Published in

Frontiers in Bioengineering and Biotechnology



FRONTIERS EBOOK COPYRIGHT STATEMENT

The copyright in the text of individual articles in this ebook is the property of their respective authors or their respective institutions or funders. The copyright in graphics and images within each article may be subject to copyright of other parties. In both cases this is subject to a license granted to Frontiers.

The compilation of articles constituting this ebook is the property of Frontiers.

Each article within this ebook, and the ebook itself, are published under the most recent version of the Creative Commons CC-BY licence. The version current at the date of publication of this ebook is CC-BY 4.0. If the CC-BY licence is updated, the licence granted by Frontiers is automatically updated to the new version.

When exercising any right under the CC-BY licence, Frontiers must be attributed as the original publisher of the article or ebook, as applicable.

Authors have the responsibility of ensuring that any graphics or other materials which are the property of others may be included in the CC-BY licence, but this should be checked before relying on the CC-BY licence to reproduce those materials. Any copyright notices relating to those materials must be complied with.

Copyright and source acknowledgement notices may not be removed and must be displayed in any copy, derivative work or partial copy which includes the elements in question.

All copyright, and all rights therein, are protected by national and international copyright laws. The above represents a summary only. For further information please read Frontiers' Conditions for Website Use and Copyright Statement, and the applicable CC-BY licence.

ISSN 1664-8714
ISBN 978-2-8325-3945-3
DOI 10.3389/978-2-8325-3945-3

About Frontiers

Frontiers is more than just an open access publisher of scholarly articles: it is a pioneering approach to the world of academia, radically improving the way scholarly research is managed. The grand vision of Frontiers is a world where all people have an equal opportunity to seek, share and generate knowledge. Frontiers provides immediate and permanent online open access to all its publications, but this alone is not enough to realize our grand goals.

Frontiers journal series

The Frontiers journal series is a multi-tier and interdisciplinary set of open-access, online journals, promising a paradigm shift from the current review, selection and dissemination processes in academic publishing. All Frontiers journals are driven by researchers for researchers; therefore, they constitute a service to the scholarly community. At the same time, the *Frontiers journal series* operates on a revolutionary invention, the tiered publishing system, initially addressing specific communities of scholars, and gradually climbing up to broader public understanding, thus serving the interests of the lay society, too.

Dedication to quality

Each Frontiers article is a landmark of the highest quality, thanks to genuinely collaborative interactions between authors and review editors, who include some of the world's best academicians. Research must be certified by peers before entering a stream of knowledge that may eventually reach the public - and shape society; therefore, Frontiers only applies the most rigorous and unbiased reviews. Frontiers revolutionizes research publishing by freely delivering the most outstanding research, evaluated with no bias from both the academic and social point of view. By applying the most advanced information technologies, Frontiers is catapulting scholarly publishing into a new generation.

What are Frontiers Research Topics?

Frontiers Research Topics are very popular trademarks of the *Frontiers journals series*: they are collections of at least ten articles, all centered on a particular subject. With their unique mix of varied contributions from Original Research to Review Articles, Frontiers Research Topics unify the most influential researchers, the latest key findings and historical advances in a hot research area.

Find out more on how to host your own Frontiers Research Topic or contribute to one as an author by contacting the Frontiers editorial office: frontiersin.org/about/contact

Biodegradation of plastics

Topic editors

Zhanyong Wang — Shenyang Agricultural University, China

Fan Li — Northeast Normal University, China

Aamer Ali Shah — Quaid-i-Azam University, Pakistan

Ken'ichiro Matsumoto — Hokkaido University, Japan

Martin Koller — University of Graz, Austria

Citation

Wang, Z., Li, F., Shah, A. A., Matsumoto, K., Koller, M., eds. (2023). *Biodegradation of plastics*. Lausanne: Frontiers Media SA. doi: 10.3389/978-2-8325-3945-3

Table of contents

- 04 **Editorial: Biodegradation of plastics**
Martin Koller, Ken'ichiro Matsumoto, Zhanyong Wang, Fan Li and Aamer Ali Shah
- 07 **Isolation, Identification, and Characterization of Polystyrene-Degrading Bacteria From the Gut of *Galleria Mellonella* (Lepidoptera: Pyralidae) Larvae**
Shan Jiang, Tingting Su, Jingjing Zhao and Zhanyong Wang
- 16 **Assessing the Biodegradation of Vulcanised Rubber Particles by Fungi Using Genetic, Molecular and Surface Analysis**
R. Andler, V. D'Afonseca, J. Pino, C. Valdés and M. Salazar-Viedma
- 27 **Current Knowledge on Polyethylene Terephthalate Degradation by Genetically Modified Microorganisms**
Aneta K. Urbanek, Katarzyna E. Kosiorowska and Aleksandra M. Mironczuk
- 42 **Two Extracellular Poly(ϵ -caprolactone)-Degrading Enzymes From *Pseudomonas hydrolytica* sp. DSWY01^T: Purification, Characterization, and Gene Analysis**
Linying Li, Xiumei Lin, Jianfeng Bao, Hongmei Xia and Fan Li
- 51 **Bioconversion of Terephthalic Acid and Ethylene Glycol Into Bacterial Cellulose by *Komagataeibacter xylinus* DSM 2004 and DSM 46604**
Asiyah Esmail, Ana T. Rebocho, Ana C. Marques, Sara Silvestre, Alexandra Gonçalves, Elvira Fortunato, Cristiana A. V. Torres, Maria A. M. Reis and Filomena Freitas
- 62 **Characterization of Polymer Degrading Lipases, LIP1 and LIP2 From *Pseudomonas chlororaphis* PA23**
Nisha Mohanan, Chun Hin Wong, Nediljko Budisa and David B. Levin
- 77 **Synthesis of Poly(Hexamethylene Succinate-Co-Ethylene Succinate) Copolymers With Different Physical Properties and Enzymatic Hydrolyzability by Regulating the Ratio of Monomer**
Menglu Li, Jing Jing and Tingting Su
- 87 **On the quest for novel bio-degradable plastics for agricultural field mulching**
Sami Ullah Dar, Zizhao Wu, Linyi Zhang, Peirong Yu, Yiheng Qin, Yezi Shen, Yunfan Zou, Leslie Poh, Yoav Eichen and Yigal Achmon
- 100 **Biodegradation of Low-Density Polyethylene—LDPE by the Lepidopteran *Galleria Mellonella* Reusing Beekeeping Waste**
Orlando Poma, Betty Ricce, Jeyson Beraún, Jackson Edgardo Perez Carpio, Hugo Fernandez and Juan Soria



OPEN ACCESS

EDITED AND REVIEWED BY

Ana Júlia Cavaleiro,
University of Minho, Portugal

*CORRESPONDENCE

Martin Koller,
✉ martin.koller@uni-graz.at

SPECIALTY SECTION

This article was submitted to Bioprocess Engineering, a section of the journal Frontiers in Bioengineering and Biotechnology

RECEIVED 30 March 2023

ACCEPTED 27 March 2023

PUBLISHED 03 April 2023

CITATION

Koller M, Matsumoto K, Wang Z, Li F and Shah AA (2023), Editorial: Biodegradation of plastics.
Front. Bioeng. Biotechnol. 11:1150078.
doi: 10.3389/fbioe.2023.1150078

COPYRIGHT

© 2023 Koller, Matsumoto, Wang, Li and Shah. This is an open-access article distributed under the terms of the [Creative Commons Attribution License \(CC BY\)](https://creativecommons.org/licenses/by/4.0/). The use, distribution or reproduction in other forums is permitted, provided the original author(s) and the copyright owner(s) are credited and that the original publication in this journal is cited, in accordance with accepted academic practice. No use, distribution or reproduction is permitted which does not comply with these terms.

Editorial: Biodegradation of plastics

Martin Koller^{1*}, Ken'ichiro Matsumoto², Zhanyong Wang³, Fan Li⁴ and Aamer Ali Shah⁵

¹Research Management and Service, Institute of Chemistry, University of Graz, Graz, Austria, ²Research Group of Biotechnology, Laboratory of Biomolecular Engineering, Faculty of Engineering, Division of Applied Chemistry, Hokkaido University, Sapporo, Japan, ³Biological Science and Technology College, Shenyang Agricultural University, Shenyang, China, ⁴School of Life Sciences, Northeast Normal University, Changchun, China, ⁵Department of Microbiology, Quaid-i-Azam University, Islamabad, Pakistan

KEYWORDS

biodegradability, plastic, plastic wastes, microbial biodegradation, enzymes

Editorial on the Research Topic Editorial: Biodegradation of plastics

Currently, humankind faces severe threats connected to aggravating climate crisis, shortage of fossil resources, and increasing quantities of waste consisting of petrochemistry-based plastics. Despite the fact that such plastics, since the mid of the last century, brought numerous benefits and advantages to our society by being stable, versatile, and of low specific mass, they have a dark side: Due to the lacking adaptation of nature to these xenobiotic materials, which were not present on Earth only some decades ago, they are highly recalcitrant towards biodegradation, i.e., their disintegration into non-toxic final products such as CO₂ or CH₄ by the action of living organisms or biocatalytic parts thereof. One could literally state that “plastics are forever!” Nowadays, reports estimate a total quantity of almost three billion tons having been produced since the onset of plastic commercialization; about 400 million tons plastics are being produced annually at the moment, with a strongly increasing trend especially in emerging and developing countries (Mukherjee and Koller, 2022). Only part of spent plastic waste undergoes a controlled end-of-life scenario like mechanical or chemical recycling or thermal conversion for energy recovery, while this later option is heavily disputed due to the obstacles connected to formation of surplus CO₂ and toxic gases. Moreover, existing recycling and incineration plants are of insufficient capacities to handle the steadily increasing quantities of plastic waste of petrochemical origin, especially full-carbon-backbone plastics like polyolefins, but also poly (ethylene terephthalate) (PET) or poly (urethanes). However, the lion's share of spent plastic is littering aquatic and terrestrial environments as macro- and microplastic waste, causing impacts on the biosphere that are only just beginning to be fully understood.

Currently, there are two scenarios to overcome these issues: One option is to switch to plastic biopolymers. Tremendous research is currently dedicated to such materials, which are both biobased and biodegradable, with microbial polyhydroxyalkanoates (PHA) probably being the most prominent example. However, there are still impediments on the way towards replacing petroplastics by bio-inspired alternatives, such as high production costs, fluctuating material quality, and an often-lacking match between customer expectations and *de facto* material performance. The second option is biodegradation of present petroplastics, as it is the topic of the Research Topic at hand.

During the last years, several organisms have been shown to contribute to degradation of said petrochemical plastics. However, the number of these organisms is still scarce, and these processes occur at rather low rates. The enzymatic machinery responsible for plastic biodegradation typically shows low affinity to the plastic substrate, operates with insufficiently deciphered reaction mechanisms, or is inefficiently expressed by the organisms. Especially, we are aware of a deep knowledge gap between preliminary research data, postulating degradability of a given polymer by certain strains or enzymes on lab scale, and, on the other hand, large scale degradation experiments performed under diverse realistic environmental conditions. What is needed to overcome existing bottle necks are progress in the field of microbiology of plastics' biodegradation and advanced biotechnological approaches. New powerful strains are waiting for their discovery as toolboxes containing enzymes for plastic biodegradation. This research needs to encompass the holistic elucidation of the metabolic pathways active during plastic biodegradation, identification of relevant genes and enzymes expressed by them, assessment of enzymes in terms of activity and stability, and genetic engineering to obtain tailor-made whole cell biocatalysts for plastic biodegradation, and strategies of biosynthetic biology, supported by bioinformatic tools.

So, there is definitely a lot to be achieved in this challenging scientific field, and a lot of research activity in this direction is witnessed globally. This gave reason to launch this Research Topic of Frontiers in Bioengineering and Biotechnology dedicated to Biodegradation of Plastics. A total of nine research groups of exceptional reputation in the global scientific community contributed their recent research outcomes to this issue, which contains eight original research articles and one comprehensive review paper. The subsequent paragraphs present the individual specific contributions in a nutshell:

In their comprehensive review, Urbanek et al. introduce the current state of research on biodegradation of PET, a heavily utilized petroplastic polymer, which frequently undergoes mechanical recycling, thus contributing to microplastic formation. Authors demonstrate that isolated wild type organisms showing PET degrading activity are of insufficient efficiency to provide a solution to overcome the problems associated to PET waste. Therefore, it is shown how strategies of metabolic engineering of microbes and protein engineering can enhance biodegradation of PET.

Jiang et al. dedicated their article to biodegradation of the polyolefin poly (styrene) (PS), a full-carbon-backbone petroplastic also produced at enormous quantities. Authors were able to isolate a PS-degrading bacterium from the digestive system of *Galleria mellonella* wax moth larvae that were fed with PS foam. Isolated bacterium was identified as *Massilia* sp. FS 1903. Biodegradation of PS films by this bacterium was studied via scanning electron microscopy and X-ray energy dispersive spectrometry, and water contact angle measurements quantified the increasing hydrophilicity of PS films during incubating with the bacterium by formation of oxygen-bearing groups on the surface. Incubation experiments demonstrated a significant mass loss of PS films after 30 days, which outperforms results for PS biodegradation reported for other biological systems.

Poma et al. resorted also to *G. mellonella* wax moths in the larval stage for plastic degradation studies. Here, authors aimed at biodegradation of low-density poly (ethylene) (LDPE). Insects were conditioned by three different beekeeping residues (beeswax, balanced diet, and wheat bran), and fed with LDPE for different times. LDPE biodegradation was monitored via RAMAN spectroscopy and mass loss measurements. Best results for LDPE biodegradation were obtained when exposing larvae conditioned with beeswax for 36 h.

Dar et al. addressed the topic of "plasticulture," hence, the agricultural application of plastics. These authors developed and characterized novel potentially biodegradable polymers. On the one hand, polymers consisting of ionic liquid monomers were prepared via photo radical induced polymerization; on the other hand, PE-like n-alkane disulfide polymers were produced from 1,ω-di-thiols through thermally activated air oxidation. These polymers were subjected towards soil biodegradation studies under controlled conditions, monitoring the formation of volatile degradation products by a respirometer and an advanced proton-transfer-reaction time-of-flight mass spectrometer system. While polymers based on ionic liquids did not demonstrate significant biodegradation, the disulfide-based polymer of 1,10-n-decane dithiol reached 20% degradation under basic soil conditions at room temperature within 3 months. This study demonstrates that introducing disulfide groups into the PE backbone is an option to make this material higher prone to biodegradation.

Li et al. studied the performance of two extracellular enzymes produced by *Pseudomonas hydrolytica* sp. DSWY01T for biodegradation of the synthetic polyester poly (ε-caprolactone) (PCL). Enzymes were purified, characterized, and the related genes were analyzed in details. Two novel PCL-degrading enzymes, PCLase I and PCLase II, were studied; both enzymes were able to hydrolyze PCL into monomers and oligomers, with PCLase I having shown to outperform biodegradation performance of PCLase II. Via sequence analysis and substrate specificity analysis, it was shown that PCLase I and PCLase II were a cutinase and a lipase, respectively, with optima for temperature and pH-value at 50°C and 9.0 (PCLase I) and 40°C and 10.0 (PCLase II).

A related organism, *Pseudomonas chlororaphis* PA23, was considered by Mohanan et al. for enzymes catalyzing biodegradation of different (bio)polymers. Two genes encoding the intracellular lipases LIP1 and LIP2 were identified, characterized and expressed in the host *Escherichia coli*. Encoded lipases LIP1 and LIP2 revealed strongly different amino acid sequences, catalytic mechanisms, substrate specificities, and polymer hydrolysis rates. It was shown that the recombinant LIP1 expressed in *E. coli* had best hydrolytic activity at 45°C and pH 9.0, this activity increased in presence of calcium cations. Maximum activity of LIP2, which was unaffected by calcium, was demonstrated at 40°C and pH 8.0. Both enzymes exhibited a broad substrate range; LIP1 and LIP2 were able to hydrolyze different types of PHAs, polylactic acid (PLA), and para-nitrophenyl (pNP) alkanoates. Moreover, some hydrolytic activity of these enzymes on the synthetic plastics PCL and poly (ethylene succinate) (PES) was discovered, thus making them of interest for biodegradation of polyesters of petrochemical origin.

In their study, Li et al. developed poly (hexamethylene succinate-co-ethylene succinate) [P(HS-co-ES)] copolymers with

varying physical properties and enzymatic hydrolyzability *via* melting polycondensation of monomers (hexylene succinate and ethylene succinate). Properties (crystallinity, thermal and mechanical characteristics, wettability, and susceptibility to enzymatic attack) were varied by changing the ratio of the two monomers. Enzymatic hydrolysis rates of all prepared copolyesters outperformed those of the corresponding homopolyesters [poly (hexylene succinate) and poly (ethylene succinate)]. It was shown that the copolyester containing 51% ethylene succinate did not fully degrade; this material is of interest for long-term applications. In contrast, copolyesters with 13% and 76% ethylene succinate rapidly degraded; they are auspicious materials for short-term applications, where fast degradation is desired.

Andler et al. addressed the problems associated to the enormous quantities of car tire waste consisting of vulcanized rubber, which is very resistant towards biodegradation due to its highly hydrophobic cross-linked structure, very hard to recycle, and contributes significantly to the global microplastic formation. Authors investigated a total of ten fungal strains over a period of 1 month for their biodegradation performance of vulcanized rubber particles; mass loss and surface structure changes were monitored. As major outcome, cultivations of the white rot fungi *Trametes versicolor* and *Pleurotus ostreatus* achieved a mass reduction of the polymer of 7.5% and 6.1%, respectively, after 4 weeks. Genome sequence analysis of both strains showed that these organisms possess a higher number of sequences for laccases and manganese peroxidases, two crucial extracellular enzymes for many oxidative reactions. This was experimentally confirmed by the high activity of laccase and peroxidase when cultivating the two fungal strains on rubber particles in comparison to rubber-free cultivation setups. Authors suggest that their results might pave the way towards efficient bio-inspired solutions for vulcanized rubber biodegradation in the future.

An intriguing approach for combining plastic upcycling and production of biopolymers was presented by Esmail et al. These researchers found out that the bacterial strains *Komagataeibacter xylinus* DSM 2004 and DSM 46604 are able to produce bacterial cellulose, a polysaccharide of high market potential, from conversion of terephthalic acid and ethylene glycol, the building blocks of the petroplastic PET. The two strains revealed different cultivation performance on these unusual substrates; strain DSM 2004 achieved higher productivity for bacterial cellulose than strain

DSM 46604, which, in contrast to DSM 2004, was unable to grow on ethylene glycol as the sole carbon source, but utilized mixtures of ethylene glycol and terephthalic acid. For both strains, cellulose formation was enhanced by co-feeding of glucose. A new downstream process was developed in this study for preparation of highly pure bacterial cellulose, encompassing dissolution of the polysaccharide in aqueous NaOH solution. Interestingly, bacterial cellulose produced by *K. xylinus* DSM 2004 and DSM 46604, respectively, showed different crystallinity and fiber diameters.

We are convinced that respected readers will draw the necessary inspiration from the presented articles for their own research work in the field of plastic biodegradation and related scientific areas. Most of all, we expect we expect that this book will provide the scientific community with the brainstorm it needs to eventually come up with efficient solutions to deal with the plastic dilemma.

Author contributions

MK: Research Topic editor; Main activities for drafting of the editorial KKM: Research Topic editor; Revision of draft. ZW: Research Topic editor; Revision of draft. FL: Research Topic editor; Revision of draft. AS: Research Topic editor; Revision of draft.

Conflict of interest

The authors declare that the research was conducted in the absence of any commercial or financial relationships that could be construed as a potential conflict of interest.

Publisher's note

All claims expressed in this article are solely those of the authors and do not necessarily represent those of their affiliated organizations, or those of the publisher, the editors and the reviewers. Any product that may be evaluated in this article, or claim that may be made by its manufacturer, is not guaranteed or endorsed by the publisher.

Reference

- Mukherjee, A., and Koller, M. (2022). Polyhydroxyalkanoate (PHA) biopolyesters – circular materials for sustainable development and growth. *Chem. Biochem. Eng. Q.* 36 (4), 273–293. doi:10.15255/CABEQ.2022.2124



Isolation, Identification, and Characterization of Polystyrene-Degrading Bacteria From the Gut of *Galleria Mellonella* (Lepidoptera: Pyralidae) Larvae

Shan Jiang¹, Tingting Su¹, Jingjing Zhao^{1*} and Zhanyong Wang^{2*}

¹School of Petrochemical Engineering, Liaoning Petrochemical University, Fushun, China, ²Department of Biotechnology, College of Bioscience and Biotechnology, Shenyang Agricultural University, Shenyang, China

OPEN ACCESS

Edited by:

Madalena Santos Alves,
University of Minho, Portugal

Reviewed by:

Andreas Vilcinskas,
University of Giessen, Germany
Xiaobo Liu,
Guangdong Technion-Israel Institute
of Technology, China

*Correspondence:

Jingjing Zhao
jingjing6180@126.com
Zhanyong Wang
wangzy125@gmail.com

Specialty section:

This article was submitted to
Bioprocess Engineering,
a section of the journal
Frontiers in Bioengineering and
Biotechnology

Received: 04 July 2021

Accepted: 09 August 2021

Published: 18 August 2021

Citation:

Jiang S, Su T, Zhao J and Wang Z
(2021) Isolation, Identification, and
Characterization of Polystyrene-
Degrading Bacteria From the Gut of
Galleria Mellonella (Lepidoptera:
Pyralidae) Larvae.
Front. Bioeng. Biotechnol. 9:736062.
doi: 10.3389/fbioe.2021.736062

Polystyrene (PS) is a widely used petroleum-based plastic, that pollutes the environment because it is difficult to degrade. In this study, a PS degrading bacterium identified as *Massilia* sp. FS1903 was successfully isolated from the gut of *Galleria mellonella* (Lepidoptera: Pyralidae) larvae that were fed with PS foam. Scanning electron microscopy and X-ray energy dispersive spectrometry showed that the structure and morphology of the PS film was destroyed by FS 1903, and that more oxygen appeared on the degraded PS film. A water contact angle assay verified the chemical change of the PS film from initially hydrophobic to hydrophilic after degradation. X-ray photoelectron spectroscopy further demonstrated that more oxygen-containing functional groups were generated during PS degradation. After 30 days of bacterial stain incubation with 0.15 g PS, 80 ml MSM, 30°C and PS of Mn 64400 and Mw 144400 Da, the weight of the PS film significantly decreased, with $12.97 \pm 1.05\%$ weight loss. This amount of degradation exceeds or is comparable to that previously reported for other species of bacteria reported to degrade PS. These results show that *Massilia* sp. FS1903 can potentially be used to degrade PS waste.

Keywords: galleria mellonella, gut microbiome, polystyrene, biodegradation, massilia sp.

INTRODUCTION

Petroleum-based plastics are artificial organic polymers, obtained from natural gas or oil and used for a variety of civil and industrial applications (Suman et al., 2020). According to new data, the global output of petroleum-based plastic materials has increased to approximately 359 million tons per year, the demand for them account for approximately 80% of the total plastics used (PlasticsEurope, 2019). Polyethylene, polypropylene, polyvinyl chloride, polystyrene (PS), polyurethane and polyethylene terephthalate plastics are the main types of petroleum-based plastics (Wei and Zimmermann, 2017). Because of their profound stability and the lack of suitable degradation methods, these plastics gradually accumulate in the environment, leading to a sharp increase in environmental contamination and substantial waste (Barnes et al., 2009). Researchers have even detected plastic fragments in deep sea sediments at a depth of 5,000 m. These forms of plastic are absorbed by marine organisms, which cause serious health problems for these organisms and may also affect human health (Rochman et al., 2015; Zhang et al., 2020).

PS, as the third most important petroleum-based plastic, is used for packaging containers, disposable cups and insulating materials, and comprises about 7% of the total amount of plastics produced (Ho et al., 2018; Urbanek et al., 2020). Because of its long persistence in the environment, PS wastes biodegradation efficiency is extremely low in natural ecosystems, and caused serious environmental pollution (Wilkes and Aristilde, 2017). Therefore, researchers around the world are exploring various PS high-efficiency degradation pathways without secondary pollution. Recently, many researchers began to investigate the biodegradation potential of intestinal microorganisms, especially in insect larvae with chewing mouthparts. Yang et al. (2015) isolated a PS-degrading bacterial strain *Exiguobacterium* sp. YT2 from the gut of *Tenebrio molitor*. This research showed that over a 30-days incubation period, YT2 formed a biofilm covering PS, resulting in obvious pits and cavities on the PS film surfaces. Over a 60-days incubation period, a suspension culture of strain YT2 degraded $7.4 \pm 0.4\%$ of the PS pieces. Another group of researchers subsequently showed that a previously untested strain of *T. molitor* larvae could degrade PS (Yang et al., 2017). Moreover, Peng et al. (2019) compared the PS degradation capability of *T. molitor* and *Tenebrio obscurus*. The results demonstrated that the ability of the *T. obscurus* gut to degrade PS is higher than that of *T. molitor* and that the PS consumption rate is also greater. After 31 days of feeding, the molecular weight of residual PS in the frass of *T. obscurus* decreased by 26.03%. Other insect species also have the same abilities as mealworms to degrade PS. Yang et al. (2020) showed that *Zophobas atratus* can use PS foam as their only food source, and various techniques have been used to demonstrate that the depolymerization of long-chain PS molecules and the subsequent formation of low-molecular-weight products occur in the larval gut. On the basis of this research, *Pseudomonas* sp., which can degrade PS, was isolated from the gut of *Z. atratus* larvae by Kim et al. (2020). Likewise, Wang et al. (2020) observed that *Tribolium castaneum* larvae can chew and eat PS foam, and finally successfully isolated a bacterial strain, identified as *Acinetobacter* sp. AnTc-1, from the gut of these larvae. Woo et al. (2020) reported PS biodegradation by the larvae of *Plesiophthalmus davidis* and isolated a bacterial strain *Serratia* sp. WSW (KCTC 82146) from their gut flora.

Galleria mellonella (Lepidoptera: Pyralidae) is a common agricultural pest that destroys the structure of honeycombs and are generally considered to be of no benefit to human beings; however, it has been discovered that *G. mellonella* larvae can eat and biodegrade polyethylene and PS (Lou et al., 2020). According to previous reports, this phenomenon is likely related to the gut microorganisms of these insects (Yang et al., 2015; Peng et al., 2019; Yang et al., 2020). In addition, some microbes from the gut of *G. mellonella* larvae related to the degradation of PE has been confirmed, and a PE degrading strain *Enterobacter* sp. D1 has been successfully screened (Bombelli et al., 2017; Ren et al., 2019; Cassone et al., 2020). However, there are few studies on PS degrading bacteria from the gut of *G. mellonella* larvae. In this study, a PS degrading bacterium was successfully isolated from the larval gut and identified by phylogenetic analysis combined with physiological and biochemical indicators. To determine the extent

of PS degradation by the bacterium, the physicochemical properties of the degraded PS film were studied by a scanning electron microscope (SEM), X-ray energy dispersive spectrometer (EDS), water contact angle (WCA), and X-ray photoelectron spectroscopy (XPS) analyses.

MATERIALS AND METHODS

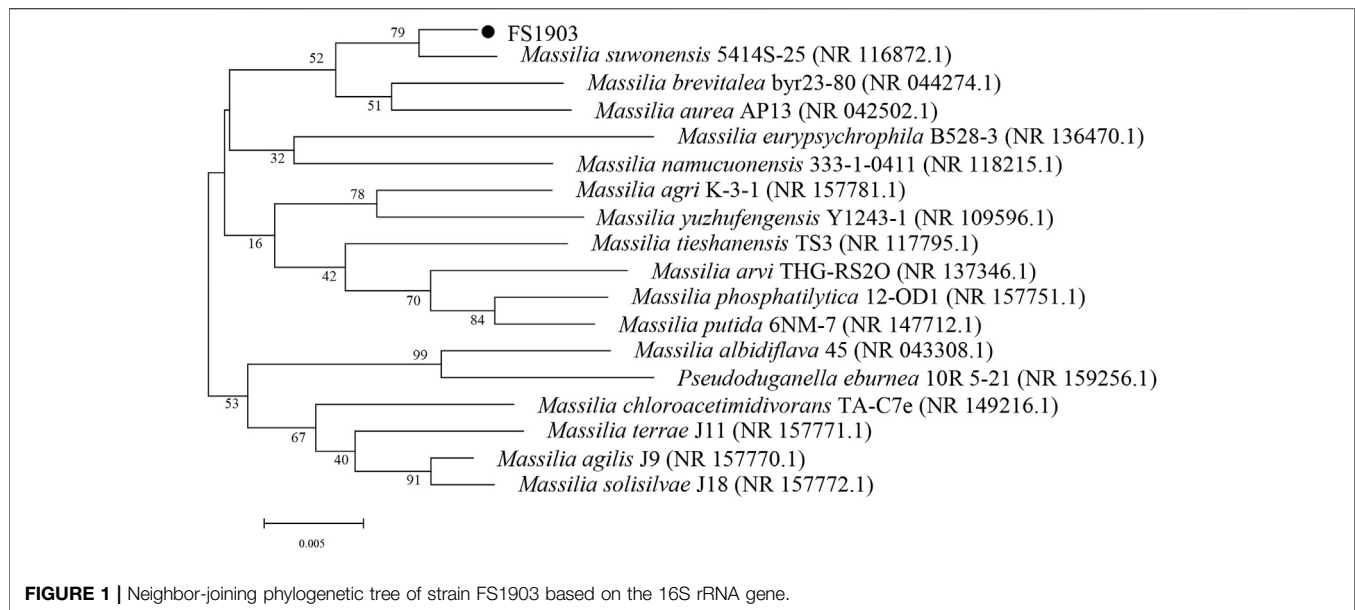
Experimental Materials

G. mellonella larvae were purchased from Huiyude Co. (Tianjin, China). PS foam board was obtained from Nannan Building Materials Co. (Zhejiang, China) and contained polystyrene purity over 98%. The number-average molecular weight (M_n) and weight-average molecular weight (M_w) of the PS were 64400 and 144,400 Da, respectively, as measured by gel permeation chromatography. The PS film for microbial degradation was prepared using the previous method (Yang et al., 2015) and fine-tuned for this study: the foam PS was dissolved in dichloromethane (0.03 g/ml) and then the solution was spread on a glass plate, after 5 h, the resulting film was removed from the glass plate and immobilized in a fume hood for 3 days at room temperature. The film was then rinsed with de-ionized water and dried before use. The thickness of the prepared film was approximately 0.02 mm.

The composition of the mineral salts medium (MSM, pH = 7.01) was as follows: 4.54 g/L KH_2PO_4 , 11.94 g/L $\text{Na}_2\text{HPO}_4 \cdot 12\text{H}_2\text{O}$, 1.0 g/L NH_4Cl , 0.5 g/L MgSO_4 , 0.005 g/L CaCl_2 , 0.002 g/L FeSO_4 , 0.001 g/L MnSO_4 and 0.002 g/L ZnSO_4 . The Luria-Bertaini (LB) medium was prepared by dissolving 10 g NaCl, 10 g tryptone, and 5 g yeast extract in 1 L deionized water. 15 g agar was added to prepare the LB agar medium. 0.9 g NaCl was dissolved in 100 ml deionized water to prepare saline. All media buffers and solutions were subjected to high-pressure steam sterilization (121°C, 103.4 kPa, 20 min). All other chemical reagents used in this study were analytical reagent grade and obtained from commercial sources.

Screening of Strains for PS Degradation Ability

Larvae ($n = 200$) were fed with PS foam for 21 days, and then 10 larvae were collected. After sterilization, the larvae were dissected and then the intestinal tissue was placed into a 1.5 ml centrifuge tube containing 1 ml of normal saline, and then shaken on a vortex mixer for 5 min. A pure intestinal cell suspension was obtained and used as a bacterial inoculum to enrich PS-degrading bacteria. A 1 ml aliquot of the suspension was transferred into a 250-ml Erlenmeyer flask with 80 ml MSM and 0.15 g PS film (1×3 mm), which was shaken on a rotary shaker (120 rpm) at room temperature. After 60 days, the remaining PS film was removed, and the enrichment culture was dispersed on LB agar plates. After culturing for 24 h at room temperature, colonies were picked and then spread on fresh LB agar plates until a pure colony was finally obtained according to the standard methodology of bacterial isolation (Yang et al., 2015). After the pure bacterial isolates were grown in liquid LB medium for 12 h, the cells were collected by centrifugation (10000 rpm) and then washed with sterile water



to remove residual medium. This step was repeated until there were no remaining nutrients. Next, the collected cells were resuspended in sterile water and then diluted 100 times to obtain a cell suspension (Yang et al., 2015). The cell suspension (0.4 ml) was distributed evenly on the surface of a MSM plate, which was then covered with PS film. Two control groups were set up. One was only inoculated with bacterial culture, while the other was only covered with PS film. All plates were cultured in triplicate at 30°C for 30 days. Place an open Petri dish with distilled water in the incubator to prevent the plates from drying. Changes in the film and bacterial growth were regularly observed. The remaining larvae were refrigerated at 4°C after pupation for subsequent use.

Sequencing and Phylogenetic Analysis

Genomic DNA used for 16S rDNA amplification was extracted from the cells during the logarithmic growth stage using the TIANamp Bacteria DNA Kit (Tiangen Biotech Co., Ltd., Beijing, China). Next, PCR amplification and agarose gel electrophoresis were performed to verify successful extraction. The gene was amplified using the universal primers 27-F (5'-AGAGTTTGA TCCTGGCTCAG-3') and 1492-R (5'-GGTTACCTTGTTACG ACTT-3'). Amplicons in the gel were recovered using TIANquick Midi Purification Kit (Tiangen Biotech Co., Ltd., Beijing, China), and then sequenced using a kit from Sangon Biotech Co., Ltd. (Shanghai, China). The obtained sequences were aligned with known organisms in the GenBank database using the Basic Local Alignment Search Tool (BLAST) created by the National Center for Biotechnology Information (NCBI, Bethesda, MD, United States). A phylogenetic tree was constructed with MEGA5.0 software using the neighbor-joining method. Bootstraps of the supporting tree branches were constructed with 1,000 replications and the default settings. A total of 17 16S rRNA sequences were used for the phylogenetic analyses, and the accession numbers of these sequences are shown in **Figure 1**.

Determination of Microbial Physiological and Biochemical Indicators

The determination of microbial physiological and biochemical indicators was carried out using the method of bacterial identification in the "Berger's Bacterial Identification Manual" (eighth edition) and Identification Manual of Common Bacteria System (Buchanna & Gibbons 1984; Dong & Cai 2001).

Performance Analysis of the Surface of the PS Film

An SEM (SU8010, Hitachi, Tokyo, Japan) was used to inspect the biofilm that formed on the PS film and the holes in the PS film after degradation. To observe the presence and growth of microorganisms, the PS films that covered the agar plates were removed after 30 days, fixed with 2.5% glutaraldehyde for 3 h and dehydrated with an ethanol gradient (30, 50, 70, 90 and 100%) for 15 min (Wang et al., 2020). To detect changes in the physical and chemical properties of the PS film, the films were immersed in a 2% (w/v) SDS aqueous solution for 4 h, and then washed with de-ionized water to completely remove the biofilm from the surface. The PS film from the uninoculated control was also treated in the same way (Sivan et al., 2006). To verify changes in the elemental composition of the PS film surface during the degradation process, a module connected to the SEM (EDS (SU8010, Hitachi, Tokyo, Japan) was used to evaluate the differences in the composition of the carbon and oxygen elements before and after degradation.

The WCA (DSA100, KRUS, Hamburg, Germany) was used to analyze changes in the hydrophilicity of the PS film surface. The contact angle was measured under static conditions at room temperature. The PS film was washed three times with SDS solution and then de-ionized water, and the contact angle measurement was estimated five times.

To investigate degradation and determine the variations of functional groups on the surface of the PS film, XPS (ESCALAB

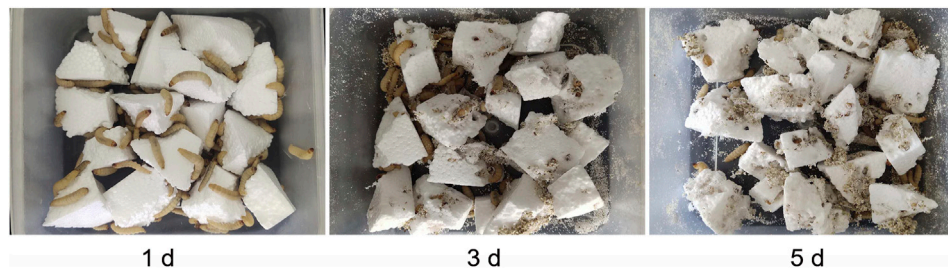


FIGURE 2 | Holes formed by *G. mellonella* larvae after feeding on PS foam for 1, 3 and 5 days.

Xi+, Thermo Fisher, Massachusetts, United States) was used to measure the binding energy. The PS film (1 cm × 1 cm) was fixed on a carbon ribbon and measured within the energy range of 2 + P–300eV, C1s.

Biodegradation Assay

After overnight incubation in 4 ml liquid LB medium, bacteria were collected by centrifugation for 10 min at 10,000 rpm, and then washed three times with 4 ml of saline. PS film (1 cm × 3 cm, 0.15 g) was added into a 250-ml Erlenmeyer flask containing 80 ml MSM. A 1 ml suspension of the bacterial culture was added into the flask, which was then incubated on an orbital shaker (150 rpm) at 30°C. This method was a slight modification of the following reported scheme (Wang et al., 2020) because the PS powder was replaced with a film; the reaction system volume was doubled; the temperature and speed were fine-tuned higher; and the reaction time was 30 days. The PS film incubated in MSM without bacteria served as a control. The weight loss assay was replicated three times. After a 30-days incubation, the PS films were harvested (Mor and Sivan, 2008).

The weight loss of the PS film was calculated using the following formula:

$$\text{Percentage of weight loss} = 100\% \times \frac{(\text{Initial PS weight} - \text{Final PS weight})}{\text{Initial PS weight}}$$

Statistical Analysis

Statistical ANOVAs were performed using SPSS 20.0 (SPSS Inc., Chicago, United States) to evaluate the differences in contact angle changes and weight loss produced by bacteria. Pairwise comparisons were analyzed with the student's t-test, as all data were normally distributed. All error values are reported as the mean value ± standard deviation.

RESULTS

Feeding Behavior of *G. mellonella* Larvae on PS Foam

G. mellonella larvae were fed with PS for 21 days. By the third day of feeding, the PS foam block was already full of holes and a small amount of block was gnawed and attached to the culture container. By the fifth day, the whole culture container was covered with PS debris (Figure 2). After consuming the PS foam diet for 21 days,

the larva appeared to be normal and they produced a normal amount of silk. These results suggested that the PS diet did not harm the larvae over a short-term feeding period.

Preliminary Screening of Strains With PS Degradation Ability

After 2 months enrichment culture, when compared with the control group, a turbid liquid was observed in the experimental group, indicating that some intestinal bacteria with the ability to degrade and use PS as a nutrition source may have been enriched. After cultivation and purification, a pure colony named as FS1903 was finally obtained. When cultivated on solid LB medium, FS1903 were round with clear edges and a slightly yellowish color (Figure 3A). The shape of the bacterial cells examined with an SEM. The results showed that FS1903 cells are an elliptical rod shape approximately 1.5 μm long and 0.5 μm in diameter (Figure 3B). To verify the PS degrading ability of FS1903, a PS film (50 mm × 50 mm) was supplied as the sole carbon source on top of an MSM plate that was spread with the cell suspension. After 30 days cultivation, when compared with control group (Figure 3C), some small colonies were observed under the PS film and a linear bacterial lawn appeared at the edge of the film in the experimental group (Figure 3D). This provides evidence that FS1903 isolated from the gut of *G. mellonella* larvae can degrade PS.

Physiological and Biochemical Test of the Tested Strain

The result of strain culturing showed that the tested strain is short rod-shaped bacterium, is motile by a terminal flagellum; forms smooth, round yellow-white colonies on LB medium; and optimum growth at 30°C and pH 7.0. Physiological and biochemical characteristics of the strain were listed in Table 1. According to the physiological and biochemical characteristics results, the strain is similar to the microorganisms of the genus *Massilia* (Shen et al., 2013; Orthova et al., 2015). In addition, bacteria of this family are often isolated from the rumen or the large intestine of humans and animals (Kämpfer et al., 2012), this is also in line with our research.

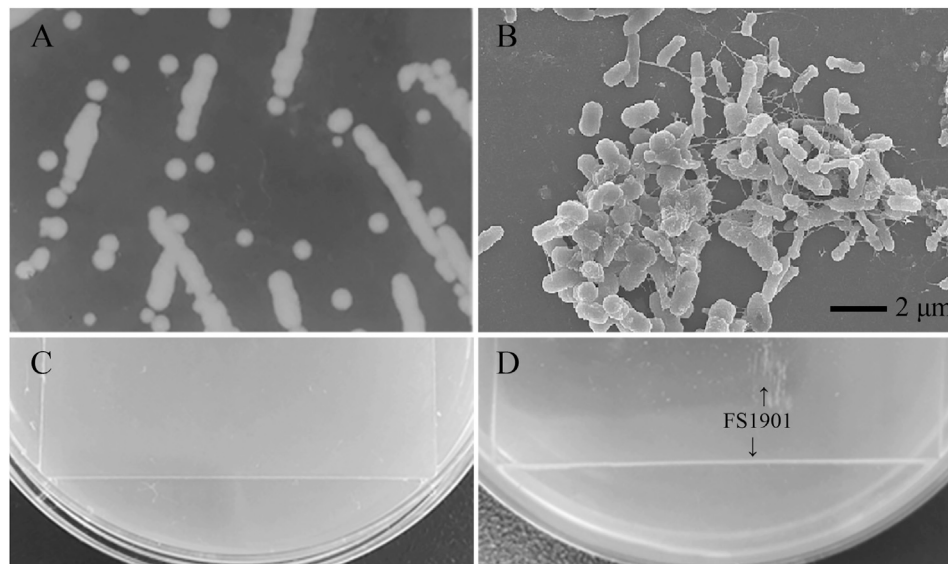


FIGURE 3 | Colonies of FS1903 on LB agar plates (A); SEM of FS 1903 (B); the control (C); and the colonies and lawn of FS1903 on the PS film on the MSM plate (D).

Sequencing and Phylogenetic Tree Construction of FS1903

A phylogenetic tree of FS1903 and other *Massilia* bacteria was constructed based on the 16S rRNA gene (Figure 1). According to the phylogenetic tree, FS1903 and *Massilia suwonensis* 5414s-25 were on the same branch and closely related with high sequence similarity of 79%. Combined with the physiological and biochemical test, tested strain can be identified as the genus *Massilia*, and then the strain was named *Massilia* sp. FS 1903. The 16S rRNA gene sequence of this bacterium was deposited in the GenBank database under accession number MW138062.

Observation of the Biofilm Formed on the PS Film Surface

The biofilm was scanned with an SEM to more closely examine the effects of the colonization of the PS film surface by FS 1903. After 30 days of cultivation, the PS film surface was examined before and after the microorganisms were completely washed off, and the results showed that the PS film was damaged by the bacteria (Figure 4A,B). In contrast, the surface of the uncultured control was smooth (Figure 4C) without any defects. These observations revealed that the bacteria caused pits and cavities on the film surface. The maximum width of a typical cavity was approximately 4 μm (Figure 4D).

Analysis of the Composition of the PS Film Surface

The carbon and oxygen composition on the PS surface where the bacteria grew was analyzed by EDS to determine the effects of the bacteria on the composition of the film. There were no obvious

TABLE 1 | Physiological and biochemical characteristics of strain FS1903.

Characteristic	FS1903
Maltose	+
Glucose	+
Lactose	-
Rhamnose	+
Sucrose	+
Arabinose	+
Starch	+
Esculin	+
Sorbitol	-
Inositol	+
L-tyrosine hydrolysis	-
V-P (2d)	-
V-P (6d)	-
Contact enzyme	+
Propionate	+
gelatin liquefaction	+

differences in the number of carbon atoms between the PS in the control group and the experimental group (Figure 5). However, more oxygen atoms were detected in the experimental group, which shows that oxidation occurred.

Oxidation was confirmed by measuring changes in the contact angle of water droplets on the PS surface, which is indicative of the surface hydrophobicity of the PS film. The results show that the contact angle of the experimental group was $66.1 \pm 5.1^\circ$, while that of the control group was $96.0 \pm 3.8^\circ$ (Figure 6). Compare to the control, the contact angle of the experimental group was significantly decreased ($p < 0.01$). This decrease in the contact angle shows that the surface tension of water decreased, because of the insertion of oxygen on the surface of PS during the oxidation

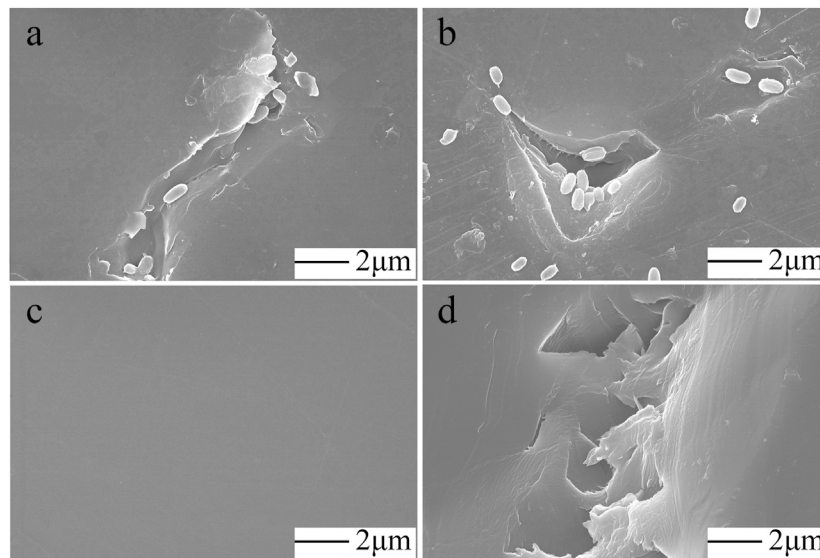


FIGURE 4 | SEM observations. FS1903 cells on the degraded PS film (A, B), control (C) and cavities and pits on the surface caused by incubation with FS 1903 (D).

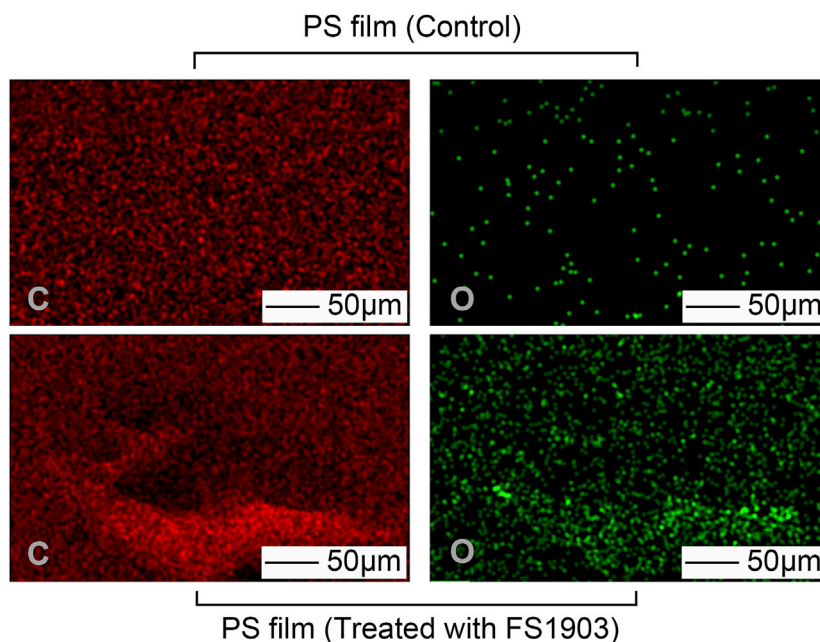


FIGURE 5 | Changes in atomic composition of the PS film surface after treatment with FS 1903. Note: “C” represents carbon and “O” represents oxygen.

process. Oxidation during PS degradation converts hydrophobic regions to hydrophilic ones, thereby changing the chemical properties of the PS surface (Gu, 2003). FS1903 colonization reduced the hydrophobicity of the PS film and at the same time the film was damaged, the decreased hydrophobicity reduced the resistance to bacterial cells to subsequent PS degradation.

XPS was used to analyze changes in the surface chemical composition and functional groups. **Figure 7** shows the comparison (0–900 eV) of the XPS scanning spectra of the PS

film for the inoculated experimental and non-inoculated control groups. The control group had only surface carbon at peak of 284.8 eV, while the PS inoculated with strain FS 1903 except 284.8 eV had another obvious peak at 532.3 eV that represented the amount of surface oxygen (**Figure 7A**). The XPS spectra of C1s on the PS film surface inoculated with strain FS1903 versus the control was compared (**Figure 7B**), and it showed that culturing with the FS1903 caused a notable decrease of the C-C group (284.8 eV). Meanwhile, compare to the control

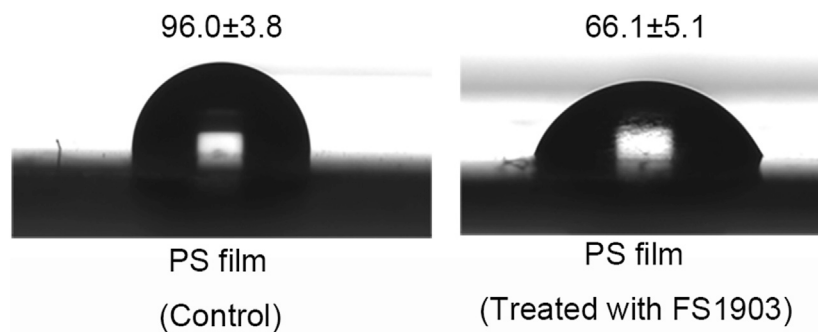


FIGURE 6 | WCA of PS film without or with inoculation by strain FS1903.

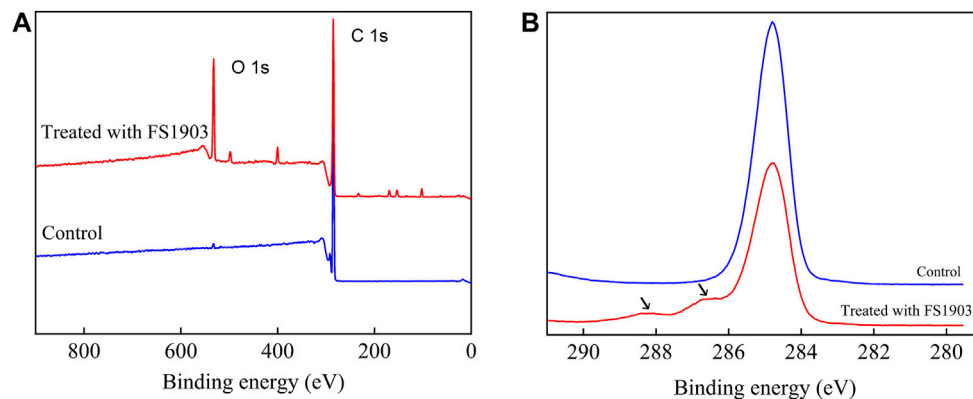


FIGURE 7 | XPS scanning (A) and C1s spectra (B) of the control and the residual PS films inoculated with FS1903.

group with one peak, the PS inoculated with strain FS 1903 had another peak at 286.5 eV, which was assigned to the C–O group. This implies that part of the C–C groups in the PS was oxidized to alcohol and carboxylic-acid-like compounds (Shang et al., 2003). In addition, on the PS film surface inoculated with strain FS 1903, another new peak appeared at 288 eV, which was assigned to the C=O group. These observations all demonstrate a transition from a C–C bond to C=O and C–O bonds during the degradation process. Furthermore, these results indicate that strain FS1903 is capable of attacking or oxidizing the PS structure to produce more polar derivatives. This change in binding energy confirms that oxidation occurs during FS1903-mediated degradation. The results are in accordance with previous work (Yang et al., 2015; Kim et al., 2020).

Biodegradation Assay

To confirm the degradation ability of strain FS 1903, we calculated the weight loss after infestation with the bacteria. After cultivation with the bacteria for 30 days, the weight loss of PS treated with strain FS1903 was $12.97 \pm 1.05\%$, which was significantly decreased compared with the control group ($p < 0.01$). Furthermore, FS1903 degraded the PS without being supplied with nutritional supplements, such as yeast extract or gelatin.

DISCUSSION

According to previous literature (Yang et al., 2015; Yang et al., 2018; Peng et al., 2019), using antibiotics to inhibit gut microorganisms of certain insects that can feed on plastic directly leads to the loss of the insects' ability to degrade plastic. At the same time, microorganisms that can degrade plastic polyethylene or PS from insect intestinal microbiomes were isolated (Yang et al., 2015; Kim et al., 2020; Wang et al., 2020). Therefore, it is clear that plastic-degrading bacteria do exist in the gut of some insects. Since the *G. mellonella* larvae have the ability to eat polystyrene and still grow normally, we preliminarily speculated that there may be microorganisms that can digest PS in the gut of these larvae. Our results confirmed this hypothesis and screened a strain of PS degrading bacteria.

The most notable and fundamental characteristic of bacteria-mediated plastic degradation processes is the formation of a biofilm on the plastic surface (Kim et al., 2020). Biofilms form on a substrate surface and can further penetrate into the materials to erode and deteriorate them (Chauhan et al., 2018; Liu et al., 2020). Adherence of bacterial cells to the polymer surface is the first and most basic step of subsequent biodegradation (Esmaili et al., 2013). In this study, the bacterial strain FS 1903 can form a biofilm on PS film. After the biofilm is formed, PS is oxidized.

Oxidation, transform the PS surface from hydrophobic to hydrophilic, is a key step in PS biodegradation (Tribedi and Sil, 2014). The oxidation in the experimental group is attributed to the functional groups (such as hydroxyl or carbonyl groups) formed via β -oxidation (Bode et al., 2000). This phenomenon caused by an enzyme or a variety of enzymes secreted by bacterial cells attaching to PS film that promotes the degradation and oxidation of PS (Mohan et al., 2020). According to the analysis results of the composition, contact angle, and functional groups of the PS film surface, oxidation was produced in the PS films treated by FS 1903. These results confirmed that FS1903 can destroy the physical integrity of a PS film and degrade it.

Although the physics and chemistry changes in the PS inoculated with the bacteria demonstrate the degradation by FS 1903, the most direct evidence of PS biodegradation is its weight loss (Yang et al., 2015; Kim et al., 2020; Wang et al., 2020). *Rhodococcus* C208 and *Exiguobacterium* sp. YT2 have been previously shown to reduce the PS weight by 0.8% in 56 days and 7.4% in 60 days, respectively (Mor and Sivan, 2008; Yang et al., 2017). *Acinetobacter* sp. AnTc-1 can degrade PS powder, with a weight loss of $12.14 \pm 1.4\%$ after 60 days of cultivation (Wang et al., 2020). Compared to these other bacterial strains, FS1903 produced a higher weight loss in less time and demonstrated a comparable potential in degrading PS. However, the weight loss is very low compared to the direct consumption of PS by insect larvae. Previous researches have reported that plastic-degrading microorganisms demonstrate expedited degradation within the insect gut environment (Przemieniecki et al., 2020; Brandon et al., 2021). This phenomenon implies that the insect host may play a role in the plastic biodegradation process. *G. mellonella* larvae have been shown that they retain the capacity to metabolize polyethylene when their gut microbiome activity is suppressed (Kong et al., 2019). In addition, Brandon et al. (2021) and Tsochatzis et al. (2021) provide evidence that insect larvae secrete emulsifying factors or enzymes that mediate plastic biodegradation. These studies indicate that using insect larvae to degrade plastic is a complex system in which the larvae host and its gut microbiome collaborate to work. This may be the reason for the low weight loss of PS degradation by FS1903 only. Therefore, further identification key functional enzymes from larvae host and gut microbiome related to the depolymerization and biodegradation of PS is needed.

REFERENCES

- Barnes, D. K. A., Galgani, F., Thompson, R. C., and Barlaz, M. (2009). Accumulation and Fragmentation of Plastic Debris in Global Environments. *Phil. Trans. R. Soc. B* 364, 1985–1998. doi:10.1098/rstb.2008.0205
- Bode, H. B., Zeeck, A., Plückhahn, K., and Jendrossek, D. (2000). Physiological and Chemical Investigations into Microbial Degradation of Synthetic Poly(*Cis* -1,4-isoprene). *Appl. Environ. Microbiol.* 66, 3680–3685. doi:10.1128/AEM.66.9.3680-3685.2000
- Bombelli, P., Howe, C. J., and Bertocchini, F. (2017). Polyethylene Bio-Degradation by Caterpillars of the Wax Moth *Galleria Mellonella*. *Curr. Biol.* 27, R292–R293. doi:10.1016/j.cub.2017.02.060

CONCLUSION

This is the first study to identify a PS-degrading strain of bacteria isolated from the gut of *G. mellonella* larvae. The degradation ability of this strain FS1903 was comparable or better than any other bacterial strain previously identified. Optimization of conditions to simulate the intestinal environment and improve the degradation efficiency of these bacteria *in vitro* is currently being investigated in our laboratory. In addition, further work is needed to determine if the larvae have the ability to degrade other common plastics (such as polyethylene, polypropylene, polyvinyl chloride and polyethylene terephthalate), and to identify the mechanisms and pathways involved in this biodegradation.

DATA AVAILABILITY STATEMENT

The datasets presented in this study can be found in online repositories. The names of the repository/repositories and accession number(s) can be found below: <https://www.ncbi.nlm.nih.gov/nuccore/MW138062.1>.

ETHICS STATEMENT

The animal study was reviewed and approved by International Association of Veterinary Editors guidelines.

AUTHOR CONTRIBUTIONS

SJ, TS, JZ and ZW: conceptualization. SJ: methodology, data curation. SJ and TS: formal analysis. SJ and JZ: writing—original draft. JZ and ZW: writing—review and editing. All authors contributed to manuscript revision, read, and approved the submitted version.

FUNDING

This work was supported by the Education Department of Liaoning Province (L2019040); the Natural Science Foundation of Liaoning Province (2020-BS-229); Liaoning Revitalization Talents Program (XLYC1807034); the Talent Scientific Research Funds of Liaoning Petrochemical University (2019XJL-012).

- Brandon, A. M., Garcia, A. M., Khlystov, N. A., Wu, W.-M., and Criddle, C. S. (2021). Enhanced Bioavailability and Microbial Biodegradation of Polystyrene in an Enrichment Derived from the Gut Microbiome of *Tenebrio molitor* (Mealworm Larvae). *Environ. Sci. Technol.* 55 (3), 2027–2036. doi:10.1021/acs.est.0c04952
- Buchanna, R. E., and Gibbons, N. E. (1984). *Bergey's Manual of Determinative Bacteriology*. The Eighth Edition. Beijing: Science Press.
- Cassone, B. J., Grove, H. C., Elebute, O., Villanueva, S. M. P., and Lemoine, C. M. R. (2020). Role of the Intestinal Microbiome in Low-Density Polyethylene Degradation by Caterpillar Larvae of the Greater Wax Moth, *Galleria Mellonella*. *Proc. R. Soc. B* 287, 20200112. doi:10.1098/rspb.2020.0112

- Chauhan, D., Agrawal, G., Deshmukh, S., Roy, S. S., and Priyadarshini, R. (2018). Biofilm Formation by *Exiguobacterium* sp. DR11 and DR14 Alter Polystyrene Surface Properties and Initiate Biodegradation. *RSC Adv.* 8, 37590–37599. doi:10.1039/C8RA06448B
- Dong, X. Z., and Cai, M. Y. (2001). *Manual for Systematic Identification of Common Bacteria*. Beijing: Science Press.
- Esmaili, A., Pourbabaee, A. A., Alikhani, H. A., Shabani, F., and Esmaili, E. (2013). Biodegradation of Low-Density Polyethylene (LDPE) by Mixed Culture of *Lysinibacillus Xylanilyticus* and *Aspergillus niger* in Soil. *PLoS One* 8, e71720. doi:10.1371/journal.pone.0071720
- Gu, J.-D. (2003). Microbiological Deterioration and Degradation of Synthetic Polymeric Materials: Recent Research Advances. *Int. Biodeterior. Biodegrad.* 52, 69–91. doi:10.1016/S0964-8305(02)00177-4
- Ho, B. T., Roberts, T. K., and Lucas, S. (2018). An Overview on Biodegradation of Polystyrene and Modified Polystyrene: the Microbial Approach. *Crit. Rev. Biotechnol.* 38, 308–320. doi:10.1080/07388551.2017.1355293
- Kämpfer, P., Lodders, N., Martin, K., and Falsen, E. (2012). *Massilia Oculi* Sp. nov., Isolated from a Human Clinical Specimen. *Int. J. Syst. Evol. Microb.* 62 (Pt 2), 364–369. doi:10.1099/ijs.0.032441-0
- Kim, H. R., Lee, H. M., Yu, H. C., Jeon, E., Lee, S., Li, J., et al. (2020). Biodegradation of Polystyrene by *Pseudomonas* Sp. Isolated from the Gut of Superworms (Larvae of *Zophobas Atratus*). *Environ. Sci. Technol.* 54, 6987–6996. doi:10.1021/acs.est.0c01495
- Kong, H. G., Kim, H. H., Chung, J.-h., Jun, J., Lee, S., Kim, H.-M., et al. (2019). The *Galleria Mellonella* Hologenome Supports Microbiota-independent Metabolism of Long-Chain Hydrocarbon Beeswax. *Cel Rep.* 26, 2451–2464. doi:10.1016/j.celrep.2019.02.018
- Liu, X., Koestler, R. J., Warscheid, T., Katayama, Y., and Gu, J.-D. (2020). Microbial Deterioration and Sustainable Conservation of Stone Monuments and Buildings. *Nat. Sustain.* 3, 991–1004. doi:10.1038/s41893-020-00602-5
- Lou, Y., Ekaterina, P., Yang, S.-S., Lu, B., Liu, B., Ren, N., et al. (2020). Biodegradation of Polyethylene and Polystyrene by Greater Wax Moth Larvae (*Galleria Mellonella* L.) and the Effect of Co-diet Supplementation on the Core Gut Microbiome. *Environ. Sci. Technol.* 54, 2821–2831. doi:10.1021/acs.est.9b07044
- Mohan, N., Montazer, Z., Sharma, P. K., and Levin, D. B. (2020). Microbial and Enzymatic Degradation of Synthetic Plastics. *Front. Microbiol.* 11, 580709. doi:10.3389/fmicb.2020.580709
- Mor, R., and Sivan, A. (2008). Biofilm Formation and Partial Biodegradation of Polystyrene by the Actinomycete *Rhodococcus Ruber*. *Biodegradation* 19, 851–858. doi:10.1007/s10532-008-9188-0
- Orthová, I., Kämpfer, P., Glaeser, S. P., Kaden, R., and Busse, H.-J. (2015). *Massilia Norwicensis* Sp. nov., Isolated from an Air Sample. *Int. J. Syst. Evol. Microb.* 65, 56–64. doi:10.1099/ijs.0.068296-0
- Peng, B.-Y., Su, Y., Chen, Z., Chen, J., Zhou, X., Benbow, M. E., et al. (2019). Biodegradation of Polystyrene by Dark (*Tenebrio Obscurus*) and Yellow (*Tenebrio Molitor*) Mealworms (Coleoptera: Tenebrionidae). *Environ. Sci. Technol.* 53, 5256–5265. doi:10.1021/acs.est.8b06963
- PlasticsEurope (2019). *Plastics-the Facts 2019. An Analysis of European Plastics Production, Demand and Waste Data*. Available at: <https://www.plasticseurope.org/en/resources/publications/1804-plastics-facts-2019> (Accessed October 17, 2019).
- Przemieniecki, S. W., Kosewska, A., Ciesielski, S., and Kosewska, O. (2020). Changes in the Gut Microbiome and Enzymatic Profile of *Tenebrio Molitor* Larvae Biodegrading Cellulose, Polyethylene and Polystyrene Waste. *Environ. Pollut.* 256, 113265. doi:10.1016/j.envpol.2019.113265
- Ren, L., Men, L., Zhang, Z., Guan, F., Tian, J., Wang, B., et al. (2019). Biodegradation of Polyethylene by *Enterobacter* Sp. D1 from the Guts of Wax Moth *Galleria Mellonella*. *Ijerph* 16, 1941. doi:10.3390/ijerph16111941
- Rochman, C. M., Tahir, A., Williams, S. L., Baxa, D. V., Lam, R., Miller, J. T., et al. (2015). Anthropogenic Debris in Seafood: Plastic Debris and Fibers from Textiles in Fish and Bivalves Sold for Human Consumption. *Sci. Rep.* 5, 14340. doi:10.1038/srep14340
- Shang, J., Chai, M., and Zhu, Y. (2003). Solid-phase Photocatalytic Degradation of Polystyrene Plastic with TiO₂ as Photocatalyst. *J. Solid State. Chem.* 174, 104–110. doi:10.1016/S0022-4596(03)00183-X
- Shen, L., Liu, Y., Wang, N., Yao, T., Jiao, N., Liu, H., et al. (2013). *Massilia Yuzhufengensis* Sp. nov., Isolated from an Ice Core. *Int. J. Syst. Evol. Microb.* 63, 1285–1290. doi:10.1099/ijs.0.042101-0
- Sivan, A., Szanto, M., and Pavlov, V. (2006). Biofilm Development of the Polyethylene-Degrading Bacterium *Rhodococcus Ruber*. *Appl. Microbiol. Biotechnol.* 72, 346–352. doi:10.1007/s00253-005-0259-4
- Suman, T. Y., Li, W.-G., Alif, S., Faris, V. R. P., Amarnath, D. J., Ma, J.-G., et al. (2020). Characterization of Petroleum-Based Plastics and Their Absorbed Trace Metals from the Sediments of the Marina Beach in Chennai, India. *Environ. Sci. Eur.* 32, 110. doi:10.1186/s12302-020-00388-5
- Tribedi, P., and Sil, A. K. (2014). Cell Surface Hydrophobicity: A Key Component in the Degradation of Polyethylene Succinate by *Pseudomonas* Sp. AKS2. *J. Appl. Microbiol.* 116, 295–303. doi:10.1111/jam.12375
- Tsochatzis, E. D., Berggreen, I. E., Norgaard, J. V., Theodoridis, G., and Dalsgaard, T. K. (2021). Biodegradation of Expanded Polystyrene by Mealworm Larvae under Different Feeding Strategies Evaluated by Metabolic Profiling Using GC-TOF-MS. *Chemosphere* 281, 130840. doi:10.1016/j.chemosphere.2021.130840
- Urbanek, A. K., Rybak, J., Wróbel, M., Leluk, K., and Mironczuk, A. M. (2020). A Comprehensive Assessment of Microbiome Diversity in *Tenebrio molitor* Fed with Polystyrene Waste. *Environ. Pollut.* 262, 114281. doi:10.1016/j.envpol.2020.114281
- Wang, Z., Xin, X., Shi, X., and Zhang, Y. (2020). A Polystyrene-Degrading *Acinetobacter* Bacterium Isolated from the Larvae of *Tribolium castaneum*. *Sci. Total Environ.* 726, 138564. doi:10.1016/j.scitotenv.2020.138564
- Wei, R., and Zimmermann, W. (2017). Microbial Enzymes for the Recycling of Recalcitrant Petroleum-based Plastics: How Far Are We? *Microb. Biotechnol.* 10, 1308–1322. doi:10.1111/1751-7915.12710
- Wilkes, R. A., and Aristilde, L. (2017). Degradation and Metabolism of Synthetic Plastics and Associated Products by *Pseudomonas* sp.: Capabilities and Challenges. *J. Appl. Microbiol.* 123, 582–593. doi:10.1111/jam.13472
- Woo, S., Song, I., and Cha, H. J. (2020). Fast and Facile Biodegradation of Polystyrene by the Gut Microbial flora of *Plesiophthalmus Davidis* Larvae. *Appl. Environ. Microbiol.* 86, e01361–20. doi:10.1128/AEM.01361-20
- Yang, Y., Yang, J., Wu, W.-M., Zhao, J., Song, Y., Gao, L., et al. (2015). Biodegradation and Mineralization of Polystyrene by Plastic-Eating Mealworms: Part 2. Role of Gut Microorganisms. *Environ. Sci. Technol.* 49, 12087–12093. doi:10.1021/acs.est.5b02663
- Yang, S.-S., Brandon, A. M., Andrew Flanagan, J. C., Yang, J., Ning, D., Cai, S.-Y., et al. (2018). Biodegradation of Polystyrene Wastes in Yellow Mealworms (Larvae of *Tenebrio molitor* Linnaeus): Factors Affecting Biodegradation Rates and the Ability of Polystyrene-Fed Larvae to Complete Their Life Cycle. *Chemosphere* 191, 979–989. doi:10.1016/j.chemosphere.2017.10.117
- Yang, S.-S., Wu, W.-M., Brandon, A. M., Fan, H.-Q., Receveur, J. P., Li, Y., et al. (2018). Ubiquity of Polystyrene Digestion and Biodegradation within Yellow Mealworms, Larvae of *Tenebrio molitor* Linnaeus (Coleoptera: Tenebrionidae). *Chemosphere* 212, 262–271. doi:10.1016/j.chemosphere.2018.08.078
- Yang, Y., Wang, J., and Xia, M. (2020). Biodegradation and Mineralization of Polystyrene by Plastic-Eating Superworms *Zophobas Atratus*. *Sci. Total Environ.* 708, 135233. doi:10.1016/j.scitotenv.2019.135233
- Zhang, D., Liu, X., Huang, W., Li, J., Wang, C., Zhang, D., et al. (2020). Microplastic Pollution in Deep-Sea Sediments and Organisms of the Western Pacific Ocean. *Environ. Pollut.* 259, 113948. doi:10.1016/j.envpol.2020.113948

Conflict of Interest: The authors declare that the research was conducted in the absence of any commercial or financial relationships that could be construed as a potential conflict of interest.

Publisher's Note: All claims expressed in this article are solely those of the authors and do not necessarily represent those of their affiliated organizations, or those of the publisher, the editors and the reviewers. Any product that may be evaluated in this article, or claim that may be made by its manufacturer, is not guaranteed or endorsed by the publisher.

Copyright © 2021 Jiang, Su, Zhao and Wang. This is an open-access article distributed under the terms of the Creative Commons Attribution License (CC BY). The use, distribution or reproduction in other forums is permitted, provided the original author(s) and the copyright owner(s) are credited and that the original publication in this journal is cited, in accordance with accepted academic practice. No use, distribution or reproduction is permitted which does not comply with these terms.



Assessing the Biodegradation of Vulcanised Rubber Particles by Fungi Using Genetic, Molecular and Surface Analysis

R. Andler^{1*}, V. D'Afonseca², J. Pino¹, C. Valdés² and M. Salazar-Viedma³

¹Escuela de Ingeniería en Biotecnología, Centro de Biotecnología de los Recursos Naturales (Cenbio), Universidad Católica del Maule, Talca, Chile, ²Centro de Investigación de Estudios Avanzados del Maule, Vicerrectoría de Investigación y Postgrado, Universidad Católica del Maule, Talca, Chile, ³Laboratorio de Genética y Microevolución, Facultad de Ciencias Básicas, Universidad Católica del Maule, Talca, Chile

OPEN ACCESS

Edited by:

Aamer Ali Shah,
Quaid-i-Azam University, Pakistan

Reviewed by:

Ziaullah Shah,
CECOS University, Pakistan
Fariha Hasan,
Quaid-i-Azam University, Pakistan

*Correspondence:

R. Andler
randler@ucm.cl

Specialty section:

This article was submitted to
Bioprocess Engineering,
a section of the journal
Frontiers in Bioengineering and
Biotechnology

Received: 19 August 2021

Accepted: 06 October 2021

Published: 18 October 2021

Citation:

Andler R, D'Afonseca V, Pino J, Valdés C and Salazar-Viedma M (2021)
Assessing the Biodegradation of
Vulcanised Rubber Particles by Fungi
Using Genetic, Molecular and
Surface Analysis.
Front. Bioeng. Biotechnol. 9:761510.
doi: 10.3389/fbioe.2021.761510

Millions of tonnes of tyre waste are discarded annually and are considered one of the most difficult solid wastes to recycle. A sustainable alternative for the treatment of vulcanised rubber is the use of microorganisms that can biotransform polymers and aromatic compounds and then assimilate and mineralise some of the degradation products. However, vulcanised rubber materials present great resistance to biodegradation due to the presence of highly hydrophobic cross-linked structures that are provided by the additives they contain and the vulcanisation process itself. In this work, the biodegradation capabilities of 10 fungal strains cultivated in PDA and EM solid medium were studied over a period of 4 weeks. The growth of the strains, the mass loss of the vulcanised rubber particles and the surface structure were analysed after the incubation period. With the white rot fungi *Trametes versicolor* and *Pleurotus ostreatus*, biodegradation percentages of 7.5 and 6.1%, respectively, were achieved. The FTIR and SEM-EDS analyses confirmed a modification of the abundance of functional groups and elements arranged on the rubber surface, such as C, O, S, Si, and Zn, due to the biological treatment employed. The availability of genomic sequences of *P. ostreatus* and *T. versicolor* in public repositories allowed the analysis of the genetic content, genomic characteristics and specific components of both fungal species, determining some similarities between both species and their relationship with rubber biodegradation. Both fungi presented a higher number of sequences for laccases and manganese peroxidases, two extracellular enzymes responsible for many of the oxidative reactions reported in the literature. This was confirmed by measuring the laccase and peroxidase activity in cultures of *T. versicolor* and *P. ostreatus* with rubber particles, reaching between 2.8 and 3.3-times higher enzyme activity than in the absence of rubber. The integrative analysis of the results, supported by genetic and bioinformatics tools, allowed a deeper analysis of the biodegradation processes of vulcanised rubber. It is expected that this type of analysis can be used to find more efficient biotechnological solutions in the future.

Keywords: laccase, peroxidase, *Pleurotus ostreatus*, rubber biodegradation, rubber recycling, *Trametes versicolor*, vulcanized rubber

INTRODUCTION

The automotive industry has generated an enormous amount of tyre waste, where landfill is not a viable or sustainable alternative (Bowles et al., 2020). In nature, we can find biological degradation mechanisms carried out by microorganisms with the capacity to use a wide range of compounds such as natural polymers. However, tyre waste has a highly complex structure, preventing effective natural biodegradation processes. Since only 20–25% w/w of a tyre corresponds to natural rubber and the remaining percentage to a mixture of synthetic rubber, carbon black, antioxidants, accelerators, retardants, elemental sulphur, among other compounds (Stevenson et al., 2008), cell colonisation and, consequently, biodegradation is inhibited. In addition to the highly resistant chemicals as part of the tyre, the high degree of crosslinking and the low or no reactivity of the functional groups in the tyre structure make the mixing of this residue with other materials a major challenge (Andler, 2020; Simon-Stöger and Varga, 2021).

Several tyre-recycling processes have been described, and most of them are focused on the modification of the chemical structure and, thus, achieving devulcanisation. These include chemical processes using different peroxides (Rooj et al., 2011; Sabzekar et al., 2015; Hejna et al., 2019), physical processes such as grinding, ultrasound, microwaves or thermo-mechanical processes (Feng and Isayev, 2006; Wang et al., 2013; Formela and Cysewska, 2014; Garcia et al., 2015; Asaro et al., 2018; Formela et al., 2019; Li et al., 2020) and biological processes using microorganisms, mainly bacteria (Tatangelo et al., 2016; Ghavipanjeh et al., 2018; Aboelkheir et al., 2019; Kaewpetch et al., 2019).

The biodegradation of unvulcanised rubber, such as natural rubber, latex or poly (*cis*-1, 4-isoprene), has previously been studied in detail. Those studies pointed out that the main microorganisms responsible for performing polymer cleavage into oligomers are actinomycetes belonging to the genera *Gordonia*, *Streptomyces*, *Nocardia*, *Actinoplanes*, among others (Jendrossek et al., 1997). The metabolic pathways involved during the oxidation of oligo (*cis*-1,4-isoprene) molecules by β -oxidation (Hiessl et al., 2012) and cell cultures, using the polymer as sole carbon source, have also been described (Andler et al., 2018b). Furthermore, the enzymes responsible for the first oxidative attack, the so-called “rubber oxygenases,” have been studied biochemically (Jendrossek and Birke, 2019) and have been used for *in vitro* applications (Andler et al., 2018a, 2020). However, biodegradation studies using vulcanised rubber are scarce, and much remains to be understood.

Fungi are characterised by their biochemical and ecological capacity to degrade contaminants of different nature and varied chemical structures (Harms et al., 2011). They present a series of unique characteristics for the biodegradation of pollutants or toxic substances, including their ability to extend through substrates because of their filamentous structure, powerful enzyme production system and the capacity to produce natural surfactants that favour the degradative process (Sánchez, 2020). The biodegradation of synthetic polymers using fungi has been extensively studied using polyethylene

terephthalate (PET), polyethylene (PE), polypropylene (PP), polyvinyl chloride (PVC) and polystyrene (PS) plastics. While commercial plastics also contain additives that impart the physicochemical properties of interest to the final product and prolong the life of plastic products (Hahladakis et al., 2018), the amount of these additives relative to the polymer is considerably lower when compared to the amount of additives present in tyres (Altenhoff et al., 2019).

Given the similarity between lignocellulosic biomass and the additives present in tyres, with many of them being aromatic compounds, white-rot fungi are excellent candidates for detoxifying tyre waste. In a previous study, the degradative capacity of 15 fungi was analysed using the additive Poly R-478 as a model aromatic compound. The authors found that the fungi *Pleurotus sajor-caju*, *Trametes versicolor* and *Resinicium bicolor* had a higher incidence of decolorising the additive and maintained their extracellular enzymatic activity after cultivation (Bredberg et al., 2002).

Despite the important degradative capacity of fungi, given their high metabolic rate and tremendous capacity for the degradation and mineralisation of various environmental pollutants, there is little information regarding their potential use as catalysts for rubber wastes. In this study, we analysed the effects generated on the surface of vulcanised rubber particles after incubation with different fungal species and their linkage with the possible enzymes responsible for these modifications, using molecular and bioinformatics tools.

MATERIALS AND METHODS

Rubber Particles

Rubber particles (RP) were purchased from Trelleborg AB, Germany. For all experiments performed, a particle size between 1 and 2 mm was used. To avoid contamination, rubber particles were washed with 70% ethanol, dried at 80°C for 24 h and sterilised at 121°C for 20 min in separate aluminium envelopes.

Growth Experiments

Ten different fungal species, namely *Coriolus multicolor*, *Gonnoderma aplanatum*, *Lentinula edodes*, *Lenzites trabea*, *Lenzites betulinus*, *Pleurotus ostreatus*, *Pleurotus eryngii*, *Postia placenta*, *Stereum hirsutum* and *Trametes versicolor*, were studied. The strains were incubated at 28°C using plates with potato dextrose agar (PDA) and malt extract agar (MEA). After obtaining a fully grown plate, 0.5 g of rubber particles was added to each plate under sterile conditions and incubated for 4 weeks. Each experiment was performed in triplicate.

Recovery of Rubber Particles

After the incubation period, the rubber particles were carefully collected from the agar plate under sterile conditions and washed with 70% ethanol and 10% sodium hypochlorite until total removal of the fungi. Subsequently, the solvent was removed, and the rubber particles were dried at 50°C for 72 h. Control samples were treated under the same conditions to prevent the

potential oxidative effect of sodium hypochlorite from affecting subsequent analyses.

Mass Reduction Measurement

The mass of the rubber particles was analysed before and after the incubation period with the fungi. The loss of mass was calculated as follows:

$$\% \text{weight reduction} = \frac{(m_i - m_f)}{m_i} \cdot 100, \quad (1)$$

where m_i is the initial mass of the rubber particles and m_f is the final mass of the rubber particles.

FTIR Analysis

10 mg of dried rubber particles were analysed by attenuated total reflectance (ATR-FTIR). The infrared spectra were obtained using an FTIR spectrometer (Agilent, Cary 630) with the ATR technique. Absorbance was measured in the wavelength range of 400–40,00 cm^{-1} , with a resolution of 4 cm^{-1} . For each sample, 64 scans were performed, and the background was subtracted using the Agilent MicroLab PC software.

Scanning Electron Microscopy

An electron microscope TESCAN VEGA 3 with probe EDS BRUKER QUANTAX was used. The method was based on the ASTM E1508 standard “Standard Guide for Quantitative Analysis by Energy-Dispersive Spectroscopy”. Samples were covered by a cathodic spray system with Palladium Gold in the Hummer 6.2 equipment.

Enzyme Activity Assay

Liquid cultures of *T. versicolor* and *P. ostreatus* were performed by cutting three $1 \times 1 \text{ cm}^2$ plugs from fully grown PDA plates and poured into 250-ml shake flasks with 50 ml of potato dextrose broth (PDB). Sterile rubber particles were incorporated to the flasks while the corresponding controls did not contain rubber particles. Cultivations were performed at 30 °C, 100 rpm for 5 days. Supernatants were obtained by centrifugation at $10,000 \times g$ for 20 min at 4°C and used for enzyme activity measurements.

Laccase and peroxidase activities were quantified spectrophotometrically (Agilent, Cary 100 Bio) at 415 nm by detecting the oxidation of 2,20-azino-bis(3-ethylbenzothiazoline-6-sulfonate) (ABTS). For laccase activity, 100 μL of sample were mixed with a solution containing 900 μL of 10 mM ABTS and 0.2 M sodium acetate pH 5.0. For peroxidase activity, 100 μL of sample were mixed with a solution containing 800 μL of 10 mM ABTS and 100 M sodium acetate pH 5.0 and 100 μL of 20 mM H_2O_2 .

Genomic Data Collection of Fungal Species

Two Basidiomycetes species were selected in this study as sample sets of the biodegradation of vulcanised rubber. Publicly available genomic assemblies were downloaded from the Joint Genome Institute's fungal genome portal MycoCosm (Grigoriev et al., 2014), JGI Genome Portal - unified access to all JGI genomic datasets (Mukherjee et al., 2021) and NCBI Genome Assembly (Schoch et al., 2020).

Bioinformatic Analysis

Two specific enzymes (laccase EC 1.10.3.2 and manganese peroxidase EC 1.11.1.13) were searched in sequences deposited in a public database for the 10 fungal species analysed in this study. The database used consisted of identical protein groups of the National Center for Biotechnology Information (www.ncbi.nlm.nih.gov).

For analysis of the similarity at the amino acid level among the sequences of laccases and manganese peroxidase, we used the MEGA-X (Kumar et al., 2018) and T-COFFEE (https://coffee.crg.cat/apps/tcoffee/) (Notredame et al., 2000) software packages with the default parameters. To generate the protein alignment figures, the ESPript 3.0 software (https://esprict.ibcp.fr/) (Robert and Gouet, 2014) was used, highlighting the regions with higher similarity among the sequences: black represents 100% similarity, grey represents 90 to 80% and white similarity below 70%. Each analysis used sequences of laccases and manganese peroxidase separately from *Pleurotus ostreatus* and *Trametes versicolor*.

To evaluate the presence of a conserved domain among the sequences of laccases and manganese peroxidase from *P. ostreatus* and *T. versicolor*, we used the Conserved Domain Database (CDD) from the NCBI (https://www.ncbi.nlm.nih.gov/Structure/cdd/cdd.shtml) and PFAM (http://pfam.xfam.org/) programmes (Lu et al., 2020).

RESULTS AND DISCUSSION

Fungal Growth in the Presence of Vulcanised Rubber Particles

The fungal strains were evaluated in terms of radial growth when incubated in PDA and EM media in Petri dishes, and no significant differences were found between the culture media used (data not shown). **Figure 1A** shows some of the fungi incubated with the vulcanised rubber particles already incorporated. There was a different fungus-rubber interaction depending on the fungal strain used. Three different behaviours stand out, namely total coating, partial coating and zero coating. Of the 10 strains analysed, only *P. ostreatus* and *T. versicolor* achieved a total coating of the vulcanised rubber particles, whereas the strains *C. multicolor*, *L. edodes*, *L. betulinus* and *P. eryngii* showed partial coating. The time required to reach a fully-grown plate was different for each fungus, which was qualitatively analysed by the relative growth rate (**Figure 1B**). Based on this, *P. ostreatus* obtained complete growth in the shortest time (between 24 and 30 h), followed by *P. eryngii* and *T. versicolor* (from 36 to 42 h). In general, the observations of the level of coating were related to the percentage mass loss of the vulcanised rubber particles at the end of the incubation periods, while the relative growth rate was not always a precise indicator. The highest mass loss was $7.5 \pm 0.3\%$, obtained after cultivation with *T. versicolor*, followed by $6.1 \pm 0.4\%$ obtained with *P. ostreatus*. Based on these results, vulcanised rubber particles treated with *T. versicolor* and *P. ostreatus* strains were selected for surface analysis.

Bredberg et al. (2002) studied the detoxification of vulcanised rubber by different wood-rotting fungi, using the aromatic

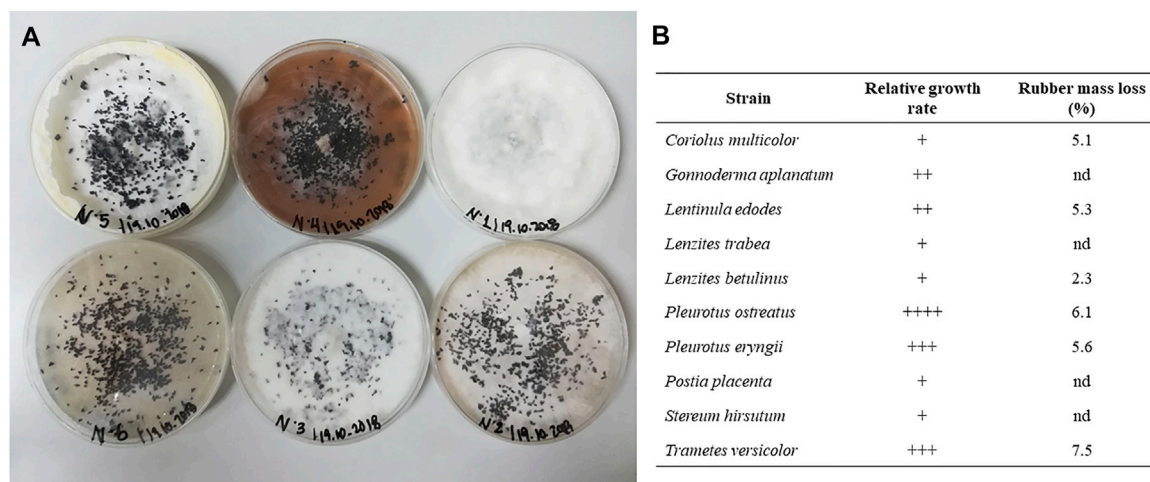


FIGURE 1 | (A) Growth of fungal species in the presence of vulcanised rubber particles. **(B)** Relative growth rate and rubber mass reduction of the 10 fungal species after incubation.

polymeric dye polyvinylamine sulfonate anthrapyridone (Poly-R478) as a model compound. The authors showed that only three strains were able to biodegrade Poly-R478, namely *Pleurotus sajor-caju*, *T. versicolor* and *Recinicium bicolor*. Subsequently, they used the treated rubber in cultures with *Acidithiobacillus ferrooxidans* and reached higher growth rates compared to rubber without fungal treatment. It was assumed that the extracellular enzymes from the selected fungi degraded aromatic structures and that the rubber obtained had a reduced toxicity. As in our study, only the cultures with white rot fungi obtained positive results.

Surface Analysis of Rubber Particles After Fungal Incubation

Changes in the rubber surface were analysed by FTIR (Figure 2). The functional groups observed may indicate the presence of compounds such as black carbon, aromatic oils, antioxidants, accelerators, among others (Altenhoff et al., 2019). Doublet was observed between 2,926 and 2,853 cm^{-1} (stretching of CH_2), which was drastically reduced after the treatment, with the greatest reduction in *T. versicolor* with EM medium and *P. ostreatus* with EM medium (Gorassini et al., 2016). A loss of a signal was also observed at approximately 1,715 cm^{-1} in the treatment with *T. versicolor* on EM and PDA media and for *P. ostreatus* on EM and PDA media, corresponding to carbonyl groups ($\text{C}=\text{O}$), which are typical of the rubber chain (Gorassini et al., 2016). A band at approximately 1,550 cm^{-1} , associated with carboxylate or conjugated ketone, was totally lost after cultivation of both fungal species (Stelescu et al., 2017). After incubation with *T. versicolor*, a small band close to 1,455 cm^{-1} , assigned to C-H bending of CH_2 , was maintained in PDA, but it decreased using EM. However, for *P. ostreatus*, the band decreased for the assay with PDA and increased significantly in the treatment with EM. Most likely, the sporulation of the fungus was influenced when PDA medium was used, and therefore, the enzymatic metabolism

involved in the decrease of the band was influenced by the sporulation process stimulated by PDA (Su et al., 2012). We detected a variation in the polymer structure after treatments corresponding to alkene groups ($-\text{C}=\text{CH}$) at a wavelength of 874 cm^{-1} . This band was not present in the control, but it appeared after incubation with *T. versicolor* and *P. ostreatus* on both media (Colom et al., 2016). One reason for this may be the exposure of groups related to isoprene and butadiene present in rubber, which, before treatment, were hidden in more interior areas of the material.

These results show that the treatment using *T. versicolor* with EM allowed a greater transformation of the surface of the rubber material, suggesting that the EM medium favours the degradation in a better way than PDA for *T. versicolor*. For *P. ostreatus*, the PDA medium allowed, in general, a greater decrease in bands versus the control. The EM medium could stimulate the generation of secondary metabolites, allowing a more efficient degradation of rubber compared to the type of metabolites stimulated by the PDA medium.

We used SEM analysis to demonstrate the changes in the rubber surface against mechanical, chemical or biological treatments (Li et al., 2012; Aboelkheir et al., 2019). In this study, SEM analysis revealed morphological changes of the analysed rubber surface after biological treatments (*P. ostreatus* and *T. versicolor* using PDA medium) in comparison with the control at 500x (Figure 3). In both treatments, particle size was approximately 500 to 1,200 μm and was therefore not influenced by the treatments, in contrast to a previous study (Li et al., 2012). The size reported in this work is compatible with treatments with lower-performance grinding. When comparing the control versus the biological treatments, an increase in the roughness of the material was observed, which was similar for *T. versicolor* and *P. ostreatus*. After the treatment, the surface showed cracks, facilitating the breaking of the rubber particles by subsequent treatments, such as mechanical ones, since they can spread rapidly, generating fractures (Kroon, 2011). This

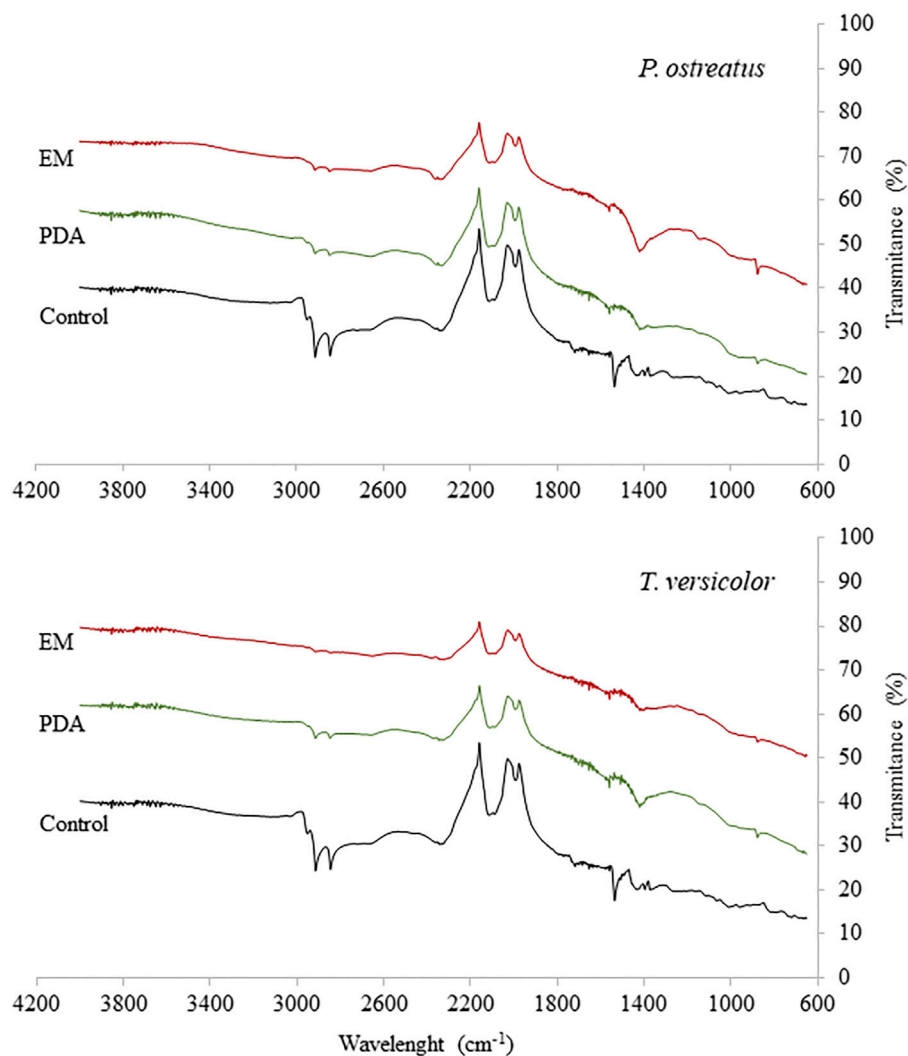


FIGURE 2 | FTIR spectrum of vulcanised rubber particles after incubation with *Trametes versicolor* and *Pleurotus ostreatus* using PDA and EM medium.

result is also related to the elemental analysis of C, O, S, Si, and Zn on the rubber surface (**Table 2**), where the carbon content decreased in the rubber particles subjected to the treatments. The opposite was observed for O and S; it should be noted that the PDA medium lacks sulphates, and therefore, the increase in S and O is not a result of the culture medium. We therefore recommend that the rubber particles were washed with ethanol and a solution of chlorine before superficial analysis (see Methodology), and therefore, the increases in Si and Zn after the biological treatment are not due to contamination, as both elements are commonly present in tyres (Adathodi et al., 2018; Altenhoff et al., 2019). Zinc is used in the non-accelerated vulcanisation of rubber, whereas silicium is used as a filler (Rattanasom et al., 2007). With *P. ostreatus*, a higher percentage of Si was detected compared to *T. versicolor*, whereas for Zn, the percentage was higher with the use of *T. versicolor*. The changes at the surface can be attributed to oxidation-reduction reactions by the enzymes secreted by the microorganisms, exposing a different proportion of the elements

initially arranged on the surface. It is suggested that the observed changes were due to enzymatic processes related to the assimilation of microorganisms towards the components present on the surface of the treated material, which is corroborated by the loss of rubber mass after treatment.

Laccase and Peroxidase Activity

Laccase and peroxidase activities were detected in all the conducted experiments (**Figure 4**). In cultures of *T. versicolor*, the presence of rubber particles revealed a 2.8-fold increase of laccase activity and 3.3-fold increase of peroxidase activity compared to the cultures without rubber particles. Likewise in cultures of *P. ostreatus*, laccase and peroxidase activities increased by double when rubber particles were in the cultivation medium. A maximum laccase activity of 0.128 U ml^{-1} was calculated for *T. versicolor* cultures, a 18% more than for *P. ostreatus* cultures. An enhanced laccase and peroxidase activity can be achieved by the addition of different mediators into the cultivation medium such

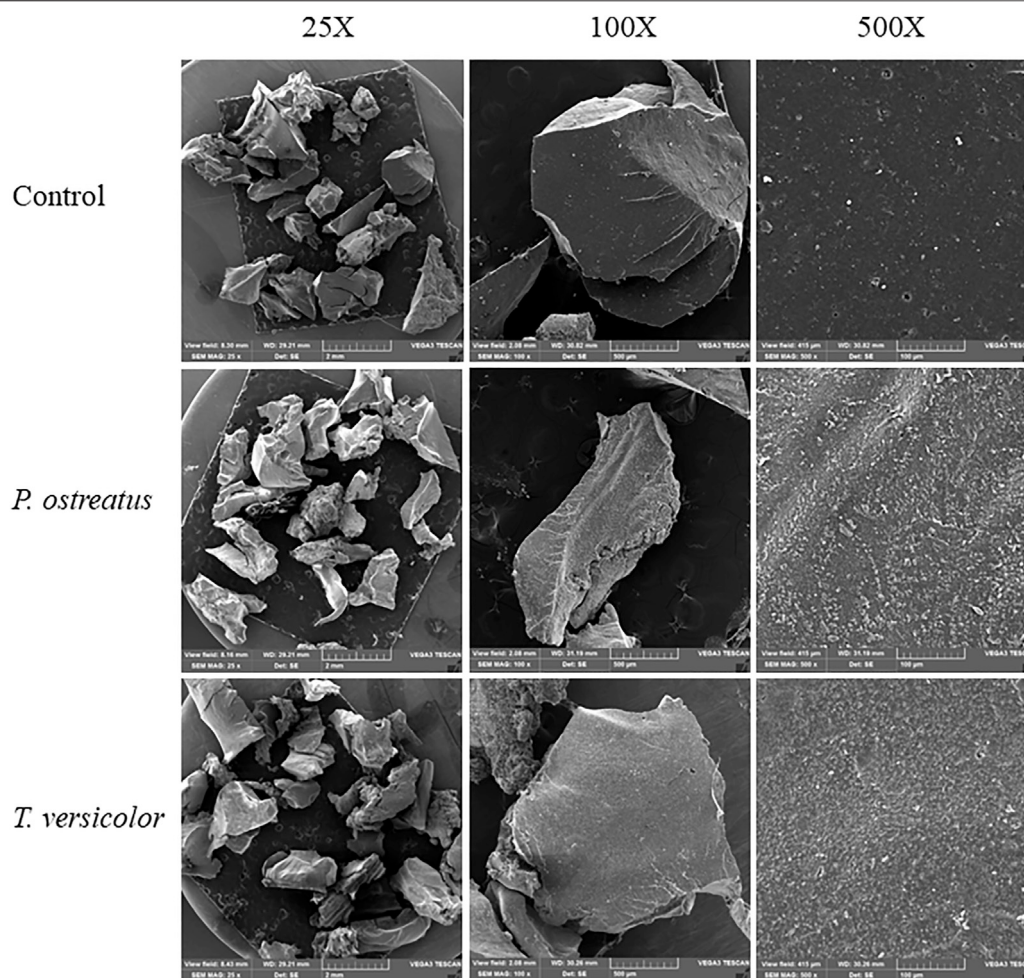


FIGURE 3 | SEM-EDS analysis of vulcanised rubber particles.

as xylinine, ferulic acid, veratryl alcohol, pyrogallol and copper (Vranska et al. 2016), enzymes like feruloyl esterase, aryl-alcohol oxidase, quinone reductases, lipases, catechol 2, 3-dioxygenase (Kumar and Chandra 2020) or by culture media optimization (Wang et al., 2014; Hahn Schneider 2018). The increase of the laccase and peroxidase activity in the cultures of *T. versicolor* and *P. ostreatus* predicts the affinity of these ligninolytic enzymes for aromatic substrates present in the rubber composition.

The presence of laccase and peroxidase enzymes has been described during the degradation process of natural rubber by the bacteria *Bacillus subtilis* (Nayanashree and Thippeswamy, 2015). Nevertheless, the enzymatic mechanism is still unknown and rubber oxygenases (Lcp, RoxA, RoxB) have been well characterized for the cleavage of natural rubber (Andler et al., 2018a; Jendrossek and Birke, 2020). The complexity of working with multi-components substrates as rubber is to reveal which of those parts are directly related to the activity of the extracellular enzymes. The current work has shown that the presence of rubber act as an inducer of laccase and peroxidase activities, and provides a more concrete result in the role of these groups of enzymes for vulcanized rubber biodegradation. However, it would be

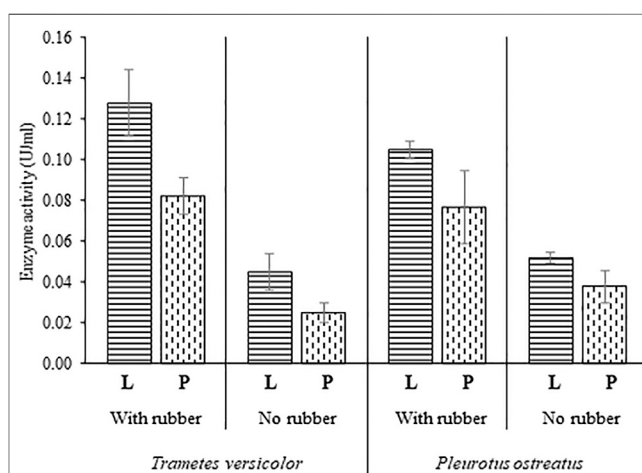


FIGURE 4 | Laccase and peroxidase activity in cultures of *Trametes versicolor* and *Pleurotus ostreatus* in the presence and the absence of vulcanized rubber particles. L, laccase, P, peroxidase. Measurements were carried out in triplicates.

TABLE 1 | General features of the genome of *P. ostreatus* and *T. versicolor*.

Feature	<i>Pleurotus ostreatus</i>	<i>Trametes versicolor</i>
Chromosomes	11	N/A
Genome size (Mbp)	34,3	44,79
GC content, %	50.85	57.7
DNA scaffolds	12 and 572	283
Total No. TE	253	233
Genes total number	12,330	14,572
Protein coding genes	12,330	14,302
Protein coding genes with function prediction	706	N/A
Protein coding genes with enzymes	1,677	N/A
Non coding genes	315	234
Pseudo genes	3	2

necessary to study the effect of laccases and peroxidases with each of the different components of vulcanized rubber to gain a deeper understanding of the reaction mechanisms.

Genomic Insights Into the Pathways for Rubber Degradation

Obtaining genome data is the initial step in understanding the biology of *P. ostreatus* and *T. versicolor*. Fungi present a wide variety of functional proteins that play different roles in the acquisition of nutrients and protection against nearby organisms or unfavourable environmental conditions (Kim et al., 2016).

The genomes of *P. ostreatus* and *T. versicolor* have been sequenced, and an analysis of the published fungal genomes, sourced from the public database (Grigoriev et al., 2014; Schoch et al., 2020; Mukherjee et al., 2021), revealed that the *P. ostreatus* haploid genome contains 11 chromosomes, with a length of 34.3 Mbp and a G + C content of ~51%. For *T. versicolor*, there is no information in the public database about the number of chromosomes; however, the total genomic size is 44.8 Mb, with a G + C content of ~58% (Table 1). Although there is a large variation in the genome size in fungi, the average genome size of fungal species taken during this study was 40.0 Mb. Fungal species harbour small genomes with highly specific genic regions and reduced non-coding regions (Galagan et al., 2003; Martinez et al., 2004). Fungi belonging to the phylum Basidiomycota have an average genome size of 46 Mb (Mohanta and Bae, 2015). In line with this, the sequenced genomes of *Pleurotus* taxa were assembled to less than 50 M bp but exhibited large numbers of annotated protein-coding genes and few constituent TEs (Table 1). However, as mentioned before, there were genome size variations among the two species, which could have arisen from unequal TE variations. The number of transposable elements (TEs), including retrotransposons and DNA transposons, accounted for approximately 253 of the *P. ostreatus* genome and 233 of the *T. versicolor* genome. For *P. ostreatus*, it was possible to determine notable genomic differences in the regions corresponding to TEs, where 80 identified TE families represented 2.5–6.2% of the genome sizes (Téllez-Téllez and Díaz-Godínez, 2019). Transposable elements are undoubtedly an important source

of genetic variation in fungi, as previously found for other fungal species (Labbé et al., 2012).

Considering the coding gene sequences in fungi, on average, the Basidiomycota group encodes for 15,431.51 genes in their genomes. The average numbers of annotated genes are 12,330 for *P. ostreatus* per genome and 14,572 for the *T. versicolor* genome (Table 1). For the noncoding gene, we found scaffolds of the genome assembly, with 315 and 234 genes, respectively. There were three and two pseudogenes predicted, corresponding to 0.24% of the genome assembly of *P. ostreatus* and 0.014% of the genome assembly of *T. versicolor*.

Comparative analysis of fungal genomes showed that fungi are highly divergent. The *P. ostreatus* genome sequence assembly was distributed across of 12 and 572 scaffolds. Of these, 56 were smaller than 1 kb (Alfaro et al., 2016; Castanera et al., 2016). The genome of *T. versicolor* comprised only 283 scaffolds. The average protein coding genes in *P. ostreatus* were 12,330, with 14,302 for *T. versicolor*. These coding genes have homologues with known proteins deposited in the NCBI nr, Pfam, SwissProt and TrEMBL databases.

Both fungal species can partially degrade vulcanised rubber, and genome data revealed that both of fungi encode for a large set of enzymes involved in the degradation of rubber materials. The protein coding genes with enzymes for *P. ostreatus* included 1,677 genes (Table 1). For *T. versicolor*, such data were not available in the public repositories. However, based on a previous study, *T. versicolor* has an expansion of the AA2 gene family (26 genes), a feature that is also found in the central polyporoid clade (Miyachi et al., 2018). The putative peroxidase genes (PoPOD) were obtained from the Joint Genome Institute (JGI) (Mukherjee et al., 2021). The gene density and the mean size of the protein-coding genes in both species of fungi used in this study secrete different enzymes, among which are laccases, manganese peroxidases, versatile peroxidases, glycosylhydrolases, peptidases and fungal esterases/lipases (Ruiz-Dueñas et al., 2011). These enzymes can degrade complex compounds such as lignin as well as certain industrial pollutants contaminating vulcanised rubber. Despite the advances in comparative genomics, the genera *Pleurotus* and *Trametes* are under-exploited, and a variety of potential biotechnological applications in different industries can be elucidated based on their genomes.

TABLE 2 | Number of laccases and manganese peroxidase in the genomes of fungi species studied.

Fungi species	Laccase	Manganese peroxidase
<i>Coriolus multicolor</i>	NA	NA
<i>Ganoderma applanatum</i>	NA	3
<i>Lentinula edodes</i>	48	9
<i>Lenzites trabea</i>	NA	NA
<i>Lenzites betulinus</i>	7	NA
<i>Pleurotus eryngii</i>	30	1
<i>Pleurotus ostreatus</i>	44	17
<i>Postia placenta</i>	4	NA
<i>Stereum hirsutum</i>	13	2
<i>Trametes versicolor</i>	37	14

Bioinformatic Analysis for Rubber Bioremediation

Laccase and Manganese Peroxidase in the Fungi Genomes

The genomic data of several species evaluated in this work revealed information concerning the presence of laccases and manganese peroxidase enzymes. For the species *L. edodes*, *L. betulinus*, *P. eryngii*, *P. ostreatus*, *P. placenta*, *S. hirsutum* and *T. versicolor*, database searches revealed the presence of several sequences of laccase already sequenced; the species *L. edodes*, *P. ostreatus*, *T. versicolor* and *P. eryngii* showed the highest number of laccase sequences (Table 2). In addition, the species *G. applanatum*, *L. edodes*, *P. eryngii*, *P. ostreatus*, *S. hirsutum* and *T. versicolor* also presented several sequences of manganese peroxidase already characterised. Species such as *L. edodes*, *P. ostreatus* and *T. versicolor* presented the highest number of characterised enzymes of manganese peroxidase in the evaluated database (Table 2). In our experiments, these species showed a high ability to degrade rubber. The high number of deposited sequences of laccase and manganese peroxidase for these species could reinforce their role as microorganisms that can degrade rubber and other polymers naturally, using laccase and manganese peroxidase enzymes (Nayanashree and Thippeswamy, 2015). However, the species *C. multicolor* and *L. trabea* presented no sequences of both mentioned enzymes. Also, *G. applanatum* had no deposited sequence of laccase; *L. betulinus* and *P. placenta* had no sequences of manganese peroxidase in the database used in this study.

Conservation Among Laccases and Manganese Peroxidase Enzymes From *P. ostreatus* and *T. versicolor*

Laccase presented three multicopper oxidase-conserved domains in its structure, namely Cu-oxidase, Cu-oxidase 2 and Cu-oxidase 3. For all sequences, these domains were located in the same region. For Cu-oxidase 3 domain, its location in the sequences started around the 31 amino acid position; it had a size of around 119 amino acids. The Cu-oxidase domain started from the 160 to 169 amino acid position and presented about 159 amino acids. The Cu-oxidase 2 domain started in the 366 to 388 amino acid position and generally had a size of 137 amino acids. These domains can use copper ions as cofactors to oxidise a broad range of substrates (Nayanashree and Thippeswamy, 2015; Arregui et al., 2019).

Manganese peroxidase has two conserved domains: a peroxidase domain with 229 amino acids and another domain, the so-called “peroxidase extension region,” with a size of 79 amino acids. The peroxidase domain in the sequences starts from 49 to 53 amino acid position and the peroxidase extension region from 279 to 286 amino acid position. These enzymatic domains are involved in oxidative reactions that use hydrogen peroxide as the electron acceptor (Nayanashree and Thippeswamy, 2015; Wang et al., 2016; Arregui et al., 2019).

For alignment at the amino acid level of laccase sequences from *P. ostreatus*, 18 sequences were used, and from *T. versicolor*, 23 sequences were used. All partial sequences were removed from the alignment analysis. Laccases from *P. ostreatus* showed a size of around 530 amino acids and a different pattern of the amino acid content; they were divided into four group of laccases. For *T. versicolor*, the laccases showed an average size of 520 amino acids and showed the same behaviour as those from *P. ostreatus* regarding the amino acid content; they were divided into three groups. In the evaluated database, the information about the specific name of each laccase in both species was inconsistent, making it difficult to predict the correct name per group. However, based on the amino acid alignment and the similarity, the laccase groups were determined.

In *P. ostreatus*, the groups of alignment represented for A and B presented high similarity among their amino acid contents of the studied sequences; however, for the groups C and D, the sequences were almost identical (see **Supplementary Figure S1** online). In *T. versicolor*, group A also presented a high similarity among the amino acid contents of the sequences, and groups B and C were almost identical (see **Supplementary Figure S2** online).

Regarding manganese peroxidase, we also evaluated its amino acid conservation among all sequences deposited in the NCBI database. Both species presented manganese peroxidase with a size of around 360 amino acids. For *P. ostreatus*, we evaluated 11 sequences and for *T. versicolor* 10 sequences. Similar to the laccase analysis, all partial sequences were removed from the alignment analysis. The species *P. ostreatus* presented four groups based on the amino acid contents of the sequences (see **Supplementary Figure S3** online). The groups A, B and C were almost identical, and group D of manganese peroxidase presented high similarity regarding the amino acid content. The species *T. versicolor* had two groups of manganese peroxidases enzymes (see **Supplementary Figure S4** online), presenting high similarity among the sequences for the group representing A, while for the group B, the sequences are almost identical. When generating an alignment using all sequences together, one analysis for laccase and another analysis for manganese peroxidase, the level of amino acid similarity decreased (data not shown). Only separated regions of conserved domains were maintained. These results indicate the presence of different isoforms of laccases and manganese peroxidase in the genomes of these two studied fungi or the lack of genomic information in the accessed database (Yuan et al., 2016).

CONCLUSION

Sustainable solutions for the management of toxic solid wastes, such as vulcanised rubber, are of great importance, and the use of

microorganisms has great potential. However, the hydrophobic nature and the large amounts of additives present in the material prevent high biodegradation rates. In this study, we analysed the degradation potential of different fungal strains, finding two white rot fungi that stood out, namely *T. versicolor* and *P. ostreatus*. The effects of biological treatments in terms of surface modifications and the presence of laccase and peroxidase activity were linked to genomic and bioinformatic analyses. We found a strong relationship between the percentage of biodegradation of rubber particles and the availability of laccase and manganese peroxidase enzymes in these species, two of the main enzymes used in the bioremediation of xenobiotics. The results obtained are promising, highlighting white rot fungi as potent biodegrading agents. Among the most interesting considerations is the non-specificity of the enzymatic attack provided by these fungi, which is necessary in highly recalcitrant materials such as tyre waste. Given the complexity of the biodegradation of vulcanised rubber, integrated and comprehensive studies are required to achieve a deeper understanding and to postulate new biotechnological processes for more effective biodegradation or biotransformation.

DATA AVAILABILITY STATEMENT

The original contributions presented in the study are included in the article/**Supplementary Material**, further inquiries can be directed to the corresponding author.

REFERENCES

- Aboelkheir, M. G., Bedor, P. B., Leite, S. G., Pal, K., Toledo Filho, R. D., and Gomes de Souza, F. (2019). Biodegradation of Vulcanized SBR: A Comparison between *Bacillus Subtilis*, *Pseudomonas aeruginosa* and *Streptomyces* Sp. *Sci. Rep.* 9. doi:10.1038/s41598-019-55530-y
- Alfaro, M., Castanera, R., Lavin, J. L., Grigoriev, I. V., Oguiza, J. A., Ramírez, L., et al. (2016). Comparative and Transcriptional Analysis of the Predicted Secretome in the Lignocellulose-Degrading Basidiomycete fungus *Pleurotus Ostreatus*. *Environ. Microbiol.* 18, 4710–4726. doi:10.1111/1462-2920.13360
- Altenhoff, A.-L., de Witt, J., Andler, R., and Steinbüchel, A. (2019). Impact of Additives of Commercial Rubber Compounds on the Microbial and Enzymatic Degradation of Poly(*cis*-1,4-Isoprene). *Biodegradation* 30, 13–26. doi:10.1007/s10532-018-9858-5
- Andler, R., Altenhoff, A.-L., Mäsing, F., and Steinbüchel, A. (2018a). *In Vitro* studies on the Degradation of Poly(*cis*-1,4-isoprene). *Biotechnol. Prog.* 34, 890–899. doi:10.1002/btpr.2631
- Andler, R. (2020). Bacterial and Enzymatic Degradation of Poly(*cis*-1,4-Isoprene) Rubber: Novel Biotechnological Applications. *Biotechnol. Adv.* 44, 107606. doi:10.1016/j.biotechadv.2020.107606
- Andler, R., Hiessl, S., Yücel, O., Tesch, M., and Steinbüchel, A. (2018b). Cleavage of Poly(*cis*-1,4-Isoprene) Rubber as Solid Substrate by Cultures of *Gordonia Polyisoprenivorans*. *New Biotechnol.* 44, 6–12. doi:10.1016/j.nbt.2018.03.002
- Andler, R., Valdés, C., Díaz-Barrera, A., and Steinbüchel, A. (2020). Biotransformation of Poly(*cis*-1,4-Isoprene) in a Multiphase Enzymatic Reactor for Continuous Extraction of Oligo-Isoprenoid Molecules. *New Biotechnol.* 58, 10–16. doi:10.1016/j.nbt.2020.05.001
- Arregui, L., Ayala, M., Gómez-Gil, X., Gutiérrez-Soto, G., Hernández-Luna, C. E., Herrera De Los Santos, M., et al. (2019). Laccases: Structure, Function, and Potential Application in Water Bioremediation. *Microb. Cel Fact* 18. doi:10.1186/s12934-019-1248-0

AUTHOR CONTRIBUTIONS

RA conceptualised, analyzed the data and edited the manuscript, VD conducted the experiments, analyzed the data and drafted the manuscript, JP conducted the experiments, helped in providing information and preparation of tables and figures, CV analyzed the data and drafted the manuscript, MS analyzed the data and drafted the manuscript. All authors read and approved the final manuscript.

FUNDING

This research was financially supported by FONDECYT Grant 11190220 from ANID (Chile).

ACKNOWLEDGMENTS

The authors acknowledge the receipt of the Fondecyt Grant 11190220 from ANID (Chile).

SUPPLEMENTARY MATERIAL

The Supplementary Material for this article can be found online at: <https://www.frontiersin.org/articles/10.3389/fbioe.2021.761510/full#supplementary-material>

- Asaro, L., Gratton, M., Seghar, S., and Ait Hocine, N. (2018). Recycling of Rubber Wastes by Devulcanization. *Resour. Conservation Recycling* 133, 250–262. doi:10.1016/j.resconrec.2018.02.016
- Bowles, A. J., Fowler, G. D., O'Sullivan, C., and Parker, K. (2020). Sustainable Rubber Recycling from Waste Tyres by Waterjet: A Novel Mechanistic and Practical Analysis. *Sustain. Mater. Tech.* 25, e00173. doi:10.1016/j.susmat.2020.e00173
- Bredberg, K., Erik Andersson, B., Landfors, E., and Holst, O. (2002). Microbial Detoxification of Waste Rubber Material by wood-rotting Fungi. *Bioresour. Technol.* 83, 221–224. doi:10.1016/S0960-8524(01)00218-8
- Castanera, R., López-Varas, L., Borgognone, A., LaButti, K., Lapidus, A., Schmutz, J., et al. (2016). Transposable Elements versus the Fungal Genome: Impact on Whole-Genome Architecture and Transcriptional Profiles. *Plos Genet.* 12, e1006108. doi:10.1371/journal.pgen.1006108
- Colom, X., Faliq, A., Formela, K., and Cañavate, J. (2016). FTIR Spectroscopic and Thermogravimetric Characterization of Ground Tyre Rubber Devulcanized by Microwave Treatment. *Polym. Test.* 52, 200–208. doi:10.1016/j.polymertesting.2016.04.020
- Feng, W., and Isayev, A. I. (2006). Recycling of Tire-Curing Bladder by Ultrasonic Devulcanization. *Polym. Eng. Sci.* 46, 8–18. doi:10.1002/pen.20449
- Formela, K., and Cysewska, M. (2014). Efficiency of Thermomechanical Reclaiming of Ground Tire Rubber Conducted in Counter-rotating and Co-rotating Twin Screw Extruder. *Polimery* 59, 231–238. doi:10.14314/polimery.2014.231
- Formela, K., Hejna, A., Zedler, L., and Colom, J. (2019). Microwave Treatment in Waste Rubber Recycling - Recent Advances and Limitations. *Express Polym. Lett.* 13, 565–588. doi:10.3144/expresspolymlett.2019.48
- Galagan, J. E., Calvo, S. E., Borkovich, K. A., Selker, E. U., Read, N. O., Jaffe, D., et al. (2003). The Genome Sequence of the Filamentous Fungus *Neurospora Crassa*. *Nature* 422. doi:10.1038/nature01554
- García, P. S., de Sousa, F. D. B., de Lima, J. A., Cruz, S. A., and Scuracchio, C. H. (2015). Devulcanization of Ground Tire Rubber: Physical and Chemical

- Changes after Different Microwave Exposure Times. *Express Polym. Lett.* 9, 1015–1026. doi:10.3144/expresspolymlett.2015.91
- Ghaviapanjeh, F., Ziaei Rad, Z., and Pazouki, M. (2018). Devulcanization of Ground Tires by Different Strains of Bacteria: Optimization of Culture Condition by Taguchi Method. *J. Polym. Environ.* 26, 3168–3175. doi:10.1007/s10924-017-1169-0
- Gorassini, A., Adami, G., Calvini, P., and Giacomello, A. (2016). ATR-FTIR Characterization of Old Pressure Sensitive Adhesive tapes in Historic Papers. *J. Cult. Heritage* 21, 775–785. doi:10.1016/j.culher.2016.03.005
- Grigoriev, I. V., Nikitin, R., Haridas, S., Kuo, A., Ohm, R., Otilar, R., et al. (2014). MycoCosm portal: Gearing up for 1000 Fungal Genomes. *Nucl. Acids Res.* 42, D699–D704. doi:10.1093/nar/gkt1183
- Hahladakis, J. N., Velis, C. A., Weber, R., Iacovidou, E., and Purnell, P. (2018). An Overview of Chemical Additives Present in Plastics: Migration, Release, Fate and Environmental Impact during Their Use, Disposal and Recycling. *J. Hazard. Mater.* 344, 179–199. doi:10.1016/j.jhazmat.2017.10.014
- Harms, H., Schlosser, D., and Wick, L. Y. (2011). Untapped Potential: Exploiting Fungi in Bioremediation of Hazardous Chemicals. *Nat. Rev. Microbiol.* 9, 177–192. doi:10.1038/nrmicro2519
- Hejna, A., Klein, M., Saeb, M. R., and Formela, K. (2019). Towards Understanding the Role of Peroxide Initiators on Compatibilization Efficiency of Thermoplastic Elastomers Highly Filled with Reclaimed GTR. *Polym. Test.* 73, 143–151. doi:10.1016/j.polymertesting.2018.11.005
- Hiessl, S., Schuldes, J., Thürmer, A., Halbsguth, T., Bröker, D., Angelov, A., et al. (2012). Involvement of Two Latex-Clearing Proteins during Rubber Degradation and Insights into the Subsequent Degradation Pathway Revealed by the Genome Sequence of *Gordonia Polyisoprenivorans* Strain VH2. *Appl. Environ. Microbiol.* 78, 2874–2887. doi:10.1128/AEM.07969-11
- Jendrossek, D., and Birke, J. (2019). Rubber Oxygenases. *Appl. Microbiol. Biotechnol.* 103, 125–142. doi:10.1007/s00253-018-9453-z
- Jendrossek, D., Tomasi, G., and Kroppenstedt, R. (1997). Bacterial Degradation of Natural Rubber: A Privilege of Actinomycetes. *FEMS Microbiol. Lett.* 150, 179–188. doi:10.1016/S0378-1097(97)00072-4
- Kaewpetch, B., Prasongsuk, S., and Poompradub, S. (2019). Devulcanization of Natural Rubber Vulcanizates by *Bacillus Cereus* TISTR 2651. *Express Polym. Lett.* 13, 877–888. doi:10.3144/expresspolymlett.2019.76
- Kim, K.-T., Jeon, J., Choi, J., Cheong, K., Song, H., Choi, G., et al. (2016). Kingdom-wide Analysis of Fungal Small Secreted Proteins (SSPs) Reveals Their Potential Role in Host Association. *Front. Plant Sci.* 7. doi:10.3389/fpls.2016.00186
- Kroon, M. (2011). Steady-state Crack Growth in Rubber-like Solids. *Int. J. Fract.* 169, 49–60. doi:10.1007/s10704-010-9583-5
- Kumar, A., and Chandra, R. (2020). Ligninolytic Enzymes and its Mechanisms for Degradation of Lignocellulosic Waste in Environment. *Heliyon* 6. e03170 doi:10.1016/j.heliyon.2020.e03170
- Kumar, S., Stecher, G., Li, M., Knyaz, C., and Tamura, K. (2018). MEGA X: Molecular Evolutionary Genetics Analysis across Computing Platforms. *Mol. Biol. Evol.* 35, 1547–1549. doi:10.1093/molbev/msy096
- Labbé, J., Murat, C., Morin, E., Tuskan, G. A., Le Tacon, F., and Martin, F. (2012). Characterization of Transposable Elements in the Ectomycorrhizal Fungus *Laccaria Bicolor*. *PLoS One* 7. e40197 doi:10.1371/journal.pone.0040197
- Lakshmi Adathodi et al., L., Raja Murugadoss, L. A. e. a., and Gaddam, K. (2018). A Comparative Study on Vehicular Tyre Rubber and Aircraft Tyre Rubber, A Review Based on SEM, EDS and XRD Analysis. *Ijimperd* 8, 1227–1234. doi:10.24247/ijimperdapr2018141
- Li, X., Xu, X., and Liu, Z. (2020). Cryogenic Grinding Performance of Scrap Tire Rubber by Devulcanization Treatment with ScCO₂. *Powder Tech.* 374, 609–617. doi:10.1016/j.powtec.2020.07.026
- Li, Y., Zhao, S., and Wang, Y. (2012). Microbial Desulfurization of Ground Tire Rubber by *Sphingomonas* sp.: A Novel Technology for Crumb Rubber Composites. *J. Polym. Environ.* 20, 372–380. doi:10.1007/s10924-011-0386-1
- Lu, S., Wang, J., Chitsaz, F., Derbyshire, M. K., Geer, R. C., Gonzales, N. R., et al. (2020). CDD/SPARCLE: The Conserved Domain Database in 2020. *Nucleic Acids Res.* 48, D265–D268. doi:10.1093/nar/gkz991
- Martinez, D., Larrondo, L. F., Putnam, N., Gelpke, M. D. S., Huang, K., Chapman, J., et al. (2004). Genome Sequence of the Lignocellulose Degrading Fungus *Phanerochaete Chrysosporium* Strain RP78. *Nat. Biotechnol.* 22, 695–700. doi:10.1038/nbt967
- Miyauchi, S., Rancon, A., Drula, E., Hage, H., Chaduli, D., Favel, A., et al. (2018). Integrative Visual Omics of the white-rot Fungus *Polyporus Brumalis* Exposes the Biotechnological Potential of its Oxidative Enzymes for Delignifying Raw Plant Biomass. *Biotechnol. Biofuels* 11. doi:10.1186/s13068-018-1198-5
- Mohanta, T. K., and Bae, H. (2015). The Diversity of Fungal Genome. *Biol. Proced. Online* 17. doi:10.1186/s12575-015-0020-z
- Mukherjee, S., Stamatis, D., Bertsch, J., Ovchinnikova, G., Sundaramurthi, J. C., Lee, J., et al. (2021). Genomes OnLine Database (GOLD) v.8: Overview and Updates. *Nucleic Acids Res.* 49, D723–D733. doi:10.1093/nar/gkaa983
- Nayanashree, G., and Thippeswamy, B. (2015). Biodegradation of Natural Rubber by Laccase and Manganese Peroxidase Enzyme of *Bacillus Subtilis*. *Environ. Process.* 2, 761–772. doi:10.1007/s40710-015-0118-y
- Notredame, C., Higgins, D. G., and Heringa, J. (2000). T-coffee: a Novel Method for Fast and Accurate Multiple Sequence Alignment 1 Edited by J. Thornton. *J. Mol. Biol.* 302, 205–217. doi:10.1006/jmbi.2000.4042
- Rattanasom, N., Saowapark, T., and Deepresertkul, C. (2007). Reinforcement of Natural Rubber with Silica/carbon Black Hybrid Filler. *Polym. Test.* 26, 369–377. doi:10.1016/j.polymertesting.2006.12.003
- Robert, X., and Gouet, P. (2014). Deciphering Key Features in Protein Structures with the New ENDscript Server. *Nucleic Acids Res.* 42, W320–W324. doi:10.1093/nar/gku316
- Rooj, S., Basak, G. C., Maji, P. K., and Bhowmick, A. K. (2011). New Route for Devulcanization of Natural Rubber and the Properties of Devulcanized Rubber. *J. Polym. Environ.* 19, 382–390. doi:10.1007/s10924-011-0293-5
- Ruiz-Dueñas, F. J., Fernández, E., Martínez, M. J., and Martínez, A. T. (2011). *Pleurotus Ostreatus* Heme Peroxidases: An In Silico Analysis from the Genome Sequence to the Enzyme Molecular Structure. *Comptes Rendus Biologies* 334, 795–805. doi:10.1016/j.crv.2011.06.004
- Sabzkar, M., Chenar, M. P., Mortazavi, S. M., Kariminejad, M., Asadi, S., and Zohuri, G. (2015). Influence of Process Variables on Chemical Devulcanization of Sulfur-Cured Natural Rubber. *Polym. Degrad. Stab.* 118, 88–95. doi:10.1016/j.polymdegradstab.2015.04.013
- Sánchez, C. (2020). Fungal Potential for the Degradation of Petroleum-Based Polymers: An Overview of Macro- and Microplastics Biodegradation. *Biotechnol. Adv.* 40. 107501 doi:10.1016/j.biotechadv.2019.107501
- Schneider, W. D. H., Fontana, R. C., Mendonça, S., de Siqueira, F. G., Dillon, A. J. P., and Camassola, M. (2018). High Level Production of Laccases and Peroxidases from the Newly Isolated white-rot Basidiomycete *Marasmiellus Palmivorus* VE111 in a Stirred-Tank Bioreactor in Response to Different Carbon and Nitrogen Sources. *Process Biochem.* 69, 1–11. doi:10.1016/j.procbio.2018.03.005
- Schoch, C. L., Ciufu, S., Domrachev, M., Hottot, C. L., Kannan, S., Khovanskaya, R., et al. (2020). NCBI Taxonomy: A Comprehensive Update on Curation, Resources and Tools. *Database* 2020. doi:10.1093/database/baaa062
- Simon-Stöger, L., and Varga, C. (2021). PE-contaminated Industrial Waste Ground Tire Rubber: How to Transform a Handicapped Resource to a Valuable One. *Waste Manag.* 119, 111–121. doi:10.1016/j.wasman.2020.09.037
- Stelcescu, M.-D., Manaila, E., Craciun, G., and Chirila, C. (2017). Development and Characterization of Polymer Eco-Composites Based on Natural Rubber Reinforced with Natural Fibers). Development and characterization of polymer eco-composites based on natural rubber reinforced with natural fibers. *Materials*, 10, 787. doi:10.3390/ma10070787
- Stevenson, K., Stallwood, B., and Hart, A. G. (2008). Tire Rubber Recycling and Bioremediation: A Review. *Bioremediation J.* 12, 1–11. doi:10.1080/10889860701866263
- Su, Y. Y., Qi, Y. L., and Cai, L. (2012). Induction of Sporulation in Plant Pathogenic Fungi. *Mycology* 3. doi:10.1080/21501203.2012.719042
- Tatangelo, V., Mangili, I., Caracino, P., Anzano, M., Najmi, Z., Bestetti, G., et al. (2016). Biological Devulcanization of Ground Natural Rubber by *Gordonia Desulfuricans* DSM 44462T Strain. *Appl. Microbiol. Biotechnol.* 100, 8931–8942. doi:10.1007/s00253-016-7691-5
- Téllez-Téllez, M., and Díaz-Godínez, G. (2019). Omic Tools to Study Enzyme Production from Fungi in the *Pleurotus* Genus. *BioRes* 14, 2420–2457. doi:10.15376/biores.14.1.2420-2457
- Vrsanska, M., Voberkova, S., Langer, V., Palovcikova, D., Moulick, A., Adam, V., et al. (2016). Induction of Laccase, Lignin Peroxidase and Manganese

- Peroxidase Activities in White-Rot Fungi Using Copper Complexes. *Molecules* 21, 1553. doi:10.3390/molecules21111553
- Wang, F., Hu, J.-H., Guo, C., and Liu, C.-Z. (2014). Enhanced Laccase Production by *Trametes versicolor* Using Corn Steep Liquor as Both Nitrogen Source and Inducer. *Bioresour. Tech.* 166, 602–605. doi:10.1016/j.biortech.2014.05.068
- Wang, N., Ren, K., Jia, R., Chen, W., and Sun, R. (2016). Expression of a Fungal Manganese Peroxidase in *Escherichia coli*: A Comparison between the Soluble and Refolded Enzymes. *BMC Biotechnol.* 16. doi:10.1186/s12896-016-0317-2
- Wang, X., Shi, C., Zhang, L., and Zhang, Y. (2013). Effects of Shear Stress and Subcritical Water on Devulcanization of Styrene-Butadiene Rubber Based Ground Tire Rubber in a Twin-Screw Extruder. *J. Appl. Polym. Sci.* 130, 1845–1854. doi:10.1002/app.39253
- Yuan, X., Tian, G., Zhao, Y., Zhao, L., Wang, H., and Ng, T. B. (2016). Biochemical Characteristics of Three Laccase Isoforms from the Basidiomycete *Pleurotus Nebrodensis*. *Molecules* 21, 203. doi:10.3390/molecules21020203

Conflict of Interest: The authors declare that the research was conducted in the absence of any commercial or financial relationships that could be construed as a potential conflict of interest.

Publisher's Note: All claims expressed in this article are solely those of the authors and do not necessarily represent those of their affiliated organizations, or those of the publisher, the editors and the reviewers. Any product that may be evaluated in this article, or claim that may be made by its manufacturer, is not guaranteed or endorsed by the publisher.

Copyright © 2021 Andler, D'Afonseca, Pino, Valdés and Salazar-Viedma. This is an open-access article distributed under the terms of the Creative Commons Attribution License (CC BY). The use, distribution or reproduction in other forums is permitted, provided the original author(s) and the copyright owner(s) are credited and that the original publication in this journal is cited, in accordance with accepted academic practice. No use, distribution or reproduction is permitted which does not comply with these terms.



Current Knowledge on Polyethylene Terephthalate Degradation by Genetically Modified Microorganisms

Aneta K. Urbanek^{†‡}, Katarzyna E. Kosiorowska[†] and Aleksandra M. Mironczuk^{*}

Department of Biotechnology and Food Microbiology, Wrocław University of Environmental and Life Sciences, Wrocław, Poland

OPEN ACCESS

Edited by:

Aamer Ali Shah,
Quaid-i-Azam University, Pakistan

Reviewed by:

Liyan Song,
Chongqing Institute of Green and
Intelligent Technology (CAS), China
Dirk Tischler,
Ruhr University Bochum, Germany
Qurrat Ul Ain Rana,
Quaid-i-Azam University, Pakistan

*Correspondence:

Aleksandra M. Mironczuk
aleksandra.mironczuk@upwr.edu.pl
orcid.org/0000-0003-1604-1635

[†]These authors share first authorship

[‡]Present address:

Aneta K. Urbanek,
Department of Biotransformation,
University of Wrocław, Wrocław,
Poland

Specialty section:

This article was submitted to
Bioprocess Engineering,
a section of the journal
Frontiers in Bioengineering and
Biotechnology

Received: 05 September 2021

Accepted: 11 November 2021

Published: 30 November 2021

Citation:

Urbanek AK, Kosiorowska KE and
Mironczuk AM (2021) Current
Knowledge on Polyethylene
Terephthalate Degradation by
Genetically Modified Microorganisms.
Front. Bioeng. Biotechnol. 9:771133.
doi: 10.3389/fbioe.2021.771133

The global production of polyethylene terephthalate (PET) is estimated to reach 87.16 million metric tons by 2022. After a single use, a remarkable part of PET is accumulated in the natural environment as plastic waste. Due to high hydrophobicity and high molecular weight, PET is hardly biodegraded by wild-type microorganisms. To solve the global problem of uncontrolled pollution by PET, the degradation of plastic by genetically modified microorganisms has become a promising alternative for the plastic circular economy. In recent years many studies have been conducted to improve the microbial capacity for PET degradation. In this review, we summarize the current knowledge about metabolic engineering of microorganisms and protein engineering for increased biodegradation of PET. The focus is on mutations introduced to the enzymes of the hydrolase class—PETase, MHETase and cutinase—which in the last few years have attracted growing interest for the PET degradation processes. The modifications described in this work summarize the results obtained so far on the hydrolysis of polyethylene terephthalate based on the released degradation products of this polymer.

Keywords: plastic degradation, genetic engineering, microorganisms, PET, protein

INTRODUCTION

Worldwide plastic production reached 348 million metric tons in 2017, and this number increases annually by ~5% (PlasticEurope, 2019; Brahney et al., 2020). Predictions about plastic waste accumulation in ecosystems suggest that in 2050 cumulative plastic waste production will reach over 25 billion tonnes, i.e., 3 times the current level (Geyer et al., 2017). The high resilience and persistence of plastic, previously considered an advantage, nowadays leads to the uncontrolled accumulation of waste in every ecosystem on the planet. Most plastics never completely disappear and only get fragmented into smaller pieces. The formed microplastics (1 µm–5 mm) and nanoplastics (<1 µm) spread all over the globe, reaching pristine regions separated from human activity. For instance, plastic particles have been found in the Arctic Polar Circle (Cózar et al., 2017), Antarctica (Waller et al., 2017), the high mountains (French Pyrenees) (Allen et al., 2019), the Mariana Trench (Gangadoo et al., 2020) and even in the rain in protected areas (Brahney et al., 2020). Easily transported microplastics are extremely dangerous to marine and seacoast animals. It is estimated that more than 800 animal species are affected by plastic waste, and around 90% of all seabirds ingest plastic (Wilcox et al., 2015). Both nanoplastics and microplastics were found in zooplankton and phytoplankton (Rummel et al., 2017), which are consumed by organisms from higher levels of the food chain. Hence microplastics are consumed and accumulated by invertebrates (Thompson et al., 2004). Moreover, it was shown that nanoplastics may reduce the survival of aquatic zooplankton and penetrate the blood-brain barrier in fish and cause behavioural disorders (Mattsson

et al., 2017). A recent study showed that crop plants are capable of effective uptake of microplastic and its transport from the roots to the shoots (Li et al., 2020). As it turns out, the ubiquitous plastics also affect the human body. The presence of microplastics was found in the lungs (Pauly et al., 1998) and faecal samples (Schwabl et al., 2019). *In vitro* studies have demonstrated the ability of microplastics to induce an immune response, oxidative stress, cytotoxicity, alteration of membrane integrity and variation in gene expression (Maeza et al., 2021).

Most of the produced plastic material has a fossil origin. Thermoplastic materials such as polyethylene (PE), polyurethane (PUR), polyvinyl chloride (PVC), polypropylene (PP), polystyrene (PS) and polyethylene terephthalate (PET) represent 80% of total global plastic usage (PlasticEurope, 2019). One of the most popular plastic materials used for packing (such as the production of bottles) is PET. PET is a polar, linear polymer of repeating units of aromatic terephthalic acid (TPA) and ethylene glycol (EG). The PET monomer is designated bis(2-hydroxyethyl) terephthalate (BHET). Owing to excellent mechanical and thermal properties, PET is mainly used for beverage bottles, foil, textile fibres and food containers (Danso et al., 2019; Taniguchi et al., 2019; Hiraga et al., 2020). The global production of PET reached 33 million metric tons in 2015 (Geyer et al., 2017) and is still increasing. The problem that has arisen with such enormous production of PET is partially solved by recycling. The main goal of recycling is to obtain new PET or recover the primary components such as TPA and EG so that they can be used as feedstock (Lange 2002). Nowadays, the recycling of PET is mainly based on chemical and mechanical methods. For instance, the mechanical recycling method for PET, melt extrusion, results in the production of rPET fibres from PET bottle waste (Park and Kim 2014), whereas the most common chemical method, glycolysis, degrades PET to BHET with a yield as high as 95% (Imran et al., 2013; Liu et al., 2020). Although these methods are commonly used, they still have some limitations such as spontaneous degradation during the lifetime of new PET obtained after re-extrusion (Park and Kim 2014) or requirement of high temperature (150–300°C) and catalysts in the glycolysis reaction. Especially using catalysts (metal-based, organic or ionic liquids) leads to the high cost of reagents and methodologies, a negative environmental impact and sometimes to the limitation to small-scale trials of reactions (Liu et al., 2020; Sang et al., 2020). In recent years, biological methods have been developed alongside the chemical and mechanical methods of PET recycling. Biological methods are promising and eco-friendly solutions for the decomposition of PET waste. Although PET is labelled as non-biodegradable, much research succeeded in the use of microorganisms or enzymes to break it down. A flagship example is the discovery of the bacterium *Ideonella sakaiensis* 201-F6 and the enzymes PETase and MHETase (Yoshida et al., 2016; Furukawa et al., 2019), which are the focus of many scientists due to very promising aspects of future management of PET. Other enzymes such as cutinases Thc_Cut1 and Thc_Cut2 from *Thermobifida cellulosilytica* DSM44535 (Acero et al., 2011), cutinase FsC from *Fusarium solani pisi* (Egmont and de Vlieg, 2000), cutinase HiC from *Humicola insolens* and lipase CALB from *Candida antarctica* (Carniel et al., 2017) or cutinase

TfH from *Thermobifida fusca* DSM43793 (Müller et al., 2005) are also the subject of numerous studies. To date, scientists have verified 27 enzymes that degrade synthetic polymers (Danso et al., 2019), among which enzymes involved in the degradation of PET are typical serine hydrolases, e.g., cutinases (EC 3.1.1.74), lipases (EC 3.1.1.3), and carboxylesterases (EC 3.1.1.1) (Roth et al., 2014). Despite the knowledge of many enzymes, there are many unsolved issues regarding their practical use to degrade PET such as low thermal stability or transfer on an industrial scale (Sang et al., 2020). Much more investigation is needed for mutational developments of the enzyme's active site, which may help to overcome the limitations.

The degradability of the polymer depends on different factors such as shape, size, presence of various substituents, e.g., chloride atoms or benzene rings, and it decreases with the increase in the molecular weight (Kumari et al., 2019; Rose et al., 2020). The bottlenecks in plastic biodegradation are their high hydrophobicity, crystallinity, strong chemical bonds and high molecular weight (Urbanek et al., 2018). In the past years, a number of studies have been conducted in order to show that many microorganisms and enzymes are capable of degrading plastic. Researchers were mostly focused on the biodegradation performed by wild-type strains, isolated directly from different environments, especially from plastic contaminated areas.

Although this approach is justified due to the ubiquity of microorganisms and their diverse biodegradability, current studies should be more focused on improving these properties. Published reports show that naturally isolated microorganisms possess a limited capability for plastic degradation. Thus, more efficient production of enzymes and the improvement of enzymes' activity that would target specific materials with greater selectivity is a key to the improvement of the biodegradation rate of plastic. Employing metabolic engineering provides powerful opportunities in this field (Figure 1).

Here, we present the possibilities of genetic manipulation in order to obtain mutant enzymes with improved catalytic activity and thermostability in the hydrolysis of polyethylene terephthalate (PET) and other polymers.

Enzymes Involved in PET Degradation

Mostly, the biodegradation of PET is possible by the enzymatic activity of cutinases (EC 3.1.1.74) or PETase (EC 3.1.1.101) with the cooperation of MHETase (EC 2.1.1.102). A number of cutinases with PET biodegradable activity were found, e.g., cutinase from *Humicola insolens* (HiC), *Thermobifida fusca* (TfCut2), leaf-branch compost (LCC) (Tournier et al., 2020), and *Ideonella sakaiensis* (PETase and MHETase) (Yoshida et al., 2016; Furukawa et al., 2019). Cutinases are able to hydrolyse both ester bonds found in aliphatic and aromatic polyesters, hence their wide application in degradation studies of a broad range of plastic polymers (Sulaiman et al., 2012; Liu et al., 2019a). In contrast, PETase can hydrolyse ester bonds present only in aromatic polyesters (Austin et al., 2018). Enzymes involved in PET degradation belong to the esterase subclass and possess a catalytic triad characteristic for α/β -hydrolases (Ser-His-Asp). Ester bond hydrolysis is provided due to the nucleophilic

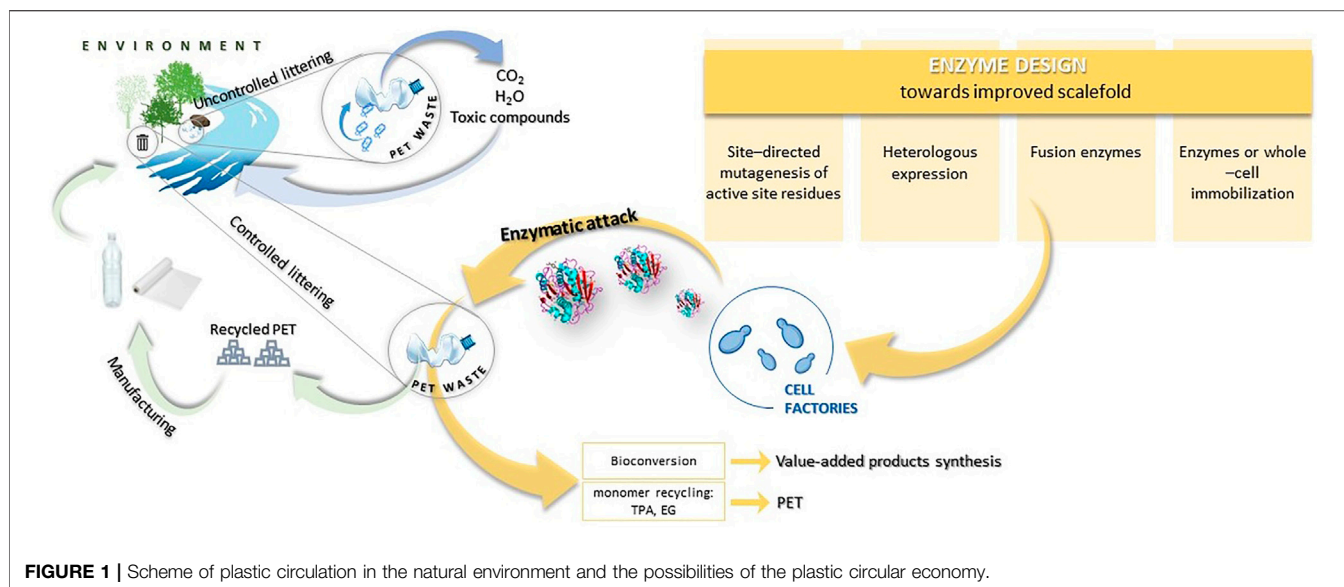


FIGURE 1 | Scheme of plastic circulation in the natural environment and the possibilities of the plastic circular economy.

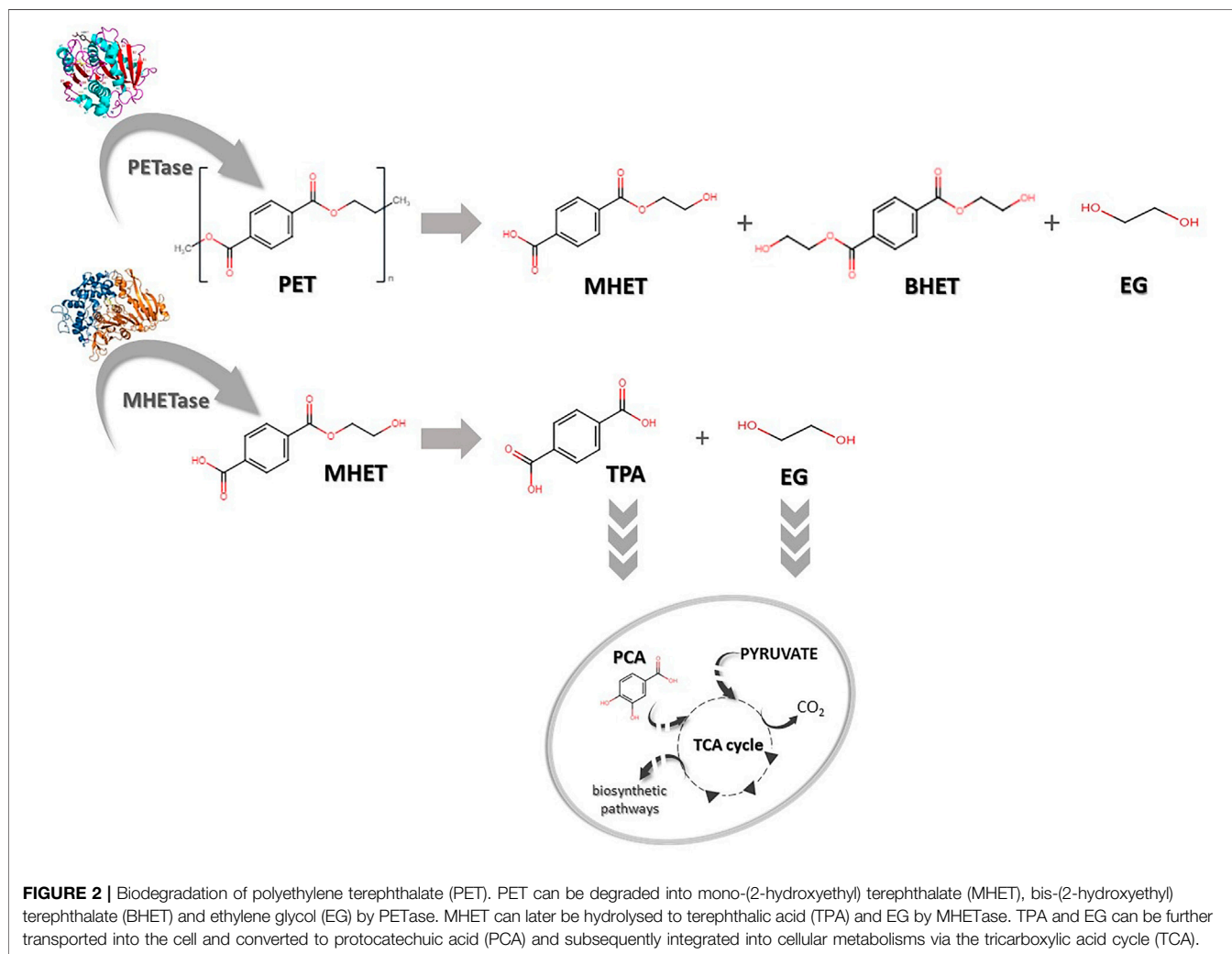


FIGURE 2 | Biodegradation of polyethylene terephthalate (PET). PET can be degraded into mono-(2-hydroxyethyl) terephthalate (MHET), bis-(2-hydroxyethyl) terephthalate (BHET) and ethylene glycol (EG) by PETase. MHET can later be hydrolysed to terephthalic acid (TPA) and EG by MHETase. TPA and EG can be further transported into the cell and converted to protocatechuic acid (PCA) and subsequently integrated into cellular metabolisms via the tricarboxylic acid cycle (TCA).

TABLE 1 | Genetic modifications of enzyme structure for enhancement of biodegradable abilities towards plastic.

Wild-type enzyme/strain	Wild-type microorganisms	Substrate specificity	Vector and host	Improvement in activity	Mutation's information	References
PETase	<i>Ideonella sakaiensis</i>	PET	Plasmid: pET28a; Host: <i>E. coli</i> BL21 (DE3)	-R61A: 1.6 fold -L88F: 2.0 fold -I179F: 15.0 fold ^a	mutagenesis of six key residues around the substrate-binding groove in order to: create space around the active site; increase the hydrophobicity of the amino acids around the active site; improve the affinity of the amino acids around the active site for PET	Ma et al. (2018)
PETase	<i>Ideonella sakaiensis</i>	PET	Plasmid: pET-21b; Host: <i>E. coli</i> BL21-CodonPlus (DE3) RIPL	-S131A: not detected -D177A: not detected -H208A: not detected -W130A: increased -W130H: increased -M132A: decreased -W156A: decreased -A180I: no change marked -Q90A: decreased -S185H: increased -S209F: decreased -W68L: decreased -Q153L: no change marked -R94A: decreased -N212A: decreased ^b	structure-guided site-directed mutagenesis in: the active sites; substrate binding pockets; the residues involved in stabilizing the rigidity of the active site	Liu et al. (2018a)
PETase	<i>Ideonella sakaiensis</i> 201-F6	PET; PEF	Plasmid: pET-21b(+); Host: <i>E. coli</i> C41(DE3)	-S238F/W159H: 4.13% higher ^c	site-directed mutagenesis to narrow the PETase active site: S238 to provide new π -stacking and hydrophobic interactions to adjacent terephthalate moieties: His159 to allow the PET polymer to sit deeper within the active-site channel	Austin et al. (2018)
PETase	<i>Ideonella sakaiensis</i> 201-F6	PET	Plasmid: pET32a; Host: <i>E. coli</i> XL1-Blue	-S131A: decreased -R103G: decreased -C174S: decreased -C210S: decreased -W156A: decreased -S185H: decreased -I179A: decreased -W130A: decreased -W130H: decreased -M132A: decreased -Y58A: 80.73% MHET production; TPA production decreased -T59A: full activity in producing MHET; TPA production decreased ^d	site-directed mutagenesis to determine apo- and complex crystal structures of PETase and to identify key residues requires for catalysis by, for instance, disruption intra-molecular disulfide bridges DS1 or substitution His residue in the corresponding position	Han et al. (2017)
PETase	<i>Ideonella sakaiensis</i>	PET	Plasmid: pET15b; pET15a; Host: <i>E. coli</i> Rosetta gami-B	-S160A: almost complete loss -D206A: almost complete loss -H237A: almost complete loss -Y87A: 5% hydrolytic activity -M161A: 52% hydrolytic activity -W185A: 5% hydrolytic activity	structural and site-directed mutagenesis in order to confirm the residues involved in enzymatic catalysis and substrate binding: three catalytic residues S160, D206 and H237 replacement with A; four subsite I residues Y87, W185, M161 and I208 replacement with A; three subsite II residues W159,	Joo et al. (2018)

(Continued on following page)

TABLE 1 | (Continued) Genetic modifications of enzyme structure for enhancement of biodegradable abilities towards plastic.

Wild-type enzyme/strain	Wild-type microorganisms	Substrate specificity	Vector and host	Improvement in activity	Mutation's information	References
				-I208A: 46% hydrolytic activity -W159A: 8% hydrolytic activity -S238A: similar hydrolytic activity -N241A: 18% hydrolytic activity -R280A: similar hydrolytic activity -W159H: dramatically decreased -S238F: dramatically decreased -C203A/C239A: dramatically decreased ^e	S238, and N241 replacement with A, W159 and S238 residues replacement with H and F; deletion of additional disulfide bond	
cutinase Thc_Cut2	<i>Thermobifida cellulolytica</i> DSM44535	PET	Plasmid: pET26b(+); Host: <i>E. coli</i> BL21-Gold(DE3)	-R19S: 3.4 fold -R29N: 17.6 fold -A30V: 17.0 fold -Q65E: decreased -L183A: 1.4 fold -R187K: 4.9 fold -double mutant R29N A30V: 8.4 fold -triple mutant R19S R29N A30V: 7.2 fold ^a	site-directed mutagenesis of amino acids located outside the active site on the Thc_Cut2 surface—exchange of selected side chains with the corresponding side chains of more active Thc_Cut1	Herrero Acero et al., 2013
cutinase	<i>Fusarium solani</i> pisi	PET	Plasmid: pET25b(+); Host: <i>E. coli</i> BL21 (DE3)	-L81A: 4.0 fold -L182A: 5.2 fold -N84A: 1.7 fold -V184A: 2.0 fold -L189A: decreased ^f	site-directed mutagenesis to create more space in the active site of the cutinase	Araújo et al. (2007)
cutinase Tfu_0883	<i>Thermobifida fusca</i>	PET	Plasmid: pET20b; Host: <i>E. coli</i> BL21 (DE3)	-I218A: 1.2 fold -Q132A/T101A: 1.6 fold ^f	site-directed mutagenesis to create space and to increase hydrophobicity of the catalytic side	Silva et al. (2011)
cutinase TfCut2	<i>Thermobifida fusca</i> KW3	PET	Plasmid: not mentioned; Host: <i>E. coli</i> BL21 (DE3)	-G62A: 4.0 fold	exchange of selected amino acid residues of active site in a substrate binding groove of TfCut2 with those present in cutinase LCC	Wei et al. (2016)
cutinase-type polyesterase (Cut190)	<i>Saccharomonospora viridis</i> AHK190	PET	Plasmid: pGEM-T; pQE80L; Host: <i>E. coli</i> DH5α; <i>E. coli</i> Rosetta-gami B (DE3)	-S226P: 1.4 fold -S226P/R228S: 2.1 fold -S226P/R228S/T262K: 2.2 fold ^g	cloning a putative cutinase gene (cut190); site-directed mutagenesis to substitute: S226 with P and R228 with the neutral S, T262 with K to enhance the salt-bridge formation	Kawai et al. (2014)
LC-cutinase	leaf-branch compost	PET	Plasmid: pHK; Host: <i>E. coli</i> DH5α; <i>E. coli</i> BL21 (DE3)	- <i>C. thermocellum</i> DSM1313:pHK-LCC: 62% ^h	insertion of the signal peptide sequence of cellulose Cel48S and a constitutive promoter of gene Clo1313_2638 (P ₂₆₃₈) to <i>Clostridium thermocellum</i> for the secretory production of LCC	Yan et al. (2020)

(Continued on following page)

TABLE 1 | (Continued) Genetic modifications of enzyme structure for enhancement of biodegradable abilities towards plastic.

Wild-type enzyme/strain	Wild-type microorganisms	Substrate specificity	Vector and host	Improvement in activity	Mutation's information	References
LC-cutinase	leaf-branch compost	PET	Plasmids: pET21b(+); pET26b(+); Host: <i>E. coli</i> BL21 (DE3)	-WCCG: 90% in 10.5 h -ICCG: 90% in 9.3 h ⁱ	site-specific saturation mutagenesis in the first contact shell of groove; replacing the divalent-metal-binding site with a disulfide bridge; mutations to improve thermostability	Tournier et al. (2020)
LC-cutinase	leaf-branch compost	PET	Plasmid: PET28; PJ912; Host: <i>E. coli</i> BL21 DE3; <i>P. pastoris</i>	-LCC-NG -LCC-G: induction of aggregation 10°C higher than LCC-NG; improvement in the catalytic performance for PET hydrolysis; the rate of aggregation was found to be slower	site directed mutagenesis to introduce three putative N-glycosylation sites to improve LCC resistance for aggregation	Shirke et al. (2018)
cutinase TfCut2, LC-cutinase, carboxyl esterase TfCa	<i>Thermobifida fusca</i> KW3	PET	Plasmid: pET-20b(+); Host: <i>E. coli</i> BL21(DE3)	-TfCa/LCC: 47.9% weight loss/24 h -TfCut2/LCC: 20.4% weight loss/24 h ⁱ	site-directed mutagenesis for immobilization of TfCa on SulfoLink resin by addition an oligopeptide of G-S-C at the C-terminus of TfCa	Barth et al., 2016; Oeser et al., 2010
cutinase (Cut) and lipase (Lip)	<i>Thermomyces lanuginosus</i> (Lip); <i>Thielavia terrestris</i> NRRL 8126 (Cut)	PVAC; PCL	Plasmid: pPICZαA; Host: <i>E. coli</i> DH5α; <i>P. pastoris</i> KM71H	-Lip-Cut: 13.3, 11.8 and 5.7 times higher compared to Lip, Cut and Lip/Cut mixture, respectively	construction of chimeric lipase-cutinase (Lip-Cut) system overexpressed in <i>P. pastoris</i> to enhance the synergistic action of both enzymes	Liu et al., 2018b; Liu et al., 2019b
cutinase 1 (Thc_Cut1)	<i>Thermofida cellulolytica</i>	PET, PBS, PHBV	Plasmid: pMK-T; pPICZαB; Host: <i>E. coli</i> XL-10 cells; <i>P. pastoris</i> KM71H	-Thc_Cut1_koAsn: no significant differences (PET) ^d -Thc_Cut1_koST: no significant differences (PET) ^d ; 92% of weight loss (PBS) ^k	knock out of the three glycosylation sites at N29, N49, N161 (Thc_Cut1_koAsn) and S31, T51, S163 (Thc_Cut1_koST) by changing the nucleotide sequence to investigate the influence of glycosylation on the activity and stability	Gamerith et al. (2017)
polyhydroxybutyrate depolymerase (PA_PBM) and polyamidase (PA)	<i>Alcaligenes faecalis</i> (PA_PBM); <i>Nocardia farcinica</i> IMA 10152A (PA)	PUR	Plasmid: pET26b(+); Host: <i>E. coli</i> XL10-Gold; <i>E. coli</i> BL21	-fusion polyamidase PA_PBM: 4 fold	C-terminal fusion of a hydrophobic binding module of PA_PBM to PA to target the catalytic domain to the polyester interface more effectively	Gamerith et al. (2016)
Alkane hydroxylase	<i>Pseudomonas</i> sp. E4	LMWPE	Plasmid: pUC19; Host: <i>E. coli</i> BL21	-recombinant cell viable even after the biodegradation tests at 37 °C for 80 days	expression of alkane hydroxylase gene (<i>alkB</i>) in <i>E. coli</i> BL21 to mineralize LMWPE	Yoon et al. (2012)

^aexpressed by kinetic parameters (kcat/KM).^bexpressed by PET, degradation efficiency towards PET, bottle.^cexpressed by the loss in the absolute crystallinity.^dexpressed by the production levels of MHET, and TPA.^eexpressed hydrolytic activity using BHET, as a substrate.^fexpressed by released TPA, during hydrolytic activity towards PET.^gexpressed as enzyme activity measured under standard conditions.^hexpressed by the weight loss of PCL, films.ⁱexpressed as enzymatic depolymerization of post-consumer PET, waste.^jexpressed by PET, degradation efficiency towards PET, films.^kexpressed by the weight loss of PBS, films.

attack by the serine oxygen to the carbonyl carbon present in the ester bond. Negatively charged aspartate stabilizes positively charged histidine residue; thus the established charge transfer

network enables serine to carry out a nucleophilic attack (Han et al., 2017). So far, homology has been found in the sequences of cutinases and PETase. Yoshida et al. (2016) observed 51%

similarity in amino acid sequence with the hydrolase present in *Thermobifida fusca* (TfH). Furthermore, similar to cutinase from *Fusarium solani*, PETase from *Ideonella sakaiensis* has two disulfide bridges that stabilize the structure of the enzyme molecule. Moreover, as was demonstrated before, an additional disulfide bond in PETase influences the thermal stability of the enzyme (Matak and Moghaddam, 2009; Joo et al., 2018). Phylogenetic analyses performed comparing these two enzymes have also revealed the presence of a highly conserved region recognized as a nucleophilic elbow that contains serine in the central part of the consensus sequence (Joo et al., 2018). Despite the similarities, an important difference is the width of the active site cleft, in comparison with cutinase from TfH; this slot is three times larger at its widest point in PETase (Austin et al., 2018). Furthermore, the residues surrounding the nucleophilic serine in the catalytic triad were found to be considerably different, which affects the substrate selectivity represented by these enzymes (Liu et al., 2018b).

Recently, many studies have been conducted to improve and better understand the mechanisms of action of these enzymes, especially PETase or MHETase (Oda 2021; Pinto et al., 2021). PETase is recognized as being responsible for hydrolytic conversion of PET into oligomers of mono-2-hydroxyethyl terephthalate (MHET), whereas MHETase hydrolyses MHET into terephthalic acid (TPA) and ethylene glycol (EG) (Figure 2). Thus, recombination and overexpression of those enzymes may be crucial for more efficient degradation of PET as well as monomer recycling (TPA and EG) and for bioconversion to high-value compounds (Furukawa et al., 2019; Taniguchi et al., 2019).

In mechanisms of enzymatic degradation of polyesters, such as PET, apart from plastic properties, the protein structure plays a key role. Especially, the regions on the surface outside the active site of the enzymes and binding modules are essential, both in interaction with the polymer and during the hydrolysis (Acero et al., 2013). For instance, Liu et al. (2018a) assumed in their study that the wide substrate-binding pocket of PETase is critical for PET hydrolysis (Liu et al., 2018b). In contrast, Austin et al. (2018) narrowed the binding cleft and observed improvement in PET degradation (Austin et al., 2018). It should also be emphasized that mutations are frequently used to create greater space in the active sites to fit the large, inaccessible polymer particles and to construct a more hydrophobic substrate-binding site (Araújo et al., 2007). Silva et al. (2011) noted that levels of adsorption to the PET surface are affected by the hydrophobic character of the enzyme active site (Silva et al., 2011). Thus, almost all modifications are related to the active sites of enzymes or their external part (Table 1). Unfortunately, during the creation of enhanced mutants, some obstacles arise. For instance, one of the difficulties emerging during enzymatic degradation of PET by PETase is the location of the enzyme inside the cells. It is perceived as a limiting factor in direct contact of PETase with the solid PET. The consequence is difficulty in establishing a high-throughput screening method in the evaluation of the hydrolysis rate by the modified strains. Fortunately, the solution is an application of developed cell-free protein-expression systems. The system is known as a useful tool in

functional and structural proteomics for proteins that could not be expressed *in vivo* in bacterial cells. Furthermore, the system offers several advantages in comparison to traditional cell-based expression methods. First of all, it allows for easy modification of reaction conditions, shortening expression time or reducing the volume of reaction. The productivity exceeds hundreds of micrograms of protein per millilitre of reaction volumes. Interestingly, in the light of the PET problem mentioned above, application of a cell-free protein-expression system allows for the direct contact of expressed protein with solid PET, providing high-throughput screening of PET hydrolytic enzymes (Murthy et al., 2004; Katzen et al., 2005; Ma et al., 2018).

Engineering of PETase

In 2016 Yoshida et al. published a report about the newly isolated bacterium *Ideonella sakaiensis* 201-F6 that was able to use PET as its major carbon and energy source (Yoshida et al., 2016). Because knowledge of the protein structure is crucial for its further modifications, shortly afterwards many reports about *I. sakaiensis* PETase (IsPETase, EC 3.1.1.101) structure were published. It was shown that this enzyme is a hydrolase and possesses a strictly conserved active site with a Ser-His-Asp catalytic triad and contains an optimal substrate binding site to hold four mono(2-hydroxyethyl) terephthalate (MHET) moieties of PET. PETase enzyme exhibits an optimum pH range of 7–9 and the stability between pH 6 and 10 (Liu et al., 2019b). For purified PETase enzyme applied on PET film, pH 9.0 was identified as optimal, whereas the optimum temperature was estimated as 30°C (Han et al., 2017). PETase exhibits lower activity on *p*-nitrophenol-linked aliphatic esters in comparison to other cutinases, but towards PET the enzyme exhibits 5.5- to 120-fold higher activity compared to the other enzymes (Han et al., 2017; Joo et al., 2018). Attempts to improve the native PETase enzyme from *Ideonella sakaiensis*, which requires a mild environment for growth, are motivated by the relatively low stability of this enzyme. Introducing modifications to the amino acid chain may result in enhanced thermal stability by this protein and could help it maintain activity for a longer time (Joo et al., 2018). Mostly the enzyme's improvement is focused on site-directed mutagenesis. In the study of Joo et al. (2018) among 14 mutants, created by structural and site-directed mutagenesis, only the variant IsPETase^{R280A}, where the arginine (R) in position 280 was replaced with alanine (A), showed increased activity of PETase. The activity towards PET film as a substrate increased by 22.4% in 18 h and 32.4% in 36 h in TPA and MHET release in comparison to IsPETase^{W/T}. This mutant also expressed hydrolytic activity using BHET as a substrate at a similar level compared to the wild-type PETase (Joo et al., 2018).

The subsequent study focused on analysing the structure of the PETase enzyme molecule, comparing it to other α/β -hydrolases enzymes, and performing the most promising modifications that could affect the thermal properties of this protein (Son et al., 2019). The possibility for enhancement of the PETase enzyme was the introduction of two mutations that, as previously, would allow the establishment of additional hydrogen bonds to stabilize the molecule. For this purpose, an IsPETase variant possesses

changes in serine (S) located at position 121 (to aspartic acid (D) or glutamic acid (E)) and aspartate (D) (to histidine (H)) in position 186 resulting in the S121D/D186H and S121E/D186H mutants have been established.

In other studies, Son et al. (2019) have applied a previous achievement of generating the PETase R280A mutant in the work of Joo et al. (2018) and introduced it to the S121E/D186H mutant described above. The study showed that the obtained triple mutant (S121E/D186H/R280A) degrades PET 13.9-fold better than the native protein and 2.3-fold than the previously established R280A protein variant.

Next, Dai et al. (2021) proceeded with further prospectively profitable changes to the structure of this protein variant. The changes in the enzyme were based on the addition of hydrophobic substrate-binding domains such as CBM (cellulose-binding domain), PBM (poly(3-hydroxybutyrate)) binding domain and HFB4 (hydrophobin) to the C-terminus end of PETase. Authors supposed that the presence of CBM, PBM or HFB4 domain in the protein structure could improve the enzyme binding to the hydrophobic surface of PET molecules, which would be associated with an enhanced level of plastic degradation by these mutants. The effect of the implemented modifications was tested based on the amount of PET degradation products (TPA and MHET) released during the incubation with the novel mutants compared to IsPETase D121E/D186H/R280A (IsPETaseEHA). The experiments showed that among the three obtained mutants (IsPETaseEHA_CBM, IsPETaseEHA_PBM, IsPETaseEHA_HFB4), only the protein containing an additional CBM domain improves PET degradation. Increase in PET breakdown products concentration was 2.28-fold increased in comparison to the original mutant and was 251.5 μM of total hydrolysis products. The two remaining variants significantly reduced PET degradation capacity (Dai et al., 2021).

In the study Han et al. (2017) created 12 mutants in order to identify key residues required for catalysis, most of them showed decreased activity in production levels of MHET and TPA compared to the wild-type PETase. Only variant Y58A (possessing change in tyrosine (Y) at position 58 to alanine (A)) exhibited 80.73% MHET production compared to MHET released by wild-type PETase and T59A, which showed full activity in producing MHET. However, in both cases, TPA production decreased (Han et al., 2017). Ma et al. (2018) aimed to create novel high-efficiency PETase mutants through mutagenesis of six key residues around the substrate-binding groove of PETase. By application of a rapid cell-free screening system, they obtained three mutants. In comparison with wild-type PETase, the R61A (exchange in arginine (R) to alanine (A)), L88F (leucine (L) in position 88 changed to phenylalanine (F)), and I179F (isoleucine (I) exchanged to phenylalanine (F)) mutants exhibited 1.4, 2.1 and 2.5 fold increases in the enzymatic affinity to PET, respectively. The strongest catalytic activity expressed by TPA concentration and by weight loss of PET film incubated with purified enzyme was shown by the I179F mutant (6.38 mmol L^{-1} of released TPA after 48 h of incubation and 22.5 $\text{mg per } \mu\text{mol L}^{-1}$ PETase per day). L88F and R61A mutants reached 17.5 and 13.5 $\text{per } \mu\text{mol L}^{-1}$ PETase

per day, respectively, whereas the degradation rate of wild-type PETase was only 8.2 $\text{mg per } \mu\text{mol L}^{-1}$ PETase per day. Furthermore, scanning electron microscopy (SEM) was used to observe the changes in the morphology of the PET film surface after treatment with the I179F mutant in comparison to the negative control. The surface of the PET film was roughened and eroded, and a large number of holes were observed (Ma et al., 2018). In the study of Liu et al. (2018b) structure-guided site-directed mutagenesis was used to improve PETase catalytic efficiency. Several mutants were created with mutations in the active sites, substrate binding pockets or in the residues involved in stabilizing the rigidity of the active site. The hydrolytic activity of PETase was analysed with respect to BHET. Only two mutants described as W130H, where tryptophan (W) has been replaced by histidine (H) and S209F possessing serine (S) exchange to phenylalanine (F), showed increased activity. Interestingly, the authors performed a PETase activity assay on PET drinking bottles. Similarly, only two mutants, described as W130A and W130H, had higher hydrolytic activity towards PET bottles in comparison to unmodified PETase (Liu et al., 2018a). However, PETase retains the ancestral α/β -hydrolase fold with a core consisting of eight β -strands and six α -helices and exhibits a more open active-site cleft than cutinases. Austin et al. (2018) narrowed the binding cleft *via* site-directed mutagenesis of two active-site residues and surprisingly observed improved PET degradation. They created the double mutant S238F/W159H (with serine (S) in position 238 replaced with phenylalanine (F) and tryptophan (W) in position 159 exchanged to histidine (H)) that altered important substrate-binding interactions. The S238 mutation provided new *p*-stacking and hydrophobic interactions to adjacent terephthalate moieties, while the conversion to His159 from the bulkier Trp allowed the PET polymer to sit deeper within the active-site channel. Moreover, in the study, it was demonstrated that the mutant could degrade polyethylene-2,5-furandicarboxylate (PEF), which is a PET replacement. The results suggested that PETase is not fully optimized for crystalline PET degradation (Austin et al., 2018).

Another modification of PETase was performed using the Premuse tool (Meng et al., 2021), by which the selected putative mutations in the protein structure could correspond to natural future evolution in the amino acid chain of the protein. A thorough in-silico analysis highlighted the potential positive effect of the W159H/F229Y mutation to boost the catalytic capacity of PETase. The newly obtained PETase double mutant having modified tryptophan (W) at position 159 to histidine (H) and phenylalanine (F) at position 229 to tyrosine (Y) showed higher thermal stability compared to the wild-type enzyme and the single variants of the mutant proteins (W159H and F229Y). The authors indicated that IsPETase W159H/F229Y after 24 h reaction at 40 °C resulted in a 40-fold increased amount of degradation products in comparison with the native enzyme, however, the authors did not report the specific values of the obtained concentrations of the released compounds (Meng et al., 2021).

Engineering of MHETase

The MHETase discovery occurred at a similar time as PETases, but it is not as well studied an enzyme as PETase despite the fact that they are cooperatively responsible for the degradation of PET by *Ideonella sakaiensis* 201-F6 (Tanasupawat et al., 2016). Structurally, MHETase is an α/β hydrolase that exhibits high substrate specificity and its catalytic triad is formed by S225-H528-D492. Additionally, the domain arrangement is similar to those observed in feruloyl esterases but in contrast to them, MHETase exists as a monomer instead of a dimeric structure (Sagong et al., 2020). MHETase possesses optimum temperature at 45°C and a wide range of pH activity between 6.5–9.0 (Palm et al., 2019). Similar to other hydrolases, MHETase performs a nucleophilic attack on the carbonyl carbon via serine (Pinto et al., 2021).

The metabolic engineering of MHETase is not yet as strongly advanced as that of PETase described in detail in the previous section. Nevertheless, we can highlight several examples of previous studies in which modifications in the amino acid sequence of this protein have been undertaken. One of the earliest MHETase mutagenesis was carried out during the work on the determination of its exact structure and involved an amino acid change within the active site of the enzyme. Palm et al. (2019) have generated a number of mutants to identify key amino acid residues in terms of enzyme activity. Their study revealed that one of the key amino acids responsible for substrate binding is Phe495, whose replacement with alanine (A) resulted in the formation of the F495A protein variant. Studies of catalytic properties of this mutant have shown that the turnover rate of MHET compared to the wild-type enzyme was more than 2 times lower and was about 5 s⁻¹ (Palm et al., 2019).

The subsequent study involving engineering MHETase to enable its degradation of BHET was conducted by Sagong et al. (2020). Investigations performed by these researchers indicated that MHETase can bind to BHET as substrate, however, the hydrolysis activity is very low. Studies with targeted mutagenesis indicated an important role of hydrophobic residues Leu254, Trp397, Phe415 and Phe495 in substrate binding and enzymatic catalysis. Sagong et al. (2020) have performed several mutations that significantly affected BHET binding by the created mutants. All of them were based on mutagenesis at phenylalanine position 424 (F424), and for three mutants (F424N, F424V, and F424I), a significant, more than 3-fold increase in activity against BHET relative to native MHETase was observed. Additional arginine point mutation at position 411 to lysine (R411K) was also found to result in a 1.7-fold increase in activity against BHET substrate compared to the wild-type enzyme. Based on the results, further mutagenesis was performed incorporating the revealed properties of the single mutants, which resulted in the formation of double protein variants (R411K/F424N, R422K/F424V, and R411K/F424I). The relative activity to BHET for the resulting mutants was 8.7, 10.5 and 11.1%, respectively than the native MHETase possessing 1% relative activity towards this substrate. Further studies on the MHETase mutants were conducted based on a previous report by Palm et al. (2019) in which an important role for the S416A mutation was identified. The resulting R411K/

S416A/F424I triple mutant was shown to be 15.3-fold more active against BHET than wild-type MHETase. Activity assays against amorphous PET film were performed on the triple mutant in two variants: without prior hydrolysis of IsPETaseEHA and after incubation with the modified PETase enzyme (see the paragraph on PETase protein engineering above for a detailed description of this mutant). As expected, neither the wild-type MHETase nor the enhanced triple mutant showed activity against PET films without prior IsPETaseEHA pre-treatment. Interestingly, the researchers found that with the use of PET film pre-treated for 10 days with IsPETaseEHA, both the wild-type MHETase enzyme and the triple mutant R411K/S416A/F424I showed activity against PET film. Specified values obtained in this study after 72 h was about 8 μ M of released degradation products by mutant variant, while for the control (wild-type MHETase) it was 4 μ M (Sagong et al., 2020).

Modification of Cutinases

Cutinases (EC 3.1.1.74) are similar to PETase. They belong to the α/β hydrolases group and possess the classical catalytic triad Ser-His-Asp. In nature, cutinases are produced by plant pathogens to hydrolyse the polyesters of the cutin and the suberin layers. In addition, cutinases are able to catalyse reactions with various polyesters and other substrates such as long-chain triacylglycerols or waxes (Nyyssola, 2015). Cutinases possess a wide spectrum of pH optima, where most prefer neutral or alkaline pH. For the thermophilic bacteria *Thermobifida fusca*, researchers indicate a range of pH at 6.8–9 with optimum pH at 8.0 at an optimum temperature of 50–55 °C (Acero et al., 2011; Hegde and Veeranki, 2013). In the case of fungal cutinase using the example of cutinase from *Fusarium solani*, the optimum enzyme condition was determined in the range of pH 7.5–10 (Chen et al., 2008; Baker et al., 2012) and the optimum temperature range for this cutinase has been indicated at 25°C (Baker et al., 2012), 30°C (Chen et al., 2008) and 40°C (Pio and Macedo, 2009).

Since cutinases are universal and efficient esterases, their modification toward PET degradation has been done (Acero et al., 2013). The effect of site-directed mutagenesis, which exchanges selected surface-located amino acids between two polyester hydrolases from *thermobifida cellulolytica* DSM44535, has been studied. As a result, six single mutants, one double mutant and one triple mutant were obtained. The degradation level of amorphous PET films was tested by enzymatic hydrolysis with the use of derived cutinases and quantification of the released degradation products (TA-terephthalic acid and MHET-mono-(2-hydroxyethyl) terephthalate). Incubation of PET with unmodified cutinase Thc_Cut2 as a control was provided. PET hydrolysis was performed for 2 days at 50°C at pH 7.0 with the 200 μ g/mL-1 of enzyme on pre-washed PET films with Triton-X 100 (Acero et al., 2013). The pre-treatment of non-ionic surfactant used in this study may lead to a decrease in the hydrophobicity of the polymer surface and consequently facilitate the binding of the enzyme with the substrate (Caparanga et al., 2009; Mohanan et al., 2020). Kinetic parameters for the mutants compared to the Thc_Cut2 (9 s-1mM-1) were performed, as a result, mutants carrying Arg29Asn (15 s-1mM-1) and/or Ala30Val (153 s-1mM-

1) exchanges showed considerably higher specific activity and higher k_{cat}/K_M values on soluble substrates. However, it should be noted that a triple mutant enzyme with Arg19Ser introduction negatively influenced all the parameters (Acero et al., 2013). Experiments performed on PET film, based on the measurement of TA and MHET released during hydrolysis showed that there is no significant increase in MHET concentration. However, an increased amount of TA released during PET degradation compared to Thc_Cut2 occurred for Ala30Val, Arg29Asn_Ala30Val and Arg19Ser_Arg29Asn_Ala30Val mutations. The highest TA concentrations measured in this experiment were 400 and 370 mM for Arg29Asn_Ala30Val and Arg19Ser_Arg29Asn_Ala30Val, respectively. Interestingly, the introduced Gln65Glu mutation resulted in a 36% decrease in the concentration of the amount of breakdown products for 3PET and completely inhibited PET degradation, despite the fact that kinetic parameters did not remarkably differ compared to the Thc_Cut2.

In other studies, a cutinase from *Fusarium solani pisi* was genetically modified to enhance its enzymatic activity. Site-directed mutagenesis targeted the region near the active site and as a result, two mutants with enhanced activity towards polyester fibres were obtained, named L81A and L182A. They showed an activity increase of four- and five-fold, respectively, when compared with the wild type, for PET fibres. The authors explained the increase in activity of these mutations by higher stabilization of TI and better accommodation of the substrate (Araújo et al., 2007).

Another successful improvement of the enzymatic degradation of PET was presented in the study of Silva et al. (2011). The active site of cutinase Tfu_0883 from *Thermobifida fusca* was modified by site-directed mutagenesis to increase the affinity of cutinase to PET and the ability to hydrolyse it. The mutation I218A (isoleucine (I) replacement to alanine(A)) was designed to create space and the double mutation Q132A/T101A possessing glutamine (Q) and tyrosine (T) replaced with alanine (A) was designed both to create space and to increase hydrophobicity. The activity of both single and double mutants exhibited considerably higher hydrolysis efficiency towards PET fibres—a double mutant exhibited 1.6-fold increased hydrolysis activity (Silva et al., 2011).

In a similar study conducted by Wei et al. (2016), mutagenesis was used to increase the activity of the cutinase TfCut2 from *Thermobifida fusca*. By exchanging selected amino acid residues of the active site in a substrate-binding groove of TfCut2 with those present in LCC, mutants with increased PET hydrolytic activity were obtained. The most active mutants were G62A, possessing glutamine (G) replaced by alanine (A) and G62A/I213S where additional exchange of isoleucine (I) by serine (S) was done. As a result, a 2.7-fold increase in weight loss of PET films was obtained compared to the wild-type enzyme. Moreover, kinetic analysis based on the released PET hydrolysis products confirmed the superior hydrolytic activity of G62A with a fourfold higher hydrolysis rate constant and a 1.5-fold lower substrate-binding constant than those of the wild-type enzyme (Wei et al., 2016). Next, the mutant TfCut2 G62A obtained by

Wei et al. (2016) was a subject of the interesting study of Furukawa et al. (2019). In the study, it was found that low-crystallinity PET (lcPET) hydrolysis may be increased by the addition of a cationic surfactant that attracts enzymes near the lcPET film surface via electrostatic interactions. This approach was applicable to the mutant TfCut2 G62A/F209A and wild-type TfCut2. As a result, the degradation rate of TfCut2 G62A/F209A in the presence of the cationic surfactant (dodecyl trimethyl ammonium) increased 12.7 times over that of wild-type TfCut2 in the absence of the surfactant. A positive effect of surfactant addition was evident for the native enzyme as well as all mutants used except H129E/F209S. The long-duration reaction showed that lcPET film had the fastest biodegradation rate of lcPET film so far ($97 \pm 1.8\%$ within 30 h) (Furukawa et al., 2019). It was also noted that the addition of a cationic surfactant, as well as the increased reaction temperature, results in enhanced hydrophobic interactions between the enzyme and the plastic surface, and consequently increases the amount of enzyme bound to the lcPET surface (Furukawa et al., 2019). Moreover, higher temperature raises the mobility of the polymer chain, which further facilitates the binding of the enzyme to the substrate (Ronkvist et al., 2009).

Tournier et al. (2020) found that leaf-branch compost cutinase (LCC) demonstrated the highest thermostability and was at least 33 times more efficient than other enzymes tested in their study. In differential scanning fluorimetry experiments it was shown that LCC is thermally stabilized in the presence of calcium ions. To avoid salt supplementation, the authors focused on improving the activity and thermostability of LCC by enzyme engineering. By using the alternative strategy of replacing the divalent metal binding with a disulfide bond the researchers obtained thermal stabilization of LCC without dependence on calcium ions. Moreover, by site-direct saturation mutagenesis, they tested 209 mutants. Most of the modified variants showed less than 1% specific activity in comparison to the wild-type LCC, but the F243I and F243W mutations, in which phenylalanine (F) at position 243 was replaced with isoleucine (I) or tryptophan (W), showed elevated activity. The obtained cutinase variants gained specific activity by 27 and 18%, respectively. Finally, they obtained an enhanced PET hydrolase that was able to depolymerize over 90% PET into monomers in over 10 h (10.5 and 9.3 h for mutants WCCG (F243W/D238C/S283C/Y127G) and ICCG (F243I/D238C/S283C/Y127G), respectively with the use of 3 mg of enzyme per 1 g of PET. The productivity of ICCG mutant was determined at 16.7 g of terephthalic acid per litre per hour at 72°C, which is a 98-fold increase compared to TfCut2 investigated before (Wei et al., 2019). Wild type LCC enzyme achieved only 53% of conversion after 20 h, which corresponds with its lower thermostability in comparison to the mutants. Although X-ray crystallography showed no substantial difference between parental LCC and ICCG, molecular-dynamic simulations revealed that mutations introduced in ICCG facilitated the catalytic binding of 2-HE(MHET)3 compared with parental LCC (Tournier et al., 2020).

Kawai et al. (2014) created a Cut190 (S226P/R228S), a double mutant enzyme for PET degradation. They cloned the cutinase gene (cut190) from *Saccharomonospora viridis* AHK190 and

expressed it in *Escherichia coli* Rosetta-gami B (DE3). It was observed that the substitution of Ser226 with Pro and Arg228 with Ser yielded the highest activity and thermostability of the new enzyme. Also, they noted that the presence of the Ca^{2+} ion enhanced the enzyme activity and thermostability in comparison to both the wild-type enzyme and mutant Cut190. Circular dichroism suggested that the Ca^{2+} changes the tertiary structure of Cut190 (S226P/R228S) (Kawai et al., 2014). High-level expression of LCC was also achieved due to insertion of the signal peptide sequence of cellulose Cel48S and a constitutive promoter of the gene Clo1313_2638 (P2638) in *Clostridium thermocellum*. Improved degradation of commercial PET films was observed and maximum weight loss (approximately 62%) was achieved after 14 days of incubation at 60°C (Yan et al., 2020).

Genetic engineering may also be a solution to many problems related to the stability of enzymes. For instance, Shirke et al. (2018) underlined that aggregation is emerging as a major factor that reduces LCC kinetic stability. In its native state, LCC is highly prone to aggregation owing to electrostatic interactions. Since LCC precipitates even at room temperature and low concentrations, the purification and storage of enzymes require salt concentrations that vary with protein concentration. Moreover, efficient PET hydrolysis requires a temperature around 70°C, which is very close to the temperature of LCC structure loss. To overcome these problems, Shirke et al. (2018) proposed the expression of native LCC in *Pichia pastoris*, resulting in the production of glycosylated LCC (LCCG). They introduced three putative N-glycosylation sites, which improved resistance to aggregation even at high-temperature conditions, leading to a 10°C increase in the thermal aggregation point and a significant increase in kinetic stability. Furthermore, glycosylation resulted in improved catalytic PET hydrolysis (Shirke et al., 2018). On the other hand, Gamerith et al. (2017) aimed to investigate the influence of glycosylation on the activity and stability of cutinase 1 (Thc_Cut1) from *Thermobifida cellulosilytica*. They expressed Thc_Cut1 and two glycosylation site knockout mutants, Thc_Cut1_koAsn and Thc_Cut1_koST, in *P. pastoris*. However, the created mutants hydrolysed aromatic (PET) and aliphatic (PHBV and PBS) polyester powders at very different rates based on quantification of released products by HPLC. Thc_Cut1_koST was the most effective among all enzymes. The highest TPA yield was obtained for Thc_Cut1_koST mutant, which caused hydrolysis of 24% of the starting PET powder amount. Due to the fact that the Thc_Cut1_koST mutant exhibited higher protein production yield in engineered *P. pastoris* yeast, this variant was used in further studies on PHBV and PBS degradation. The authors did not observe significant differences in PHBV degradation between Thc_Cut1 and Thc_Cut1_koST mutants, due to the similar amounts of 3-HBA (3-hydroxybutyric acid) at around 0.5 mM after 96 h of incubation. A similar trend was observed by investigating a PBS film weight loss, where a 92% decrease in the mass of polymer film was obtained for the applied mutant and 41% for Thc_Cut1 within 96 h of hydrolysis (Gamerith et al., 2017).

Although the main focus in genetic engineering of microorganisms and enzymes with biodegradation activity is

directed towards PET, some studies present results for other plastics. For instance, the alkane hydroxylase gene (alkB) from *Pseudomonas* sp. E4 was expressed in *E. coli* BL21. A recombinant strain secreted recombinant alkane hydroxylase (AH) and was able to mineralize 19.3% of the low molecular weight polyethylene (LMWPE) to CO_2 after incubation in the compost for 80 days at 37°C, while the recipient cell was not active at all toward LMWPE biodegradation (Yoon et al., 2012).

Synergistic Activity of Chimeric Enzymes

Chimeric enzymes, also known as fusion proteins, are proteins formed by combining two or more unrelated genes that originally encoded distinct proteins. The resulting proteins exhibit the attributes of all the proteins used in the fusion and constitute a single, combined molecule. Suitably designed hybrid proteins offer many opportunities due to their wide range of properties and can be used in many fields (Yu et al., 2015). Thus, the application of multiple enzyme systems for the biodegradation of plastic seems to be a very promising solution. It is reasonable to assume that enzymes might be used synergistically with other enzymes in polymer degradation due to the complementary properties of both enzymes in both catalysis pattern and substrate specificity (Liu et al., 2019b). A prime example is the connection of two enzymes in the biodegradation of PET. It is known that during PET degradation, accumulating MHET is an important factor that limits the efficiency of hydrolysis. To avoid this problem, the recombinant expression and purification of TfCut2 from *Thermobifida fusca* KW3 and LC-cutinase (LCC) were proposed. In the study of Barth et al. (2016) the dual system was LCC or TfCut2 combined with immobilized TfCa on the SulfoLink resin—which was generated by the addition of oligopeptide of glycine-serine-cysteine at the C-terminus via site-directed mutagenesis. The introduction of the C-terminal oligopeptide did not cause a significant reduction in its hydrolytic activity against *p*-NPB, BHET and MHET. The immobilized enzyme maintained approximately 94% of its initial activity at 60°C, whereas free TfCa resulted in a complete loss of activity at 55°C. Moreover, the usage of a dual enzyme reaction system with LCC or TfCut2 caused a 47.9% or 20.4% weight loss, respectively, of the PET films after a reaction time of 24 h (Barth et al., 2016). An artificial chimeric enzyme was also constructed by Liu et al. (2018a). In their study lipase (Lip) from *Thermomyces lanuginosus* and cutinase (Cut) from *Thielavia terrestris* NRRL 8126 were used for the construction of bifunctional lipase-cutinase (Lip-Cut) by end-to-end fusion and overexpression in *Pichia pastoris* (Liu et al., 2018b). Lip-Cut exhibited a more efficient degradation ability towards poly(ϵ -caprolactone) (PCL). The weight loss of PCL films was 13.3, 11.8, and 5.7 times higher (at 6 h) than those obtained by Lip, Cut and the Lip/Cut mixture, respectively. GC-MS analysis revealed that the main products produced during hydrolysis were 6-hydroxyhexanoic acid and 3-caprolactone. Moreover, SEM analysis showed that the surface of the PCL film became rougher and more holes were observed after 4 h of treatment with bifunctional Lip-Cut than in the case of other enzymes after 48 h (Liu et al., 2019a). Gamerith et al. (2016), using C-terminal fusion, fused a hydrophobic binding module of polyhydroxybutyrate depolymerase (PA_PBM) from

Alcaligenes faecalis to polyamidase (PA) from *Nocardia farcinica* IMA 10152A. The fusion polyamidase (PA_PBM) indeed resulted in a more active enzyme on commercial polyurethane copolymers as indicated by the release of 4,4'-diaminodiphenylmethane (MDA) and different oligomers (Gamerith et al., 2016).

An interesting improvement of PET degradation was the two-enzyme system described by Knott et al., 2020. In that study, the authors constructed an MHETase: PETase chimeric protein covalently linking the C-terminus of MHETase to the N-terminus of PETase of varying glycine-serine linker lengths (8, 12 or 20 aa residues). All chimeric proteins exhibit improved PET and MHET turnover relative to the free enzymes. Hydrolysis of amorphous PET incubated with 0.25 mg of PETase and 0.5 mg of MHETase per gram of PET resulted in the release of 0.25 mM MHET and TPA by PETase and 0.45 mM MHET when co-incubated with the two enzymes. The use of the MP8, MP12 and MP20 chimeras increased the amount of TPA released threefold (1.4, 1.45, and 1.5 mM, respectively). Interestingly, the chimeric constructs linking the C-terminus of PETase to the N-terminus of MHETase were not capable of expressing the protein (Knott et al., 2020).

Another enhancement of PETase based on the implementation of hybrid proteins to increase its activity and thermal stability was performed by Chen et al. (2021). The work conducted by these researchers involved the addition of an amino acid chain containing glutamic acid (E) and lysine (K) to the C-terminus of the PETase enzyme, which resulted in the formation of different PETase-EK fusion protein variants (5, 10 and 30 kDa). Thermal stability assays performed for the obtained mutants compared to the native PETase showed that each of the obtained proteins exhibited better stability (80% activity after 6 h incubation at 40°C) than the native enzyme (65% activity after incubation under the same conditions). The ability to degrade PET was verified by the number of released degradation products during incubation with amorphous PET film and PET bottle film. The experiment demonstrated that each mutant caused a significantly higher level of PET degradation (on both plastic type materials used) compared to the wild-type enzyme. The best results were obtained with PETase-EK30, which after 6 days of incubation at 40°C resulted in the release of 302.4 and 146.2 µM total MHET and TPA after incubation with amorphous PET film and PET bottles, respectively. The incubation with the native enzyme resulted in the release of 32.8 and 13.9 µM of MHET and TPA for the appropriate substrates, correspondingly. It is worth noting that for the native enzyme, from day 1 of incubation to day 6, the amount of products released did not change significantly. In the case of the mutants, a progressive increase in the amount of breakdown products was noted from day 1 to day 4 of incubation, while between days 4 and 6 the measured concentrations were at equivalent amounts (Chen et al., 2021).

Prospective Applications of Modified Microorganisms and Engineered Proteins in PET Waste Management

Since 1964 production of plastic has increased twentyfold, but almost 50 years after the introduction of the recycling process, only 14% of plastic packing is collected for reuse. PET used in

bottles has the highest recycling rate, but globally only 7% of it is recycled bottle-to-bottle. Most of the plastic products after a single use are landfilled, and 32% escape the collection system to the natural environment (Ellen MacArthur Foundation and World Economic Forum, 2014; http://www3.weforum.org/docs/WEF_The_New_Plastics_Economy.pdf). The growing amount of plastic waste has forced the scientific community to look at this global issue. So far the published reports have shown that naturally isolated microorganisms possess a limited capability for plastic degradation, and it might take decades before microbes adapt to use plastic as a carbon source. The published data on genetically modified microorganisms or chemically engineered enzymes suggest that this direction offers a promising method for plastic waste management. Nowadays, through the chemical engineering of enzymes such as modification of the active site or by introducing new bonds, we can avoid cofactor supplementation with the simultaneous multifold improvement of their activities, reduction of the reaction time and increase of their thermal stability. The latter factor might be crucial since hydrolysis of PET needs a higher temperature than the glass transition temperature (T_g), which is 67–81 °C. A highly interesting approach that can be applied to PET degradation technology in the future is the concept of nano-immobilization of enzymes to improve their tolerance to temperature and pH. The first attempts to use immobilized enzymes have been recently achieved successfully (Jia et al., 2021). Another perspective, which should be included in the discussion, is the possibility of reuse of the products of PET degradation (such as EG and TPA) to synthesize a new PET with similar properties as a virgin PET. This will result in reduced demand for fossil substrates for plastic synthesis and simultaneously may be a branch where the use of immobilized enzymes can bring additional benefits. Prospectively, due to restrictions and concerns over the use of GMOs worldwide, safer and easier to safely handle modified proteins may become an alternative to the long-known bioremediation or biological recycling, which seems to be a distant goal when using GMMs. The application of enzymatic recycling with the use of enhanced mutants of PETase cutinase may be one solution in the future to reduce the level of contamination, and to our knowledge, such application is one of the latest developments in this field (Singh et al., 2021).

An interesting attempt was made by Roberts et al. (2020), where a microbial consortium of *Pseudomonas* and *Bacillus* species was applied to synergic PET degradation. Such a study may bring additional perspective about applying an enzymatic cocktail as a possibility to provide ester bond hydrolysis in PET formulated with engineered hydrolases. Despite the fact that microorganisms able to produce PET-degrading enzymes and capable of growing degradation products as the sole carbon source can be found in nature, the efficiency of PET hydrolysis is generally low. The other perspective that can be taken into consideration in further application attempts of genetic engineering and protein modification methods is related to the successful attempt to obtain microalgae capable of producing PETase enzyme (Kim et al., 2020). The use of an improved mutant of this protein in similar studies could

greatly enhance the research conducted in this area and bring interesting adaptive solutions for photosynthesizing eukaryotes.

In the future probably we will be able to use plastic wastes as a low-cost substrate for genetically modified microorganisms to produce value-added products such as enzymes, fatty acids, organic acids and others. As emphasized in this review, genetically modified microorganisms are a promising alternative for the plastic circular economy.

CONCLUSION

As the production of plastics is still increasing, enzymatic hydrolysis of PET and other plastic is gaining importance and interest from researchers. This way of degradation of plastic is evaluated as an environmentally friendly, novel strategy for the recycling of post-consumer plastic materials. Thus, in order to better adapt the enzymes to synthetic polymers, the use of genetic engineering may be a key to solving the plastic pollution problem. However, the engineering of novel hydrolases exhibiting highly efficient and specific catalytic

properties towards PET materials remains a challenge. All findings presented above may provide further options to obtain effective enzymes for biocatalytic plastic recycling processes.

AUTHOR CONTRIBUTIONS

AU wrote the manuscript and made the figures, KK wrote the manuscript, AM wrote and revised the manuscript.

FUNDING

This work was supported by the National Science Centre, Poland under Grant UMO-2017/27/B/NZ9/02218. The publication fee is financed under the Leading Research Groups support project from the subsidy increased for the period 2020–2025 in the amount of 2% of the subsidy referred to Art. 387 (3) of the Law of 20 July 2018 on Higher Education and Science, obtained in 2019.

REFERENCES

- Allen, S., Allen, D., Phoenix, V. R., Le Roux, G., Durántez Jiménez, P., Simonneau, A., et al. (2019). Atmospheric Transport and Deposition of Microplastics in a Remote Mountain Catchment. *Nat. Geosci.* 12 (5), 339–344. doi:10.1038/s41561-019-0335-5
- Araújo, R., Silva, C., O'Neill, A., Micaelo, N., Guebitz, G., Soares, C. M., et al. (2007). Tailoring Cutinase Activity towards Polyethylene Terephthalate and Polyamide 6,6 Fibers. *J. Biotechnol.* 128 (4), 849–857. doi:10.1016/j.jbiotec.2006.12.028
- Austin, H. P., Allen, M. D., Donohoe, B. S., Rorrer, N. A., Kearns, F. L., Silveira, R. L., et al. (2018). Characterization and Engineering of a Plastic-Degrading Aromatic Polyesterase. *Proc. Natl. Acad. Sci. USA* 115 (19), E4350–E4357. doi:10.1073/pnas.1718804115
- Baker, P. J., Poultney, C., Liu, Z., Gross, R., and Montclare, J. K. (2012). Identification and Comparison of Cutinases for Synthetic Polyester Degradation. *Appl. Microbiol. Biotechnol.* 93, 229–240. doi:10.1007/s00253-011-3402-4
- Barth, M., Honak, A., Oeser, T., Wei, R., Belisário-Ferrari, M. R., Then, J., et al. (2016). A Dual Enzyme System Composed of a Polyester Hydrolase and a Carboxylesterase Enhances the Biocatalytic Degradation of Polyethylene Terephthalate Films. *Biotechnol. J.* 11 (8), 1082–1087. doi:10.1002/biot.201600008
- Brahney, J., Hallerud, M., Heim, E., Hahnenberger, M., and Sukumaran, S. (2020). Plastic Rain in Protected Areas of the United States. *Science* 368 (6496), 1257–1260. doi:10.1126/science.aaz5819
- Caparanga, A. R., Basilia, B. A., Dagbay, K. B., and Salvacion, J. W. L. (2009). Factors Affecting Degradation of Polyethylene Terephthalate (PET) during Pre-filtration Conditioning. *Waste Management* 29, 2425–2428. doi:10.1016/j.wasman.2009.03.025
- Carniel, A., Valoni, E., Nicomedes, J., Gomes, A. d. C., and Castro, A. M. d. (2017). Lipase from *Candida antarctica* (CALB) and Cutinase from *Humicola insolens* Act Synergistically for PET Hydrolysis to Terephthalic Acid. *Process Biochem.* 59, 84–90. doi:10.1016/j.procbio.2016.07.023
- Chen, K., Hu, Y., Dong, X., and Sun, Y. (2021). Molecular Insights into the Enhanced Performance of Eukaryotic PETase toward PET Degradation. *ACS Catal.* 11, 7358–7370. doi:10.1021/acscatal.1c01062
- Chen, S., Tong, X., Woodard, R. W., Du, G., Wu, J., and Chen, J. (2008). Identification and Characterization of Bacterial Cutinase. *J. Biol. Chem.* 283, 25854–25862. doi:10.1074/jbc.M800848200
- Cózar, A., Martí, E., Duarte, C. M., García-de-Lomas, J., van Sebille, E., Ballatore, T. J., et al. (2017). The Arctic Ocean as a Dead End for Floating Plastics in the North Atlantic branch of the Thermohaline Circulation. *Sci. Adv.* 3 (4), e1600582. doi:10.1126/sciadv.1600582
- Dai, L., Qu, Y., Huang, J. W., Hu, Y., Hu, H., Li, S., et al. (2021). Enhancing PET Hydrolytic Enzyme Activity by Fusion of the Cellulose-Binding Domain of Cellobiohydrolase I from *Trichoderma reesei*. *J. Biotechnol.* 334, 47–50. doi:10.1016/j.jbiotec.2021.05.006
- Danso, D., Chow, J., and Streit, W. R. (2019). Plastics: Environmental and Biotechnological Perspectives on Microbial Degradation. *Appl. Environ. Microbiol.* 85, e01095–19. doi:10.1128/AEM.01095-19
- Egmond, M., and de Vlieg, J. (2000). Fusarium Solani Pisi Cutinase. *Biochimie* 82 (11), 1015–1021. doi:10.1016/s0300-9084(00)01183-4
- Ellen MacArthur Foundation and World Economic Forum (2014). Ellen MacArthur Foundation and World Economic Forum. http://www3.weforum.org/docs/WEF_The_New_Plastics_Economy.pdf.
- Furukawa, M., Kawakami, N., Tomizawa, A., and Miyamoto, K. (2019). Efficient Degradation of Poly(ethylene Terephthalate) with *Thermobifida fusca* Cutinase Exhibiting Improved Catalytic Activity Generated Using Mutagenesis and Additive-Based Approaches. *Sci. Rep.* 9, 16038. doi:10.1038/s41598-019-52379-z
- Gamerith, C., Herrero Acero, E., Pellis, A., Ortner, A., Vielnascher, R., Luschig, D., et al. (2016). Improving Enzymatic Polyurethane Hydrolysis by Tuning Enzyme Sorption. *Polym. Degrad. Stab.* 132, 69–77. doi:10.1016/j.polymdegradstab.2016.02.025
- Gamerith, C., Vastano, M., Ghorbanpour, S. M., Zitzenbacher, S., Ribitsch, D., Zumstein, M. T., et al. (2017). Enzymatic Degradation of Aromatic and Aliphatic Polyesters by *P. pastoris* Expressed Cutinase 1 from *Thermobifida cellulolytica*. *Front. Microbiol.* 8, 938. doi:10.3389/fmicb.2017.00938
- Gangadoo, S., Owen, S., Rajapaksha, P., Plaisted, K., Cheeseman, S., Haddara, H., et al. (2020). Nano-plastics and Their Analytical Characterisation and Fate in the marine Environment: From Source to Sea. *Sci. Total Environ.* 732, 138792. doi:10.1016/j.scitotenv.2020.138792
- Geyer, R., Jambeck, J. R., and Law, K. L. (2017). Production, Use, and Fate of All Plastics Ever Made. *Sci. Adv.* 3 (7), e1700782. doi:10.1126/sciadv.1700782
- Han, X., Liu, W., Huang, J.-W., Ma, J., Zheng, Y., Ko, T.-P., et al. (2017). Structural Insight into Catalytic Mechanism of PET Hydrolase. *Nat. Commun.* 8 (1), 2106. doi:10.1038/s41467-017-02255-z
- Herrero Acero, E., Ribitsch, D., Dellacher, A., Zitzenbacher, S., Marold, A., Steinkellner, G., et al. (2013). Surface Engineering of a Cutinase

- from Thermobifida Cellulosilytica for Improved Polyester Hydrolysis. *Biotechnol. Bioeng.* 110 (10), 2581–2590. doi:10.1002/bit.24930
- Herrero Acero, E., Ribitsch, D., Steinkellner, G., Gruber, K., Greimel, K., Eiteljoerg, I., et al. (2011). Enzymatic Surface Hydrolysis of PET: Effect of Structural Diversity on Kinetic Properties of Cutinases from Thermobifida. *Macromolecules* 44, 4632–4640. doi:10.1021/ma200949p
- Hiraga, K., Taniguchi, I., Yoshida, S., Kimura, Y., and Oda, K. (2020). Biodegradation of Waste PET. *EMBO Rep.* 21 (2), e49826. doi:10.15252/embr.201949826
- Imran, M., Kim, D. H., Al-Masry, W. A., Mahmood, A., Hassan, A., Haider, S., et al. (2013). Manganese-, Cobalt-, and Zinc-Based Mixed-Oxide Spinel as Novel Catalysts for the Chemical Recycling of Poly(ethylene Terephthalate) via Glycolysis. *Polym. Degrad. Stab.* 98 (4), 904–915. doi:10.1016/j.polymdegradstab.2013.01.007
- Jia, Y., Samak, N. A., Hao, X., Chen, Z., Yang, G., Zhao, X., et al. (2021). Nano-immobilization of PETase Enzyme for Enhanced Polyethylene Terephthalate Biodegradation. *Biochem. Eng. J.* 176, 108205. doi:10.1016/j.bej.2021.108205
- Joo, S., Cho, I. J., Seo, H., Son, H. F., Sagong, H.-Y., Shin, T. J., et al. (2018). Structural Insight into Molecular Mechanism of Poly(ethylene Terephthalate) Degradation. *Nat. Commun.* 9 (1), 382. doi:10.1038/s41467-018-02881-1
- Katzen, F., Chang, G., and Kudlicki, W. (2005). The Past, Present and Future of Cell-free Protein Synthesis. *Trends Biotechnol.* 23 (3), 150–156. doi:10.1016/j.tibtech.2005.01.003
- Kawai, F., Oda, M., Tamashiro, T., Waku, T., Tanaka, N., Yamamoto, M., et al. (2014). A Novel Ca²⁺-Activated, Thermostabilized Polyesterase Capable of Hydrolyzing Polyethylene Terephthalate from Saccharomonospora Viridis AHK190 Functional Expression of Polyethylene Terephthalate-Degrading Enzyme (PETase) in green Microalgae. *Appl. Microbiol. Biotechnol. Microb. Cell Fact.* 9819 (24), 100531–100649. doi:10.1186/s12934-020-01355-8
- Knott, B. C., Erickson, E., Allen, M. D., Gado, J. E., Graham, R., Kearns, F. L., et al. (2020). Characterization and Engineering of a Two-Enzyme System for Plastics Depolymerization. *Proc. Natl. Acad. Sci. USA* 117 (41), 25476–25485. doi:10.1073/pnas.2006753117
- Kumari, A., Chaudhary, D. R., and Jha, B. (2019). Destabilization of Polyethylene and Polyvinylchloride Structure by marine Bacterial Strain. *Environ. Sci. Pollut. Res.* 26 (2), 1507–1516. doi:10.1007/s11356-018-3465-1
- Lange, P. (2002). Sustainable Development: Efficiency and Recycling in Chemicals Manufacturing. *Green. Chem.* 4 (6), 546–550. doi:10.1039/b207546f
- Li, L., Luo, Y., Li, R., Zhou, Q., Peijnenburg, W. J. G. M., Yin, N., et al. (2020). Effective Uptake of Submicrometre Plastics by Crop Plants via a Crack-Entry Mode. *Nat. Sustainability* 3, 929–937. doi:10.1038/s41893-020-0567-9
- Liu, B., He, L., Wang, L., Li, T., Li, C., Liu, H., et al. (2018a). Protein Crystallography and Site-Direct Mutagenesis Analysis of the Poly(ethylene Terephthalate) Hydrolase PETase from Ideonella Sakaiensis. *Chembiochem* 19 (14), 1471–1475. doi:10.1002/cbic.201800097
- Liu, C., Shi, C., Zhu, S., Wei, R., and Yin, C.-C. (2019b). Structural and Functional Characterization of Polyethylene Terephthalate Hydrolase from Ideonella Sakaiensis. *Biochem. Biophysical Res. Commun.* 508, 289–294. doi:10.1016/j.bbrc.2018.11.148
- Liu, M., Yang, S., Long, L., Cao, Y., and Ding, S. (2018b). Engineering a Chimeric Lipase-Cutinase (Lip-Cut) for Efficient Enzymatic Deinking of Waste Paper. *BioResources* 13 (1), 981–996.
- Liu, M., Zhang, T., Long, L., Zhang, R., and Ding, S. (2019a). Efficient Enzymatic Degradation of Poly (ε-caprolactone) by an Engineered Bifunctional Lipase-Cutinase. *Polym. Degrad. Stab.* 160, 120–125. doi:10.1016/j.polymdegradstab.2018.12.020
- Liu, Y., Yao, X., Yao, H., Zhou, Q., Xin, J., Lu, X., et al. (2020). Degradation of Poly(ethylene Terephthalate) Catalyzed by Metal-free Choline-Based Ionic Liquids. *Green. Chem.* 22, 3122–3131. doi:10.1039/d0gc00327a
- Ma, Y., Yao, M., Li, B., Ding, M., He, B., Chen, S., et al. (2018). Enhanced Poly(ethylene Terephthalate) Hydrolase Activity by Protein Engineering. *Engineering* 4 (6), 888–893. doi:10.1016/j.eng.2018.09.007
- Matak, M. Y., and Moghaddam, M. E. (2009). The Role of Short-Range Cys171-Cys178 Disulfide Bond in Maintaining Cutinase Active Site Integrity: A Molecular Dynamics Simulation. *Biochem. Biophysical Res. Commun.* 390, 201–204. doi:10.1016/j.bbrc.2009.09.073
- Mattsson, K., Johnson, E. V., Malmendal, A., Linse, S., Hansson, L.-A., and Cedervall, T. (2017). Brain Damage and Behavioural Disorders in Fish Induced by Plastic Nanoparticles Delivered through the Food Chain. *Sci. Rep.* 7 (1), 11452. doi:10.1038/s41598-017-10813-0
- Meng, X., Yang, L., Liu, H., Li, Q., Xu, G., Zhang, Y., et al. (2021). Protein Engineering of Stable IsPETase for PET Plastic Degradation by Premuse. *Int. J. Biol. Macromolecules* 180, 667–676. doi:10.1016/j.ijbiomac.2021.03.058
- Mohan, N., Montazer, Z., Sharma, P. K., and Levin, D. B. (2020). Microbial and Enzymatic Degradation of Synthetic Plastics. *Front. Microbiol.* 11, 580709. doi:10.3389/fmicb.2020.580709
- Murthy, T. V. S., Wu, W., Qiu, Q. Q., Shi, Z., LaBaer, J., and Brizuela, L. (2004). Bacterial Cell-free System for High-Throughput Protein Expression and a Comparative Analysis of *Escherichia coli* Cell-free and Whole Cell Expression Systems. *Protein Expr. Purif.* 36 (2), 217–225. doi:10.1016/j.pep.2004.04.002
- Müller, R. J., Schrader, H., Profe, J., Dresler, K., and Deckwer, W. D. (2005). Enzymatic Degradation of Poly(ethylene Terephthalate): Rapid Hydrolyse Using a Hydrolase from T. Fusca. *Macromol. Rapid Commun.* 26, 1400–1405. doi:10.1002/marc.200500410
- Nyyssölä, A. (2015). Which Properties of Cutinases Are Important for Applications? *Appl. Microbiol. Biotechnol.* 99 (12), 4931–4942. doi:10.1007/s00253-015-6596-z
- Oda, M. (2021). Structural Basis for Ca²⁺-dependent Catalysis of a Cutinase-like Enzyme and its Engineering: Application to Enzymatic PET Depolymerization. *Biophysics* 18, 168–176. doi:10.2142/biophysico.bppb-v18.018
- Palm, G. J., Reisky, L., Böttcher, D., Müller, H., Michels, E. A. P., Walczak, M. C., et al. (2019). Structure of the Plastic-Degrading Ideonella Sakaiensis MHETase Bound to a Substrate. *Nat. Commun.* 10, 1–10. doi:10.1038/s41467-019-09326-3
- Park, S. H., and Kim, S. H. (2014). Poly (Ethylene Terephthalate) Recycling for High Value Added Textiles. *Fashion and Textiles* 1, 1. doi:10.1186/s40691-014-0001-x
- Pauly, J. L., Stegmeier, S. J., Allaart, H. A., Cheney, R. T., Zhang, P. J., Mayer, A. G., et al. (1998). Inhaled Cellulosic and Plastic Fibers Found in Human Lung Tissue. *Cancer Epidemiol. Biomarkers Prev.* 7 (5), 419–428.
- Pinto, A. V., Ferreira, P., Neves, R. P. P., Fernandes, P. A., Ramos, M. J., and Magalhães, A. L. (2021). Reaction Mechanism of MHETase, a PET Degrading Enzyme. *ACS Catal.* 11, 10416–10428. doi:10.1021/acscatal.1c02444
- Pio, T. F., and Macedo, G. A. (2009). Chapter 4 Cutinases: Properties and Industrial Applications. *Adv. Appl. Microbiol.* 66, 77–95. doi:10.1016/S0065-2164(08)00804-6
- PlasticEurope (2019). Plastic-the Facts 2019. An Analysis of European Plastic Production, Demand and Waste Data. https://www.plasticseurope.org/application/files/9715/7129/9584/FINAL_web_version_Plastics_the_facts2019_14102019.pdf
- Roberts, C., Edwards, S., Vague, M., León-Zayas, R., Scheffer, H., Chan, G., et al. (2020). Environmental Consortium Containing Pseudomonas and Bacillus Species Synergistically Degrades Polyethylene Terephthalate Plastic. *mSphere* 5, 1–20. doi:10.1128/msphere.01151-20
- Ronkvist, Å. M., Xie, W., Lu, W., and Gross, R. A. (2009). Cutinase-Catalyzed Hydrolysis of Poly(ethylene Terephthalate). *Macromolecules* 42, 5128–5138. doi:10.1021/ma9005318
- Rose, R. S., Richardson, K. H., Latvanen, E. J., Hanson, C. A., Resmini, M., and Sanders, I. A. (2020). Microbial Degradation of Plastic in Aqueous Solutions Demonstrated by CO₂ Evolution and Quantification. *Int. J. Mol. Sci.* 21 (4), 1176. doi:10.3390/ijms21041176
- Roth, C., Wei, R., Oeser, T., Then, J., Föllner, C., Zimmermann, W., et al. (2014). Structural and Functional Studies on a Thermostable Polyethylene Terephthalate Degrading Hydrolase from Thermobifida Fusca. *Appl. Microbiol. Biotechnol.* 98, 7815–7823. doi:10.1007/s00253-014-5672-0
- Rummel, C. D., Jahnke, A., Gorokhova, E., Kühnel, D., and Schmitt-Jansen, M. (2017). Impacts of Biofilm Formation on the Fate and Potential Effects of Microplastic in the Aquatic Environment. *Environ. Sci. Technol. Lett.* 4 (7), 258–267. doi:10.1021/acs.estlett.7b00164
- Sagong, H.-Y., Seo, H., Kim, T., Son, H. F., Joo, S., Lee, S. H., et al. (2020). Decomposition of the PET Film by MHETase Using Exo-PETase Function. *ACS Catal.* 10, 4805–4812. doi:10.1021/acscatal.9b05604
- Sang, T., Wallis, C. J., Hill, G., and Britovsek, G. J. P. (2020). Polyethylene Terephthalate Degradation Under Natural and Accelerated Weathering Conditions. *Eur. Polym. J.* 136, 109873. doi:10.1016/j.eurpolymj.2020.109873

- Schwabl, P., Köppel, S., Königshofer, P., Bucsics, T., Trauner, M., Reiberger, T., et al. (2019). Detection of Various Microplastics in Human Stool. *Ann. Intern. Med.* 171, 453–457. doi:10.7326/m19-0618
- Shirke, A. N., White, C., Englaender, J. A., Zwarycz, A., Butterfoss, G. L., Linhardt, R. J., et al. (2018). Stabilizing Leaf and branch Compost Cutinase (LCC) with Glycosylation: Mechanism and Effect on PET Hydrolysis. *Biochemistry* 57 (7), 1190–1200. doi:10.1021/acs.biochem.7b01189
- Silva, C., Da, S., Silva, N., Matamá, T., Araújo, R., Martins, M., et al. (2011). Engineered *Thermobifida Fusca* Cutinase with Increased Activity on Polyester Substrates. *Biotechnol. J.* 6 (10), 1230–1239. doi:10.1002/biot.201000391
- Singh, A., Rorrer, N. A., Nicholson, S. R., Erickson, E., DesVeaux, J. S., Avelino, A. F. T., et al. (2021). Techno-economic, Life-Cycle, and Socioeconomic Impact Analysis of Enzymatic Recycling of Poly(ethylene Terephthalate). *Joule* 5, 2479–2503. doi:10.1016/j.joule.2021.06.015
- Son, H. F., Cho, I. J., Joo, S., Seo, H., Sagong, H.-Y., Choi, S. Y., et al. (2019). Rational Protein Engineering of Thermo-Stable PETase from *Ideonella Sakaiensis* for Highly Efficient PET Degradation. *ACS Catal.* 9, 3519–3526. doi:10.1021/acscatal.9b00568
- Sulaiman, S., Yamato, S., Kanaya, E., Kim, J.-J., Koga, Y., Takano, K., et al. (2012). Isolation of a Novel Cutinase Homolog with Polyethylene Terephthalate-Degrading Activity from Leaf-branch Compost by Using a Metagenomic Approach. *Appl. Environ. Microbiol.* 78, 1556–1562. doi:10.1128/AEM.06725-11
- Tanasupawat, S., Takehana, T., Yoshida, S., Hiraga, K., and Oda, K. (2016). *Ideonella Sakaiensis* Sp. nov., Isolated from a Microbial Consortium that Degrades Poly(ethylene Terephthalate). *Int. J. Syst. Evol. Microbiol.* 66 (8), 2813–2818. doi:10.1099/ijsem.0.001058
- Taniguchi, I., Yoshida, S., Hiraga, K., Miyamoto, K., Kimura, Y., and Oda, K. (2019). Biodegradation of PET: Current Status and Application Aspects. *ACS Catal.* 9, 4089–4105. doi:10.1021/acscatal.8b05171
- Thompson, R. C., Olson, Y., Mitchell, R. P., Davis, A., Rowland, S. J., John, A. W. G., et al. (2004). Lost at Sea: Where is All the Plastic? *Science* (80-) 304, 838. doi:10.1126/science.1094559
- Tournier, V., Topham, C. M., Gilles, A., David, B., Folgoas, C., Moya-Leclair, E., et al. (2020). An Engineered PET Depolymerase to Break Down and Recycle Plastic Bottles. *Nature* 580 (7802), 216–219. doi:10.1038/s41586-020-2149-4
- Urbanek, A. K., Rymowicz, W., and Mirończuk, A. M. (2018). Degradation of Plastics and Plastic-Degrading Bacteria in Cold marine Habitats. *Appl. Microbiol. Biotechnol.* 102 (18), 7669–7678. doi:10.1007/s00253-018-9195-y
- Waller, C. L., Griffiths, H. J., Waluda, C. M., Thorpe, S. E., Loaiza, I., Moreno, B., et al. (2017). Microplastics in the Antarctic marine System: an Emerging Area of Research. *Sci. Total Environ.* 598, 220–227. doi:10.1016/j.scitotenv.2017.03.283
- Wei, R., Breite, D., Song, C., Gräsig, D., Ploss, T., Hille, P., et al. (2019). Biocatalytic Degradation Efficiency of Postconsumer Polyethylene Terephthalate Packaging Determined by Their Polymer Microstructures. *Adv. Sci. (Weinh)* 6, 1900491. doi:10.1002/advs.201900491
- Wei, R., Oeser, T., Schmidt, J., Meier, R., Barth, M., Then, J., et al. (2016). Engineered Bacterial Polyester Hydrolases Efficiently Degrade Polyethylene Terephthalate Due to Relieved Product Inhibition. *Biotechnol. Bioeng.* 113 (8), 1658–1665. doi:10.1002/bit.25941
- Wilcox, C., Van Seville, E., and Hardesty, B. D. (2015). Threat of Plastic Pollution to Seabirds Is Global, Pervasive, and Increasing. *Proc. Natl. Acad. Sci. USA* 112 (38), 11899–11904. doi:10.1073/pnas.1502108112
- Yan, F., Wei, R., Cui, Q., Bornscheuer, U. T., and Liu, Y. J. (2020). Thermophilic Whole-Cell Degradation of Polyethylene Terephthalate Using Engineered *Clostridium Thermocellum*. *Microb. Biotechnol.* 14, 374–385. doi:10.1111/1751-7915.13580
- Yoon, M. G., Jeon, H. J., and Kim, M. N. (2012). Biodegradation of Polyethylene by a Soil Bacterium and AlkB Cloned Recombinant Cell. *J. Bioremediation Biodegradation* 3 (4), 145. doi:10.4172/2155-6199.1000145
- Yoshida, S., Hiraga, K., Takehana, T., Taniguchi, I., Yamaji, H., Maeda, Y., et al. (2016). A Bacterium that Degrades and Assimilates Poly(ethylene Terephthalate). *Science* 351 (6278), 1196–1199. doi:10.1126/science.aad6359
- Yu, K., Liu, C., Kim, B.-G., and Lee, D.-Y. (2015). Synthetic Fusion Protein Design and Applications. *Biotechnol. Adv.* 33, 155–164. doi:10.1016/j.biotechadv.2014.11.005

Conflict of Interest: The authors declare that the research was conducted in the absence of any commercial or financial relationships that could be construed as a potential conflict of interest.

Publisher's Note: All claims expressed in this article are solely those of the authors and do not necessarily represent those of their affiliated organizations, or those of the publisher, the editors and the reviewers. Any product that may be evaluated in this article, or claim that may be made by its manufacturer, is not guaranteed or endorsed by the publisher.

Copyright © 2021 Urbanek, Kosiorowska and Mirończuk. This is an open-access article distributed under the terms of the Creative Commons Attribution License (CC BY). The use, distribution or reproduction in other forums is permitted, provided the original author(s) and the copyright owner(s) are credited and that the original publication in this journal is cited, in accordance with accepted academic practice. No use, distribution or reproduction is permitted which does not comply with these terms.



Two Extracellular Poly(ϵ -caprolactone)-Degrading Enzymes From *Pseudomonas hydrolytica* sp. DSWY01^T: Purification, Characterization, and Gene Analysis

Linying Li^{1,2}, Xiumei Lin³, Jianfeng Bao¹, Hongmei Xia^{1,4} and Fan Li^{1,2*}

¹School of Life Sciences, Northeast Normal University, Changchun, China, ²Engineering Research Center of Glycoconjugates, Ministry of Education, Changchun, China, ³Changchun GeneScience Pharmaceutical Co., Ltd., Changchun, China, ⁴National Demonstration Center for Experimental Biology Education, Northeast Normal University, Changchun, China

OPEN ACCESS

Edited by:

Tajalli Keshavarz,
University of Westminster,
United Kingdom

Reviewed by:

Jayati Ray Dutta,
Birla Institute of Technology and
Science, India
Michail N. Isupov,
University of Exeter, United Kingdom

*Correspondence:

Fan Li
lif885@nenu.edu.cn

Specialty section:

This article was submitted to
Bioprocess Engineering,
a section of the journal
Frontiers in Bioengineering and
Biotechnology

Received: 15 December 2021

Accepted: 02 March 2022

Published: 18 March 2022

Citation:

Li L, Lin X, Bao J, Xia H and Li F (2022)
Two Extracellular Poly(ϵ -caprolactone)-
Degrading Enzymes From
Pseudomonas hydrolytica sp.
DSWY01^T: Purification,
Characterization, and Gene Analysis.
Front. Bioeng. Biotechnol. 10:835847.
doi: 10.3389/fbioe.2022.835847

Poly(ϵ -caprolactone) (PCL) is an artificial polyester with commercially promising application. In this study, two novel PCL-degrading enzymes named PCLase I and PCLase II were purified to homogeneity from the culture supernatant of an effective polyester-degrading bacterium, *Pseudomonas hydrolytica* sp. DSWY01^T. The molecular masses of PCLase I and PCLase II were determined to be 27.5 and 30.0 kDa, respectively. The optimum temperatures for the enzyme activities were 50 and 40°C, and the optimum pH values were 9.0 and 10.0, respectively. The two enzymes exhibited different physical and chemical properties, but both enzymes could degrade PCL substrates into monomers and oligomers. Weight loss detection and scanning electron microscopy revealed that PCLase I had more effective degradation ability than PCLase II. The genes of the two enzymes were cloned on the basis of the peptide fingerprint analysis results. The sequence analysis and substrate specificity analysis results showed that PCLase I and PCLase II were cutinase and lipase, respectively. Interface activation experiment also confirmed this conclusion. Structural analysis and modeling were further performed to obtain possible insights on the mechanism.

Keywords: poly(ϵ -caprolactone), *Pseudomonas hydrolytica*, PCL-degrading enzyme, cutinase, lipase

INTRODUCTION

In recent years, biodegradable and biocompatible polyesters such as poly(3-hydroxybutyrate) (PHB), poly(butylene succinate) (PBS), poly(ϵ -caprolactone) (PCL), and poly(lactic acid) (PLA) have been widely used in packaging, medical, and ecological applications due to the adverse effects of traditional plastics on the environment (Ikada and Tsuji, 2000; Gross and Kalra, 2002; Woodruff and Huttmacher, 2010; Gautam et al., 2013). Among these materials, PCL is a semi-crystalline linear aliphatic polyester that is ring-opening polymerized by ϵ -caprolactone (Lovera et al., 2007). The excellent properties of PCL, including its biocompatibility, low melting point, and high processability, make it useful in different industries.

PCL can be completely degraded by microorganisms in the environment, but the speed of its degradation varies due to environmental differences (Min et al., 2007; Cho et al., 2011). Various PCL-degrading bacteria or fungi have been isolated, and previous research have shown that PCL-degrading enzymes from microorganisms mediate PCL degradation (Murphy et al., 1996; Murphy et al., 1998;

Khatiwala et al., 2008; Sekiguchi et al., 2011; Abdel-Motaal et al., 2014). Previous works have reported that some PCL-degrading enzymes are lipases, whereas some are cutinases that degrade cutin under natural conditions. However, existing research still focuses mainly on the evaluation of PCL degradation performance, and the systematic investigation of PCL-degrading enzymes' mechanism is limited.

The biodegradation of PCL is an unusual feature considering that PCL is a chemically synthesized polymer. PCL's hydrolysis mechanism by various enzymes can provide valuable information for the synthesis of novel biodegradable materials. PCL-degrading enzymes derived from microorganisms are also environment-friendly catalysts that can be used in polyester recycling, and these enzymes can be effectively applied to the controlled degradation and recycling of PCL. Several studies have recently been conducted on the use of PCL degradation in blended materials for the preparation of porous scaffolds or modification of polymers (Kikkawa et al., 2010; Ju et al., 2014). The exploitation and application of different types of PCL-degrading enzymes are indispensable in these studies.

In a previous work, we screened a bacterial strain that can degrade several kinds of polyesters from activated sludge. The strain was identified to be a new species of *Pseudomonas* named *Pseudomonas hydrolytica* sp. DSWY01^T (Zhou et al., 2020). In the current study, two PCL-degrading enzymes were simultaneously purified from the strain; their enzymatic properties and PCL degradation behavior were examined. The possible mechanism of enzyme function was determined according to the enzyme's sequence and structural information.

MATERIALS AND METHODS

Chemicals, Materials, and Methods

PCL with a molecular weight of 80,000 g/mol was obtained from Solvay Interlox Ltd., and PCL film prepared by hot pressing was provided by Changchun Institute of Applied Chemistry. Pylsurf A210G was acquired from Daiichi Kogyo Seiyaku (Japan). DEAE Sepharose Fast Flow and Sephadex G-75 columns were obtained from GE Healthcare Bio-Sciences AB (Sweden). Unless otherwise stated, all chemicals used were of analytical grade.

Bacterial Strains, Plasmids, and Medium

P. hydrolytica DSWY01^T was screened and preserved in our laboratory. A mineral medium containing 0.1% PCL, 1.194% Na₂HPO₄·12H₂O, 0.554% KH₂PO₄, 0.1% NH₄Cl, 0.05% MgSO₄·7H₂O, and 0.0005% CaCl₂·2H₂O was used for the strain cultivation. The gene was cloned into plasmid pET-22b (+) and transformed into competent cells of *Escherichia coli* BL21 (DE3) for heterologous expression.

Purification of PCL-Degrading Enzymes

P. hydrolytica sp. DSWY01^T was fermented in PCL-emulsified medium at 37°C for 48 h, and the culture supernatant was obtained by centrifugation at 12,000 rpm for 20 min. After being dialyzed against 20 mM Na₂HPO₄-NaH₂PO₄ buffer (pH 7.6), the sample was applied to DEAE Sepharose Fast Flow (1.0 ×

20 cm) (pH 7.6) and eluted with a linear gradient of NaCl from 0 to 1.0 M. The unpurified active fractions were further applied to DEAE Sepharose Fast Flow (1.0 × 20 cm) (pH 9.0) or Sephadex G-75, which were eluted with NaCl (0–1.0 M) and 0.02 M phosphate buffer (pH 7.6), respectively. All of the steps were performed at 4°C.

Enzyme Assay and Protein Measurement

Initially, 0.1% (w/v) of PCL was emulsified with 0.01% (w/v) of Pylsurf A210G and used as the substrate. PCL-degrading enzyme at appropriate concentration was mixed with the substrate and kept at 50°C for 20 min to assay the activity. The decrease in the PCL emulsions' turbidity was measured using a UV spectrophotometer. One unit (U) of enzymatic activity was defined as the amount of enzyme required to reduce absorbance by 0.001 at 650 nm per min (Shirakura et al., 1986). The protein concentration was determined via Coomassie Brilliant Blue method, with bovine serum albumin as the standard.

Effects of pH and Temperature on the PCL-Degrading Activity of the Purified Enzymes

The PCL-degrading activity of the purified enzymes was assayed in 0.2 M buffers of various pHs (citrate buffer, pH 4–6; Na₂HPO₄-NaH₂PO₄ buffer, pH 6–8; Tris-HCl buffer, pH 8–9; Gly-NaOH buffer, pH 9–12) to determine the optimum pH. The optimal temperature was determined by measuring the enzyme's activity at temperatures ranging from 30 to 75°C. To evaluate the pH stability and thermostability of the purified enzymes, the enzyme was kept either at a pH ranging from 3 to 12 at 4°C for 24 h or at temperatures ranging from 20 to 70°C for 2 h; residual activity was then assayed under standard conditions.

Effects of Metal Ions, Inhibitors, and Organic Solvents on the PCL-Degrading Activity of the Purified Enzymes

Several metal ions, including Mg²⁺, Na⁺, Ca²⁺, Zn²⁺, Co²⁺, Fe³⁺, Fe²⁺, Cu²⁺, and Mn²⁺, ethylenediaminetetraacetic acid (EDTA), and PMSF, were added to the reaction with final concentrations of 1 mM or 10 mM to determine their effects on the PCL-degrading activity of the purified enzymes. The effects of various chemical reagents, including methanol, ethanol, glycerol, Tween-80, and Triton X-100, were assayed with final concentrations of 1% (v/v) and 10% (v/v). The activity of the enzyme incubated without any metal ion and chemical was considered 100%.

Substrate Specificity of the PCL-Degrading Enzymes

PLA, PHB, PBS, tributyrin, olive oil, apple peel cutin, and various *p*NP esters, including *p*NP acetate (C2), *p*NP butyrate (C4), *p*NP caprylate (C8), *p*NP laurate (C12), and *p*NP myristate (C14), were used as substrates to determine the substrate specificity of PCL-degrading enzyme. The degradation of PLA, PHB, PBS, and *p*NP esters was assayed using a spectrophotometer (Kazenwadel et al., 2012). The degradation of tributyrin and olive oil was determined

by titration (Prazeres et al., 2006), and the degradation of cutin was determined by weighing method.

Determination of Hydrolysis Products of the PCL-Degrading Enzymes

PCL-degrading enzymes were incubated with PCL-emulsified substrate at 50°C for 30 min, and the supernatant was collected and analyzed by tandem quadrupole mass spectrometry (MS) (Quattro Premier XE) with capillary voltage of 3.0 kV, cone voltage of 20 V, and source temperature of 110°C. The same sample incubated with enzyme inactivated by boiling was used as a control.

Degradation of Poly(ϵ -Caprolactone) Film by the PCL-Degrading Enzymes

PCL films (10 × 10 × 0.2 mm) were incubated with 1 ml of PCL-degrading enzyme (0.2 mg/ml) at 45°C. The enzyme solution was changed every 24 h, and the films were taken out at the same interval to be completely vacuum dried at room temperature. The film's weight was then measured to obtain the weight loss curve (Shi et al., 2020).

SEM Observations

The surface morphologies of the PCL films with different degradation degrees were observed through a Hitachi S570 SEM (Japan) at an acceleration voltage of 15 kV. The surface of each PCL film was sprayed with gold before analysis.

Gene Cloning and Sequence Analysis

The protein band of the PCL-degrading enzyme was excised from SDS-PAGE gel. After trypsin digestion, the sample was subjected to matrix-assisted laser desorption/ionization time-of-flight MS (MALDI-TOF-MS, 4,700 Proteomics Analyzer, Tianjin Biotechnology Inc., China). The results were compared and analyzed in MASCOT Peptide Mass Fingerprint database. Primers were designed on the basis of the sequence with 100% identity in the database, and the PCL-degrading enzyme gene fragments were amplified by PCR using strain genome as template. The domain of the PCL-degrading enzyme was predicted by Inter Pro Scan, and the signal peptide was predicted by Signal P4.1 Server. The secondary structure was predicted on the online software PSIPred, and the three-dimensional spatial structure was found in UniProt protein database or constructed using SWISS-MODEL.

RESULTS

Purification of PCL-Degrading Enzyme

Two PCL-degrading enzymes were purified to homogeneity from the culture supernatant of *P. hydrolytica* sp. DSWY01^T as described in "Materials and methods." The component named PCLase I was purified by a combination of DEAE-Sepharose chromatographic steps eluted at pH 7.6 and pH 9.0, respectively, and another component named PCLase II was obtained by a

combination of DEAE-Sepharose and further Sephadex G-75 column chromatography. **Table 1** summarizes the enzymes' purification. The molecular masses of PCLase I and PCLase II were determined by SDS-PAGE analysis to be 27.5 and 30.0 kDa, respectively (**Figure 1**).

Effects of Temperature and pH on the PCL-Degrading Activity of Purified Enzymes

The PCL-degrading activities of the purified enzymes were detected at different temperatures ranging from 20 to 70°C. The purified PCLase I and PCLase II exhibited the maximum degrading activity at 50 and 40°C, respectively (**Figure 2A**). The two PCL-degrading enzymes were moderately stable at temperatures up to 50°C. However, when the temperature increased to 60°C, the activity of PCLase I was almost lost after 2 h of incubation, whereas PCLase II retained more than 80% of the enzymatic activity (**Figure 2B**).

The optimum pH for PCLase I and PCLase II were observed to be pH 9.0 and pH 10.0, respectively, and almost no activity was detected under acidic conditions (**Figure 2C**). PCLase I and PCLase II were stable at pH conditions ranging from 6.0 to 12.0, and PCLase I showed remarkable stability at pH 12.0 with activity of approximately 100% (**Figure 2D**).

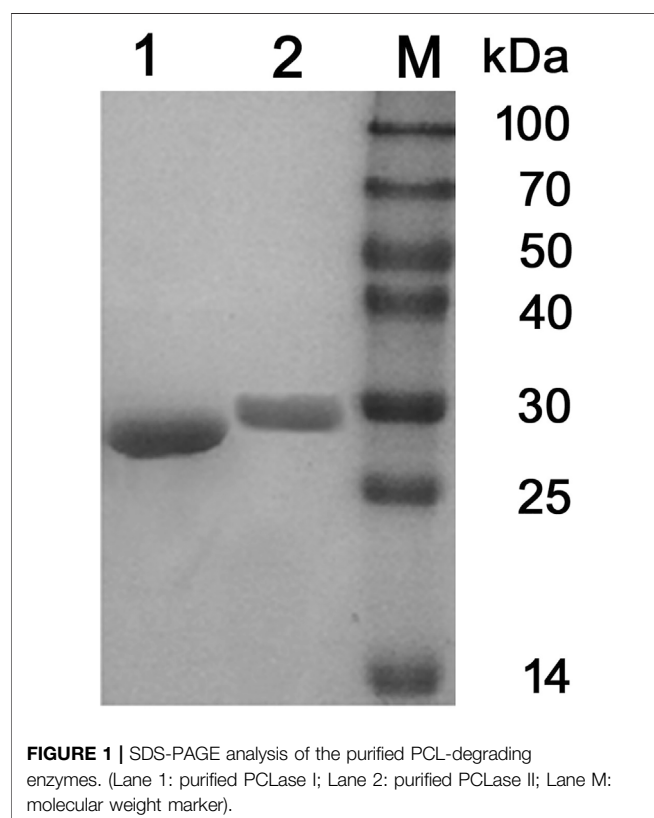
Effects of Metal Ions and Chemicals on the PCL-Degrading Activity of Purified Enzymes

The effects of various metal ions on the activity of the purified enzymes are listed in **Table 2**. The results showed that 1 mM of Mg²⁺ and Ca²⁺ significantly enhanced the activity of the two PCL-degrading enzymes. When the ion concentration was increased to 10 mM, these two ions had a stronger promotion on PCLase I, reaching 833 and 226% of the original activity. However, these ions significantly inhibited the activity of PCLase II with approximately 60% activity remaining. In addition, 1 mM of Fe³⁺ and Fe²⁺ significantly enhanced PCLase I's activity while inhibiting PCLase II's activity to be 80.77 and 91.16%, respectively. By contrast, Co²⁺ and Cu²⁺ enhanced the activity of PCLase II and inhibited that of PCLase I. Specifically, Co²⁺ completely inactivated PCLase I. These differences indicate the amino acids involved in the degradation function of the two enzymes may be different in property.

Table 3 shows the effects of chemicals on the purified enzymes. PCLase I and PCLase II were tolerant to tested organic solvents and had more than 80% activity remaining at 1 and 10% concentrations, respectively. Surfactant Triton X-100 strongly inhibited the activity of these two PCL-degrading enzymes, and almost no activity was detected even at 1% concentration. Tween-80 at 1% concentration slightly inhibited the activity of PCLase I, but almost completely inhibited that of PCLase II; when the concentration was increased to 10%, the inhibition on both enzymes was significant. These results indicated that the active centers of the two PCL-degrading enzymes may have a hydrophobic region that is necessary for their functions.

TABLE 1 | Purification of the PCL-degrading enzymes from the supernatant of *pseudomonas hydrolytica* sp. DSWY01^T.

Components	Steps	Total proteins (mg)	Total activities (U)	Specific activities (U/mg)	Purification (fold)	Yield (%)
Culture supernatant		120.9	19,945.5	164.9	1.0	100.0
lyophilized dialysate		43.9	12880.4	293.4	1.8	64.6
PCLase I	DEAE-Sepharose (pH7.6)	21.8	7,384.7	338.7	2.1	37.0
	DEAE-Sepharose (pH9.0)	4.5	3,728.9	828.6	5.0	18.7
PCLase II	DEAE-Sepharose (pH7.6)	18.0	5,884.7	326.9	2.0	29.5
	Sephadex G-75	3.9	2,578.9	661.3	4.0	12.9



Substrate Specificity of the Purified Enzymes

The activities of PCLase I and PCLase II were tested on several representative substrates. **Table 4** shows that aside from PCL, these two PCL-degrading enzymes could also degrade PBS, *p*NP ester, tributyrin, and olive oil, while neither enzyme degraded PLA. In addition, PCLase I degraded crude cutin and did not degrade PHB; by contrast, PCLase II degraded PHB while had no degrading activity on cutin. These results indicated that PCLase I may be a cutinase, whereas PCLase II is an esterase that does not degrade cutin.

Determination of Enzymatic Hydrolysis Products

The products of PCL degradation by purified PCL-degrading enzymes were identified by MS. **Figure 3** shows that unlike the control group, monomers (peak at *m/z* 131.0), dimers (peak at

m/z 245.3), trimers (peak at *m/z* 359.5), and tetramers (peak at *m/z* 473.6) were detected in the samples. These results indicated that the catalytically active centers of the two purified PCL-degrading enzymes may be able to bind to long-chain substrates containing several PCL monomers and cleave the ester bonds in them. This mode is different with several reported PHB depolymerases which can only cleave the substrate from the chain end and release monomers or dimers (Zhou et al., 2009; Wang et al., 2012; Li et al., 2018).

Degradation and SEM Observation of the PCL Films Degraded by Purified Enzymes

The weight loss of the films caused by enzymatic hydrolysis can be used as an index to measure the enzymatic degradation ability. **Figure 4** presents the weight loss plot of the PCL films with degradation time. The relationship between the weight loss of the PCL films and degradation time was close to linear for PCLase I, and the loss of the films degraded by PCLase I reached 70% after 3 days of incubation. This degradation trend is consistent with the result of cutinase degradation of the PCL film reported by Shi (Shi et al., 2020). However, the degradation profile of PCLase II is different from that of PCLase I. Its plot could be divided into a slow stage (0–3 days) and a fast stage (3–8 days) (**Figure 4**). The weight loss was achieved at approximately 75% after 8 days of incubation. These results showed that different enzymes have varying degradation rates for PCL solid materials, which may be attributed to different enzymatic hydrolysis modes. Shi also has similar findings, but the difference from the results of the current study is that the speed of PCL degradation by *Candida antarctica* lipase that Shi used was initially fast and then slowed down (Shi et al., 2020); additionally, the specific mechanism requires further research.

SEM micrographs of the PCL films degraded by the two purified enzymes are shown in **Figure 5**. The PCL film's surface was smooth before enzymatic hydrolysis. However, as the enzymatic hydrolysis time increased; the film surface was damaged to varying degrees. The appearance of spherulites in the degradation process showed that the PCL-degrading enzyme preferentially degrades the film's amorphous regions, and then degrades the crystalline regions. The SEM results also showed that aside from the degradation rates of PCLase I and PCLase II, their degradation modes also vary. **Figure 5B** and **5D** show that when the degradation rate was 30%, the film degraded by PCLase I appeared to be a lamellar structure with no spherulites, whereas the film degraded by PCLase II presented spherulites, suggesting that the action of PCLase II may be deeper.

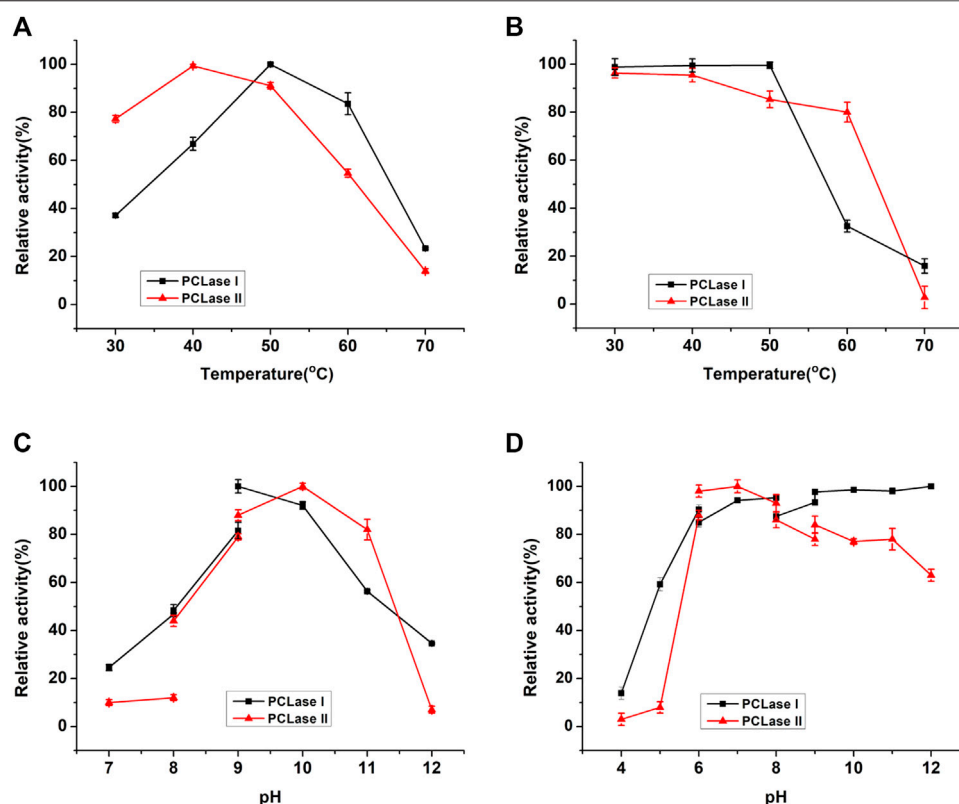


FIGURE 2 | Effects of temperature and pH on the enzymatic activity of the purified PCL-degrading enzymes. **(A)** Temperature dependence of enzymatic activity; **(B)** Thermostability of the purified enzymes; **(C)** pH dependence of enzymatic activity; **(D)** Stability of the purified enzymes at different pH conditions.

TABLE 2 | Effects of metal ions on the activity of the two PCL-degrading enzymes.

Metal ions	Residual activity (%)			
	PCLase I		PCLase II	
	1 mM	10 mM	1 mM	10 mM
Mg ²⁺	169.80 ± 4.90	833.60 ± 3.20	220.57 ± 0.90	61.06 ± 2.39
Na ⁺	106.60 ± 0.60	88.00 ± 1.20	115.50 ± 0.49	64.98 ± 2.21
Ca ²⁺	149.00 ± 1.20	226.30 ± 2.30	132.55 ± 1.64	66.80 ± 2.73
Zn ²⁺	17.30 ± 1.00	-	22.48 ± 0.57	-
Co ²⁺	0	-	110.38 ± 0.71	-
Fe ³⁺	227.80 ± 16.50	-	80.77 ± 0.99	-
Fe ²⁺	166.00 ± 1.90	-	91.16 ± 0.54	-
Cu ²⁺	88.20 ± 0.50	-	108.99 ± 0.36	-
Mn ²⁺	41.50 ± 2.40	-	99.37 ± 1.18	-

- Means that the effect of the metal ion could not be detected for the precipitate.

Cloning, Expression, and Sequence Analysis of PCL-Degrading Enzymes

The two purified PCL-degrading enzymes were analyzed by MALDI-TOF-MS. The peptide fingerprints showed that PCLase I had 100% similarity to a hypothetical protein (WP_004373894.1) from *Pseudomonas mendocina* ymp and that PCLase II had 100% similarity to a lactonizing lipase (WP_003239806.1) from the same strain. The primers were designed according to the homologous

sequence and applied for PCR amplification using the genome of *P. hydrolytica* sp. DSWY01^T as template. The sequencing results showed that the amplified fragment sequences were consistent with the homologous sequence derived from *P. mendocina* ymp. Amplified genes, excluding the putative signal peptide sequence, were cloned and expressed in *E. coli* (DE3). The detection showed that the expressed recombinant enzymes have PCL-degrading activity, and their molecular weights were consistent with the

TABLE 3 | Effects of chemicals on the activity of the two PCL-degrading enzymes.

Organic solvent	Residual activity (%)			
	PCLase I		PCLase II	
	1%	10%	1%	10%
Methanol	84.50 \pm 0.49	128.10 \pm 1.50	95.34 \pm 0.60	87.06 \pm 1.35
Ethanol	96.60 \pm 0.80	125.50 \pm 3.30	91.71 \pm 0.56	83.42 \pm 0.60
Glycerol	108.80 \pm 1.30	108.10 \pm 1.40	95.19 \pm 1.27	81.95 \pm 1.43
Tween-80	86.80 \pm 0.20	0	1.85 \pm 0.72	1.78 \pm 1.93
Triton X-100	0	0	0.98 \pm 0.15	0.63 \pm 0.45

TABLE 4 | Substrate specificity of the two PCL-degrading enzymes.

Substrate	PCLase I	PCLase II
PCL	+	+
PHB	–	+
PLA	–	–
PBS	+	+
pNPC2-C16	+	+
Tributyrin	+	+
Olive oil	+	+
Crude cutin	+	–

+ Means that the enzyme has the degrading ability, and – means no degrading ability.

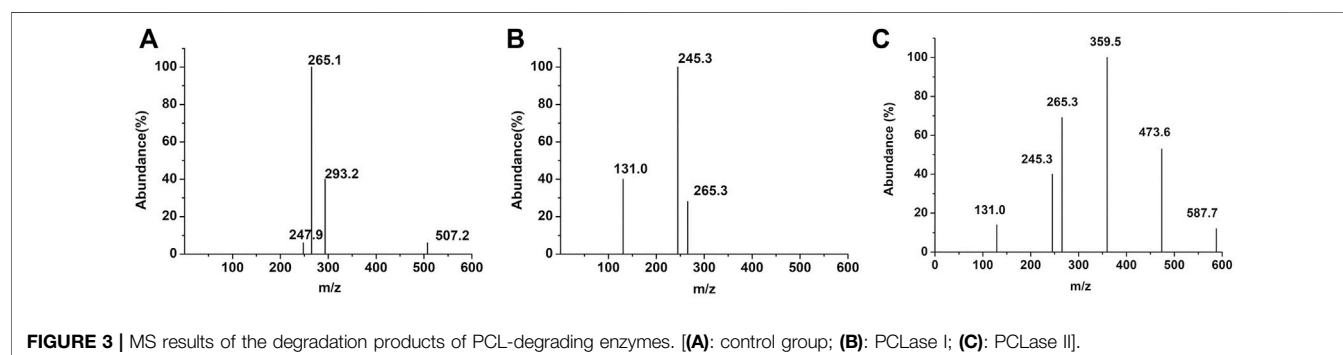
previously purified PCLase I and PCLase II. This result indicated that the two DNA fragments (i.e., *pcl1* and *pcl2*) obtained through peptide fingerprinting and homologous amplification were indeed genes encoding PCLase I and PCLase II.

Pcl1 comprised an ORF of 843 nucleotides encoded with a protein of 280 residues, with a theoretical molecular weight of 29.63 kDa and a theoretical pI of 8.55, predicted with a 22-amino acid signal peptide at the N-terminal region. *Pcl2* comprised an ORF of 954 nucleotides encoded with a protein of 317 residues, with a theoretical molecular weight of 33.20 kDa and a theoretical pI of 6.59, predicted with a 24-amino acid signal peptide at the N-terminal region. Both enzymes belonged to α/β hydrolase family and contained catalytic triad composed of Ser148-Asp198-His228 and Ser111-Asp261-His283 in the active center, respectively. The two enzymes both had a single catalytic structure with no substrate binding domain, which is different from solid-phase substrate hydrolases, such as cellulase and polyhydroxybutyrate depolymerase (Mattinen et al., 1997; Shin et al., 2002; Hiraishi et al., 2006).

DISCUSSION

P. hydrolytica sp. DSWY01^T is a strain screened in our laboratory in a previous research. This strain has been found to have the ability to degrade polyesters, including PHB and PLA (Zhou et al., 2020). In the current study, two PCL-degrading enzymes were purified from the strain's fermentation supernatant. These results indicated that the strain had good application potential in the degradation, recycling, and transformation of polymer polyesters.

Microorganisms usually secrete isoenzymes to synergistically degrade macro-molecules *in vitro*. However, considering that PCL is a chemically synthesized polyester, the original function of the PCL-degrading enzymes secreted by microorganisms should not be to degrade PCL. Several enzymes secreted by the strain that degrade natural polyester more likely happened to have relatively broad substrate specificity, which recognized the PCL substrate and further broke the ester bond. The substrate specificity analysis results showed that both PCL-degrading enzymes degraded ester substrates, including olive oil and tributyrin; PCLase I significantly degraded the rough cutin of apple peel, whereas PCLase II had no such degradation ability. In addition, sequence alignment showed that PCLase II may be a lipase and that PCLase I was most similar to a hypothetical protein with an unidentified function. Considering these characteristics of the enzymes, we speculated that these two PCL-degrading enzymes possibly belong to cutinase and lipase families, respectively. To further study the properties of the PCL-degrading enzymes, we used tributyrin as substrate in an interface activity experiment. As shown in **Figure 6**, the



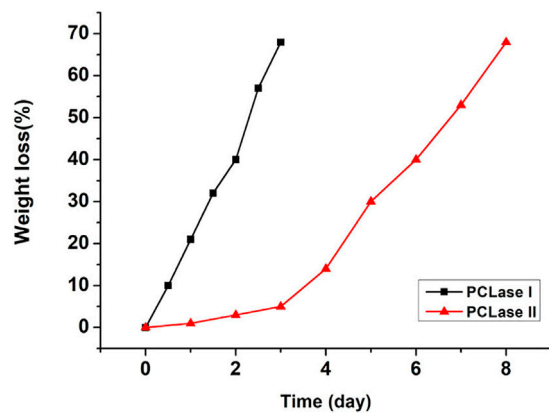


FIGURE 4 | Weight loss of the degraded PCL films.

degradation activity of PCLase I increased with the increase of the substrate concentration and showed no interface activation effect; however, the activity of PCLase II increased sharply when the tributyrin concentration was higher than 0.8 mM, showing a typical interface activation effect. This results support earlier suggestion that PCLase II is a lipase whereas PCLase I is a cutinase.

Previous research found that lipases usually have catalytic triad composed of nucleophilic-histidine acid residues; and in its open conformation, the “lid structure” at the top of the active site enables the solvent to approach the catalytic cavity centre (Brzozowski et al., 1991; Grochulski et al., 1994; Brzozowski et al., 2000). By contrast, the active region of cutinase is directly exposed to the top of the three-dimensional structure and can directly contact and interact with the substrate. In the present study, the enzymes’ sequences were blasted in the database, and the results showed that PCLase I is an enzyme with a known structure (PDB No. 2fx5) (Sibille et al., 2006) (**Figure 7A**) and that although PCLase II has no structural information, PCLase II is similar to the lipase PAL (PDB No. 1ex9.1) derived from *Pseudomonas aeruginosa* PAO1 with the sequence identity of 82.75%. We modeled the structure of PCLase II and then compared the differences in the structure of the two PCL-degrading enzymes interacting with the substrate.

Lipase PAL (1ex9.1.A) was used as a template for homologous modeling in SWISS-MODEL. The sequence alignment results between PAL and PCLase II showed that Amino Acids 30 to 317 of PCLase II corresponded to amino acids 1 to 285 of the template PAL. Unlike the α -helix in PAL, Amino Acids 226 to 232 of PCLase II formed a β -sheet. However, other components corresponded well to the template. A previous study revealed that PAL has a movable helical structure formed by amino acids 125–147 (Nardini et al.,

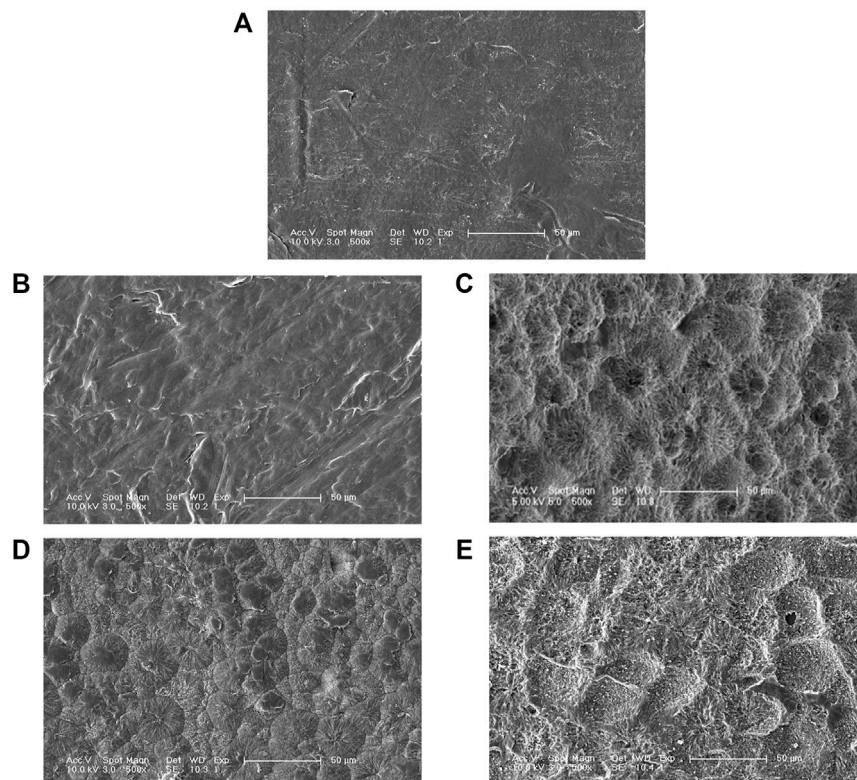


FIGURE 5 | SEM micrographs of undegraded PCL (**A**), degraded by PCLase I (**B**) 36 h; (**C**) 72 h], and PCLase II [(**D**) 5 days; (**E**) 8 days].

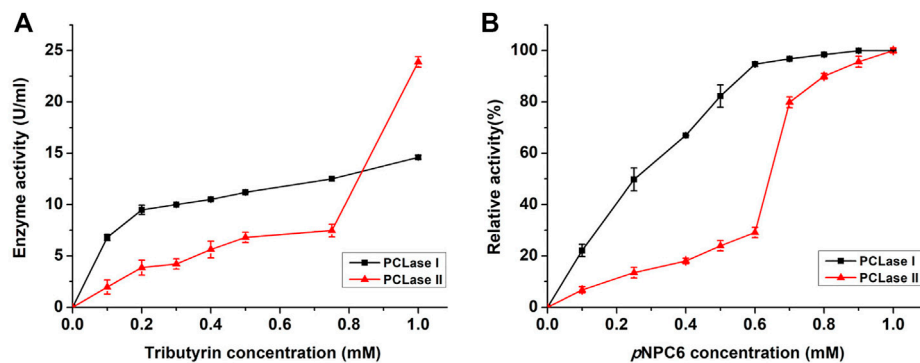


FIGURE 6 | Effects of tributyrin and pNP ester on PCL-degrading enzymes. Tributyrin (A) and pNP esters (B) were used as substrates to detect the activity of PCLase I and PCLase II under different concentrations.

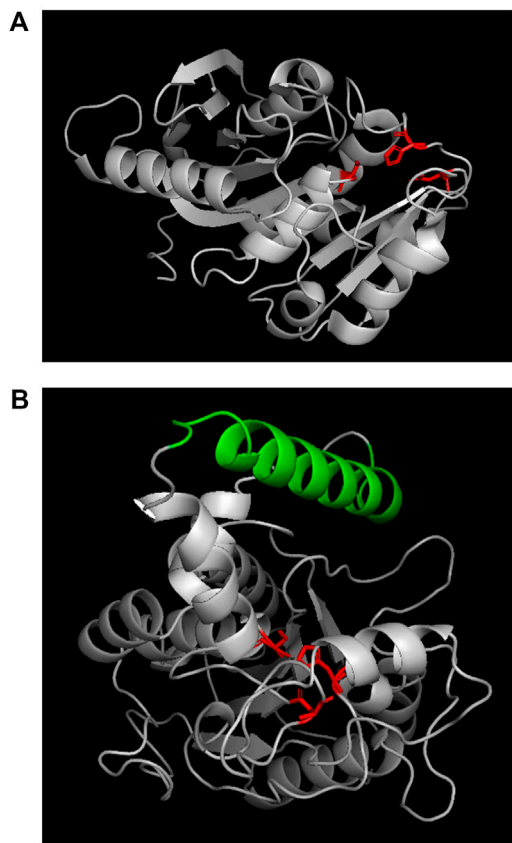


FIGURE 7 | Structures of PCLase I (A) and modeled PCLase II (B). Catalytic triad is marked in red and "lid structure" is colored in green.

2000). This structure and the surrounding structure are the key "lid structures" that can be used to control the exposure of the enzyme active site, which makes the solvent and the substrate enter the cavity where the active site is located. The helical structure of PCLase II's 155–180 amino acids is highly similar to PAL's "lid structure" (Figure 7B). Combined with PCLase II's properties, we speculate

that PCLase II belongs to lipase and that its "lid structure" may be related to the "interface activation" effect. In addition, this lid structure may also play a steric hindrance, preventing the long-chain polyester from entering the active pocket of the enzyme. This limitation may be the reason why the degradation efficiency of PCLase II to PCL film was lower than that of PCLase I.

The MS analysis results showed the presence of dimers, trimers, and tetramers in the enzymatic hydrolysis products, suggesting that these enzymes can bind to long-chain polyesters. Moreover, these enzymes can also degrade PBS polyester, indicating that the enzymes have excellent substrate versatility, which makes these enzymes have the potential to be used in the degradation and recycling of mixed biodegradable polyesters. Moreover, these properties of enzymes are valuable to the development and synthesis of derivatized polyesters based on PCL or PBS structures. In addition, these properties of enzymes make the degradation of derivatized polyesters based on PCL or PBS structures possible, which has guiding significance for the development of more types of biodegradable polyesters.

DATA AVAILABILITY STATEMENT

The original contributions presented in the study are included in the article/Supplementary Material, further inquiries can be directed to the corresponding author.

AUTHOR CONTRIBUTIONS

FL designed and supervised the study. LL, XL, and JB performed the experiments. FL, LL, and HX analyzed the data and wrote the manuscript. All authors revised the manuscript and approved the final manuscript.

FUNDING

This work was supported by the National Natural Science Foundation of China (No. 31870048).

REFERENCES

- Abdel-Motaal, F. F., El-Sayed, M. A., El-Zayat, S. A., and Ito, S.-I. (2014). Biodegradation of Poly (ϵ -Caprolactone) (PCL) Film and Foam Plastic by *Pseudozyma Japonica* Sp. nov., a Novel Cutinolytic Ustilaginomycetous Yeast Species. *Biotech.* 4, 507–512. doi:10.1007/s13205-013-0182-9
- Brzozowski, A. M., Derewenda, U., Derewenda, Z. S., Dodson, G. G., Lawson, D. M., Turkenburg, J. P., et al. (1991). A Model for Interfacial Activation in Lipases from the Structure of a Fungal Lipase-Inhibitor Complex. *Nature* 351, 491–494. doi:10.1038/351491a0
- Brzozowski, A. M., Savage, H., Verma, C. S., Turkenburg, J. P., Lawson, D. M., Svendsen, A., et al. (2000). Structural Origins of the Interfacial Activation in *Thermomyces (Humicola) Lanuginosa* Lipase. *Biochemistry* 39, 15071–15082. doi:10.1021/bi0013905
- Cho, H. S., Moon, H. S., Kim, M., Nam, K., and Kim, J. Y. (2011). Biodegradability and Biodegradation Rate of Poly(caprolactone)-Starch Blend and Poly(butylene Succinate) Biodegradable Polymer under Aerobic and Anaerobic Environment. *Waste Manag.* 31, 475–480. doi:10.1016/j.wasman.2010.10.029
- Gautam, S., Dinda, A. K., and Mishra, N. C. (2013). Fabrication and Characterization of PCL/gelatin Composite Nanofibrous Scaffold for Tissue Engineering Applications by Electrospinning Method. *Mater. Sci. Eng. C* 33, 1228–1235. doi:10.1016/j.msec.2012.12.015
- Grochulski, P., Li, Y., Schrag, J. D., and Cygler, M. (1994). Two Conformational States of *Candida Rugosalipase*. *Protein Sci.* 3, 82–91. doi:10.1002/pro.5560030111
- Gross, R. A., and Kalra, B. (2002). Biodegradable Polymers for the Environment. *Science* 297, 803–807. doi:10.1126/science.297.5582.803
- Hiraishi, T., Hirahara, Y., Doi, Y., Maeda, M., and Taguchi, S. (2006). Effects of Mutations in the Substrate-Binding Domain of Poly[(R)-3-Hydroxybutyrate] (PHB) Depolymerase from *Ralstonia Pickettii* T1 on PHB Degradation. *Appl. Environ. Microbiol.* 72, 7331–7338. doi:10.1128/aem.01187-06
- Ikada, Y., and Tsuji, H. (2000). Biodegradable Polyesters for Medical and Ecological Applications. *Macromol. Rapid Commun.* 21, 117–132. doi:10.1002/(sici)1521-3927(20000201)21:3<117::aid-marc117>3.0.co;2-x
- Ju, D., Han, L., Li, F., Chen, S., and Dong, L. (2014). Poly(ϵ -caprolactone) Composites Reinforced by Biodegradable Poly(3-Hydroxybutyrate-Co-3-Hydroxyvalerate) Fiber. *Int. J. Biol. Macromolecules* 67, 343–350. doi:10.1016/j.ijbiomac.2014.03.048
- Kazenwadel, C., Eiben, S., Maurer, S., Beutler, H., Wetzl, D., Hauer, B., et al. (2012). Thiol-functionalization of Acrylic Ester Monomers Catalyzed by Immobilized *Humicola Insolens* Cutinase. *Enzyme Microb. Technol.* 51, 9–15. doi:10.1016/j.enzmictec.2012.03.007
- Khatiwala, V. K., Shekhar, N., Aggarwal, S., and Mandal, U. K. (2008). Biodegradation of Poly(ϵ -Caprolactone) (PCL) Film by *Alcaligenes Faecalis*. *J. Polym. Environ.* 16, 61–67. doi:10.1007/s10924-008-0104-9
- Kikkawa, Y., Takahashi, M., Aoyagi, M., Suga, H., Kanesato, M., and Abe, H. (2010). Surface Patterning of Poly(ϵ -Caprolactone): Epitaxial Crystallization and Enzymatic Degradation. *Macromol. Chem. Phys.* 211, 2480–2483. doi:10.1002/macp.201000358
- Li, F., Guo, Z., Wang, N., Xia, H., Liu, D., and Chen, S. (2019). Biodegradation of Poly(3-Hydroxybutyrate)-Derived Polymers with Different 4-hydroxybutyrate Fractions by a Novel Depolymerase from *Paecilomyces* sp. 1407. *Polym. Degrad. Stab.* 159, 107–115. doi:10.1016/j.polymdegradstab.2018.11.016
- Lovera, D., Márquez, L., Balsamo, V., Taddei, A., Castelli, C., and Müller, A. J. (2007). Crystallization, Morphology, and Enzymatic Degradation of Polyhydroxybutyrate/Polycaprolactone (PHB/PCL) Blends. *Macromol. Chem. Phys.* 208, 924–937. doi:10.1002/macp.200700011
- Mattinen, M.-L., Linder, M., Teleman, A., and Annala, A. (1997). Interaction between Cellohexose and Cellulose Binding Domains from *Trichoderma Reesei* Cellulases. *FEBS Lett.* 407, 291–296. doi:10.1016/s0014-5793(97)00356-6
- Murphy, C. A., Cameron, J. A., Huang, S. J., and Vinopal, R. T. (1998). A Second Polycaprolactone Depolymerase from *Fusarium*, a Lipase Distinct from Cutinase. *Appl. Microbiol. Biotechnol.* 50, 692–696. doi:10.1007/s002530051352
- Murphy, C. A., Cameron, J. A., Huang, S. J., and Vinopal, R. T. (1996). *Fusarium* Polycaprolactone Depolymerase Is Cutinase. *Appl. Environ. Microbiol.* 62, 456–460. doi:10.1128/AEM.62.2.456-460.1996
- Nardini, M., Lang, D. A., Liebeton, K., Jaeger, K.-E., and Dijkstra, B. W. (2000). Crystal Structure of *Pseudomonas aeruginosa* Lipase in the Open Conformation. *J. Biol. Chem.* 275, 31219–31225. doi:10.1074/jbc.m003903200
- Prazeres, J. N. d., Cruz, J. A. B., and Pastore, G. M. (2006). Characterization of Alkaline Lipase from *Fusarium Oxysporum* and the Effect of Different Surfactants and Detergents on the Enzyme Activity. *Braz. J. Microbiol.* 37, 505–509. doi:10.1590/S1517-83822006000400019
- Sekiguchi, T., Saika, A., Nomura, K., Watanabe, T., Watanabe, T., Fujimoto, Y., et al. (2011). Biodegradation of Aliphatic Polyesters Soaked in Deep Seawaters and Isolation of Poly(ϵ -Caprolactone)-Degrading Bacteria. *Polym. Degrad. Stab.* 96, 1397–1403. doi:10.1016/j.polymdegradstab.2011.03.004
- Shi, K., Jing, J., Song, L., Su, T., and Wang, Z. (2020). Enzymatic Hydrolysis of Polyester: Degradation of Poly(ϵ -Caprolactone) by *Candida antarctica* Lipase and *Fusarium Solani* Cutinase. *Int. J. Biol. Macromolecules* 144, 183–189. doi:10.1016/j.ijbiomac.2019.12.105
- Shin, E.-S., Yang, M.-J., Jung, K. H., Kwon, E.-J., Jung, J. S., Park, S. K., et al. (2002). Influence of the Transposition of the Thermostabilizing Domain of *Clostridium Thermocellum* Xylanase (XynX) on Xylan Binding and Thermostabilization. *Appl. Environ. Microbiol.* 68, 3496–3501. doi:10.1128/AEM.68.7.3496-3501.2002
- Shirakura, Y., Fukui, T., Saito, T., Okamoto, Y., Narikawa, T., Koide, K., et al. (1986). Degradation of Poly(3-Hydroxybutyrate) by Poly(3-Hydroxybutyrate) Depolymerase from *Alcaligenes Faecalis* T1. *Biochim. Biophys. Acta (Bba) - Gen. Subjects* 880, 46–53. doi:10.1016/0304-4165(86)90118-2
- Sibille, N., Favier, A., Azuaga, A. I., Ganshaw, G., Bott, R., Bonvin, A. M. J. J., et al. (2006). Comparative NMR Study on the Impact of point Mutations on Protein Stability of *Pseudomonas Mendocinalipase*. *Protein Sci.* 15, 1915–1927. doi:10.1110/ps.062213706
- Tseng, M., Hoang, K.-C., Yang, M.-K., Yang, S.-F., and Chu, W. S. (2007). Polyester-degrading Thermophilic Actinomycetes Isolated from Different Environment in Taiwan. *Biodegradation* 18, 579–583. doi:10.1007/s10532-006-9089-z
- Wang, Y., Li, F., Wang, Z.-y., Liu, D.-b., Xia, H.-m., Liu, L.-f., et al. (2012). Purification and Properties of an Extracellular Polyhydroxybutyrate Depolymerase from *Pseudomonas Mendocina* DSWY0601. *Chem. Res. Chin. U.* 28, 459–464. doi:10.1007/s11274-012-1048-8
- Woodruff, M. A., and Huttmacher, D. W. (2010). The Return of a Forgotten Polymer-Polycaprolactone in the 21st century. *Prog. Polym. Sci.* 35, 1217–1256. doi:10.1016/j.progpolymsci.2010.04.002
- Zhou, H., Wang, Z., Chen, S., Liu, D., and Xia, H. (2008). Purification and Characterization of Extracellular Poly(β -Hydroxybutyrate) Depolymerase from *Penicillium* sp. DS9701-D2. *Polymer-Plastics Technol. Eng.* 48, 58–63. doi:10.1080/03602550802539627
- Zhou, S., Wang, Y., Xia, H., Liu, D., Chen, S., and Li, F. (2020). *Pseudomonas Hydrolytica* Sp. nov., Multiple Polymer-Degrading Bacteria Isolated from Soil in China. *Int. J. Syst. Evol. Microb.* 70, 3049–3054. doi:10.1099/ijsem.0.004129

Conflict of Interest: XL was employed by the company Changchun GeneScience Pharmaceutical Co., Ltd.

The remaining authors declare that the research was conducted in the absence of any commercial or financial relationships that could be construed as a potential conflict of interest.

Publisher's Note: All claims expressed in this article are solely those of the authors and do not necessarily represent those of their affiliated organizations, or those of the publisher, the editors and the reviewers. Any product that may be evaluated in this article, or claim that may be made by its manufacturer, is not guaranteed or endorsed by the publisher.

Copyright © 2022 Li, Lin, Bao, Xia and Li. This is an open-access article distributed under the terms of the Creative Commons Attribution License (CC BY). The use, distribution or reproduction in other forums is permitted, provided the original author(s) and the copyright owner(s) are credited and that the original publication in this journal is cited, in accordance with accepted academic practice. No use, distribution or reproduction is permitted which does not comply with these terms.



Bioconversion of Terephthalic Acid and Ethylene Glycol Into Bacterial Cellulose by *Komagataeibacter xylinus* DSM 2004 and DSM 46604

Asiyah Esmail^{1,2}, Ana T. Rebocho^{1,2}, Ana C. Marques³, Sara Silvestre³, Alexandra Gonçalves³, Elvira Fortunato³, Cristiana A. V. Torres^{1,2}, Maria A. M. Reis^{1,2} and Filomena Freitas^{1,2*}

¹Associate Laboratory Institute for Health and Bioeconomy, School of Science and Technology, NOVA University Lisbon, Caparica, Portugal, ²UCIBIO—Applied Molecular Biosciences Unit, Department of Chemistry, School of Science and Technology, NOVA University Lisbon, Caparica, Portugal, ³Department of Materials Science, School of Science and Technology, NOVA University Lisbon and CEMOP/UNINOVA, Caparica, Portugal

OPEN ACCESS

Edited by:

Martin Koller,
University of Graz, Austria

Reviewed by:

Carla Silva,
University of Minho, Portugal
Stanislav Obruca,
Brno University of Technology,
Czechia
Marina Tišma,
University of Osijek, Croatia

*Correspondence:

Filomena Freitas
a4406@fct.unl.pt

Specialty section:

This article was submitted to
Bioprocess Engineering,
a section of the journal
Frontiers in Bioengineering and
Biotechnology

Received: 12 January 2022

Accepted: 14 March 2022

Published: 05 April 2022

Citation:

Esmail A, Rebocho AT, Marques AC, Silvestre S, Gonçalves A, Fortunato E, Torres CAV, Reis MAM and Freitas F (2022) Bioconversion of Terephthalic Acid and Ethylene Glycol Into Bacterial Cellulose by *Komagataeibacter xylinus* DSM 2004 and DSM 46604. *Front. Bioeng. Biotechnol.* 10:853322. doi: 10.3389/fbioe.2022.853322

Komagataeibacter xylinus strains DSM 2004 and DSM 46604 were evaluated for their ability to grow and produce bacterial cellulose (BC) upon cultivation on terephthalic acid (TA) and ethylene glycol (EG), which are monomers of the petrochemical-derived plastic polyethylene terephthalate (PET). Both strains were able to utilize TA, EG, and their mixtures for BC synthesis, with different performances. *K. xylinus* DSM 2004 achieved higher BC production from TA (0.81 ± 0.01 g/L), EG (0.64 ± 0.02 g/L), and TA + EG mixtures (0.6 ± 0.1 g/L) than strain DSM 46604. The latter was unable to utilize EG as the sole carbon source and reached a BC production of 0.16 ± 0.01 g/L and 0.23 ± 0.1 g/L from TA alone or TA + EG mixtures, respectively. Further supplementing the media with glucose enhanced BC production by both strains. During cultivation on media containing TA and EG, rapid pH drop due to metabolization of EG into acidic compounds led to some precipitation of TA that was impregnated into the BC pellicles. An adaptation of the downstream procedure involving BC dissolution in NaOH was used for the recovery of pure BC. The different medium composition tested, as well as the downstream procedure, impacted the BC pellicles' physical properties. Although no variation in terms of the chemical structure were observed, differences in crystallinity degree and microstructure of the produced BC were observed. The BC produced by *K. xylinus* DSM 2004 had a higher crystallinity (19–64%) than that of the strain DSM 46604 (17–53%). Moreover, the scanning electron microscopy analysis showed a higher fiber diameter for *K. xylinus* DSM 2004 BC (46–56 nm) than for *K. xylinus* DSM 46604 (37–49 nm). Dissolution of BC in NaOH did not influence the chemical structure; however, it led to BC conversion from type I to type II, as well as a decrease in crystallinity. These results demonstrate that PET monomers, TA and EG, can be upcycled into a value-added product, BC, presenting an approach that will contribute to lessening the environmental burden caused by plastic disposal in the environment.

Keywords: bacterial cellulose, bioconversion, PET, terephthalic acid, ethylene glycol

INTRODUCTION

Polyethylene terephthalate (PET) is a polyester of terephthalic acid (TPA) and ethylene glycol (EG) monomers. PET is the most manufactured thermoplastic globally, due to its remarkable material properties, such as high tensile strength, great chemical resistance, elasticity, electrical insulating properties, and thermostability (Robertson, 2014), which grant its versatility to be used in many industries, such as packaging, textiles, electrical and electronics, and the automotive industry (Webb et al., 2013). However, PET is incredibly resistant to hydrolytic or enzymatic degradation, presenting as a considerable recalcitrant pollutant in the environment and contributing to the alarming worldwide plastic accumulation and pollution problem (Sang et al., 2020). Physical treatments, such as thermal and mechanical procedures, coupled with exposure to chemicals, namely, acids or alkali, are used to depolymerize PET into its monomers (TA and EG) or into low Mw oligomers (Thiounn and Smith, 2020). The resulting TA can be purified and utilized for producing recycled PET, thus valorizing waste PET materials.

The resulting plastic monomers are more easily degraded by microorganisms due to their higher water solubility than the original high molecular weight polymers. Therefore, they can alternatively be used by some bacteria as feedstocks for the production of value-added microbial products, such as polyhydroxyalkanoates (PHAs) (Tiso et al., 2021) and bacterial cellulose (BC) (Zhang et al., 2021). Although this strategy is still underexplored, requiring extensive research for its implementation, it arises as a very promising approach that will simultaneously contribute to mitigate the plastic waste problem, enabling plastic waste to become a resource rather than an environmental burden by adding value to them (Nikolaivits et al., 2021).

BC is a natural polysaccharide synthesized by some species of bacteria, including Gram-negative (e.g., *Acetobacter*, *Gluconacetobacter* (presently *Komagataeibacter*), and *Rhizobium*), as well as Gram-positive bacterial species such as *Sarcina ventriculi* (Carvalho et al., 2019). Among the aforementioned bacteria, *Komagataeibacter* is known to be the most efficient to produce high-quality BC for commercial use (Ruka et al., 2012). Both BC and plant-based cellulose are chemically composed of glucose molecules connected *via* acetal linkages between C1 and C4 carbons (Klemm et al., 2001). Still, there are major differences between them in terms of purity, macromolecular properties, and characteristics. Relative to plant-based cellulose, BC shows higher purity, degree of polymerization, water uptake capacity, crystallinity (up to 96%), biocompatibility, and Young's modulus (Klemm et al., 2001; Ul-Islam et al., 2012). These distinctive properties favor BC over plant-based cellulose for an array of applications in the food, cosmetics, optoelectronics, and textile industry, as well as in the biomedical field (Fortunato et al., 2016; Carvalho et al., 2019; Wang et al., 2019; Marques et al., 2021).

In accordance with this, this work assessed the capability of *Komagataeibacter xylinus* strains DSM 2004 and DSM 46604 to utilize TA and EG as carbon sources for BC production. Media

supplemented with TA and/or EG were tested for the static cultivation of both strains, as well as the same mixtures supplemented with glucose as a co-substrate. The BC pellicles obtained were extracted and characterized in terms of their physical-chemical properties and their nanostructure to evaluate the impact of the medium composition.

MATERIALS AND METHODS

Microorganisms and Media

This study was carried out using two *Komagataeibacter xylinus* strains, namely, DSM 2004 and DSM 46604, purchased from DSMZ (the German Collection of Microorganisms and Cell Cultures). The microorganisms were preserved in glycerol (20%, v/v) (99% Sigma-Aldrich), as a cryoprotectant agent, at -80°C. The inocula were prepared by inoculation of 1 ml of the cryopreserved cultures in the HS (Hestrin-Schramm) medium (Hestrin and Schramm, 1954) (per liter: glucose, 20 g; peptone, 5 g; yeast extract, 5 g; citric acid, 1.15 g; disodium hydrogen phosphate, 2.7 g; pH = 7) and incubation in an orbital shaker, at 30°C and 150 rpm, for 24 h. T-75 flasks (BIOFIL) containing 30 ml medium were inoculated with 20% (v/v) inoculum and incubated statically at 30°C, for 18 days.

The media tested consisted of the non-supplemented HS medium; HS medium supplemented with glucose (20 g/L) (reagent grade, Scharlau), TA (20 g/L) (synthesis grade, Merck), or EG (20 g/L) (Honeywell); and HS medium supplemented with mixtures of glucose, TA, and/or EG. For the preparation of culture media containing TA, sonication in an ultrasonic bath (Bandelin Sonorex Digitec Berlin) of the mixture for 30 min was performed, followed by pH adjustment to 7.0 by addition of 5 M NaOH for complete TA solubilization.

Analytical Techniques

At the end of the assays, the cellulose membranes were collected from the flasks, and the cultivation broth samples were centrifuged (10,956 × g 15 min, 4°C). The resultant supernatant was collected for glucose, TA, and EG quantification. Broth samples were also collected at the beginning of the assays for nutrient quantification.

The collected cellulose membranes were treated with 0.1 N NaOH, at 80°C, for 20 min (Costa et al., 2017), and neutralized with water in an orbital shaker for 48 h (200 rpm, at 20°C). Wet BC pellicles were weighed after alkaline treatment as well as after lyophilization (ScanVac CoolSafe™, LaboGene) at -110°C for 48 h, for BC gravimetric quantification.

In some of the assays, there was the formation of a precipitate that got impregnated into the BC pellicles. For BC purification, such pellicles were dissolved in 5 M NaOH at a concentration of 2wt% using the method described by Araújo et al. (2020). Shortly, the BC was dispersed in the alkali solvent system and kept at -20°C for 48 h. During this period, three freeze-thaw cycles were performed in which the thawed suspensions were extensively stirred (at 500 rpm, for 1 h), at 20°C. The resulting solutions were dialyzed with a 12-kDa cut-off membrane (Nadir dialysis tubing, Carl Roth, Karlsruhe, Germany) against deionized water, at a

constant stirring (200 rpm), till neutral pH and constant conductivity values (20 $\mu\text{S}/\text{cm}$) were reached. The dialyzed BC was freeze-dried and gravimetrically quantified.

For glucose and EG quantification, the cell-free supernatant was diluted in sulfuric acid (H_2SO_4 0.01 N) and filtered with modified nylon centrifugal filters (0.2 μm , VWR), at 10,000 rpm for 10 min. Glucose and EG concentration were determined by HPLC with a VARIAN Metacarb column (BioRad) coupled to a refractive index (RI) detector. The analyses were performed at 50°C, with sulfuric acid (H_2SO_4 0.01 N) as the eluent at a flow rate of 0.6 ml/min. Glucose and EG standards were used at concentrations in the range of 0.01–1.0 g/L. For TA quantification, the cell-free supernatant was filtered with modified nylon centrifugal filters (0.2 μm , VWR) and diluted with NaOH 30 mM. TA concentration was determined by HPLC, with an anion exchange column (Ionpac AS11-HC 4.6 \times 250 mm equipped with a pre-column) coupled to a conductivity detector. The analyses were performed at 30°C, with NaOH 30 mM as the eluent at a flow rate of 1.5 ml/min. TA standards were used at concentrations in the range of 0.006–1.0 g/L.

Polymer Characterization

Fourier Transform Infrared Spectroscopy

Fourier transform infrared spectroscopy (FTIR) analysis was performed with a Perkin-Elmer Spectrum Two spectrometer. The dried polymer samples were directly analyzed on the FTIR cells. The spectra were recorded between 400 and 4,000 cm^{-1} resolutions with 10 scans, at 20°C.

Scanning Electron Microscopy

To observe the nanostructure of BC, the lyophilized samples were mounted for observation with scanning electron microscopy (SEM) using double-sided carbon tape and aluminum stubs and sputter-coated with a thin layer of iridium (Q150T ES, Quorum, UK). The analysis was performed in a scanning electron microscope (Hitachi, model *Regulus* 8,220) using an acceleration voltage of 3 kV. The obtained SEM images were processed by ImageJ (NIH image).

X-Ray Diffraction

The structural analysis of the samples was performed by X-ray diffraction (XRD) using an X-ray diffractometer (PANalytical X'Pert PRO MRD) with a monochromatic Cu K α radiation source (45 kV and 40 mA) to scan the samples, which were recorded in a 2 θ range from 10° to 90° using a scan rate of 10°/min with a continuous scanning mode. The crystallinity index (CI) was calculated using the XRD deconvolution method as described by Park et al. (2010).

Thermogravimetric Analysis

Thermogravimetric (TG) measurements were carried out with a simultaneous thermal analyzer, STA 449 F3 Jupiter from NETZSCH Thermal Analysis (Wittelsbacherstraße, Germany), under nitrogen atmosphere and loading 5 mg of each material into a covered aluminum crucible. The polymers were heated up to 500°C at 10 K/min.

RESULTS AND DISCUSSION

BC Production

K. xylinus strains DSM 2004 and DSM 46604 were screened for their ability to produce BC upon cultivation on the TA and/or EG supplemented HS medium. As shown in **Table 1**, both strains were able to produce BC in most of the tested medium composition, although with different yields.

K. xylinus DSM 2004 grew on all tested media. As expected, the highest BC production was observed in the glucose-supplemented medium (2.1 ± 0.2 g/L), which is in the range of the values reported for *K. xylinus* strains in the HS medium with glucose (0.24–3.1 g/L) (Mikkelsen et al., 2009; Yang et al., 2016; Ogrizek et al., 2021). The culture was able to grow on both TA- and EG-supplemented media, producing BC at concentrations of 0.81 ± 0.01 g/L and 0.64 ± 0.02 g/L, respectively. Considering that only residual growth was observed on the non-supplemented HS medium (0.29 ± 0.02 g/L), probably by the utilization of peptone, yeast extract and/or citric acid present on the HS medium served as substrates. These results show that strain DSM 2004 was able to utilize TA and EG as carbon sources for BC production. This was confirmed by the consumption of 1.9 ± 0.1 g/L of TA and 4.2 ± 0.8 g/L of EG during the assays (**Table 1**). The highest yield on a substrate basis was obtained for TA (0.43 ± 0.02 g BC/g substrate), which was considerably higher than the values obtained for glucose or EG (0.20 ± 0.03 and 0.15 ± 0.04 g BC/g substrate, respectively).

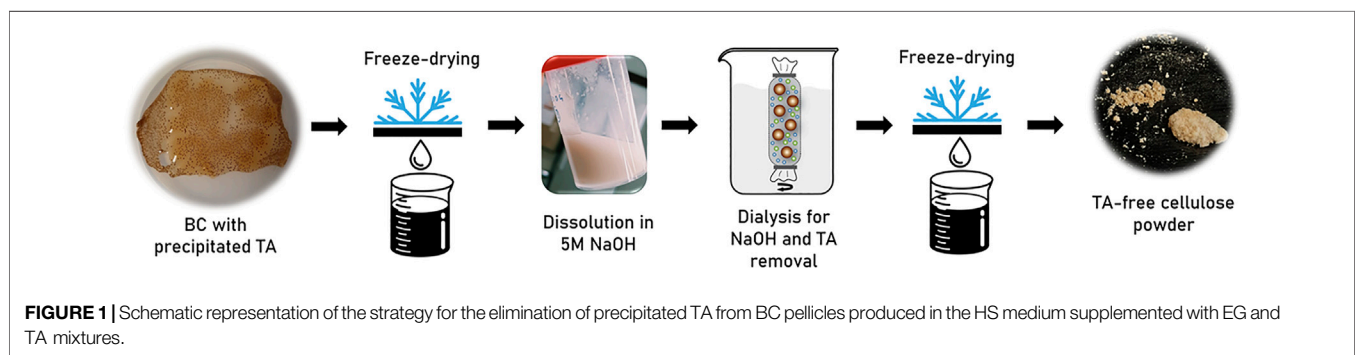
On the other hand, upon cultivation on the HS medium supplemented with TA and EG mixtures, strain DSM 2004 had a BC production of 0.60 ± 0.10 g/L, which is similar to that on EG (0.64 ± 0.02 g/L). However, in that assay, it was not possible to quantify TA due to its precipitation during cultivation that was probably caused by the decrease in the medium's pH due to the metabolization of EG into acidic metabolites produced, namely, glycolic and oxalic acids (Viinamöki et al., 2015). Since TA is only soluble in neutral to basic solutions (Palme et al., 2017), insoluble particles formed and became impregnated into the synthesized BC pellicles. TA precipitation during the TA + EG supplemented assays interfered with the gravimetric quantification of the produced BC. Hence, to overcome this, a strategy was implemented to eliminate TA precipitate from the BC pellicle. A schematic of the approach is represented in **Figure 1**. The produced BC pellicles were dissolved in 5 M NaOH using the freeze-thaw procedure described by Araújo et al. (2020) (Araújo et al., 2020), resulting in a solution of BC and TA that was dialyzed with a 12-kDa cutoff membrane against deionized water. The dialysis permitted the low molecular weight TA molecule to be eliminated from the solution, while the TA-free BC was retained inside the membrane due to its higher molecular weight and quantified by freeze-drying.

BC production on the HS medium supplemented with glucose and TA (2.0 ± 0.1 g/L) was identical to that obtained in the glucose-supplemented medium (2.1 ± 0.2 g/L) (**Table 1**), which suggests no gain on utilizing TA together with glucose. On the other hand, supplementing the medium with EG (in the glucose + EG and glucose + TA + EG assays) improved BC production

TABLE 1 | Substrate conversion, BC production, and yield of BC on a substrate basis for *K. xylinus* DSM 2004 and DSM 46604 grown on the HS medium supplemented with glucose, TA, and/or EG.

<i>K. xylinus</i>	Assay	Substrate consumption (g/L)			BC (g/L)	Yield (g_BC/G_substrate)
		Glc	TA	EG		
DSM 2004	HS	—	—	—	0.29 ± 0.02	—
	HS + Glc	10.40 ± 0.60	—	—	2.10 ± 0.20	0.20 ± 0.03
	HS + TA	—	1.90 ± 0.10	—	0.81 ± 0.01	0.43 ± 0.02
	HS + EG	—	—	4.20 ± 0.80	0.64 ± 0.02	0.15 ± 0.04
	HS + TA + EG	—	(*)	2.90 ± 2.50	0.60 ± 0.10	(*)
	HS + Glc + EG	9.30 ± 1.70	1.80 ± 0.60	—	2.00 ± 0.10	0.18 ± 0.05
	HS + Glc + TA + EG	12.60 ± 1.80	—	6.60 ± 1.10	1.00 ± 0.01	0.05 ± 0.01
DSM 46604	HS	—	—	—	0.29 ± 0.02	—
	HS + Glc	10.10 ± 0.40	—	—	0.53 ± 0.04	0.05 ± 0.01
	HS + TA	—	0.90 ± 0.30	—	0.16 ± 0.01	0.18 ± 0.08
	HS + EG	—	—	—	—	—
	HS + TA + EG	—	(*)	0.45 ± 0.50	0.23 ± 0.10	(*)
	HS + Glc + TA	9.80 ± 1.20	1.60 ± 0.05	—	0.70 ± 0.20	0.06 ± 0.02
	HS + Glc + EG	9.30 ± 1.40	—	6.10 ± 0.50	0.40 ± 0.02	0.03 ± 0.02
	HS + Glc + TA + EG	15.40 ± 1.00	(*)	8.20 ± 0.20	0.76 ± 0.10	(*)

(*)- not quantified due to TA precipitation.



(1.00 ± 0.01 g/L and 1.20 ± 0.03 g/L, respectively) compared to EG alone or TA + EG (0.64 ± 0.02 and 0.60 ± 0.1, respectively), but it was significantly lower than production from glucose alone. In those assays, despite the complete glucose consumption, the lower BC production resulted in reduced yields on the substrate (**Table 1**). These results suggest that the presence of EG in the culture medium induced metabolic pathways other than cell growth or BC synthesis. Nevertheless, the obtained BC production in the assays containing TA + EG was only slightly lower than the values reported for BC production by the bacterial isolate *Taonella mepensis* WT-6 from terylene ammonia hydrolysate (1.75–2.42 g/L) containing TA and EG (Zhang et al., 2021).

Concerning *K. xylinus* DSM 46604, it presented no cell growth on the non-supplemented HS medium or on the EG-supplemented medium (**Table 1**). Moreover, it presented significantly lower BC production in all other tested media than strain DSM 2004. However, it was able to produce BC when grown on TA (0.16 ± 0.01 g/L), despite the lower production than that observed in the glucose-supplemented medium (0.53 ± 0.04 g/L) (**Table 1**). Combining glucose and

TA as substrates resulted in a higher BC production (0.70 ± 0.20 g/L), which demonstrates that strain DSM 46604 was able to utilize both carbon sources simultaneously. Contrary to strain DSM 2004, the presence of EG in the cultivation medium was not detrimental for cell growth and BC synthesis, with slightly higher or similar production being attained in the TA + EG and glucose + TA + EG assays (0.23 ± 0.1 and 0.76 ± 0.1 g/L, respectively), compared to the TA alone and glucose + TA assays. Moreover, analogous to DSM 2004, precipitation of TA was observed for assays containing TA and EG due to the acidification of the medium. Therefore, purification of the BC pellicles was performed, as previously described, to eliminate the precipitated TA, and obtain pure BC for quantification and further characterization.

Although *K. xylinus* DSM 2004 and 46604 were able to synthesize BC using TA and/or EG, the production is lower than that observed for other *K. xylinus* strains on multiple substrates, such as waste mango pulp (6.32 g/L) (García-Sánchez et al., 2020), grape bagasse (8 g/L) (Vazquez et al., 2013), glycerol from biodiesel production (10 g/L) (Vazquez et al., 2013), cotton cloth hydrolysate (10.8 g/L) (Hong et al.,

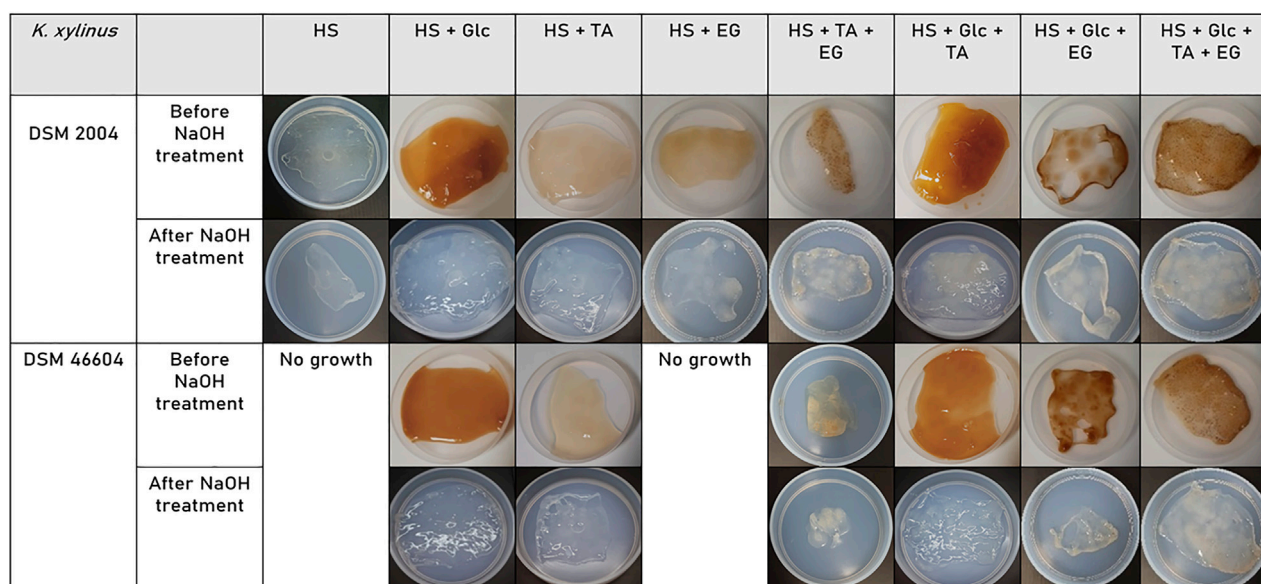


FIGURE 2 | BC pellicles produced by the cultivation of *K. xylinus* strains DSM 2004 and DSM 46604 on the HS medium supplemented with glucose, TA, and/or EG.

2012), and wheat straw acid hydrolysate (15.4 g/L) (Hong et al., 2011). Most of such feedstocks are sugar-rich materials that are easily assimilable by the cells, in contrast to TA or EG, which are not so easily metabolized by the cells. Nevertheless, these results demonstrate the synthesis of BC from PET monomers TA and EG, although the process requires further efforts for its optimization, namely, regarding the optimization of the medium composition (e.g., defining optimal carbon and nitrogen sources concentrations) and the cultivation conditions, such as the pH, temperature, and oxygen supply.

BC Characterization

The BC pellicles obtained in all assays were characterized for their morphology and physical–chemical properties.

Morphology

Figure 2 shows the wet BC pellicles in each cultivation assay, as produced and after NaOH treatment. The produced BC pellicles displayed an orange/yellowish tint before the alkaline treatment and became translucent afterward. This demonstrates the treatment was efficient on the removal of bacterial cell debris and medium remnants from the pellicles. The size and thickness of the pellicles increased accordingly to the bacterial growth and BC production (Zhong, 2020) described previously. After freeze-drying, the membranes presented a papery texture and lost their transparency, becoming white and opaque, as has been previously reported in the literature (Vasconcellos and Farinas, 2018).

The SEM images of the freeze-dried BC pellicle surface are shown in **Figure 3** for both *K. xylinus* strains. The BC obtained after elimination of the TA precipitate was not characterized since the native 3D network was disrupted by the process.

The nanostructure displayed by all samples is similar to that described for dried BC membranes, namely, a three-dimensional

porous network of continuous nanofibers (Swingler et al., 2021; Fortunato et al., 2016). The fibers' diameter ranged between 23 and 90 nm (**Table 2**), which is within the values reported for BC (20–100 nm) produced by different bacteria (Szymańska-Chargot et al., 2011; Gayathri and Srinikethan, 2019; Wang et al., 2019). Nevertheless, some differences are noticed between the samples, which might be correlated with the producing strain, as well as with the carbon source utilized for cultivation. On average, the BC produced by *K. xylinus* DSM 2004 presented a slightly higher fiber diameter (27–90 nm) than that of strain DSM 46604 (23–68 nm). Moreover, the latter structures are shown to be more tightly packed for all media tested, showing a higher number of fused fibers (**Figure 3**).

Chemical Structure

Similar FTIR spectra were obtained for the BC produced from glucose, TA and/or EG by *K. xylinus* DSM 2004 (**Figure 4A**) and DSM 46604 (**Figure 4B**), suggesting that the use of TA and/or EG had no significant influence on the chemical structure of the biopolymer synthesized. All spectra show the characteristic bonds reported for BC (Gea et al., 2011). The intense peak at $3,346\text{ cm}^{-1}$ can be attributed to the stretching of hydroxyl groups in cellulose (Deng et al., 2003). The presence of asymmetric stretching for CH_2 was revealed by the band at $2,896\text{ cm}^{-1}$ (Oh et al., 2005). Also, the bending of HCH and OCH was observed at $1,427\text{ cm}^{-1}$ (Oh et al., 2005). In addition, the spectra showed peaks at $1,360\text{--}1,315\text{ cm}^{-1}$ that may be linked to C–H bonds (Gea et al., 2011). The stretching band detected at $1,162\text{ cm}^{-1}$ is related to C–O–C asymmetric stretching and CH deformation (Kačuráková et al., 2002). Moreover, the peak appearing at $1,109\text{ cm}^{-1}$ can be associated with the stretching of C–C rings in polysaccharides (Movasaghi et al., 2008). However, some differences can be seen in the spectra of the BC samples

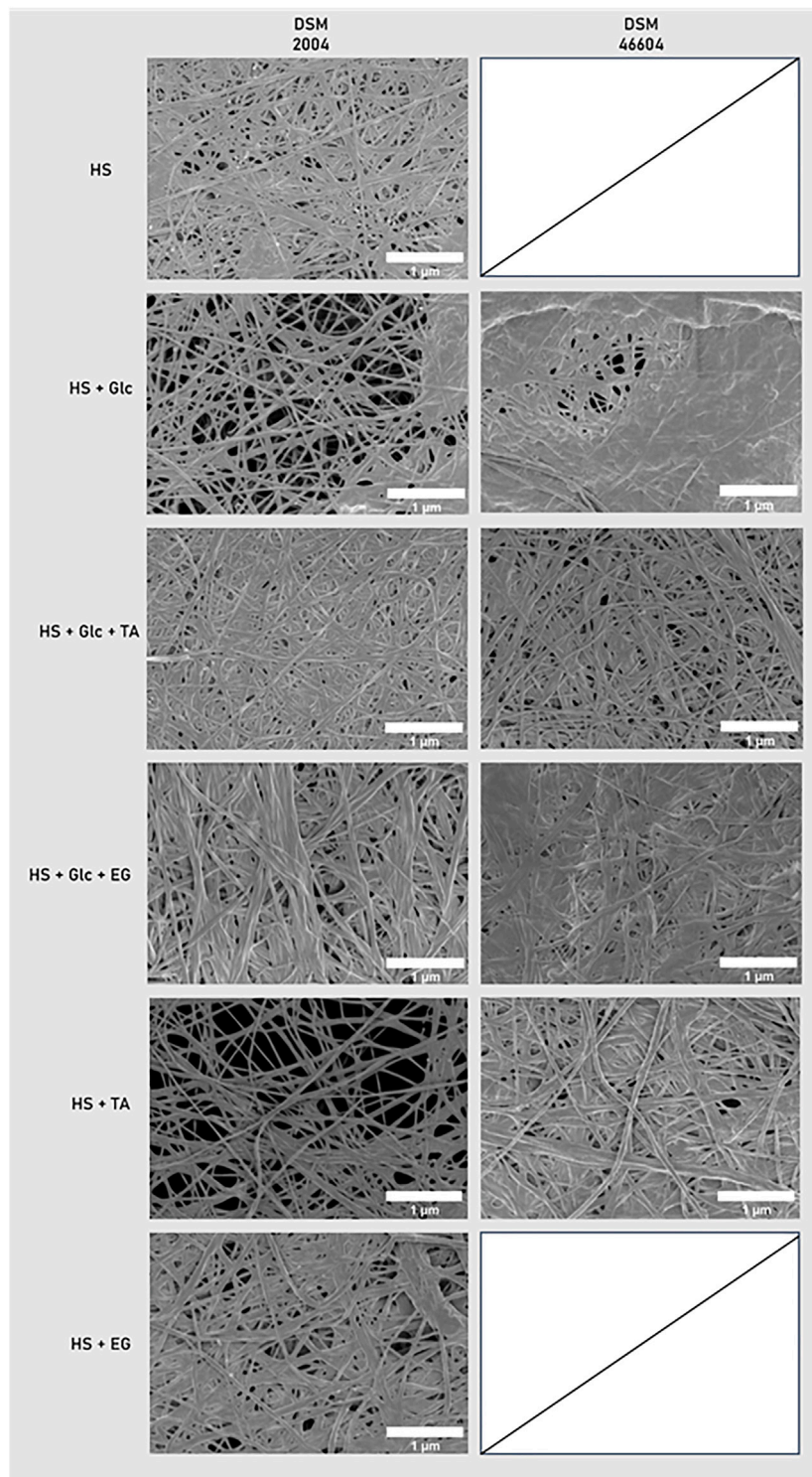


FIGURE 3 | SEM images of BC grown in glucose, TA, and EG by *K. xylinus* DSM 2004 and DSM 46604.

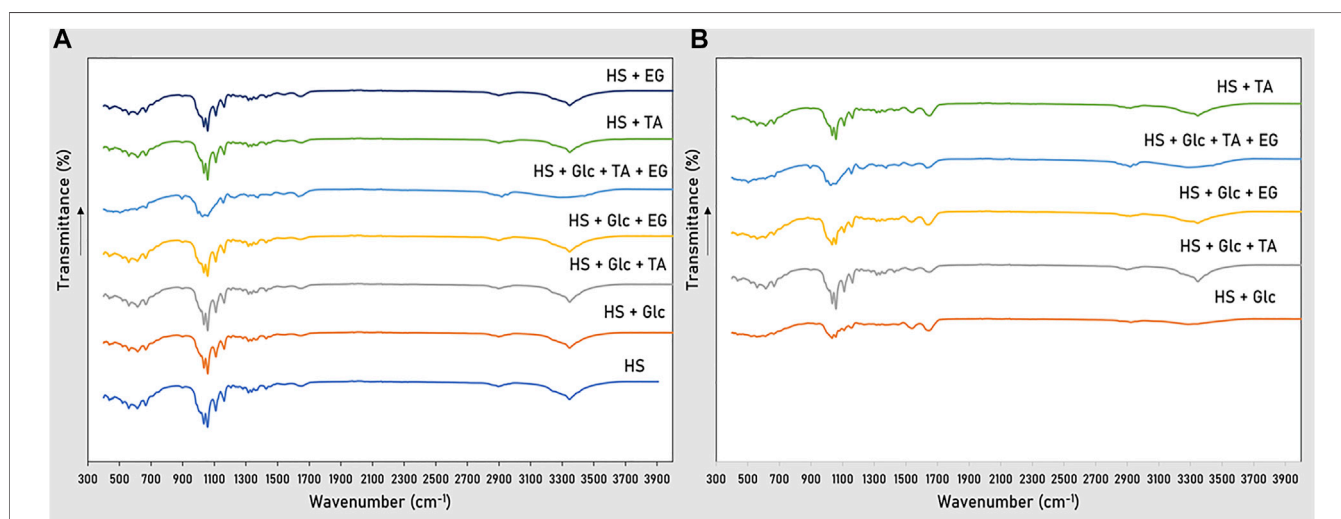
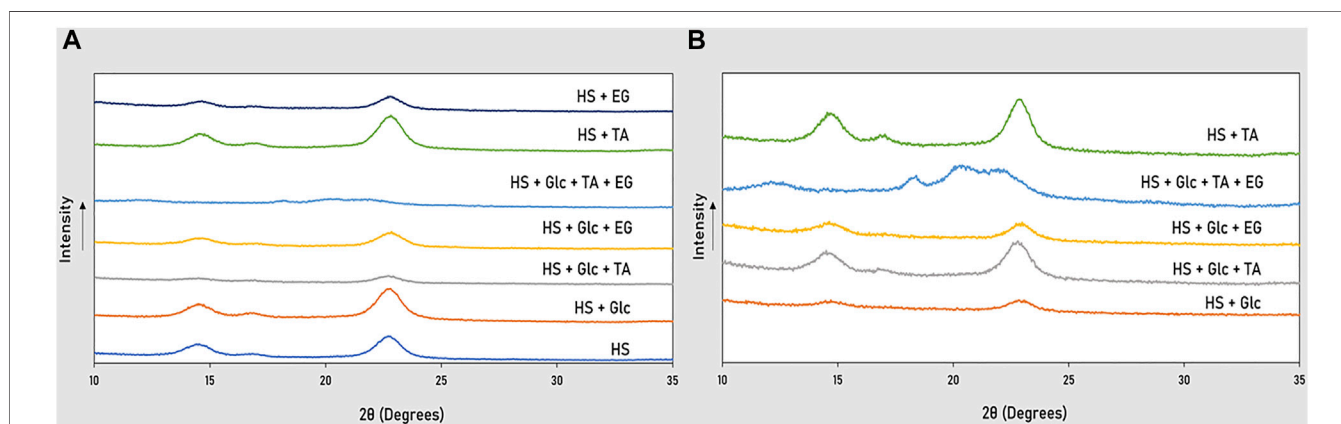
produced in the Glc + TA + EG supplemented media, namely, a lower intensity of the peaks appearing at the regions around $960\text{--}1,100\text{ cm}^{-1}$ and $3,346\text{ cm}^{-1}$, which is probably due to the processing that the pellicles were subjected for the elimination of

the precipitated TA. Furthermore, no peaks associated with the FTIR spectrum of TA (**Supplementary Appendix SA**) (Téllez et al., 2001) were noticed on the spectra of the BC samples, thus confirming the purification procedure was efficient.

TABLE 2 | Fiber diameter, crystallinity index (CI), weight loss, char yield, and degradation temperature (T_{deg}) of BC grown in glucose, TA, and EG by *K. xylinus* DSM 2004 and DSM 46604.

Strain	Assay	Fiber diameter (nm)	CI (%)	Weight loss (%)			Char yield (%)	T_{deg} (°C)
				30–100°C	225–375°C	380–500°C		
2004	HS	27–90	64	3	67	7	23	337
	HS + Glc	29–75	63	6	56	12	27	327
	HS + Glc + TA	34–84	45	5	59	9	27	334
	HS + Glc + EG	35–70	61	6	58	12	25	331
	HS + Glc + TA + EG	(*)	19	7	52	14	27	325
	HS + TA	33–68	57	4	56	13	27	333
	HS + EG	41–74	40	5	60	8	27	323
46604	HS + Glc	23–68	33	6	56	13	25	328
	HS + Glc + TA	28–55	53	5	55	13	27	331
	HS + Glc + EG	29–66	37	6	62	8	23	338
	HS + Glc + TA + EG	(*)	17	4	61	5	29	333
	HS + TA	33–63	48	4	48	10	37	315

(*)- not quantified due to TA precipitation.

**FIGURE 4** | FTIR spectra of the chemical groups present in BC grown in glucose, TA, and EG by *K. xylinus* DSM 2004 (A) and DSM 46604 (B).**FIGURE 5** | XRD diffractograms of BC grown in glucose, TA, and EG by *K. xylinus* DSM 2004 (A) and DSM 46604 (B).

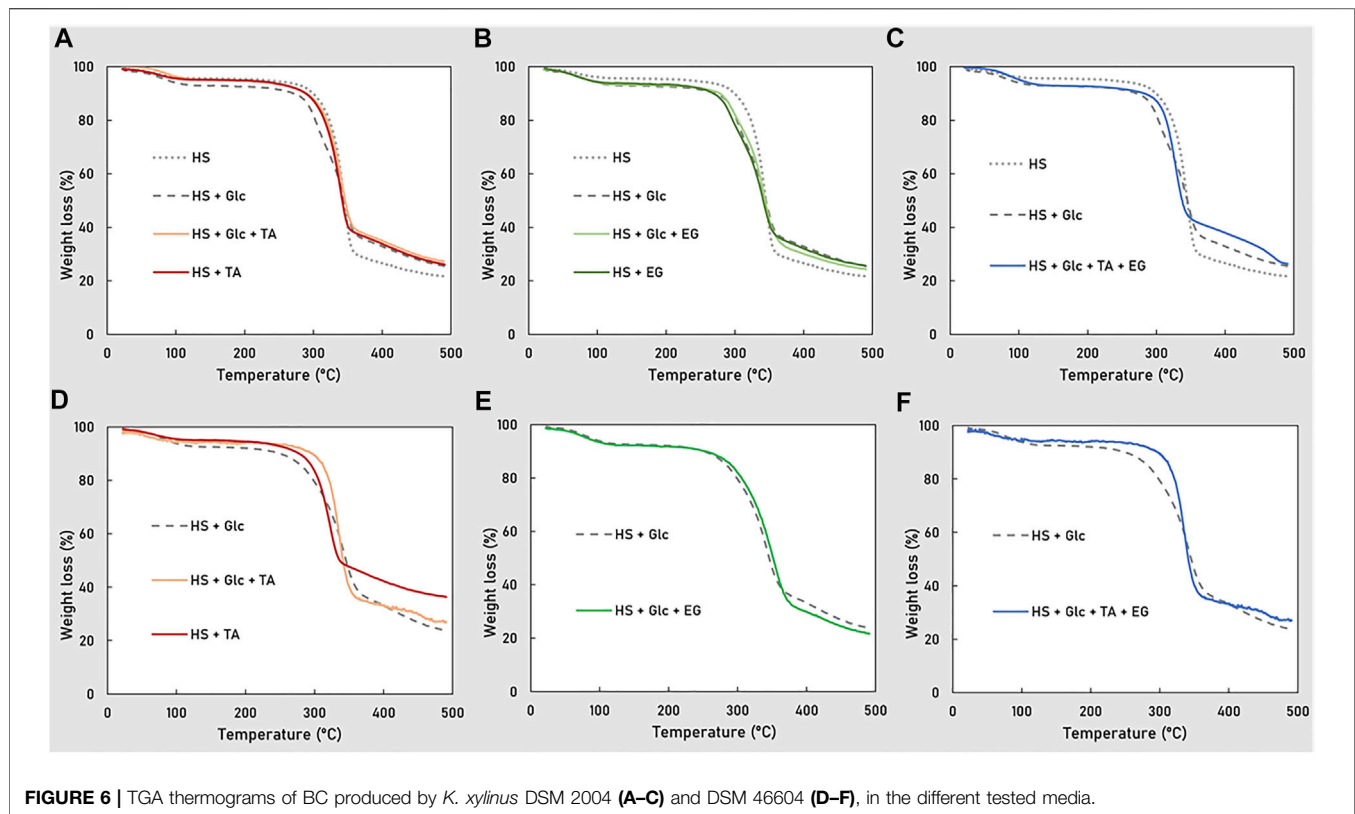


FIGURE 6 | TGA thermograms of BC produced by *K. xylinus* DSM 2004 (A–C) and DSM 46604 (D–F), in the different tested media.

Crystallinity

The structural analysis performed by XRD (Figure 5) allowed the determination of the crystallinity index (CI) of the BC produced by each strain from the different substrates (Table 2). Most samples exhibited some or all of the main reflections of the X-ray diffraction pattern of crystalline BC, presenting typical peaks for the crystalline phase with different intensities, specifically three narrow humps located at $2\theta = 15, 17,$ and 23° , corresponding to the (1–10), (110), and (200) crystal planes (Ye et al., 2019). However, the BC produced by cultivation on Glc + TA + EG by both bacterial strains that were subjected to precipitate removal showed a different profile, exhibiting a pattern of diffraction that is the characteristic of the polymorphic transformation of cellulose I to cellulose II (Pandey et al., 2014), specifically a broad hump within the $2\theta = 20\text{--}22^\circ$ region, as well as some degree of crystallinity, confirmed by two shifted small peaks in the crystalline zone near 12 and 18° . The difference in reflections by these BC samples can be explained by the fact that they were subjected to dissolution in NaOH, which has been reported to decrease BC crystallinity by cleaving inter- and intramolecular bonds and destroying the crystalline region from penetrating the amorphous area of the polymer (Pandey et al., 2014).

The CI values are well in accordance with the XRD patterns of the different BC samples (Table 2). The results differed depending on the bacterial strain used, as well as the medium components, since these conditions have been described to impact BC properties, along with pH and oxygen delivery (Pourramezan et al., 2009). BC is formed by a multistep

process of production and crystallization where the sub-fibrils of cellulose are extruded linearly through the pores at the surface of the cell membrane of the bacteria, where they are crystallized into microfibrils (Wang et al., 2019). Moreover, the rate at which the bacteria synthesizes BC also impacts the biopolymer's crystallinity (Ruka et al., 2012), which might be the case for our investigation, where *K. xylinus* DSM 2004 presented, in average, the production of BC of higher CI than *K. xylinus* DSM 46604 (19–64% against 17–53%, respectively). Moreover, the different cultivation media apparently impacted the CI of the BC that is produced differently for each bacterial strain. For strain DSM 2004, the highest CI values were found for the BC synthesized in the non-supplemented HS medium and the glucose-supplemented media (64 and 63%, respectively), decreasing for the BC produced in the presence of TA (45–57%) or EG (40–61%) (Table 2). An opposite trend was noted for strain 46604, for which the lowest CI value was observed for the BC produced in the glucose medium (33%), increasing for the biopolymers produced in the TA (48–53%) or EG (37%) supplemented media (Table 2), which may indicate that TA allowed a higher BC crystallization of that strain. These results indicate that CI is influenced by medium composition, as reported in previous studies that proved different additives (e.g., agar, carboxymethylcellulose (CMC), and sodium alginate) in the culture medium impact the productivity, crystallinity, and crystal size of BC (Cheng et al., 2009).

Thermal Properties

The thermal decomposition behavior, namely, the thermograms and the degradation temperature, of the BC produced by each strain upon cultivation on glucose, TA, and/or EG is presented in **Figure 6** and **Table 2**. All samples present a similar profile, experiencing three weight loss events (**Figure 6**), in accordance with the reported studies for BC (Gayathri and Srinikethan, 2019; Zhang et al., 2021). The first degradation step (3–7% weight loss), which occurred between 30 and 100°C, can be attributed to the loss of crystal water existing in BC samples (Zhang et al., 2021). The second and most significant weight loss (48–67%) was observed between 225 and 375°C, and is related to the pyrolysis of BC, where the main degradation of the polymer occurs (George et al., 2005). The last weight-loss step (5–14%), occurring between 380 and 500°C, corresponds to the degradation of remnant microorganisms or protein present in the samples (Zhang et al., 2021). The samples char yield at 490°C ranged between 23 and 37 (**Table 2**).

For strain DSM 2004, the BC produced in the non-supplemented medium (**Figure 6A**) had the highest T_{deg} value (337°C) and the lowest char yield (23%) (**Table 2**). In contrast, cultivation on the glucose-supplemented medium resulted in the BC with higher char yield (27%) and lower T_{deg} (327°C). The profiles for the EG and the Glc + EG samples (**Figure 6B**) were similar to that of the glucose-supplemented medium (**Figure 6A**), while the BC produced upon cultivation on TA or Glc + TA (**Figure 6A**) shows T_{deg} values (333–334°C) similar to those of the BC sample from the HS medium, but the char yield (27%) was identical to that of the HS + Glc assay. The profile for BC grown in the Glc + TA + EG mixture (**Figure 6C**) confirmed that the thermal properties of BC were not significantly impacted by TA precipitate removal in comparison to BC grown in Glc. A similar trend was noticed for strain DSM 46604, for which the TGA profiles for the BC samples produced in the presence of glucose (**Figure 6D**) were similar to those of the EG assay (**Figure 6E**), while the samples obtained in the TA and Glc + TA assays (**Figure 6D**), as well as Glc + TA + EG (**Figure 6F**), differed. Nevertheless, the T_{deg} values found for all assays were in the 315–338°C range (**Table 2**), which is among the values reported for BC (312–356°C) produced by different bacteria (George et al., 2005; Jia et al., 2017; Bekatorou et al., 2019). Despite identified differences, these results show there was no significant impact on the samples' thermal degradation profile upon cultivation on TA and/or EG.

CONCLUSION

Komagataeibacter xylinus strains DSM 2004 and DSM 46604 demonstrated their ability to grow on media supplemented with TA and/or EG, the monomers of PET. *K. xylinus* DSM 2004 displayed the most promising performance, being able to utilize

both TA and EG as sole carbon sources. Although the BC produced in all tested media had identical chemical structure and thermal behavior, their crystallinity and nanostructure varied with the producing bacterial strain, as well as with the medium composition. These promising findings pave the way for the upcycling of PET degradation monomers into a high-value biopolymer, thus contributing to the reduction of the plastics' harmful impact to the environment.

DATA AVAILABILITY STATEMENT

The raw data supporting the conclusions of this article will be made available by the authors, without undue reservation.

AUTHOR CONTRIBUTIONS

Conceptualization: AE, CT, and FF; formal analysis: AE and FF; investigation: AE; methodology: AE, AR, AM, SS, and AG; writing—original draft: AE and FF; writing—review and editing: CT, EF, MR, and FF. All authors have read and agreed to the published version of the manuscript.

FUNDING

This work was financed by national funds from FCT—Fundação para a Ciência e a Tecnologia, I.P., in the scope of the project UIDP/04378/2020 and UIDB/04378/2020 of the Research Unit on Applied Molecular Biosciences-UCIBIO and the project LA/P/0140/2020 of the Associate Laboratory Institute for Health and Bioeconomy-i4HB, the project LA/P/0037/2020 of the Associate Laboratory Institute of Nanostructures, Nanomodelling and Nanofabrication i3N, and by the European Union's Horizon 2020 research and innovation program through Project Bio Innovation of a Circular Economy for Plastics (BioICEP), under grant agreement No. 870292, supported by the National Natural Science Foundation of China (grant numbers: Institute of Microbiology, Chinese Academy of Sciences: 31961133016; Beijing Institute of Technology: 31961133015; Shandong University: 31961133014). AE and AR acknowledge FCT I.P. for PhD Grants 2021.05014. BD and 2020.06470. BD, respectively.

SUPPLEMENTARY MATERIAL

The Supplementary Material for this article can be found online at: <https://www.frontiersin.org/articles/10.3389/fbioe.2022.853322/full#supplementary-material>

REFERENCES

- Araújo, D., Alves, V. D., Marques, A. C., Fortunato, E., Reis, M. A. M., and Freitas, F. (2020). Low Temperature Dissolution of Yeast Chitin-Glucan Complex and Characterization of the Regenerated Polymer. *Bioengineering* 7, 28. doi:10.3390/bioengineering7010028
- Bekatorou, A., Plioni, I., Sparou, K., Maroutsiou, R., Tsafraikidou, P., Petsi, T., et al. (2019). Bacterial Cellulose Production Using the Corinthian Currant Finishing Side-Stream and Cheese Whey: Process Optimization and Textural Characterization. *Foods* 8, 193. doi:10.3390/foods8060193
- Carvalho, T., Guedes, G., Sousa, F. L., Freire, C. S. R., and Santos, H. A. (2019). Latest Advances on Bacterial Cellulose-Based Materials for Wound Healing, Delivery Systems, and Tissue Engineering. *Biotechnol. J.* 14, 1900059. doi:10.1002/biot.201900059
- Cheng, K.-C., Catchmark, J. M., and Demirci, A. (2009). Effect of Different Additives on Bacterial Cellulose Production by *Acetobacter Xylinum* and Analysis of Material Property. *Cellulose* 16, 1033–1045. doi:10.1007/s10570-009-9346-5
- Costa, A. F. S., Almeida, F. C. G., Vinhas, G. M., and Sarubbo, L. A. (2017). Production of Bacterial Cellulose by *Gluconacetobacter Hansenii* Using Corn Steep Liquor as Nutrient Sources. *Front. Microbiol.* 8, 2027. doi:10.3389/fmicb.2017.02027
- Deng, S., Bai, R., Hu, X., and Luo, Q. (2003). Characteristics of a Bioflocculant Produced by *Bacillus Mucilaginosus* and its Use in Starch Wastewater Treatment. *Appl. Microbiol. Biotechnol.* 60, 588–593. doi:10.1007/s00253-002-1159-5
- Fortunato, E., Gaspar, D., Duarte, P., Pereira, L., Águas, H., Vicente, A., et al. (2016). Optoelectronic Devices from Bacterial NanoCellulose. *Bacterial Nanocellulose: Biotechnol. Bio-Economy* 2016, 179–197. doi:10.1016/B978-0-444-63458-0.00011-1
- García-Sánchez, M. E., Robledo-Ortiz, J. R., Robledo-Ortiz, J. R., Jiménez-Palomar, I., González-Reynoso, O., and González-García, Y. (2020). Production of Bacterial Cellulose by *Komagataeibacter Xylinus* Using Mango Waste as Alternative Culture Medium. *Rquim* 19, 851–865. doi:10.24275/rmiq/Bio743
- Gayathri, G., and Srinikethan, G. (2019). Bacterial Cellulose Production by *K. Saccharivorans* BCI Strain Using Crude Distillery Effluent as Cheap and Cost Effective Nutrient Medium. *Int. J. Biol. Macromolecules* 138, 950–957. doi:10.1016/j.ijbiomac.2019.07.159
- Gea, S., Reynolds, C. T., Roohpour, N., Wirjosentono, B., Soykeabkaew, N., Bilotti, E., et al. (2011). Investigation into the Structural, Morphological, Mechanical and thermal Behaviour of Bacterial Cellulose after a Two-step Purification Process. *Bioresour. Technology* 102, 9105–9110. doi:10.1016/j.biortech.2011.04.077
- George, J., Ramana, K. V., Sabapathy, S. N., Jagannath, J. H., and Bawa, A. S. (2005). Characterization of Chemically Treated Bacterial (*Acetobacter Xylinum*) Biopolymer: Some Thermo-Mechanical Properties. *Int. J. Biol. Macromolecules* 37, 189–194. doi:10.1016/j.ijbiomac.2005.10.007
- Hestrin, S., and Schramm, M. (1954). Synthesis of Cellulose by *Acetobacter Xylinum*. 2. Preparation of Freeze-Dried Cells Capable of Polymerizing Glucose to Cellulose. *Biochem. J.* 58, 345–352. doi:10.1042/bj0580345
- Hong, F., Guo, X., Zhang, S., Han, S.-f., Yang, G., and Jönsson, L. J. (2012). Bacterial Cellulose Production from Cotton-Based Waste Textiles: Enzymatic Saccharification Enhanced by Ionic Liquid Pretreatment. *Bioresour. Technology* 104, 503–508. doi:10.1016/j.biortech.2011.11.028
- Hong, F., Zhu, Y. X., Yang, G., and Yang, X. X. (2011). Wheat Straw Acid Hydrolysate as a Potential Cost-Effective Feedstock for Production of Bacterial Cellulose. *J. Chem. Technol. Biotechnol.* 86, 675–680. doi:10.1002/jctb.2567
- Jia, Y., Wang, X., Huo, M., Zhai, X., Li, F., and Zhong, C. (2017). Preparation and Characterization of a Novel Bacterial Cellulose/chitosan Bio-Hydrogel. *Nanomater. Nanotechnology* 7, 184798041770717–184798041770718. doi:10.1177/1847980417707172
- Kacuráková, M., Smith, A. C., Gidley, M. J., and Wilson, R. H. (2002). Molecular Interactions in Bacterial Cellulose Composites Studied by 1D FT-IR and Dynamic 2D FT-IR Spectroscopy. *Carbohydr. Res.* 337, 1145–1153. doi:10.1016/S0008-6215(02)00102-7
- Klemm, D., Schumann, D., Udhardt, U., and Marsch, S. (2001). Bacterial Synthesized Cellulose - Artificial Blood Vessels for Microsurgery. *Prog. Polym. Sci.* 26, 1561–1603. doi:10.1016/S0079-6700(01)00021-1
- Marques, A. C., Pinheiro, T., Morais, M., Martins, C., Andrade, A. F., Martins, R., et al. (2021). Bottom-up Microwave-Assisted Seed-Mediated Synthesis of Gold Nanoparticles onto Nanocellulose to Boost Stability and High Performance for SERS Applications. *Appl. Surf. Sci.* 561, 150060. doi:10.1016/j.apsusc.2021.150060
- Mikkelsen, D., Flanagan, B. M., Dykes, G. A., and Gidley, M. J. (2009). Influence of Different Carbon Sources on Bacterial Cellulose Production by *Gluconacetobacter Xylinus* strain ATCC 53524. *J. Appl. Microbiol.* 107, 576–583. doi:10.1111/j.1365-2672.2009.04226.x
- Movasaghi, Z., Rehman, S., and ur Rehman, D. I. (2008). Fourier Transform Infrared (FTIR) Spectroscopy of Biological Tissues. *Appl. Spectrosc. Rev.* 43, 134–179. doi:10.1080/057049207018290410.1080/05704920701829043
- Nikolaivits, E., Pantelic, B., Azeem, M., Taxeidis, G., Babu, R., Topakas, E., et al. (2021). Progressing Plastics Circularity: A Review of Mechano-Biocatalytic Approaches for Waste Plastic (Re)valorization. *Front. Bioeng. Biotechnol.* 9, 535. doi:10.3389/fbioe.2021.696040
- Ogrizek, L., Lamovšek, J., Čuš, F., Leskovšek, M., and Gorjanc, M. (2021). Properties of Bacterial Cellulose Produced Using white and Red Grape Bagasse as a Nutrient Source. *Processes* 9, 1088. doi:10.3390/pr9071088
- Oh, S. Y., Yoo, D. I., Shin, Y., Kim, H. C., Kim, H. Y., Chung, Y. S., et al. (2005). Crystalline Structure Analysis of Cellulose Treated with Sodium Hydroxide and Carbon Dioxide by Means of X-ray Diffraction and FTIR Spectroscopy. *Carbohydr. Res.* 340, 2376–2391. doi:10.1016/j.carres.2005.08.007
- Palme, A., Peterson, A., de la Motte, H., Theliander, H., and Brelid, H. (2017). Development of an Efficient Route for Combined Recycling of PET and Cotton from Mixed Fabrics. *Text. Cloth. Sustain.* 3, 1. doi:10.1186/s40689-017-0026-9
- Pandey, M., Mustafa Abeer, M., and Amin, M. C. I. (2014). Dissolution study of bacterial cellulose (nata de coco) from local food industry: Solubility behavior & structural changes. *Int. J. Pharm. Pharm. Sci.* 6, 89–93. doi:10.4103/0975-7406.129179
- Park, S., Baker, J. O., Himmel, M. E., Parilla, P. A., and Johnson, D. K. (2010). Cellulose Crystallinity index: Measurement Techniques and Their Impact on Interpreting Cellulase Performance. *Biotechnol. Biofuels* 3, 1–10. doi:10.1186/1754-6834-3-10
- Pourrameza, G. Z., Roayaei, A. M., and Qezelbash, Q. R. (2008). Optimization of Culture Conditions for Bacterial Cellulose Production by *Acetobacter* Sp. 4B-2. *Biotechnology* 8, 150–154. doi:10.3923/biotech.2009.150.154
- Robertson, G. L. (2014). Food Packaging. *Encycl. Agric. Food Syst.* 3, 232–249. doi:10.1016/B978-0-444-52512-3.00063-2
- Ruka, D. R., Simon, G. P., and Dean, K. M. (2012). Altering the Growth Conditions of *Gluconacetobacter Xylinus* to Maximize the Yield of Bacterial Cellulose. *Carbohydr. Polym.* 89, 613–622. doi:10.1016/j.carbpol.2012.03.059
- Sang, T., Wallis, C. J., Hill, G., and Britovsek, G. J. P. (2020). Polyethylene Terephthalate Degradation under Natural and Accelerated Weathering Conditions. *Eur. Polym. J.* 136, 109873. doi:10.1016/j.eurpolymj.2020.109873
- Swingler, S., Gupta, A., Gibson, H., Kowalczyk, M., Heaselgrave, W., and Radecka, I. (2021). Recent Advances and Applications of Bacterial Cellulose in Biomedicine. *Polymers* 13, 412. doi:10.3390/polym13030412
- Szymańska-Chargot, M., Cybulska, J., and Zdunek, A. (2011). Sensing the Structural Differences in Cellulose from Apple and Bacterial Cell wall Materials by Raman and FT-IR Spectroscopy. *Sensors* 11, 5543–5560. doi:10.3390/s110605543
- Téllez, S., C. A., Hollauer, E., Mondragon, M. A., and Castaño, V. M. (2001). Fourier Transform Infrared and Raman Spectra, Vibrational Assignment and Ab Initio Calculations of Terephthalic Acid and Related Compounds. *Spectrochim. Acta - Part. A. Mol. Biomol. Spectrosc.* 57, 993–1007. doi:10.1016/S1386-1425(00)00428-5
- Thiounn, T., and Smith, R. C. (2020). Advances and Approaches for Chemical Recycling of Plastic Waste. *J. Polym. Sci.* 58, 1347–1364. doi:10.1002/pol.20190261
- Tiso, T., Narancic, T., Wei, R., Pollet, E., Beagan, N., Schröder, K., et al. (2021). Towards Bio-Upcycling of Polyethylene Terephthalate. *Metab. Eng.* 66, 167–178. doi:10.1016/j.jymben.2021.03.011

- Ul-Islam, M., Khan, T., and Park, J. K. (2012). Water Holding and Release Properties of Bacterial Cellulose Obtained by *In Situ* and *Ex Situ* Modification. *Carbohydr. Polym.* 88, 596–603. doi:10.1016/j.carbpol.2012.01.006
- Vasconcellos, V. M., and Farinas, C. S. (2018). The Effect of the Drying Process on the Properties of Bacterial Cellulose Films from *Gluconacetobacter Hansenii*. *Chem. Eng. Trans.* 64, 145–150. doi:10.3303/CET1864025
- Vazquez, A., Foresti, M. L., Cerrutti, P., and Galvagno, M. (2013). Bacterial Cellulose from Simple and Low Cost Production Media by *Gluconacetobacter Xylinus*. *J. Polym. Environ.* 21, 545–554. doi:10.1007/s10924-012-0541-3
- Viinamäki, J., Sajantila, A., and Ojanperä, I. (2015). Ethylene Glycol and Metabolite Concentrations in Fatal Ethylene Glycol Poisonings. *J. Anal. Toxicol.* 39, 481–485. doi:10.1093/jat/bkv044
- Wang, J., Tavakoli, J., and Tang, Y. (2019). Bacterial Cellulose Production, Properties and Applications with Different Culture Methods - A Review. *Carbohydr. Polym.* 219, 63–76. doi:10.1016/j.carbpol.2019.05.008
- Webb, H., Arnott, J., Crawford, R., and Ivanova, E. (2013). Plastic Degradation and its Environmental Implications with Special Reference to Poly(ethylene Terephthalate). *Polymers* 5, 1–18. doi:10.3390/polym5010001
- Yang, X.-Y., Huang, C., Guo, H.-J., Xiong, L., Luo, J., Wang, B., et al. (2016). Bacterial Cellulose Production from the Litchi Extract by *Gluconacetobacter Xylinus*. *Prep. Biochem. Biotechnol.* 46, 39–43. doi:10.1080/10826068.2014.958163
- Ye, J., Zheng, S., Zhang, Z., Yang, F., Ma, K., Feng, Y., et al. (2019). Bacterial Cellulose Production by *Acetobacter Xylinum* ATCC 23767 Using Tobacco Waste Extract as Culture Medium. *Bioresour. Technology* 274, 518–524. doi:10.1016/j.biortech.2018.12.028
- Zhang, Y., Chen, Y., Cao, G., Ma, X., Zhou, J., and Xu, W. (2021). Bacterial Cellulose Production from Terylene Ammonia Hydrolysate by *Taonella Mepensis* WT-6. *Int. J. Biol. Macromolecules* 166, 251–258. doi:10.1016/j.ijbiomac.2020.10.172
- Zhong, C. (2020). Industrial-Scale Production and Applications of Bacterial Cellulose. *Front. Bioeng. Biotechnol.* 8, 1425. doi:10.3389/fbioe.2020.605374

Conflict of Interest: The authors declare that the research was conducted in the absence of any commercial or financial relationships that could be construed as a potential conflict of interest.

Publisher's Note: All claims expressed in this article are solely those of the authors and do not necessarily represent those of their affiliated organizations, or those of the publisher, the editors, and the reviewers. Any product that may be evaluated in this article, or claim that may be made by its manufacturer, is not guaranteed or endorsed by the publisher.

Copyright © 2022 Esmail, Rebocho, Marques, Silvestre, Gonçalves, Fortunato, Torres, Reis and Freitas. This is an open-access article distributed under the terms of the Creative Commons Attribution License (CC BY). The use, distribution or reproduction in other forums is permitted, provided the original author(s) and the copyright owner(s) are credited and that the original publication in this journal is cited, in accordance with accepted academic practice. No use, distribution or reproduction is permitted which does not comply with these terms.



Characterization of Polymer Degrading Lipases, LIP1 and LIP2 From *Pseudomonas chlororaphis* PA23

Nisha Mohanan¹, Chun Hin Wong², Nediljko Budisa² and David B. Levin^{1*}

¹Department of Biosystems Engineering, University of Manitoba, Winnipeg, MB, Canada, ²Department of Chemistry, University of Manitoba, Winnipeg, MB, Canada

OPEN ACCESS

Edited by:

Aamer Ali Shah,
Quaid-i-Azam University, Pakistan

Reviewed by:

Rajni Hatti Kaul,
Lund University, Sweden
Qurrat Ul Ain Rana,
Quaid-i-Azam University, Pakistan

*Correspondence:

David B. Levin
david.levin@umanitoba.ca

Specialty section:

This article was submitted to
Bioprocess Engineering,
a section of the journal
Frontiers in Bioengineering and
Biotechnology

Received: 13 January 2022

Accepted: 22 March 2022

Published: 20 April 2022

Citation:

Mohanan N, Wong CH, Budisa N and
Levin DB (2022) Characterization of
Polymer Degrading Lipases, LIP1 and
LIP2 From *Pseudomonas*
chlororaphis PA23.
Front. Bioeng. Biotechnol. 10:854298.
doi: 10.3389/fbioe.2022.854298

The outstanding metabolic and bioprotective properties of the bacterial genus *Pseudomonas* make these species a potentially interesting source for the search of hydrolytic activities that could be useful for the degradation of plastics. We identified two genes encoding the intracellular lipases LIP1 and LIP2 of the biocontrol bacterium *Pseudomonas chlororaphis* PA23 and subsequently performed cloning and expression in *Escherichia coli*. The *lip1* gene has an open reading frame of 828 bp and encodes a protein of 29.7 kDa whereas the *lip2* consists of 834 bp and has a protein of 30.2 kDa. Although secondary structure analyses of LIP1 and LIP2 indicate a dominant α/β -hydrolase-fold, the two proteins differ widely in their amino acid sequences (15.39% identity), substrate specificities, and hydrolysis rates. Homology modeling indicates the catalytic serine in both enzymes located in a GX SXG sequence motif (lipase box). However, LIP1 has a catalytic triad of Ser152-His253-Glu221 with a GGX-type oxyanion pocket, whereas LIP2 has Ser138-His249-Asp221 in its active site and a GX-type of oxyanion hole residues. However, LIP1 has a catalytic triad of Ser152-His253-Glu221 with an oxyanion pocket of GGX-type, whereas LIP2 has Ser138-His249-Asp221 in its active site and a GX-type of oxyanion hole residues. Our three-dimensional models of LIP1 and LIP2 complexed with a 3-hydroxyoctanoate dimer revealed the core α/β hydrolase-type domain with an exposed substrate binding pocket in LIP1 and an active-site capped with a closing lid domain in LIP2. The recombinant LIP1 was optimally active at 45°C and pH 9.0, and the activity improved in the presence of Ca^{2+} . LIP2 exhibited maximum activity at 40°C and pH 8.0, and was unaffected by Ca^{2+} . Despite different properties, the enzymes exhibited broadsubstrate specificity and were able to hydrolyze short chain length and medium chain length polyhydroxyalkanoates (PHAs), polylactic acid (PLA), and para-nitrophenyl (pNP) alkanoates. Gel Permeation Chromatography (GPC) analysis showed a decrease in the molecular weight of the polymers after incubation with LIP1 and LIP2. The enzymes also manifested some polymer-degrading activity on petroleum-based polymers such as poly(ϵ -caprolactone) (PCL) and polyethylene succinate (PES), suggesting that these enzymes could be useful for biodegradation of synthetic polyester plastics. The study will be the first report of the complete characterization of intracellular lipases from bacterial

and/or *Pseudomonas* species. The lipases, LIP1 and LIP2 are different from other bacterial lipases/esterases in having broad substrate specificity for polyesters.

Keywords: lipase, esterase, polyhydroxyalkanoate (PHA), polylactic acid (PLA), poly(ϵ -caprolactone) (PCL), polyethylene succinate (PES), biodegradation

INTRODUCTION

Lipase enzymes (E.C.3.1.1.3), found in diverse organisms such as animals, plants, fungi, and bacteria, catalyze the hydrolysis of ester bonds in triglycerides to free fatty acids and glycerol. They act at the interface between an insoluble phase of the substrate and an aqueous phase containing the enzyme (interfacial activation) (Reis et al., 2009). A unique property of true lipases that distinguishes them from other esterases is their enhanced activity at a nonpolar-aqueous interface (Fojan et al., 2000). Lipases show a wide-range of molecular sizes, substrate/positional specificities, and catalytic activities. They have a large number of nonpolar residues near the surface that cluster around the active site (Fojan et al., 2000). Many lipases exhibit a lid-like structure, and opening of the lid exposes the hydrophobic patches in the active site, leading to catalysis at the lipid-water interface, while the closed lid conformation is inaccessible to solvent (Derewenda et al., 1992; Fojan et al., 2000). Esterases, and a few lipases, do not have a lid structure (Uppenberg et al., 1994; Longhi et al., 1997).

Microbial lipases have been investigated for their multifold applications in organic synthesis, detergent formulations, oleochemistry and nutrition (Saxena et al., 2003). To date, many bacterial lipases have been identified, cloned, and characterized (Contesini et al., 2020). However, very limited information is available on the potential application of lipases (especially intracellular lipases) for degradation of polyester polymers/plastics. Extracellular lipases purified from *Bacillus subtilis*, *Pseudomonas aeruginosa*, *Pseudomonas alcaligenes*, and *Burkholderia cepacia* (former *Pseudomonas cepacia*) degrade polyesters of ω -hydroxyalkanoic acids such as poly(ϵ -caprolactone (PCL) and poly-4-hydroxyalkanoate (P(4HB)) polymers (Jaeger et al., 1995). The extracellular lipase of a *Pseudomonas* sp. was also able to degrade PCL (Kim et al., 1992). Weak but detectable medium chain length polyhydroxyalkanoate (mcl-PHA) activity was observed with the extracellular lipases from *P. alcaligenes* and *P. aeruginosa* (Jaeger et al., 1995).

In a previous report from this lab (Sharma et al., 2019), the cell free culture supernatant of *Pseudomonas chlororaphis* PA23 was shown to hydrolyze the ester bonds of p-nitrophenyl fatty acid substrates and PHA polymers with different subunit composition. In the present study, two genes encoding intracellular lipases from *P. chlororaphis* PA23 were cloned and expressed in *E. coli* BL21(DE3) to study the enzyme properties and investigate their degradation activity toward various biodegradable polymers such as small chain length (scl-) and mcl-PHAs, polylactic acid (PLA), polyethylene succinate (PES), and PCL. This is the first report on the application testing of lipases as potential agents for the degradation of a wide-range of biobased and synthetic polyesters.

MATERIALS AND METHODS

Bacterial Strains and Plasmid

P. chlororaphis PA23 is a plant growth-promoting bacterium isolated from the soybean rhizosphere that can suppress the growth of the fungal pathogen *Sclerotinia sclerotiorum* due to its ability to synthesize phenazine and pyrrolnitrin compounds (Savchuk and Fernando, 2004; Fernando et al., 2007). *Escherichia coli* DH5 α and *E. coli* BL21 (DE3) were used as host cells for recombinant plasmid construction and protein expression, respectively. pET28a(+) (Novagen, Madison, USA) was used as an expression vector for the expression of the lipase genes, *lip1* and *lip2*. The PHA polymers used in the study were synthesized by *Pseudomonas putida* LS46 (International Depository Authority of Canada Accession Number 181110-03) (Sharma et al., 2011; Blunt et al., 2018).

Chemicals, Media and Growth Conditions

Hexanoic acid, octanoic acid, nonanoic acid, decanoic acid, polylactic acid (PLA), polycaprolactone (PCL) and polyethylene succinate (PES) was purchased from Sigma Chemical Co. (St. Louis, MO). All other analytical grade products, chemicals and dyes were from either Sigma Chemical Co. (St. Louis, MO) or Fisher Scientific (Toronto, ON). To prepare the various PHA polymers, the *P. putida* LS46 was cultivated in Ramsay's minimal medium (RMM) (Ramsay et al., 1994) at 30°C in 7 L Applicon Bioreactor with hexanoic, octanoic, nonanoic, or decanoic acid as the sole carbon source (Blunt et al., 2018). A copolymer of 3-hydroxybutyrate and 3-hydroxyvalerate [Poly (3-hydroxybutyrate-co-3-hydroxyvalerate, PHBV)] was prepared from biodiesel fatty acid supplemented with 0.5% valeric acid using *Cuprividus necator* H16 (Sharma et al., 2016). The monomer compositions of these PHA polymers were determined (Sharma et al., 2011) and are shown in Table 1. Luria Bertani (LB) broth and agar were used for the growth of *E. coli* DH5 α and *E. coli* BL21 (DE3) cells.

DNA Manipulation and Plasmid Construction

The genomic DNA of *P. chlororaphis* PA23 was isolated from LB bacterial cultures using the Wizard DNA purification kit (Promega). DNA fragments containing genes encoding the lipase enzymes, *lip1* and *lip2* were generated separately by PCR amplification from of *P. chlororaphis* PA23 chromosomal DNA using phusion DNA polymerase (Thermo Scientific) and the primer combinations listed in Table 2. The nucleotide sequences of these genes were obtained from the whole genome sequence of *P. chlororaphis*

TABLE 1 | Composition of PHA polymers used in this study.

PHA ^a	Substrate	^a Monomer composition of PHA (mol %)								
		3HB	3HV	3HHx	3HHp	3HO	3HN	3HD	3HDD	3HTD
PHBV	Glucose/Valerate	76.9	23.1	ND	ND	ND	ND	ND	ND	ND
PHHx	Hexanoic acid	ND	ND	82.4	ND	16.0	ND	1.6	ND	ND
PHO	Octanoic acid	ND	ND	6.5	ND	92.0	ND	1.5	ND	ND
PHN	Nonanoic acid	ND	ND	ND	18.7	ND	81.3	ND	ND	ND
PHD	Decanoic acid	ND	ND	5.2	ND	57.4	ND	37.0	0.4	ND

^aPHBV polymer was synthesized by *C. nector* H16 and all the other PHA polymers were synthesized by *P. putida* LS46 (Sharma et al., 2016; Blunt et al., 2018). PHBV, Poly (3-hydroxybutyrate-co-3-hydroxyvalerate); PHHx, poly(3-hydroxyhexanoate); PHO, poly(3-hydroxyoctanoate); PHN, poly(3-hydroxynonanoate); PHD, poly(3-hydroxydecanoate); ND, not detected.

TABLE 2 | Primers used for the construction of recombinant lipase, *lip1* and *lip2* in pET28a vector.

Gene	Primers used
<i>lip1</i>	FP: ATAGCTAGCACAATGACCCCTCTCTATCGC RP: ATAAAGCTTACGGATGGATGACAGGGCCTG
<i>lip2</i>	FP: ATAGCTAGCAGCACGTTAAGTTGGGTTTCGT RP: ATAAAGCTTGGCGGATTGGCGCGCTTGCG

PA23 from NCBI (Accession No. CP008696). Primers were designed to incorporate the restriction endonuclease sites *NheI* and *HindIII* at the 5'-ends of the forward and reverse primers, respectively.

The PCR reaction was carried out in a Thermocycler (Biorad, USA) under defined conditions (initial denaturation at 98°C for 30 s followed by 34 cycles of 98°C for 10 s, 66°C for 30 s and 72°C for 1 min, with final extension of 10 min at 72°C). The amplicon was cloned into the expression vector, pET-28a (+), and transformed into *E. coli* DH5 α . Transformants were selected on LB kanamycin (50 μ g/ml) plates, followed by screening of recombinants by colony PCR and restriction digestion to verify fall-out. The positive clones containing lipase genes, *lip1* and *lip2* were confirmed and verified for integration by sequencing at the nucleic acid sequencing facility MacroGen, Maryland, United States.

Sequence Analysis and Homology Modeling

Amino acid sequence similarity searches for *P. chlororaphis* PA23 lipases, LIP1 (EY04_08410) and LIP2 (EY04_09635) were carried out using Basic Local Alignment Search Tool (BLAST) for

proteins (<http://blast.ncbi.nlm.nih.gov/Blast.cgi>). The sequences used were retrieved from the Integrated Microbial Genome (IMG) (<https://img.jgi.doe.gov>) and/or NCBI (<https://www.ncbi.nlm.nih.gov>). Alignment of amino acid sequences was performed using Clustal Omega (<https://www.ebi.ac.uk/Tools/msa/clustalo/>) and Esprict 3.0 (<http://esprict.ibcp.fr/ESPrict/ESPrict/>). Amino acids contents were analyzed using the ProtParam tool (<http://web.expasy.org/protparam/>). Secondary structure predictions and other protein features were generated using the XtalPred server (<http://ffas.burnham.org/XtalPred.cgi/xtal>). The three-dimensional structures of LIP1 and LIP2 were modeled using SWISS-MODEL (Waterhouse et al., 2018). The putative thioesterase tm1040_2492 from *Silicibacter* sp. TM1040 (2PBL) for LIP1, and the monoglyceride lipase Rv0183 from *M. tuberculosis* (6EIC) (Aschauer et al., 2017, 2018) for LIP2 served as templates. A dimer of 3-hydroxyoctanoic acid (HO) was generated using Avogadro: an open-source molecular builder and visualization tool, version 1.2.0 (<http://avogadro.cc/>, Hanwellet al., 2012) and the universal force field (Rappe et al., 1992) was used for energy minimization. The dimer was docked to the LIP1 and LIP2 model using the Vinawizard in PyRx software (Dallakyan and Olson, 2015). Figures were generated using PyMOL (Molecular Graphics System, Version 2.5.2).

Expression and Purification of Recombinant LIP1 and LIP2

The recombinant plasmids carrying the lipase gene (*pET28a-lip1* and *pET28a-lip2*) were isolated using the Geneaid plasmid isolation kit and introduced into *E. coli* BL21 (DE3) expression host. *E. coli* BL21 (DE3) cells harboring the recombinant plasmid were cultivated by inoculating 1%

TABLE 3 | Putative lipases present in the genome of *Pseudomonas chlororaphis* PA23.

Lipases	Accession number	Location	Gene size (bp)	Number of amino acids (aa)	Molecular weight (kDa)
LIP1	EY04_08410	Intracellular	828	275	29.7
LIP2	EY04_09635	Intracellular	834	277	30.2
LIP3	EY04_02420	Intracellular	891	296	32.5
LIP4	EY04_21540	Extracellular	942	315	34.0
LIP5	EY04_17885	Extracellular	1905	634	69.8
LIP6	EY04_32435	Extracellular	1911	636	70

primary culture of the recombinant cells into 50 ml of LB broth supplemented with 50 µg/ml kanamycin. Cells were grown using an incubator shaker at 37°C until optical density of 0.6 at 600 nm (OD_{600}) and induced with 0.6 mM isopropyl-1thio- β -D-galactopyranoside (IPTG) for 5 h. Subsequently, the expression levels of *lip1* and *lip2* were studied at various IPTG concentrations (0.4, 0.6, 0.8 and 1.0 mM), growth temperatures (37°C, 30 and 16°C) after induction, and incubation times (4, 8, and 16 h). The cells were harvested by centrifugation, and digested in chilled lysis buffer (25 mM Tris-HCl, 10 mM $MgCl_2$, 100 mM NaCl, and 1 mg/ml lysozyme) in an ultrasound machine [10 cycles with 1 min pulse (10 s on/off)]. Recombinant enzymes were purified from the clear lysate (obtained after centrifugation at $10,000 \times g$ for 30 min) by affinity chromatography using HiTrap Ni^{2+} -NTA resins (Qiagen) under nondenaturing condition according to the manufacturer's instructions. Expression profiles and purity of recombinant proteins were analyzed by sodium dodecyl sulfate–polyacrylamide electrophoresis (SDS-PAGE).

Qualitative and Quantitative Estimation of Depolymerase/Esterase Activity of LIP1 and LIP2

To determine the depolymerase activity of the recombinant enzymes, a homogeneous latex suspension of PHA polymers synthesized by *P. putida* LS46 from hexanoic (PHHx), octanoic (PHO), nonanoic (PNO), and decanoic acids (PHD) were prepared as described by Ramsay et al. (1994). Four volumes of a PHA solution in acetone (0.1%, w/v) were added dropwise to 1 volume of cold water (5–10°C) with stirring. The acetone was removed with speed vacuum concentrators to obtain a white colloidal suspension. PHA agar plates were prepared using 10 mg PHA polymer suspension and 1.5% (wt/vol) agar in 50 mM phosphate buffer (pH 7). The enzyme solution was dropped into 5-mm-diameter wells punched into the PHA agar plates and then incubated at 30°C for 48 h. The zone of clearance around the wells indicated the depolymerase activity. The fluorescent dye, Nile red (0.0005%) was added to the plates to reveal fluorescent clear halos around the wells when irradiated with UV light (350 nm) (Kouker and Jaeger, 1987).

The PHA depolymerase activity of the enzyme was determined by measuring the turbidity decrease of the PHA suspension at OD_{650} (Tamura et al., 2011). The reaction mixture contained 1 mg PHA latex, 50 mM phosphate buffer, pH 7 and 0.025 mg enzyme solution. The turbidity decrease was measured every 24 h for 96 h. The substrate control, PHA (without the enzyme) was taken in parallel. One unit of depolymerase activity by turbidimetric assay was determined as the amount of enzyme that can decrease the absorbance (OD_{650}) by 1 absorbance unit per min. Alternatively, one unit of depolymerase activity (units_{PHA}) was the amount of enzyme that hydrolyzes 1 µg of PHA in 1 min. Parallel PHA control samples (without the enzyme) were taken. All experiments were carried out in triplicate.

The esterase activity of lipases was determined as described by Schirmer et al. (1993) using p-nitrophenyl octanoate (PNPO) as substrate. The recombinant enzyme from crude cell lysate and/or

the purified enzyme (0.025 mg) was used in a reaction with 3.9 ml PBS buffer and 100 µl substrate, PNPO (1 mM) at optimum temperature for 20 min. The reaction was stopped with 1 ml of 1 M sodium carbonate and the absorbance was recorded at OD_{420} . The substrate control, PNPO (without the enzyme) was taken in parallel. One unit of PNPO esterase activity was measured as the amount of enzyme releasing 1 µmol of p-nitrophenol per min under optimal conditions. Total protein was determined by Bradford assay using Bovine serum albumin (BSA) as the standard protein (Bradford, 1996).

Biophysical and Biochemical Properties, and Substrate Specificity of LIP1 and LIP2

To determine the effect of pH on the activity of LIP1 and LIP2, the substrate (PNPO, 1 mM) was dissolved separately in buffers with different pH values [sodium acetate buffer (50 mM, pH 4.0–5.0), sodium phosphate buffer (50 mM, pH 6.0–8.0) and glycine-NaOH buffer (50 mM, pH 9.0–10.0)], and then used in reaction mixtures with the appropriately diluted enzyme (0.025 mg) solutions prepared in the desired buffers. The effects of temperature on lipase activity were investigated by testing at different temperatures (25–55°C) for 20 min. The enzymes were exposed to different temperatures (30–60°C) for a period of 24 h to check their thermal stability. The effect of cations (chloride/sulfate salts), chelators (EDTA) and ionic and non-ionic detergents on the enzyme activities of LIP1 and LIP2 was studied by adding them to the reaction mixtures and incubating them for 20 min in 50 mM sodium phosphate buffer at their optimal pH and temperature conditions. The residual enzyme activities were determined.

The substrate specificity of the enzymes was estimated against various PHAs, PHBV, PLA, p-nitrophenylalkanoate substrates (pNP-acetate, pNP-butyrate, pNP-octanoate and pNP-decanoate), and petrochemical based polymers such as poly(ethylene succinate) [PES] and polycaprolactone (PCL) at 1 mg substrate concentration under optimal conditions for enzyme activity. V_{max} and K_m values were calculated using the Lineweaver-Burk linear regression plot. The purified enzymes, LIP1 and LIP2 were incubated with pNP octanoate substrate in concentrations ranging from 0.1–3.0 mM under optimal assay conditions.

Gel Permeation Chromatography

The molecular weights of the PHAs before and after degradation with LIP1 and LIP2 were analyzed by gel permeation chromatography (GPC). The reaction mixture containing different 10 mg polymer suspension (PHB, PHHx, PHO, PHN, PHD, PLA, PCL, and PES) prepared according to Ramsay et al. (1994) was subjected to enzymatic hydrolysis with the recombinant lipases (2.5 mg) in separate experiments. The polymer substrates (without the enzyme) were kept as controls. After 96 h incubation at optimal temperature, the reaction mixtures and substrate controls were oven dried at 60°C. After cooling, samples were chloroformed to achieve a final sample concentration of 1.5 mg/ml and filtered with 0.45 µm PTFE. All test and control sample sets were

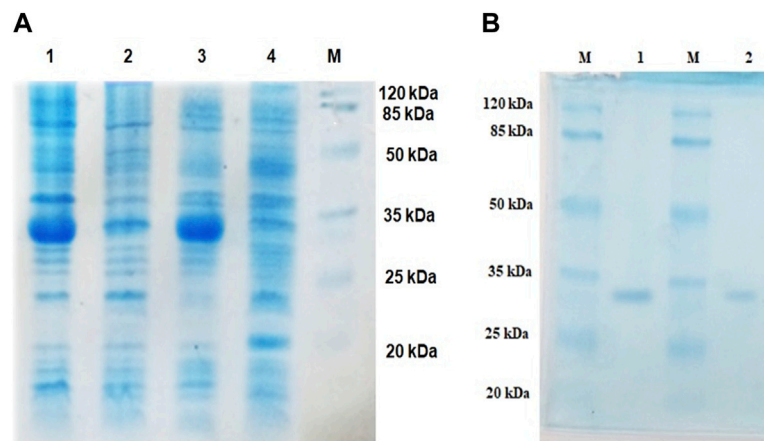


FIGURE 1 | Expression and purification profiles (SDS-PAGE) of recombinant LIP1 and LIP2; **(A)** Cell lysates of *Escherichia coli* BL21 (DE3) transformed with *pET28a-lip1* and *pET28a-lip2* Lane 1, cell lysate of induced *E. coli* BL21 (DE3) carrying *lip1-pET28a* expressing LIP1; Lane 2, the lysate of the noninduced host cells containing *lip1-pET28a*; Lane 3, cell lysate of induced *E. coli* BL21 (DE3) harboring *lip2-pET28a* with an expression band of LIP2; Lane 4, cell lysate of the non induced *E. coli* BL21 (DE3) with *lip2-pET28a* plasmid; Lane M, standard molecular weight marker (Thermo Fisher Scientific) **(B)** SDS-PAGE-purification profiles after His-Tag affinity chromatography: LIP1 (Lane 1) and LIP2 (Lane 2) on 12% SDS-PAGE; Lane M, standard molecular weight marker.

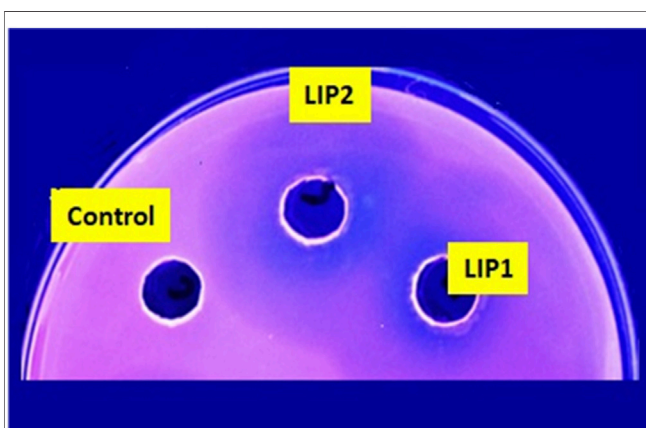


FIGURE 2 | PHA agar plate assay for testing the depolymerase/esterase activity of LIP1 and LIP2. Qualitative mcl-PHA depolymerase activity of LIP1 and LIP2 in Nile red-PHO agar plate after UV irradiation (350 nm). Twenty (20) μ g of purified LIP1 and LIP2 enzymes were added to the wells and incubated for 48 h. Substrate hydrolysis leads to the formation of fluorescent clear halos around the wells. The soluble crude extract of uninduced expression host *E. coli* BL21 (DE3) was used as control.

examined by gel permeation chromatography (GPC) using a Waters Model 1515 solvent pump with a Waters Refractive Index detector (model 2414) and the Agilent PLgel MIXED-C column (7.5 mm id: 1.5 ml/min). Data were acquired and analyzed using the Breeze 2 software (Waters Chromatography). The process was calibrated with Agilent Polystyrene EasiCal PS-1 standards (Agilent Technologies, Mississauga, Ontario, Canada). The mobile phase (HPLC grade chloroform) was run at a flow rate of 1 ml/min. The column temperature was set at 30°C and the sample injection volume was set at 20 μ l. The method was integrated with the standards to obtain the peak-average molecular weight (MP),

number-average molecular weight (M_n), weight-average molecular weight (M_w) and the polydispersity index (M_w/M_n).

RESULTS

Cloning, Expression and Purification of LIP1 and LIP2

The genome sequence of *P. chlororaphis* PA23 is available at the NCBI (<https://www.ncbi.nlm.nih.gov>) and Integrated Microbial Genome (IMG) (<https://img.jgi.doe.gov>) (Genome Acc. No. CP008696). *P. chlororaphis* PA23 possess seven genes annotated as esterase/lipase (Table 3). Of these, three encode for intracellular lipases (EY04_08410, EY04_09635, EY04_02420), three encode a signal peptide and are extracellular lipases (EY04_21540, EY04_17885, EY04_32435), and one encodes for an intracellular PHA depolymerase (EY04_01535). In our previous study, the hydrolysis of the ester bonds of p-nitrophenyl-fatty acid substrates, and the ester bonds of PHA polymers of various subunit composition by the extracellular esterases/lipases was recorded in the culture media in which *P. chlororaphis* PA23 and *A. lwoffii* were grown (Sharma et al., 2019). In the present study, two genes encoding intracellular lipases were cloned and expressed in *E. coli* BL21(DE3) to compare the properties and investigate its biodegradability in comparison with various biodegradable polymers.

Lipase genes cloned into the pET28a(+) vector and expressed in *E. coli* BL21(DE3) showed optimal expression with 0.6 mM IPTG at 37°C in 5 h (Figure 1A). The recombinant proteins were purified to homogeneity. SDS-PAGE analysis of the expressed and purified enzymes revealed molecular masses of ~30 kDa for LIP1 and LIP2, which correlated with the predicted molecular mass from its amino acid sequence (<https://web.expasy.org/protparam>) (Figures 1A,B). Qualitative assessment of the

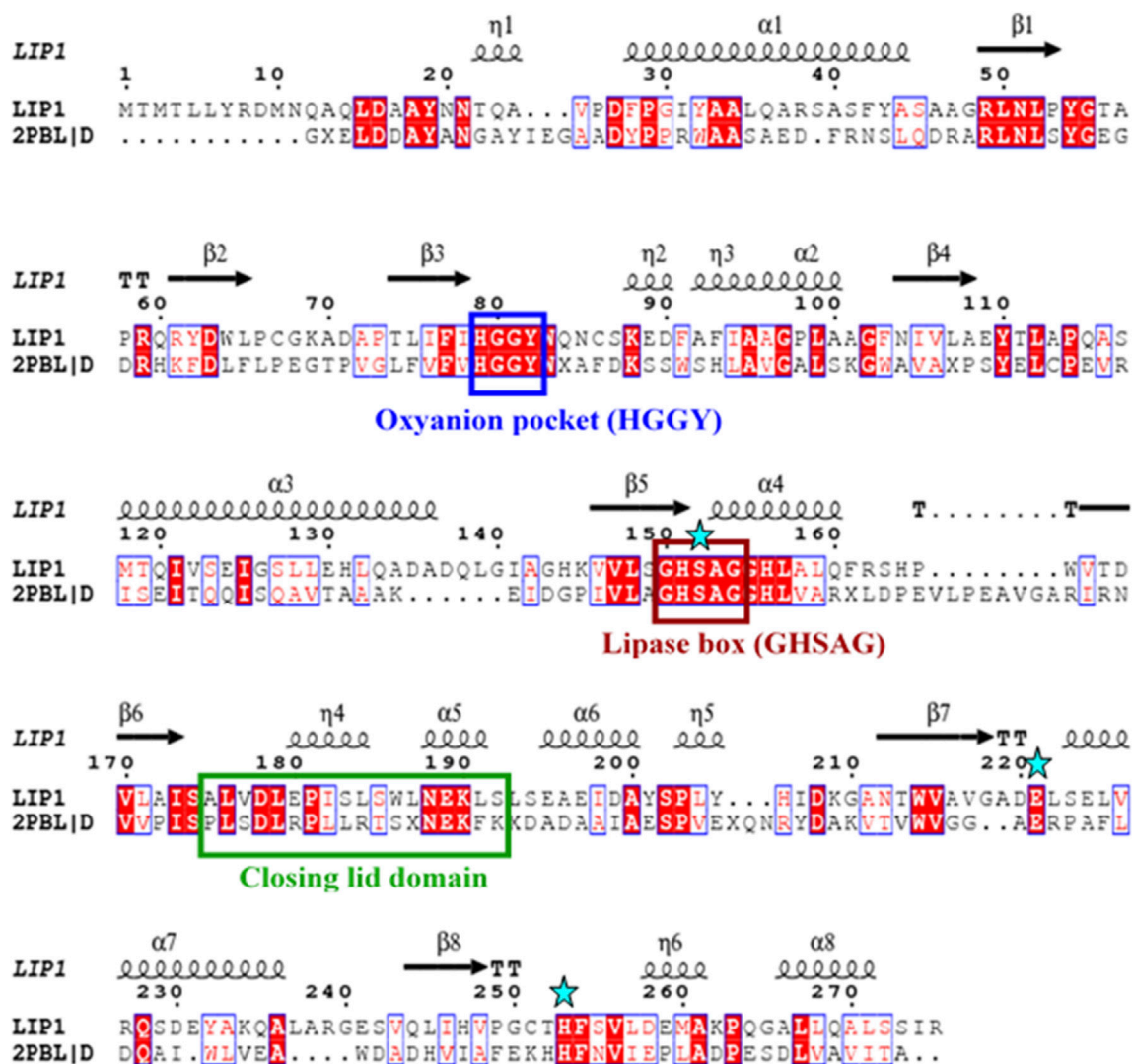


FIGURE 3 | Amino acid sequence alignment of LIP1 with putative lipase/thioesterase from *Silicibacter* sp. Tm1040 (2PBL). The lipase consensus sequence is indicated by a brown box, the residues of the oxyanion holes in a blue box, the domain of the closing lid in a green box and the residues of the catalytic triad (serine, glutamic acid and histidine) are highlighted by asterisks. α -helix and β -strands are shown at the top of the alignment.

depolymerase activity of the purified enzyme was analyzed in a PHA agar plate with Nile red fluorescent dye (Figure 2). Compared to the control strain (the soluble crude extract of uninduced recombinant *E. coli* BL21 cells containing *lip1-pET28a(+)/lip2-pET28a(+)*, the purified enzymes were able to hydrolyze PHA latex as shown by the formation of fluorescent clear halos/zones around the wells after 48 h of incubation at 30°C, under UV irradiation (350 nm) (Figure 2).

Sequence Analyses and Homology Modeling of LIP1 and LIP2

The *lip1* and *lip2* genes were found to encode enzymes with predicted molecular masses of 29.7 and 30.2 kDa, respectively. BLAST analyses of the deduced amino acid sequences (BLASTp) revealed that the enzymes, LIP1 and LIP2, belong to the lipase

superfamily and have an α/β -hydrolase fold. Alignment of the amino acid sequences of LIP1 and LIP2 revealed very low sequence identity (15.39%). However, both enzymes have the conserved sequence regions including the lipase box (GX₁SX₂G) characteristic of the lipase/esterase family and the putative oxyanion hole residues (HGGY in LIP1; HGX in LIP2) in the catalytic domain (Figures 3, 4). The x₁ sites in the lipase boxes of LIP1 and LIP2 are occupied by histidine (H151) and arginine (R137), whereas the x₂ sites contain alanine (A153) and proline (P139), respectively. The enzymes possess a catalytic triad (serine-histidine-aspartic acid/glutamic acid) characteristic of other lipases. The catalytic triad of LIP1 has Ser¹⁵²-His²⁵³-Glu²²¹ (Figure 3), while the catalytic triad of LIP2 has Ser¹³⁸-His²⁴⁹-Asp²²¹ in its active site (Figure 4).

PSI-BLAST search for LIP1 and LIP2 in the Protein Data Bank revealed several bacterial lipases as close homologues.

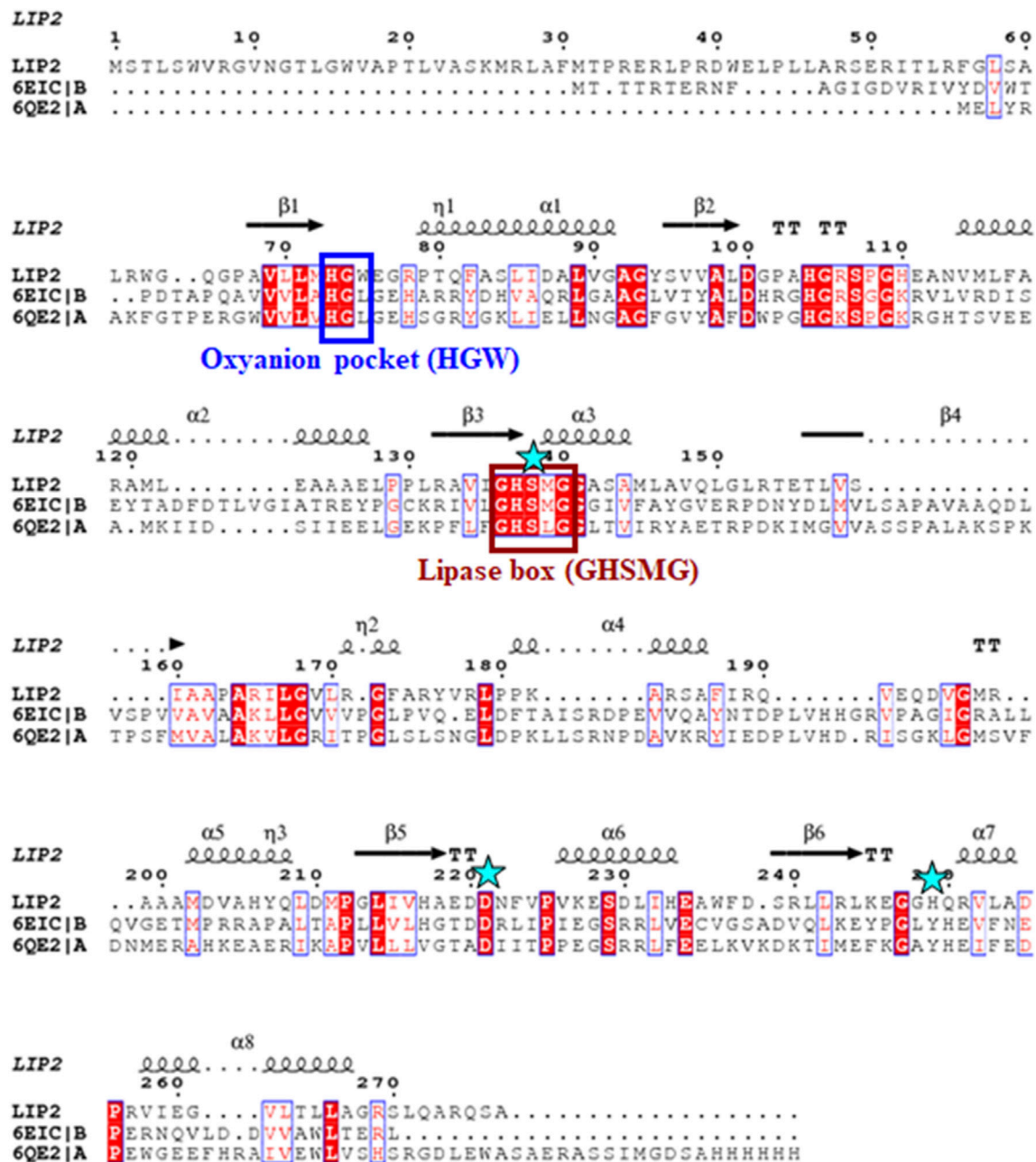


FIGURE 4 | Amino acid sequence alignment of LIP2 with the monoglyceride lipase from *Mycobacterium tuberculosis* (6EIC) and monoacylglycerol lipase from *Paleococcus ferrophilus* (6QE2). The consensus sequence of lipase is shown in a brown box, the residues of the oxyanion hole are indicated by a blue box, and the residues of the catalytic triad (serine, aspartic acid and histidine) are highlighted by asterisks. The α -helix and β -strands are shown at the top of the alignment.

The putative esterase, tm1040_2492 from *Silicibacter* sp. TM1040 (2PBL) was chosen as a template for LIP1 (27% amino acid identity and 88% similarity), and monoglyceride lipase Rv0183 from *M. tuberculosis* (6EIC) was chosen for LIP2 (24% amino acid identity and 70% similarity). **Figures 5A, 6A** show the homology model of LIP1 and LIP2, respectively, with the substrate 3-hydroxyoctanoate. The core domain of LIP1 consists of an 8-parallel stranded β -sheet (except for strand-2 which is antiparallel), whereas

LIP2 consists of a six-parallel stranded β -sheet. Multiple α -helices are located on both sides of the core β -sheet in each model. **Figures 5B,C, 6B,C** show the binding pocket of the substrate 3-hydroxyoctanoate dimer. Residues 175-192 of LIP2 are likely the closing lid domain of the substrate binding pocket, while the substrate binding pocket of LIP1 is exposed and lacks the closing lid (capping) domain. To better illustrate the substrate binding pocket, the closing lid domain is not shown in **Figure 6B**.

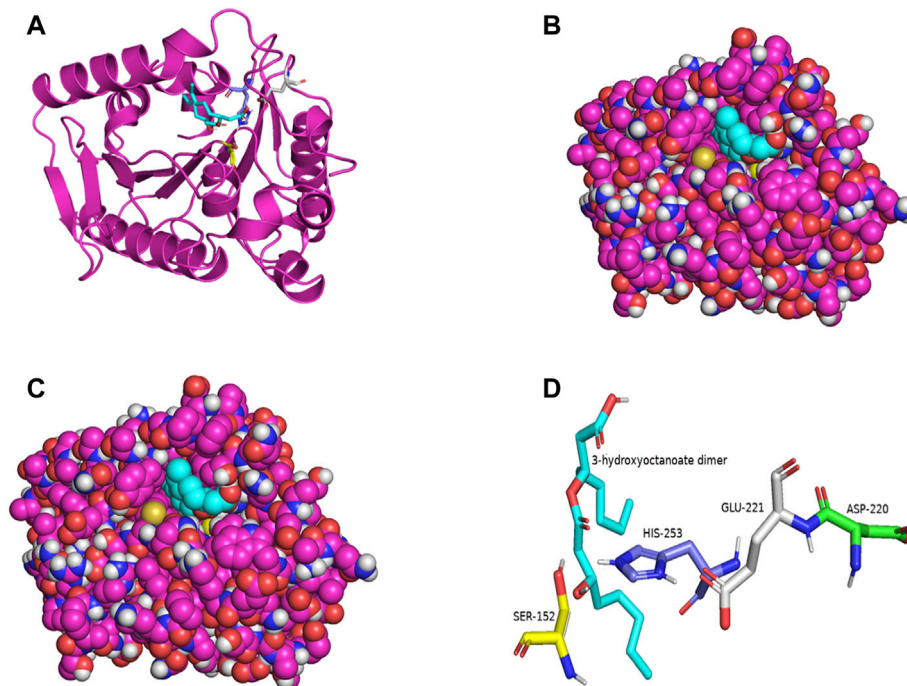


FIGURE 5 | The three-dimensional structure of LIP1 generated by homology modelling. **(A)** Ribbon plot representation of the entire LIP1 scaffold with labelled residues of the catalytic triad Ser¹⁵² (yellow) His²⁵³ (slate) Glu²²¹ (gray) in the binding pocket. The substrate 3-hydroxyoctanoate dimer (cyan) is computationally docked. **(B)** Atomic model of LIP1 with docked substrate in van der Waals representation. **(C)** Representation of the molecular surface of lipase LIP1 with the docked substrate (stick representation). **(D)** The closer view of the residues (stick model) of the catalytic triad around the substrate in the active site of LIP1, colored as in A, with Asp220 colored green. The structure is calculated using the putative esterase tm1040_2492 as template and SWISS-MODEL Program.

The catalytic triad of hydrolases and lipases usually involving closely spaced Ser-His-Asp/Glu residues is a hallmark of this enzyme class. We also identified the catalytic triad motif in both LIP1 both LIP2 and modeled their binding pockets with the substrate as shown in **Figures 5D, 6D**. In the LIP1 model, the distance between O δ of Glu²²¹ and N δ of His²⁵³ is 3.1 Å. In comparison, in the LIP2 model, the O δ of Asp²²⁰ is 12.4 Å away from His²⁵³, and therefore, Glu²²¹ acts as the acid in the catalytic triad of LIP2. The binding energy for the substrate to LIP1 and LIP2 determined in the docking experiment was calculated to be -6.4 kcal/mol and -6.1 kcal/mol, respectively. A negative free energy of binding indicates the substrate docking is spontaneous.

Characterization of the Recombinant LIP1 and LIP2

LIP1 and LIP2 were active over a wide pH range (pH 4.0–10.0) with optimal activity at pH 9.0 and pH 8.0, respectively (**Figure 7A**). LIP1 and LIP2 retained more than 50% of activity over a pH range from 8.0 to 10.0, but the enzymes showed less than 30% activity at acidic pH (4.0–6.0). LIP1 and LIP2 were optimally active at 45 and 40°C, respectively, and retained more than 50% activity when the reaction was carried out at 55°C (**Figure 7B**). Moreover, thermal inactivation experiments showed that the LIP1 retained nearly 70% activity for 24 h at 45°C (**Figure 7C**).

LIP2, on the other hand, was very stable and retained more than 80% of its activity for 24 h at 45°C. The enzymes were stable at 30°C for at least 2 months of incubation and retained nearly 100% of their activities for minimum 4 months at 4°C. Sequence analysis of LIP1 and LIP2 was performed to analyze thermophilic properties in relation to their amino acid sequence (**Table 4**). Enzyme kinetic studies using pNP-octanoate as substrate revealed that V_{\max} and K_m for LIP1 were $769.23 \mu\text{M mg}^{-1} \text{ min}^{-1}$ and 0.384 mM , respectively, whereas these values for LIP2 were $714.28 \mu\text{M mg}^{-1} \text{ min}^{-1}$ and 0.286 mM , respectively.

When the effect of cations and other compounds was examined (**Table 5**), it was found that 1 mM MgSO_4 , or 10 mM EDTA did not affect the enzyme activity, but the enzyme activity of LIP1 was increased by 50% in the presence of 1 mM CaCl_2 . The activity of LIP2 was not affected by the presence of EDTA and metal ions, indicating that it is not a metalloenzyme. The cations of magnesium, sodium and calcium are not required as cofactors for the enzyme activity. PMSF and ionic and nonionic detergents (SDS and Tween 80) inhibited the activities of both LIP1 and LIP2 (**Table 5**).

Substrate Specificity of LIP1 and LIP2

The lipase enzymes LIP1 and LIP2 showed broad substrate specificity. In particular, the enzymes demonstrated significant activity towards the ester bonds of pNP-alkanoates, which are the typical substrate for lipases (**Figure 8**). LIP1 and LIP2 hydrolyzed

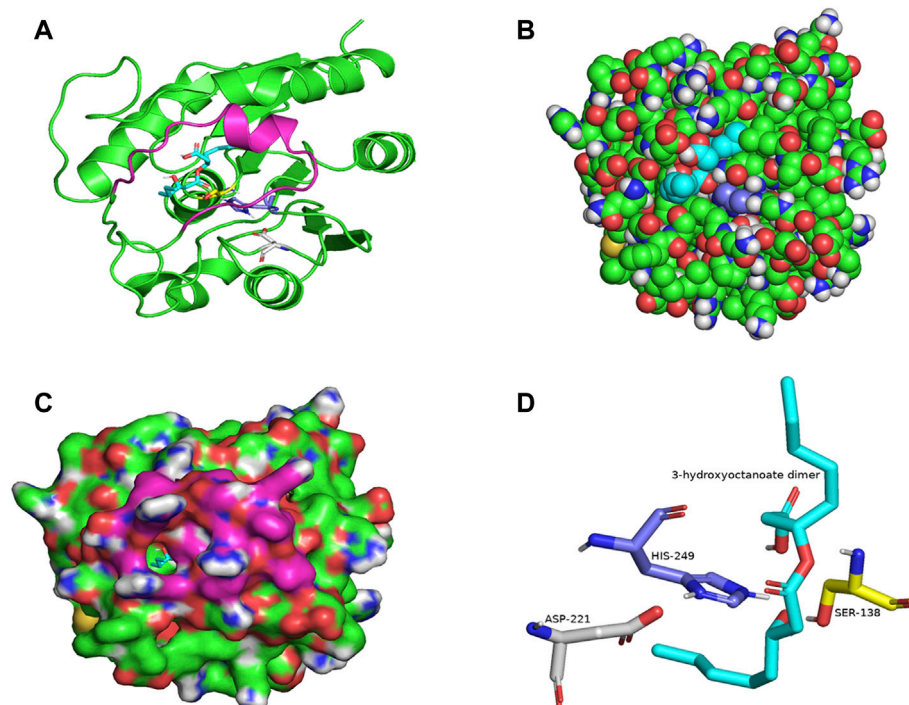


FIGURE 6 | The three-dimensional structure of LIP2 generated by homology modelling. **(A)** Ribbon plot representation of the entire LIP2 scaffold with labelled residues of the catalytic triad Ser¹³⁸ (yellow) His²⁴⁹ (slate) Asp²²¹ (gray) in the binding pocket. The model also contains the lid domain (magenta) and the active site with the docked substrate 3-hydroxyoctanoate dimer (cyan). **(B)** Atomic model of LIP2 with docked substrate in van der Waals representation. Note that the lid domain is not shown to better visualize the binding pocket. **(C)** Illustration of the lipase LIP2 surface with the docked substrate (stick representation). **(D)** The closer view of the residues (stick model) of the catalytic triad around the substrate in the active site of LIP2, colored as in A. The structure is calculated using the monoglyceride lipase Rv0183 as template and SWISS-MODEL Program.

pNP-alkanoates ranging from shorter to longer side chains, with esterase activity highest for pNP-octanoate. The relative activity of LIP1 was significantly higher (88.24%) than that of LIP2 (67.23%) for pNP-butyrate. LIP1 and LIP2 were able to hydrolyze ester bonds of β -polyhydroxyalkanoates/PHA polymers prepared from valeric acid (PHBV), hexanoic acid (PHHx), octanoic acid (PHO), nonanoic acid (PHN), and decanoic acid (PHD), as shown by the turbidimetric assays with different polymers (Table 6). The order of substrate (PHA) preference for the LIP1 was PHO > PHN > PHD > PHHx > PHBV while for LIP2 the order of substrate preference was PHO > PHN > PHHx > PHBV > PHD. With PHO as substrate, LIP1 and LIP2 had specific activity of 360.12 units_{PHA}

mg⁻¹ and 301.72 units_{PHA} mg⁻¹ of protein, respectively. Taken together, these results indicate that the enzyme has a broad substrate spectrum ranging from scl- and mcl-PHAs to pNP-alkanoates (C4 to C10). Remarkably, in addition to PHA polymers, the enzymes showed significant activity towards PLA and were able to hydrolyze synthetic polyester plastics such as PCL and PES (Table 6).

Analysis of Degradation Products

Gel Permeation Chromatography (GPC) analyses of the polymer samples before and after enzyme treatment revealed significant degradation of PHAs, PLA, and the petrochemical-based polymers, PCL and PES by both LIP1 and LIP2. The chromatograms for each set of experiments with PHBV, PHHx, PHO, PHN, PHD, PLA, PCL, and PES showed a decrease in molecular weight in the polymer samples treated with LIP1 and LIP2 relative to the untreated/control samples (Supplementary Figures S1–S8). Degradation was achieved for scl-PHA (PHBV), mcl-PHAs (PHHx, PHO, PHN, PHD), PLA, PCL and PES for both LIP1 and LIP2 after 96 h of enzyme treatment. Separate chromatograms for each of the samples are included in Supplementary Figures S1–S8. The quantitative results of GPC analysis revealed significant changes in Mw, Mn, MP, polydispersity and other related parameters

TABLE 4 | Parametric comparison and amino acid composition analysis of LIP1 and LIP2.

Amino Acid	LIP1	LIP2
% Uncharged polar residues (Gln + Asn + Thr + Ser)	20.3	13.3
% Hydrophobic residues (Ala + Val + Ile + Leu)	37.1	38.6
% Arg	3.3	9.7
% Lys	2.5	1.4
% Pro	4.7	5.8
% Cys	1.1	0
% Arg/Lys	1.32	6.93

TABLE 5 | Effects of various modulators on LIP1 and LIP2 activity.

Modulators/reagents	Final concentration	Relative activity (%)	
		LIP1	LIP2
EDTA	10 mM	98 ± 1.5	95 ± 3.1
CaCl ₂	1 mM	158 ± 3.5	82 ± 2.2
MgCl ₂	1 mM	79 ± 2.1	73 ± 1.2
NaCl	50 mM	110 ± 1.1	96 ± 0.5
PMSF	1 mM	69 ± 0.5	80 ± 3.3
Tween80	0.1%	30 ± 1.6	53 ± 0.9
SDS	5%	26 ± 1.0	19 ± 2.6
Enzyme activity (Without modulator)		100	100

^aThe values shown are the averages of three independent (biological) replicate experiments ± standard deviations.

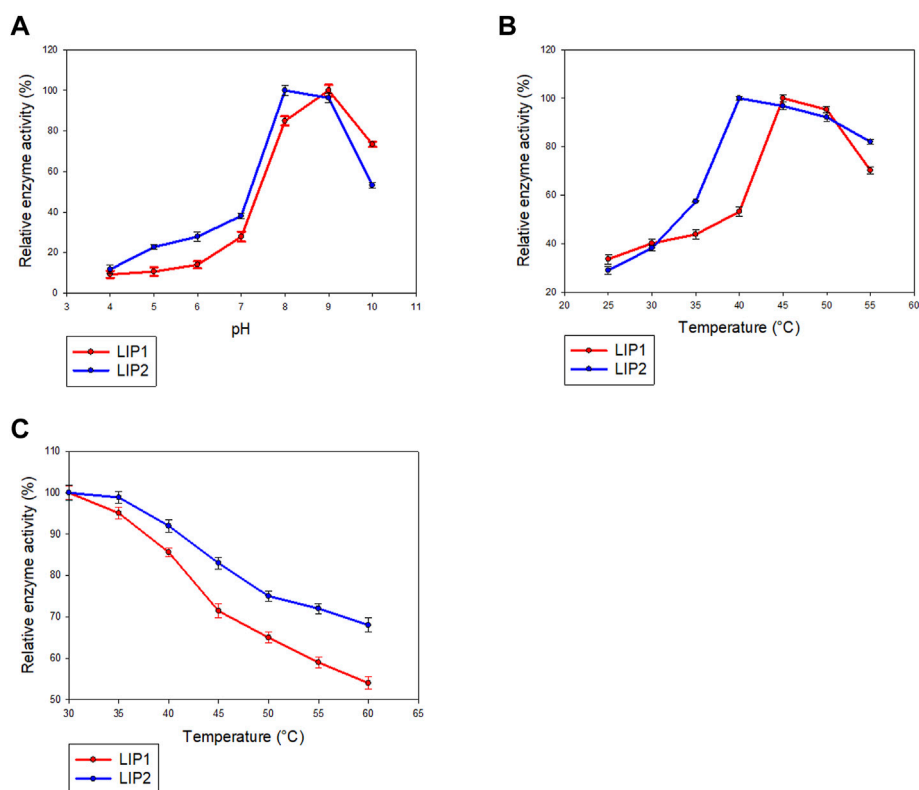


FIGURE 7 | Determination of parameters of enzymatic activity of LIP1 and LIP2. Effects of **(A)** pH and **(B)** temperature on the activity of LIP1 (red line) and LIP2 (blue line). Recombinant LIP1 and LIP2 were optimally active at pH 9.0 and 8.0, respectively. The observed maximum activity was taken as 100%. **(C)** Effect of temperature on the stability of LIP1 (red line) and LIP2 (blue line). The activity of the untreated enzyme (0.025 mg/ml) was set as 100%.

(Supplementary Table S1) for the polymers treated with LIP1 and LIP2 compared to the untreated samples/control.

DISCUSSION

Our previous report showed that the cell free culture supernatant of *P. chlororaphis* PA23 was shown to hydrolyze the ester bonds of p-nitrophenyl fatty acid substrates and PHA polymers of various subunit composition (Sharma et al., 2019). In the

present study, two genes encoding intracellular lipases (designated here as LIP1, EY04_08410 and LIP2, EY04_09635) from *P. chlororaphis* PA23 were cloned and expressed in *E. coli* BL21 (DE3). Analysis of the primary structures of the LIP1 and LIP2 enzymes revealed no significant overall sequence homology between them. However, the lipase consensus sequence motif GX₁SX₂G was found with the X₁ occupied by histidine and arginine residues in LIP1 and LIP2, respectively. In lipases and esterases, the X₁ residue is commonly occupied by a polar residue and X₂ is variable (Schirmer et al., 1993). In contrast, PHA

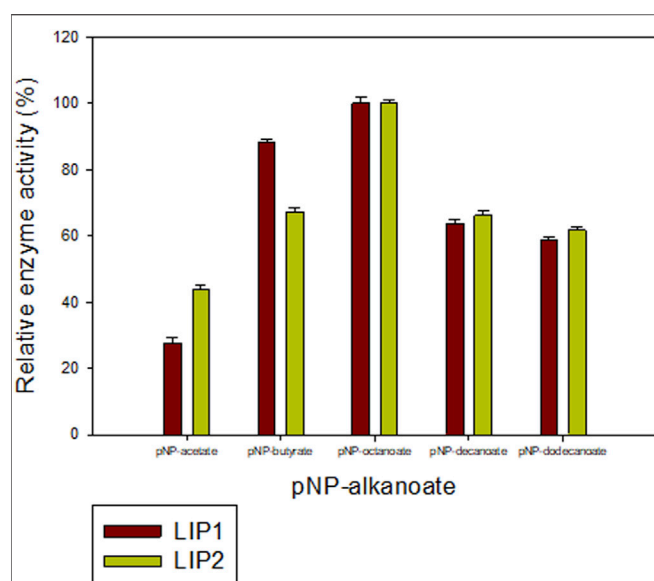


FIGURE 8 | Determination of the activities of LIP1 and LIP2 towards different substrates. Substrate specificity of lipases LIP1 (brown bars) and LIP2 (green bars) from *P. chlororaphis* PA23. The reaction mixture contained 1 mM of various p-nitrophenyl(pNP) alkanates and 0.025 mg of purified enzyme under optimal conditions of the enzymes. The maximum activity observed was taken as 100%. The 100% activity for LIP1 and LIP2 corresponded to 730.12 U mg⁻¹ and 656.56 U mg⁻¹ for pNP-octanoate, respectively.

TABLE 6 | Substrate specificity of the purified LIP1 and LIP2.

Substrate	Relative activity (%) ^a	
	LIP1	LIP2
PHA polymers		
PHBV	74.35 ± 2.2	63.45 ± 3.1
PHHx	79.31 ± 5.5	74 ± 2.6
PHO	100	100
PHN	92.33 ± 3.2	82.84 ± 4.3
PHD	83.19 ± 4.9	59.31 ± 3.6
Other biodegradable/petrochemical-based polymers		
polylactic acid (PLA)	42.32 ± 1.2	47.89 ± 4.3
poly(ε-caprolactone) (PCL)	32.96 ± 3.2	38.11 ± 1.4
poly(ethylene succinate) (PES)	17.09 ± 2.3	14.66 ± 3.7

^aThe values shown are the averages of three independent (biological) replicate experiments ± standard deviations. The pure enzyme (0.025 mg) was assayed with the indicated substrates at a final concentration of 1 mg, in all cases for 96 h. Polymer without the enzyme was taken as control. The maximum activity observed was taken as 100%. 100% activity corresponded to 360.12 U mg⁻¹ in LIP1 and 301.72 U mg⁻¹ in LIP2.

depolymerases have a hydrophobic residue at position X₁ (Knoll et al., 2009; Gangoi et al., 2012). Another conserved sequence region (HGGY- in LIP1 and HGX- in LIP2) that appears to resemble the oxyanion hole consensus sequence in lipases was observed. Depending on the amino acids involved in the formation of the oxyanion hole, lipolytic enzymes are divided into two classes, the GGGX (X can be F, L or Y) and the GX type (Fischer and Pleiss, 2003; Pleiss et al., 2000). Thus, LIP1 belongs

to the GGGX type, in which the first G is replaced by H, whereas LIP2 belongs to the GX class.

Lipases are generally highly variable in size, and sequence similarity among them is limited to short regions located around active-site residues. Arpigny and Jaeger (1999) suggested that bacterial lipases can be grouped into eight classes based on their conserved amino acid sequence regions and biochemical properties. However, the three-dimensional structures of lipases share a common folding motif in their cores, known as α/β hydrolase-fold, which is characteristic of hydrolase and/or esterase family enzymes (Ollis et al., 1992). The general α/β-hydrolase-fold consists of an eight-stranded, mostly parallel β sheet flanked by six α helices, with a catalytic triad (Ser/Asp/Cys-His-Asp/Glu); LIP1 has eight β sheets with Ser¹⁵²-His²⁵³-Glu²²¹ in its active site, while LIP2 has six β sheets and Ser¹³⁸-His²⁴⁹-Asp²²¹ as a catalytic triad.

The enzymes exhibited different pH and temperature optima/stability but were similar to the lipase from *Pseudomonas aeruginosa* MB 5001, which showed maximum esterase activity at pH 8.0 and 55°C (Chartrain et al., 1993). The lipases of psychrotrophic *Pseudomonas fluorescens* strain AFT 36 (Fox and Stepaniak, 1983) and *Pseudomonas* sp. (Choo et al., 1998) were found to be stable between pH 6 and 9. The lipases from *Pseudomonas* sp. and *P. fluorescens* strain AFT 36 were found to be stable below 60°C (Fox and Stepaniak, 1983; Dong et al., 1999). PueB lipase from *Pseudomonas chlororaphis* (Howard et al., 2001) and lipase from *Pseudomonas* sp. (Adams and Brawely, 1981) exhibited stability at 100°C. The thermal stability of LIP2 was relatively higher than that of LIP1 as inferred from the thermal inactivation studies. Sequence analysis of LIP1 and LIP2 also revealed relatively high thermostability for LIP2 compared with LIP1. LIP2 has few uncharged polar residues, a high arginine/lysine ratio and a high proline content (Table 4), the sequence based parameters which contribute to its increased thermal stability, as defined by Szilagyi and Zavodsky, 2000).

The stimulatory effect of Ca²⁺ on the LIP1 activity was similar to that observed for lipases from *Pseudomonas putida* 3SK (Lee and Rhee, 1994), *P. aeruginosa* EF2 (Gilbert et al., 1991) and *Pseudomonas* sp. 7323 (Zhang and Zeng, 2008). It has been suggested that the calcium ion is primarily involved in removal of fatty acids formed as insoluble calcium soaps during hydrolysis, thus causing a change in the interfacial substrate-water ration that is favorable for enzyme action (Brockman, 1994). The addition of calcium ion could also lead to better alignment on the substrate molecule or the formation of the calcium salts of fatty acids (Macrae and Hammond, 1985; Godtfredsen, 1990). Esterase activity was not affected by the presence of EDTA and metal ions in LIP2, suggesting that it is not a metalloenzyme and/or metal ions are not required as cofactors for enzyme activity. Similar observations were made for the lipases of *Trichosporon asteroides* strain LP005 (Dharmstithi and Ammaranond, 1996) and *Aspergillus terreus* (Yadav et al., 1998). PMSF causes sulfonylation of the O_γ atom of the active-site serine residue, thereby obliterating the catalytic region and leading to irreversible inhibition of the enzyme activity (Sharma and

TABLE 7 | Degradation of polyesters by bacterial lipases/esterases.

Bacterial source	Lipases/ Esterases	Polyesters hydrolyzed/ Degradation ability of the enzymes	Polyesters not hydrolyzed	Method Used	Activity	References
<i>Pseudomonas</i> sp.	Extracellular lipase	Polycaprolactone	—	Weight loss	—	Kim et al. (1992)
<i>Streptomyces rochei</i> , <i>Pseudomonas fragi</i> , <i>Pseudomonas</i> sp.	Extracellular lipases (commercial)	Poly(3-hydroxypropionate), Polycaprolactone	Poly(3-hydroxybutyrate) Poly(4-hydroxybutyrate) Poly(5-hydroxyvalerate) Poly(6-hydroxyhexanoate)	Weight loss of polyester films	0.3–1.0 mg weight loss	Mukai et al. (1993)
<i>Pseudomonas fluorescens</i>	Extracellular lipase (commercial)	Poly(3-hydroxypropionate) Poly(4-hydroxybutyrate) Poly(6-hydroxyhexanoate)	Poly(3-hydroxybutyrate), Poly(5-hydroxyvalerate)	Weight loss of PHA films	0.4–0.8 mg weight loss	Mukai et al. (1993)
<i>Bacillus subtilis</i> , <i>Pseudomonas aeruginosa</i> , <i>Pseudomonas alcaligenes</i> , <i>Burkholderia cepacia</i> (former <i>Pseudomonas cepacia</i>)	Extracellular lipases	pNP-palmitate, Poly(6- hydroxyhexanoate) Poly(4- hydroxybutyrate), Polycaprolactone	Poly(3-hydroxybutyrate) Poly(3-hydroxyalkanoates), Polylactic acid	Turbidimetric assay, Rhodamine agar plate assay	<i>B. subtilis</i> lipase: 0.2 × 10 ³ U/mg (pNPP) 6000 U/mg (PCL) <i>P. aeruginosa</i> lipase: 52 × 10 ³ U/mg (pNPP) 1.8 × 10 ⁶ U/ mg (PCL) <i>P. alcaligenes</i> lipase: 8 × 10 ³ U/mg (pNPP) 140,000 U/mg (PCL) <i>B. cepacia</i> lipase: 0.5 × 10 ³ U/mg (pNPP) 40,000 U/mg (PCL)	Jaeger et al. (1995)
<i>P. fluorescens</i> GK13	Extracellular esterase	pNPP	Polyhydroxyalkanoates, Polycaprolactone, Polylactic acid	Turbidimetric assay Rhodamine agar plate assay	0.4 × 10 ³ U/mg (pNPP)	Jaeger et al. (1995)
<i>Pseudomonas</i> sp. AKS2	Extracellular esterase and lipase	Low density polyethylene	-	Viability test in biofilm	-	Tribedi et al. (2015)
<i>Bacillus subtilis</i>	Extracellular lipase	pNPP, Polyhydroxyalkanoates	-	Molecular weight decrease by GPC FTIR NMR DSC	21.3% molecular weight decrease, 28.3% weight loss, 273.65 U/mg (pNPP)	Kanmani et al. (2016)
<i>Geobacillus zalihae</i>	Extracellular lipase	Poly(3-hydroxybutyrate)	-	Poly(3- hydroxybutyrate) agar plate	Clear zone around the colony	Mohamed et al. (2017)
<i>Pseudomonas chlororaphis</i> PA23- 63-1	Extracellular lipases and esterases mix	pNP-alkanoate Poly (3-hydroxybutyrate-co- 3-hydroxyvalerate) Poly(3-hydroxyhexanoate) Poly(3-hydroxyoctanoate) Poly(3-hydroxynonanoate) Poly(3-hydroxydecanoate)	Polycaprolactone, Polyethylene sulfonate	PHA agar plate assay, Turbidimetric assay, Weight loss of PHA films	4.5% weight loss, 997.7 U/mg (pNPO), 722 U/mg (PHO), Clear zone of PHA hydrolysis	Sharma et al. (2019)
<i>Pseudomonas chlororaphis</i> PA23	Intracellular lipases, LIP1 and LIP2	Poly (3-hydroxybutyrate-co- 3-hydroxyvalerate) Poly(3-hydroxyhexanoate) Poly(3-hydroxyoctanoate) Poly(3-hydroxynonanoate) Poly(3-hydroxydecanoate) Polylactic acid Polycaprolactone Polyethylene sulfonate	-	Nile blue agar plate assay, Turbidimetric assay, Molecular weight decrease by GPC	18–40% molecular weight decrease, Clear zone of PHA hydrolysis, 769.23 U mg ⁻¹ in LIP1 (pNPO), 714.28 U mg ⁻¹ in LIP2 (pNPO), 360.12 U mg ⁻¹ in LIP1 (PHO), 301.72 U mg ⁻¹ in LIP2 (PHO)	This study

^apNP, paranitrophenyl; pNPP, paranitrophenyl palmitate; pNPO, paranitrophenyl octanoate; PHA, polyhydroxyalkanoate; PHBV, Poly (3-hydroxybutyrate-co-3-hydroxyvalerate; PHO, Poly(3-hydroxyoctanoate); PLA, polylactic acid; PCL, polycaprolactone; PES, polyethylene succinate; LDPE, low density polyethylene; GPC, gel permeation chromatography; FTIR, fourier transform infrared; NMR, nuclear magnetic resonance; DSC, Differential Scanning Calorimetry.

Radha Kishan 2011). The inhibition of enzyme activity by PMSF in the enzymes was comparable to that of PseB lipase from *Pseudomonas chlororaphis*, which showed 50% inhibition with 1 mM PMSF (Howard et al., 2001). Inhibition of LIP1 and LIP2 activities by ionic and nonionic detergents, SDS and Tween 80 indicates the presence of a hydrophobic region in the catalytic center and/or a change in the active configuration of the enzyme. Inhibition of enzyme activity by SDS has been reported for lipase from *Pseudomonas putida* 3SK (Lee and Rhee, 1994), while *Thermomyces lanuginosus* lipase stays active at high SDS concentrations at alkaline pH (Rasmussen et al., 2022).

Modelling the three-dimensional structures of LIP1 and LIP2 complexed with a 3-hydroxyoctanoate dimer revealed the core domain to be of the α/β hydrolase-type with an active site capped with a closing lid domain in LIP2 and an exposed substrate binding pocket in LIP1. Most lipases function at an organic-aqueous interfaces facilitated by a mobile subdomain flap or lid located over the active site (Brocca et al., 2003; Khan et al., 2017). The lid protects the active site and is therefore responsible for catalytic activity (Barbe et al., 2009). In aqueous media, the lid is mostly closed, whereas in the presence of a hydrophobic layer, the open form is likely to be the predominant structure. The lids of lipases are amphipathic structures; in the closed form, their hydrophobic side is directed toward the catalytic pocket, while the hydrophilic side faces the solvent (Brocca et al., 2003). When the enzyme changes to the open conformation, the hydrophobic side becomes exposed so that it contributes to the substrate-binding region (Yang and Lowe, 2000). The amphipathic nature of the lid and its specific amino acid sequence are important factors contributing to the enzyme activity and specificity of lipases (Holmquist et al., 1995). However, some lipases do not have a lid structure such as CalB, the lipase from *Candida Antarctica* B (Uppenberg et al., 1994).

Interestingly, LIP1 and LIP2 showed broad substrate specificity with the ability to degrade pNP-alkanoates (C2-C12), scl- (C4) and mcl-PHAs (C6-C10), PLA, PCL and PES. The PseB lipase from *Pseudomonas chlororaphis* was also reported that have esterase activity with various pNP-alkanoates such as pNP-acetate, pNP-propionate and pNP-butyrate (Howard et al., 2001). While the LIP1 and LIP2 enzymes exhibited maximum activity with pNP-octanoate a different relative activity with the polyesters was found. LIP1 showed high relative activity to pNP-butyrate (C4) compared to LIP2. LIP1 has a comparatively high substrate preference for medium-chain PHAs which can be attribute to its high relative activity for PHO, PHN and PHD. In contrast, LIP2 has comparatively low degradation activity for PHD. The difference in substrate specificity maybe related to the different amino acid composition of the oxyanion pocket (GGX-type oxyanion in LIP1 versus GX-type in LIP2) and the active site configuration of the enzymes with different binding energy with the substrates.

PES is a poly(alkenedicarboxylate), while PCL is an aliphatic polyester composed of repeating ω -hydroxyalkanoate units. These

polymers are mainly used in thermoplastic polyurethanes among many other applications (Fatma et al., 2014). The cell-free supernatant of yeast culture, *Pseudozyma japonica*-Y7-09 showed significant ability to degrade PCL (Fatma et al., 2014). The extracellular lipases of *P. aeruginosa* revealed the degradation of aromatic-aliphatic polyesters and polyesteramides (Wilkes and Aristilde, 2017). However, none of the studies determined the degradation activity of lipases for PES (Santos et al., 2013). In contrast, both LIP1 and LIP2 were able to hydrolyze both PES and PCL to some extent. An intracellular mcl-PHA depolymerase of *Pseudomonas putida* LS46 also showed detectable activity towards PES (Mohanani et al., 2020). The Gel Permeation Chromatography revealed a significant degradation of the polymers by LIP1 and LIP2, as shown from the decrease in molecular weights of the polymers treated with the enzymes (18–40% molecular weight loss of PHAs), which clearly shows its high degradation potential compared to the known lipases/esterases. PHA treated with *Bacillus subtilis* lipase reported the molecular weight decrease of 21% (Kanmani et al., 2016). The major distinguishing feature of LIP1 and LIP2 from other lipases available in literature (Table 7) is their broad substrate specificity. In addition to PHAs, PLA and p-nitrophenyl esters of fatty acids, the enzymes were able to hydrolyze synthetic polyesters, PES and PCL. Further, majority of the studies have been done using extracellular lipases (Table 7); this report study will be the first to provide complete characterization of intracellular lipases from bacterial and/or *Pseudomonas* species for biodegradation of polymers.

CONCLUSIONS AND FUTURE PROSPECTS

The present study demonstrated the characteristic features and structure-function relationship of the two lipases, LIP1 and LIP2 of *P. chlororaphis* PA23. It provides further evidence for the remarkable versatility of lipases with respect of their potential application for the degradation of various polyesters, including pNP-alkanoates, PHAs, PLA, and to some extent, the petrochemical-based polymers, PCL and PES. Our data suggests that LIP1 and LIP2 lipases can contribute to the biodegradation of various polyesters. Thus, the increasing demand for biodegradation agents for plastics could be satisfied by the use of microbial lipases. Directed evolution strategies/mutagenesis to improve the degradation potential and/or substrate specificity of the enzymes (LIP1 and LIP2) so as to degrade other synthetic polyesters such as PE/PET as well as analysis and comparison of the degradation behavior of the wild type and mutant enzymes will be our future target. Further, future studies to determine the high-resolution 3D structure of these enzymes will shed more light in elucidating their specific interactions with polyesters and other substrates of interest. Furthermore, this structural information will be also useful in engineering binding pockets of these enzymes either by classical mutagenesis of AI-assisted directed evolution to study and/or improve or even redesign their degradation potential towards different polyesters.

DATA AVAILABILITY STATEMENT

The original contributions presented in the study are included in the article/**Supplementary Material**, further inquiries can be directed to the corresponding author.

AUTHOR CONTRIBUTIONS

NM, experimental design and implementation, analyses of data; CW, in silico analyses of protein structure; NB, financial support for CW, over sight of in silico protein structure, analyses, manuscript editing; DL, financial support of NM, overall project management, preparation of figures, manuscript editing.

REFERENCES

- Adams, D. M., and Brawley, T. G. (1981). Heat Resistant Bacterial Lipases and Ultra-high Temperature Sterilization of Dairy Products. *J. Dairy Sci.* 64, 1951–1957. doi:10.3168/jds.s0022-0302(81)82796-8
- Arpigny, J. L., and Jaeger, K.-E. (1999). Bacterial Lipolytic Enzymes: Classification and Properties. *Biochem. J.* 343, 177–183. doi:10.1042/bj3430177
- Aschauer, P., Pavkov-Keller, T., and Oberer, M. (2017). Crystal Structure of Rv0183, a Monoglyceride Lipase from *Mycobacterium tuberculosis*. *Mycobacterium Tuberculosis*. doi:10.2210/pdb6E1C/pdb
- Aschauer, P., Zimmermann, R., Breinbauer, R., Pavkov-Keller, T., and Oberer, M. (2018). The crystal Structure of Monoacylglycerol Lipase from *M. tuberculosis* Reveals the Basis for Specific Inhibition. *Sci. Rep.* 8, 8948. doi:10.1038/s41598-018-27051-7
- Barbe, S., Lafaquière, V., Guieysse, D., Monsan, P., Remaud-Siméon, M., and André, I. (2009). Insights into Lid Movements of *Burkholderia cepacia* Lipase Inferred from Molecular Dynamics Simulations. *Proteins* 77, 509–523. doi:10.1002/prot.22462
- Blunt, W., Dartiaillh, C., Sparling, R., Gapes, D., Levin, D. B., and Cicek, N. (2018). Carbon Flux to Growth or Polyhydroxyalkanoate Synthesis Under Microaerophilic Conditions is Affected by Fatty Acid Chain-Length in *Pseudomonas putida* LS46. *Appl. Microbiol. Biotechnol.* 102, 6437–6449. doi:10.1007/s00253-018-9055-9
- Bradford, M. M. (1996). A Rapid and Sensitive Method for the Quantitation of Microgram Quantities of Protein Utilizing the Principle of Protein-Dye Binding. *Anal. Biochem.* 72, 248–254. doi:10.1006/abio.1976.9999
- Brocca, S., Secundo, F., Ossola, M., Alberghina, L., Carrea, G., and Lotti, M. (2003). Sequence of the Lid Affects Activity and Specificity of *Candida rugosa* Lipase Isoenzymes. *Protein Sci.* 12, 2312–2319. doi:10.1110/ps.0304003
- Brockman, H. (1994). Dipole Potential of Lipid Membranes. *Chem. Phys. Lipids* 73, 57–79. doi:10.1016/0009-3084(94)90174-0
- Chartrain, M., Katz, L., Marcin, C., Thien, M., Smith, S., Fisher, E., et al. (1993). Purification and Characterization of a Novel Bioconverting Lipase from *Pseudomonas aeruginosa* MB 5001. *Enzyme Microb. Technology* 15, 575–580. doi:10.1016/0141-0229(93)90019-x
- Choo, D.-W., Kurihara, T., Suzuki, T., Soda, K., and Esaki, N. (1998). A Cold-Adapted Lipase of an Alaskan Psychrotroph, *Pseudomonas* sp. Strain B11-1: Gene Cloning and Enzyme Purification and Characterization. *Appl. Environ. Microbiol.* 64, 486–491. doi:10.1128/aem.64.2.486-491.1998
- Contesini, F. J., Davaño, M. G., Borin, G. P., Vanegas, K. G., Cirino, J. P. G., Melo, R. R. d., et al. (2020). Advances in Recombinant Lipases: Production, Engineering, Immobilization and Application in the Pharmaceutical Industry. *Catalysts* 10, 1032. doi:10.3390/catal10091032
- Dallakyan, S., and Olson, A. J. (2015). “Small-molecule Library Screening by Docking with PyRx,” in *Chemical Biology. Methods in Molecular Biology*. Editors J. Hempel, C. Williams, and C. Hong (New York, NY: Humana Press), 1263. doi:10.1007/978-1-4939-2269-71910.1007/978-1-4939-2269-7_19
- Derewenda, U., Brzozowski, A. M., Lawson, D. M., and Derewenda, Z. S. (1992). Catalysis at the Interface: the Anatomy of a Conformational Change in a Triglyceride Lipase. *Biochemistry* 31, 1532–1541. doi:10.1021/bi00120a034
- Dharmstithi, S., and Ammaranond, P. (1996). Purification and Characterization of Lipase from a Raw-Milk Yeast (*Trichosporon asteroides*). *Biotechnol. Appl. Biochem.* 26, 111–116.
- Dong, H., Gao, S., Han, Sp., and Cao, Sg. (1999). Purification and Characterization of a *Pseudomonas* sp. Lipase and its Properties in Non-aqueous media. *Biotechnol. Appl. Biochem.* 30, 251–256.
- Fatma, F. A., Magdi, A. E., Soadm, A. E., and Shin-ichi, I. (2014). Biodegradation of Poly(ecaprolactone) (PCL) Film and Foam Plastic by *Pseudozyma japonica* sp. nov., a Novel Cutinolytic Ustilaginomycetous Yeast Species. *Biotech* 3 (4), 507–512.
- Fernando, W. G. D., Nakkeeran, S., Zhang, Y., and Savchuk, S. (2007). Biological Control of *Sclerotinia sclerotiorum* (Lib.) de Bary by *Pseudomonas* and *Bacillus* Species on canola petals. *Crop Prot.* 26, 100–107. doi:10.1016/j.cropro.2006.04.007
- Fischer, M., and Pleiss, F. (2003). The Lipase Engineering Database: a Navigation and Analysis Tool for Protein Families. *Nucl. Acid. Res.* 31, 319–321. doi:10.1093/nar/gkg015
- Fojan, P., Jonson, P. H., Petersen, M. T. N., and Petersen, S. B. (2000). What Distinguishes an Esterase from a Lipase: A Novel Structural Approach. *Biochimie* 82, 1033–1041. doi:10.1016/s0300-9084(00)01188-3
- Fox, P. F., and Stepaniak, L. (1983). Isolation and Some Properties of Extracellular Heat-Stable Lipases from *Pseudomonas fluorescens* Strain AFT 36. *J. Dairy Res.* 50, 77–89. doi:10.1017/s0022029900032544
- Gangoiti, J., Santos, M., Prieto, M. A., de la Mata, I., Serra, J. L., and Llama, M. J. (2012). Characterization of a Novel Subgroup of Extracellular Medium-Chain-Length Polyhydroxyalkanoate Depolymerases from Actinobacteria. *Appl. Environ. Microbiol.* 78, 7229–7237. doi:10.1128/AEM.01707-12
- Gilbert, E. J., Cornish, A., and Jones, C. W. (1991). Purification and Properties of Extracellular Lipase from *Pseudomonas aeruginosa* EF2. *J. Gen. Microbiol.* 137, 2223–2229. doi:10.1099/00221287-137-9-2223
- Godtfredsen, S. E. (1990). “Microbial Lipases,” in *Microbial Enzymes and Biotechnology*. Editors W. M. Fogarty and E. T. Kelly (Amsterdam: Elsevier), 255–274. doi:10.1007/978-94-009-0765-2_7
- Hanwell, M. D., Curtis, D. E., Lonie, D. C., Vandermeersch, T., Zurek, E., and Hutchison, G. R. (2012). Avogadro: An Advanced Semantic Chemical Editor, Visualization, and Analysis Platform. *J. Cheminform* 4, 17. doi:10.1186/1758-2946-4-17
- Holmquist, M., Clausen, I. G., Patkar, S., Svendsen, A., and Hult, K. (1995). Probing a Functional Role of Glu87 and Trp89 in the Lid of *Humicola lanuginosa* Lipase through Transesterification Reactions in Organic Solvent. *J. Protein Chem.* 14, 217–224. doi:10.1007/BF01886762
- Howard, G. T., Crother, B., and Vicknair, J. (2001). Cloning, Nucleotide Sequencing and Characterization of a Polyurethanase Gene (pueB) from *Pseudomonas chlororaphis*. *Int. Biodeterioration Biodegradation* 47, 141–149. doi:10.1016/s0964-8305(01)00042-7

FUNDING

This work was funded by the Natural Sciences and Engineering Research Council of Canada (Discovery grant: RGPIN-04945-2017) and by a grant from Agriculture and Agri-Food Canada through the AgriScience BioProducts Cluster program held by Dr. Levin.

SUPPLEMENTARY MATERIAL

The Supplementary Material for this article can be found online at: <https://www.frontiersin.org/articles/10.3389/fbioe.2022.854298/full#supplementary-material>

- Jaeger, K. E., Steinbüchel, A., and Jendrossek, D. (1995). Substrate Specificities of Bacterial Polyhydroxyalkanoate Depolymerases and Lipases: Bacterial Lipases Hydrolyze poly(ω -hydroxyalkanoates). *Appl. Environ. Microbiol.* 61, 3113–3118. doi:10.1128/aem.61.8.3113-3118.1995
- Kanmani, P., Kumaresan, K., Aravind, J., Karthikeyan, S., and Balan, R. (2016). Enzymatic Degradation of Polyhydroxyalkanoate Using Lipase from *Bacillus subtilis*. *Int. J. Environ. Sci. Technol.* 13, 1541–1552. doi:10.1007/s13762-016-0992-5
- Khan, F. I., Lan, D., Durrani, R., Huan, W., Zhao, Z., and Wang, Y. (2017). The Lid Domain in Lipases: Structural and Functional Determinant of Enzymatic Properties. *Front. Bioeng. Biotechnol.* 5, 16. doi:10.3389/fbioe.2017.00016
- Kim, Y. C., Jun, H. S., Chang, H. N., and Woo, S. I. (1992). Optimal Conditions for Enzymatic Degradation of Polycaprolactone. *J. Kor. Inst. Chem. Eng.* 30, 718–724.
- Knoll, M., Hamm, T. M., Wagner, F., Martinez, V., and Pleiss, J. (2009). The PHA Depolymerase Engineering Database: a Systematic Analysis Tool for the Diverse Family of Polyhydroxyalkanoate (PHA) Depolymerases. *BMC Bioinformatics* 10, 89. doi:10.1186/1471-2105-10-89
- Kouker, G., and Jaeger, K. E. (1987). Specific and Sensitive Plate Assay for Bacterial Lipases. *Appl. Environ. Microbiol.* 53, 211–213. doi:10.1128/aem.53.1.211-213.1987
- Lee, S. Y., and Rhee, J. S. (1994). Hydrolysis of Triglyceride by the Whole Cell of *Pseudomonas Putida* 3SK in Two-phase Batch and Continuous Reactors Systems. *Biotechnol. Bioeng.* 44, 437–443. doi:10.1002/bit.260440406
- Longhi, S., Czjzek, M., Lamzin, V., Nicolas, A., and Cambillau, C. (1997). Atomic Resolution (1.0 Å) crystal Structure of Fusarium Solani Cutinase: Stereochemical Analysis. *J. Mol. Biol.* 268, 779–799. doi:10.1006/jmbi.1997.1000
- Macrae, A. R., and Hammond, R. C. (1985). Present and Future Applications of Lipases. *Biotechnol. Genet. Eng. Rev.* 3, 193–218. doi:10.1080/02648725.1985.10647813
- Mohamed, R. A., Salleh, A. B., Leow, A. T. C., Yahaya, N. M., and Abdul Rahman, M. B. (2017). Ability of T1 Lipase to Degrade Amorphous P(3HB): Structural and Functional Study. *Mol. Biotechnol.* 59, 284–293. doi:10.1007/s12033-017-0012-0
- Mohanani, N., Sharma, P. K., and Levin, D. B. (2020). Characterization of an Intracellular Poly(3-Hydroxyalkanoate) Depolymerase from the Soil Bacterium, *Pseudomonas putida* LS46. *Polym. Degrad. Stab.* 175, 109127. doi:10.1016/j.polymdegradstab.2020.109127
- Mukai, K., Doi, Y., Sema, Y., and Tomita, K. (1993). Substrate Specificities in Hydrolysis of Polyhydroxyalkanoates by Microbial Esterases. *Biotechnol. Lett.* 15, 601–604. doi:10.1007/bf00138548
- Ollis, D. L., Cheah, E., Cygler, M., Dijkstra, B., Frolow, F., Franken, S. M., et al. (1992). The α/β Hydrolase Fold. *Protein Engineering* 5, 197–211. doi:10.1093/protein/5.3.197
- Pleiss, J., Fischer, M., Peiker, M., Thiele, C., and Schmid, R. D. (2000). Lipase Engineering Database - Understanding and Exploiting Sequence-Structure-Function Relationships. *J. Mol. Catal. B-Enzymatic* 10, 491–508. doi:10.1016/s1381-1177(00)00092-8
- Ramsay, B. A., Saracovan, I., Ramsay, J. L., and Marchessault, R. H. (1994). A Method for the Isolation of Microorganisms Producing Extracellular Long-Side-Chain Poly (β -3-hydroxyalkanoate) Depolymerase. *J. Environ. Polym. Degrad.* 2, 1e7. doi:10.1007/bf02073481
- Rappe, A. K., Casewit, C. J., Colwell, K. S., Goddard III, W. A., and Skiff, W. M. (1992). UFF, a Full Periodic Table Force Field for Molecular Mechanics and Molecular Dynamics Simulations. *J. Am. Chem. Soc.* 114, 10024–10035. doi:10.1021/ja00051a040
- Rasmussen, H. O., Wollenberg, D. T. W., Wang, H., Andersen, K. K., Oliveira, C. L. P., Jorgensen, C. I., et al. (2022). The Changing Face of SDS Denaturation: Complexes of *Thermomyces lanuginosus* Lipase with SDS at pH 4.0, 6.0 and 8.0. *J. Colloid Interf. Sci.* 614, 214–232. doi:10.1016/j.jcis.2021.12.188
- Reis, P., Holmberg, K., Watzke, H., Leser, M. E., and Miller, R. (2009). Lipases at Interfaces: A Review. *Adv. Colloid Interf. Sci.* 147–148, 237–250. doi:10.1016/j.jcis.2008.06.001
- Santos, M., Gangoiiti, J., Keul, H., Moller, M., Serra, J. L., and Llama, M. J. (2013). Polyester Hydrolytic and Synthetic Activity Catalysed by the Medium-Chain-Length Poly(3-Hydroxyalkanoate) Depolymerase from *Streptomyces venezuelae* SO1. *Appl. Microbiol. Biotechnol.* 97, 211e222. doi:10.1007/s00253-012-4210-1
- Savchuk, S. C., and Fernando, W. G. D. (2004). Effect of Timing of Application and Population Dynamics on the Degree of Biological Control of *Sclerotinia sclerotiorum* by Bacterial Antagonists. *FEMS Microbiol. Ecol.* 49, 379–388. doi:10.1016/j.femsec.2004.04.014
- Saxena, R. K., Sheoran, A., Giri, B., and Davidson, W. S. (2003). Purification Strategies for Microbial Lipases. *J. Microbiol. Method.* 52, 1–18. doi:10.1016/s0167-7012(02)00161-6
- Schirmer, A., Jendrossek, D., and Schlegel, H. G. (1993). Degradation of Poly (3-Hydroxyoctanoic Acid) [P(3HO)] by Bacteria: Purification and Properties of a [P(3HO)] Depolymerase from *Pseudomonas fluorescens* GK13, Appl. Environ. Microbiol. 59, 1220e1227. doi:10.1128/AEM.59.4.1220-1227.1993
- Sharma, A., and Radha Kishan, K. V. (2011). Serine Protease Inhibitor Mediated Peptide Bond Re-synthesis in Diverse Protein Molecules. *FEBS Lett.* 585, 3465–3470. doi:10.1016/j.febslet.2011.10.004
- Sharma, P. K., Fu, J., Cicek, N., Sparling, R., and Levin, D. B. (2011). Kinetics of Medium-Chain Length Polyhydroxyalkanoate Production by a Novel Isolate of *Pseudomonas putida* LS46. *Can. J. Microbiol.* 58, 982e989. doi:10.1139/w2012-074
- Sharma, P. K., Fu, J., Spicer, V., Krokhin, O. V., Cicek, N., Sparling, R., et al. (2016). Global Changes in the Proteome of *Cupriavidus necator* H16 During Poly(3-Hydroxybutyrate) Synthesis from Various Biodiesel By-Product Substrates. *AMB Express* 6, 36. doi:10.1186/s13568-016-0206-z
- Sharma, P. K., Mohanan, N., Sidhu, R., and Levin, D. B. (2019). Colonization and Degradation of Polyhydroxyalkanoates by Lipase Producing Bacteria. *Can. J. Microbiol.* 65, 461e475. doi:10.1139/cjm-2019-0042
- Szilagyi, A., and Zavodsky, P. (2000). Structural Differences between Mesophilic, Moderately Thermophilic and Extremely Thermophilic Protein Subunits: Results of a Comprehensive Survey. *Struct. Fold Des.* 8, 493–504. doi:10.1016/s0969-2126(00)00133-7
- Tamura, K., Peterson, D., Peterson, N., Stecher, G., Nei, M., and Kumar, S. (2011). MEGA5: Molecular Evolutionary Genetics Analysis Using Maximum Likelihood, Evolutionary Distance, and Maximum Parsimony Methods. *Mol. Biol. Evol.* 28, 2731e2739. doi:10.1093/molbev/msr121
- Tribedi, P., Das Gupta, A., and Sil, A. K. (2015). Adaptation of *Pseudomonas* sp. AKS2 in Biofilm on Low-Density Polyethylene Surface: An Effective Strategy for Efficient Survival and Polymerdegradation. *Bioresour. Bioproc.* 2, 1–10. doi:10.1186/s40643-015-0044-x
- Uppenberg, J., Hansen, M. T., Patkar, S., and Jones, T. A. (1994). The Sequence, crystal Structure Determination and Refinement of Two crystal Forms of Lipase B from *Candida antarctica*. *Structure* 15, 293–308. doi:10.1016/s0969-2126(00)00031-9
- Waterhouse, A., Bertoni, M., Bienert, S., Studer, G., Tauriello, G., Gumienny, R., et al. (2018). SWISS-MODEL: Homology Modelling of Protein Structures and Complexes. *Nucleic Acids Res.* 46, W296–W303. doi:10.1093/nar/gky427
- Wilkes, R. A., and Aristilde, L. (2017). Degradation and Metabolism of Synthetic Plastics and Associated Products by *Pseudomonas* sp.: Capabilities and Challenges. *J. Appl. Microbiol.* 123, 582–593. doi:10.1111/jam.13472
- Yadav, R. P., Saxena, R. K., Gupta, R., and Davidson, S. (1998). Purification and Characterization of a Regiospecific Lipase from *Aspergillus terreus*. *Biotechnol. Appl. Biochem.* 28, 243–249.
- Yang, Y., and Lowe, M. E. (2000). The Open Lid Mediates Pancreatic Lipase Function. *J. Lipid Res.* 41, 48–57. doi:10.1016/s0022-2275(20)32073-3
- Zhang, J. W., and Zeng, R. Y. (2008). Molecular Cloning and Expression of a Cold-Adapted Lipase Gene from an Antarctic Deep Sea Psychrotrophic Bacterium *Pseudomonas* sp. 7323. *Mar. Biotechnol.* 10, 612–621. doi:10.1007/s10126-008-9099-4

Conflict of Interest: The authors declare that the research was conducted in the absence of any commercial or financial relationships that could be construed as a potential conflict of interest.

Publisher's Note: All claims expressed in this article are solely those of the authors and do not necessarily represent those of their affiliated organizations, or those of the publisher, the editors and the reviewers. Any product that may be evaluated in this article, or claim that may be made by its manufacturer, is not guaranteed or endorsed by the publisher.

Copyright © 2022 Mohanan, Wong, Budisa and Levin. This is an open-access article distributed under the terms of the Creative Commons Attribution License (CC BY). The use, distribution or reproduction in other forums is permitted, provided the original author(s) and the copyright owner(s) are credited and that the original publication in this journal is cited, in accordance with accepted academic practice. No use, distribution or reproduction is permitted which does not comply with these terms.



Synthesis of Poly(Hexamethylene Succinate-Co-Ethylene Succinate) Copolymers With Different Physical Properties and Enzymatic Hydrolyzability by Regulating the Ratio of Monomer

Menglu Li[†], Jing Jing[†] and Tingting Su^{*}

School of Petrochemical Engineering, Liaoning Petrochemical University, Fushun, China

OPEN ACCESS

Edited by:

Fan Li,
Northeast Normal University, China

Reviewed by:

Bomou Ma,
Donghua University, China
Zhiyong Wei,
Dalian University of Technology, China

*Correspondence:

Tingting Su
sutingting1978@126.com

[†]These authors have contributed
equally to this work

Specialty section:

This article was submitted to
Bioprocess Engineering,
a section of the journal
Frontiers in Bioengineering and
Biotechnology

Received: 11 March 2022

Accepted: 30 March 2022

Published: 28 April 2022

Citation:

Li M, Jing J and Su T (2022) Synthesis
of Poly(Hexamethylene Succinate-Co-
Ethylene Succinate) Copolymers With
Different Physical Properties and
Enzymatic Hydrolyzability by
Regulating the Ratio of Monomer.
Front. Bioeng. Biotechnol. 10:894046.
doi: 10.3389/fbioe.2022.894046

Poly(hexylene succinate) (PHS), poly(ethylene succinate) (PES), and their random copolyesters, poly(hexylene succinate-co-ethylene succinate) ((P(HS-co-ES))), were synthesized by melting polycondensation. Simply varying the ratios of HS/ES afforded control over the copolymer crystallinity, thermal and mechanical properties, wettability, and enzymatic hydrolyzability as shown by X-ray diffraction (XRD), differential scanning calorimetry (DSC), tensile tests, and water contact angle (WCA) measurements. The enzymatic hydrolysis rates of all prepared copolyesters were higher than those of the corresponding homopolyesters. The hydrolysis rates were affected by crystallinity, melting temperature, and hydrophobicity of the copolyesters, and therefore, the degradation rates could be tuned along with the ES content. The library of copolymers prepared here with tunable degradation rates, ranging from HS-enriched to ES-enriched copolyesters, is promising for a variety of different applications. The P(HS-co-ES51) copolyester that did not fully degrade is particularly promising for use in long-term storage applications, whereas P(HS-co-ES13) and P(HS-co-ES76) that rapidly degrade are good for use in very short-term applications.

Keywords: aliphatic polyester, poly(hexamethylene succinate-co-ethylene succinate), enzymatic hydrolysis, cutinase, physical properties

INTRODUCTION

Although the polymer-based products are widely used, traditional polymers do not easily degrade and are a major source of pollution in soil, air, and water (Papageorgiou et al., 2014; Balart et al., 2020; Blanco et al., 2020; de Araújo Veloso et al., 2021). Degradable polymers as potential green material candidates for use in such applications have received extensive attention. One promising class of degradable polymers is aliphatic polyesters which are biocompatible, biodegradable, and thermally stable. As such, copolyesters have attracted growing attention and are used in a wide range of applications, including biomedical materials, disposable packaging, and agricultural films (Pan et al., 2018; Polyák et al., 2018; Siracusa and Blanco, 2020; Kesavan et al., 2021).

Both poly(hexylene succinate) (PHS) and poly(ethylene succinate) (PES) are aliphatic polyesters with similar chemical structures. The difference between the two polyesters is the number of diol

units in the repeat units. PHS with more carbons per repeat unit not only has a faster crystallization rate and is more flexible but also has poor tensile strength and low flow melting point. In contrast, PES has a high melting point but a low elongation at break and a lower crystallization rate. Therefore, both polyesters have drawbacks and need to be modified to expand their application ranges. Yang et al. prepared poly(hexylene succinate-co-3 mol% ethylene succinate) (poly(HS-co-3 mol% ES)) copolyesters and studied their crystallization kinetics and melting behaviors (Yang and Qiu, 2013). They concluded that the two prepared P(HS-co-3 mol% ES) copolymers had the same characteristics as the pure PHS polymer, and the small number of ES units were in the amorphous regions of the copolyester, not in the crystalline PHS regions.

Few studies have considered the degradation behaviors of poly(hexamethylene succinate-co-ethylene succinate) (P(HS-co-ES)) copolyesters and associated changes in the physical properties of the polymer films before and after degradation. In this study, pure PHS, pure PES, and P(HS-co-ES) copolyesters with varying ES contents were synthesized using a two-step esterification and polycondensation reaction. The effects of the hydroxyl content on the physical properties of the resulting polyesters, including the crystal structure, thermal properties, and mechanical properties, were investigated. In addition, the polyesters were enzymatically degraded using cutinase, and the effects of polymer composition on the enzymatic hydrolysis rate are discussed. Moreover, the difference in film morphology, crystallinity, and thermal properties before and after enzymatic hydrolysis are compared.

MATERIAL AND METHODS

Material

Succinic acid (SA, 99.5%) and titanium isopropoxide (TTIP, 95%) were obtained from Shanghai Aladdin Biochemical Company (Shanghai, China). Ethylene glycol (EG, 98%), 1,6-hexanediol (HD, 98%), and decahydronaphthalene were purchased from Chengdu Aikeda Chemical Reagent Co., Ltd. (Chengdu, China). Chloroform was obtained from Shenyang Xinxing Reagent Factory (Shenyang, China). Anhydrous methanol was obtained from Tianjin Damao Chemical Reagent Factory (Tianjin, China). Cutinase was prepared following the procedure reported in our previous work (Hu et al., 2016). All chemicals and reagents were of analytical grade.

Synthesis of Polyesters and Preparation of Samples

The molar ratio of SA to total diol(s) was 1:1.1. The reagents, including SA, EG, and HD, were added to 60 ml decahydronaphthalene containing TTIP at a mass concentration of 1/600 of the total reactant mass. The esterification reaction was carried out at 140°C for 2 h under a nitrogen atmosphere, and subsequently, the polycondensation reaction was carried out at 230°C for 4 h below 3 mmHg. The products were dissolved in 100 ml of chloroform and then

precipitated into three times the volume of pre-cooled methanol. The precipitate was then washed with alcohol until the solution was clear, collected, and dried at 37°C under vacuum before use. The feed ratios of the diols used to prepare the different polymers are listed in **Table 1**.

The prepared polyesters were hot-pressed at 160°C and then cold-pressed at room temperature to obtain films with thicknesses of 1 and 0.5 mm, respectively. The 1-mm films were cut into 40 × 4 × 1 mm dumbbell-shaped pieces with a mold for the mechanical property tests. The 0.5-mm polyester films were cut into 30 × 10 × 0.5 mm rectangular pieces for the enzymatic hydrolysis and swelling experiments.

Enzymatic Hydrolysis

The polyester films (30 × 10 × 0.5 mm) were vacuum-dried until their weight was kept constant, weighed, and then placed in 10 ml of Na₂HPO₄-NaH₂PO₄ buffer (0.1 M, pH = 7.4) containing 0.096 mg/ml cutinase at 37°C. The polyester films were removed from the buffer at regular intervals, rinsed with distilled water, dried with a clean absorbent wipe, and weighed. The removed films were dried under vacuum until the mass was constant to ensure that the water was removed and re-weighed. The weight loss ratios were calculated according to **Eq. 1**:

$$R = \frac{W_0 - W_d}{W_0} \times 100\%, \quad (1)$$

where R is the weight loss ratio of the films; W_0 is the initial film weight before the hydrolysis experiments, and W_d is the film weight after the films were incubated with the enzyme solution.

Proton Nuclear Magnetic Resonance

The compositions of the polyesters were analyzed using ¹H NMR spectroscopy (Bruker BioSpin, AVANCE III HD 400, Switzerland). Deuterated chloroform (CDCl₃) was used as the solvent, and tetramethylsilane (TMS) was used as the internal standard.

Attenuated Total Reflectance Fourier Transform Spectroscopy

ATR-FTIR data were collected using the ATR mode of an FT-IR spectrometer (Agilent Cary 660, United States of America) with a slide-on ATR accessory (Agilent, United States of America). The reported spectra are the average of sixteen scans that were collected over a frequency range from 4,000 to 400 cm⁻¹ at a resolution of 2 cm⁻¹.

X-Ray Diffraction

The crystal structures of the polyester films were determined by XRD (S8 Tiger, Bruker, Germany). The XRD was equipped with Cu-Kα radiation source ($\lambda = 0.1541$ nm, 40 kV, 40 mA), and data were collected at 25°C. The scattering data were collected over a range of diffraction angles from 5 to 50° using a 0.02° step size. The crystallite sizes were evaluated from the XRD patterns according to the Debye-Scherrer Equation (Klug and Alexander, 1974).

TABLE 1 | Composition and mechanical and thermal properties of P(HS-co-ES) copolyesters.

Polyester	HD/EG	HS/ES	Tensile strength/MPa	Elongation at break/%	Young's modulus/MPa	T _m /°C	X _c /%
PHS	100/0	100/0	15.9 ± 1.9	52.5 ± 0.8	160.0 ± 2.2	55.5	50.9
P(HS-co-ES13)	80/20	87/13	13.7 ± 1.4	363.5 ± 6.4	49.8 ± 1.7	42.2	45.3
P(HS-co-ES32)	60/40	68/32	2.8 ± 0.6	66.0 ± 3.3	15.4 ± 0.5	30.6	39.5
P(HS-co-ES51)	40/60	49/51	0.4 ± 0.1	53.1 ± 1.8	3.0 ± 0.3	-	20.7
P(HS-co-ES76)	20/80	24/76	6.0 ± 0.4	7.7 ± 0.6	76.6 ± 2.6	58.2	49.8
PES	0/100	0/100	30.1 ± 1.7	8.5 ± 0.3	193.2 ± 4.7	104.1	58.3

Differential Scanning Calorimeter

The thermal properties of the polyester films were determined using DSC (TA Instruments, New Castle, DE, United States of America). The measurements were performed in a nitrogen atmosphere (50 ml/min). The polyester samples were heated from 0 to 150°C, held at 150°C for 3 min, cooled to 0°C, and then reheated to 150°C. The temperature ramp rate during all steps was 10°C/min.

Thermogravimetry

The thermal decomposition behaviors of the polyester films were studied using TG analysis (TA Instruments, Q600, United States of America). About 8 mg samples were heated from room temperature to 500°C at a rate of 10°C/min under a nitrogen atmosphere (50 ml/min).

Scanning Electron Microscopy

The surface morphologies of the polyester films before and after enzymatic hydrolysis were observed by SEM (SV810, Hitachi, Tokyo, Japan). For imaging, the film surfaces were sprayed with gold, and the films were placed on the sample stage for observation at 20 kV.

Water Contact Angle Assay

The hydrophilicity of the dried polyester films surfaces was quantified by WCA measurements (KRUS, DSA100, Hamburg, Germany). Static WCA angles were measured with an injection volume of 0.3 µL at 0.5 µL/s. The WCA values are reported as the average of five measurements at room temperature (25°C).

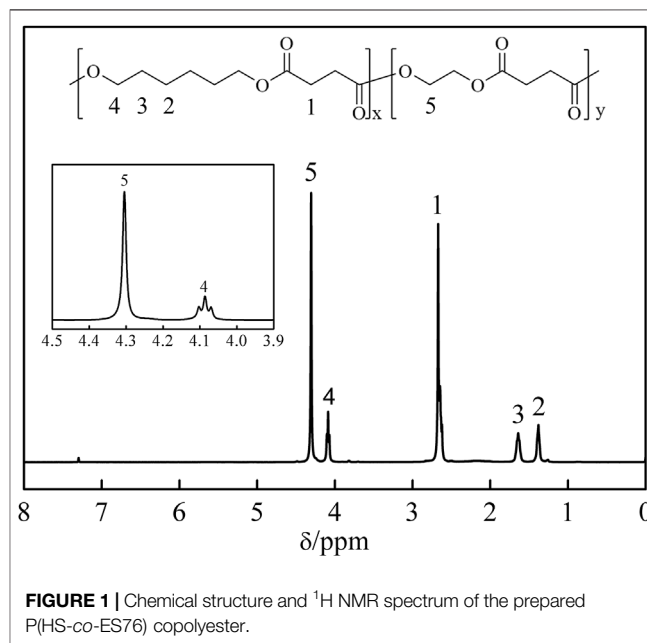
Swelling Property Analysis

The polyester films (30 × 10 × 0.5 mm) were vacuum-dried to a constant weight, weighed, and the dimensions were measured and recorded. The polyester films were immersed in 50 ml of deionized water at room temperature. After 24 h of immersion, the films were removed from water, wiped dry, weighed, and the dimensions were re-measured. The swelling degree, *Sw*, of the polyester films was calculated according to Eq. 2:

$$S_w = \frac{W_s - W_d}{W_d} \times 100\%, \quad (2)$$

and the swelling ratios (*S_r*) were determined by Eq. 3:

$$S_r = \frac{A_d}{A_s}, \quad (3)$$

**FIGURE 1** | Chemical structure and ¹H NMR spectrum of the prepared P(HS-co-ES76) copolyester.

where *W_d* is the dry wet weight of the polyester films, *W_s* is the weight of the film after it was immersed in water for 24 h, *A_d* is the side length of the dry polyester film, and *A_s* is the side length of the polyester film after it was swollen with water.

Mechanical Property

The mechanical properties of samples were analyzed using an Instron 5500R universal testing machine (Instron Corp., Canton, Massachusetts, United States of America). The measurements were performed at room temperature with a tensile speed of 20 mm/min. The mechanical testing was carried out five times.

RESULTS AND DISCUSSION

Composition of P(HS-co-ES) Copolyesters

The compositions of the synthesized P(HS-co-ES) copolyesters were determined by ¹H NMR, and the measured ¹H NMR spectrum and chemical structure for P(HS-co-ES76) are shown in Figure 1. The peak at 2.67 ppm is due to the protons on the COCH₂ group in SA, labeled as 1 in the corresponding chemical structure. The peaks at 1.38, 1.64, and 4.09 ppm are assigned to the protons labeled 2, 3, and 4 in the HS units, respectively, and the peak at 4.30 ppm is assigned to proton 5 in the ES units. The ratios of the area of peak 4 from

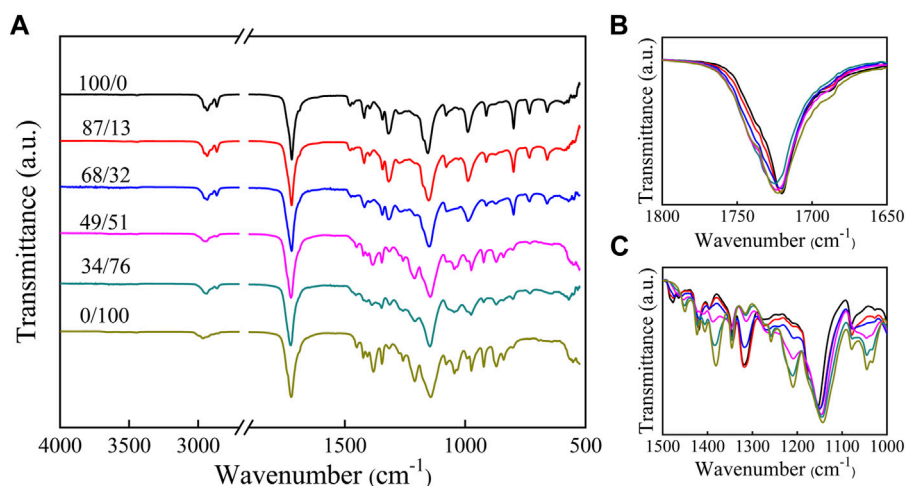


FIGURE 2 | FT-IR spectra of PHS, PES, and P(HS-co-ES) copolyesters at various frequencies: **(A)** 4,000–500 cm^{-1} ; **(B)** 1800–1,650 cm^{-1} ; and **(C)** 1,500–1,000 cm^{-1} .

$-\text{O}(\text{CH}_2)_6\text{O}-$ in the HS units to the area of peak 5 from $-\text{O}(\text{CH}_2)_2\text{O}-$ in the ES units were used to calculate the molar ratio of HS/ES in the synthesized polymers (Tan et al., 2017; Bi et al., 2018). Polymers 10, 90. doi: 10.3390/polym10010090). The experimentally determined HE/ES ratios are expressed as mol%, and the deviation from the theoretical ratios is due to the volatilization of the ethylene glycol monomer during the reaction.

Chemical Structure of P(HS-co-ES) Copolyesters

FT-IR spectra of all synthetic polyesters are shown in **Figure 2**. The peaks at 2,930 and 2,860 cm^{-1} are attributed to $-\text{CH}_2-$ stretching vibrations. The peaks at 1720 cm^{-1} are attributed to the $\text{C}=\text{O}$ stretching vibrations in the crystalline regions of the copolymers (Sato et al., 2004) and shifted to lower wavenumbers by approximately 25 cm^{-1} compared to the unconstrained $\text{C}=\text{O}$ groups due to the regular packing arrangement in the crystalline regions of the films (Sato et al., 2005). The band at 1,150 cm^{-1} is attributed to the $\text{C}-\text{O}$ vibrations in the crystalline or amorphous regions of the films (Sato et al., 2004; Sato et al., 2005). The small absorption peak near 720 cm^{-1} in the FT-IR spectra measured for the PHS, P(HS-co-ES13), and P(HS-co-ES32) is assigned to the rocking vibrations of the $-(\text{CH}_2)_4-$ structure in the dibasic hydroxyl groups in HS (Karayannidis et al., 2003). In contrast, the diols used to synthesize PES only contained one methylene group, and therefore, the polyesters containing higher molar ratios of ES content did not have an absorption peak at 720 cm^{-1} from these in-plane swinging vibrations. The absorption peaks between 1800 and 1,650 cm^{-1} in the spectra measured for the P(HS-co-ES) copolyesters were similar to those of the pure PHS and PES polymers (**Figure 2B**); however, the positions, intensities, and shapes of the absorption peaks between 1,500 and 1,000 cm^{-1} are different (**Figure 2C**). In particular, the peak positions and shapes measured for copolyesters with HS contents >51 mol% are similar to those of PHS, while the peaks of the majority of ES copolyesters are similar to those of pure PES.

Crystal Structure of P(HS-co-ES) Copolyesters

The XRD diffraction patterns and crystal sizes of P(HS-co-ES) are shown in **Figure 3**. The data in **Figure 3A** show that PHS forms a monoclinic crystal with the diffraction peaks at 21.38°, 24.33°, and 30.22° that correspond to the (220), (040), and (240) planes, respectively. Meanwhile, PES is an orthorhombic crystal with diffraction peaks at 20.13°, 22.79°, and 23.22° from the (121), (200), and (220) planes, respectively (Bai et al., 2018a; Jing et al., 2021). The XRD diffraction patterns of copolyesters with ES contents of 13 mol% and 32 mol% are similar to those of PHS, indicating that ES was amorphous in these copolymers, while the XRD diffraction pattern of the copolyester with ES content greater than or equal to 51 mol% was similar to that of PES, indicating that the ES unit was crystalline in these copolyesters.

The degree of crystallinity (X_c) in each sample was calculated from the areas of XRD diffraction peaks (Gigli et al., 2013), and the results are summarized in **Table 1**. The degree of crystallinity of all P(HS-co-ES) copolyesters is less than that of either the pure PHS or PES, regardless of the copolyester composition. The copolyester with an ES content of 51 mol% had the lowest degree of crystallinity among all the prepared polymers.

The crystallite sizes (L) were calculated from the half-width-half-max (HWHM) of the diffraction peaks using the Debye-Scherrer equation (Gigli et al., 2013). As shown in **Figure 3B**, the crystallite size of the (040) plane first increased and then decreased in the copolyesters compared to PHS, and the crystallite size of the (121) plane increased with increasing ES content. The crystallite sizes in the copolyester films are larger than those of pure PHS and PES, and the largest crystallite size was observed in the copolyester with an ES content of 76 mol% (Jing et al., 2021).

The melting temperatures (T_m) determined from the second heating curves of the DSC measurements are listed in **Table 1**. No melting peaks were observed in the copolyester with an ES content of 51 mol% due to the low crystallinity of P(HS-co-ES51). The T_m of

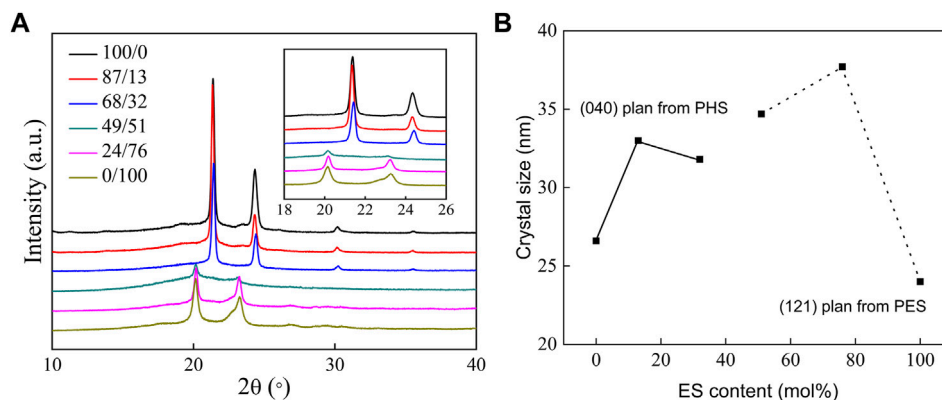


FIGURE 3 | XRD patterns of PHS, PES, and P(HS-co-ES) copolyesters **(A)** and the corresponding crystallite sizes calculated using the Debye–Scherrer equation **(B)**.

the copolyesters was lower than that of PHS and PES because introducing ES units into the copolyesters increases the number of methylene groups between the ester bonds, which reduces the chain order and packing (Nikolic and Djonlagic, 2001; Shi et al., 2019). The melting temperature also depends on the crystallite sizes in the polyester and the number of defects in the films, where the films with smaller crystals or more defects have lower T_m (Castilla-Cortázar et al., 2012). The DSC results revealed that P(HS-co-ES32) and P(HS-co-ES51) have low T_m values, while the XRD results showed that these samples had large crystal sizes, suggesting that the films formed by these two copolyesters had more crystal defects.

Mechanical Properties of P(HS-co-ES) Copolyesters

The mechanical properties of the polyesters are summarized in **Table 1**. Although the tensile strengths for the different polyesters were similar, the elongations at break varied with the copolyester composition and first increased and then decreased with an increase in the ES content. The P(HS-co-ES13) copolyester had the highest elongation at break of 363.5%, while the P(HS-co-ES76) copolyester had the lowest elongation at break of 7.7%, which was also lower than that of either the pure PHS or PES polyesters. Furthermore, comparison of the properties of the different polyesters reveals a correlation between the mechanical properties and thermal and crystal properties. The melting temperature and crystallinity of the copolyesters are lower than those of PHS and PES, while the elongations at break are higher, which may be because the degree of crystallinity decreases with increasing ES content, and the corresponding increase in the size of the amorphous regions of the films leads to a decrease in the stiffness. Meanwhile, the tensile strength and Young's modulus of P(HS-co-ES32) and P(hs-co-ES51) are very low possibly because of their low degrees of crystallinity and melting temperatures as the soft amorphous phase leads to more defects in the films and makes the copolyesters softer and less viscous at room temperature. The change in the tensile properties of P(HS-co-ES) is consistent with other reported results (Zhang et al., 2021).

Enzymatic Hydrolysis of P(HS-co-ES) Copolyesters

Figure 4A shows the weight loss of the hydrolyzed polyester films after they were incubated with cutinase at pH 7.4 and 37°C. There was no measurable weight loss in the control samples incubated in the same buffer without cutinase (data not shown). The P(HS-co-ES32) and P(HS-co-ES51) samples (**Figure 4A**) were not completely hydrolyzed during the experiments because the films curled as they degraded. The total surface area decreased during the curling process; therefore, the weight loss of the P(HS251-co-ES32) and P(HS-co-ES51) was less.

Figure 4B shows that the amount of water absorbed by the polyesters increased throughout the enzymatic hydrolysis process, where P(HS-co-ES32) adsorbed the most water absorption, followed by P(HS-co-ES52). The degree of swelling of the other four polyesters did not exceed 15%, and PHS absorbed the least water. After 4 h of incubation with the enzyme solution, the enzymatic hydrolysis rates of PHS, P(HS-co-ES13), P(HS-co-ES32), P(HS-co-ES51), P(HS-co-ES76), and PES were 42.03, 63.50, 21.61, 36.10, 48.37, and 15.74%, respectively. In addition, it took about 5, 3, 10, 8, 5, and 14 h to hydrolyze 50% of the mass of each polyester. The addition of ES significantly increased the rate of enzymatic hydrolysis of the copolyesters, with the exception of P(HS-co-ES32) and P(HS-co-ES51). P(HS-co-ES13) and P(HS-co-ES76) completely hydrolyzed in less time than pure PHS and PES, and P(HS-co-ES13) has the highest enzymatic hydrolysis rate under the same experimental conditions.

P(HS-co-ES13) has the fastest enzymatic hydrolysis rate. In the first, rapid degradation stage, the ester bonds were degraded, resulting in shorter polyester segments and significant weight loss. In the second, slower degradation stage, the terminal fragments were enzymatically hydrolyzed, forming water-soluble oligomers that dissolved away from the film surface (Rizzarelli et al., 2004; Bikiaris et al., 2006). The pH of the surrounding buffer solution decreases as the ester bonds are cleaved and water-soluble substances are produced (**Figure 4C**), and cutinase is less active at lower pHs, which leads to a slowing down of the enzymatic hydrolysis rate. The total surface area of the P(HS-co-ES32) and P(HS-co-ES51) samples

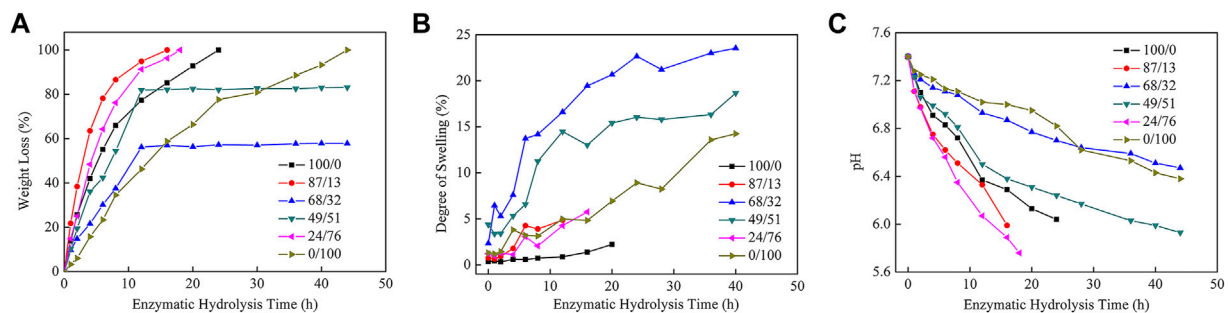


FIGURE 4 | Weight loss curves (A), degree of swelling curves (B), and pH curves (C) of polyester films after hydrolysis by cutinase.

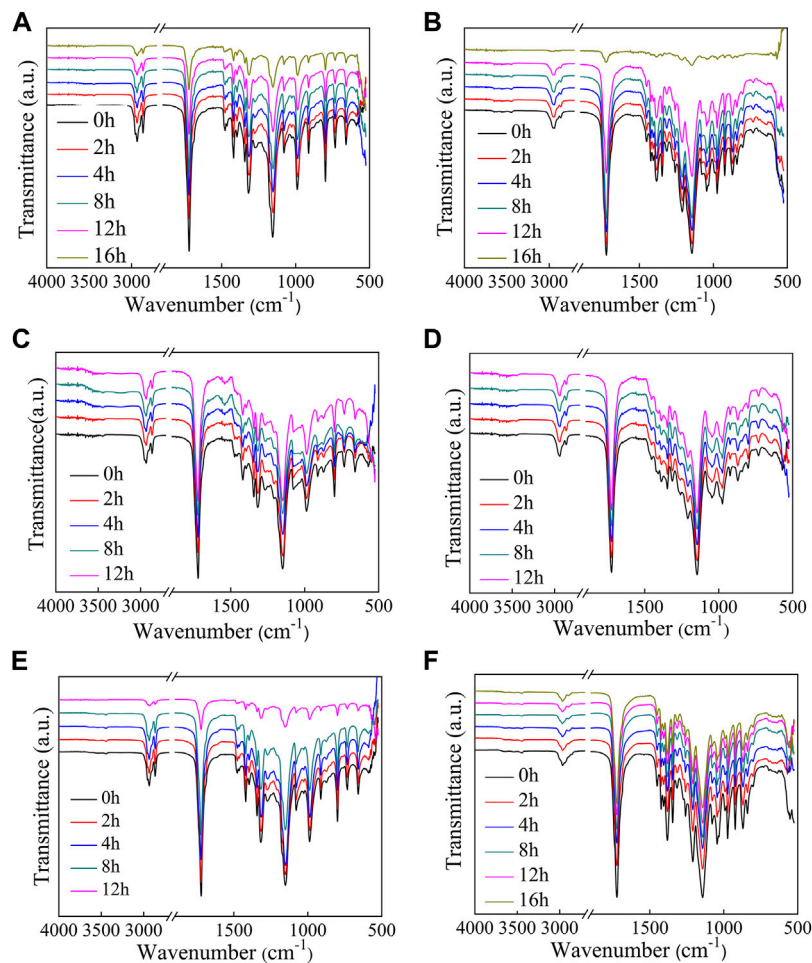


FIGURE 5 | FT-IR spectra measured of the polyesters at different extents of enzymatic hydrolysis. (A–F): PHS, P(HS-co-13ES), P(HS-co-32ES), P(HS-co-51ES), P(HS-co-76ES), and PES.

decreased when the films curled, and as a result, these samples did not completely hydrolyze. Overall, the enzymatic hydrolysis rates of these samples were relatively slow, especially in the second stage, when the enzymatic hydrolysis rate was almost zero. Except for P(HS-co-ES32) and P(HS-co-ES51), the enzymatic degradation rate of the other polyesters followed $\text{P(HS-co-ES13)} > \text{P(HS-co-ES76)} >$

$\text{PHS} > \text{PES}$. The main factors affecting enzymatic hydrolysis are hydrophilicity, melting temperature, and crystallinity, each of which is discussed in the next sections.

The FT-IR spectra of polyesters after enzymatic hydrolysis are compared in Figure 5A–F. The peak positions did not change significantly; however, the intensity of the C=O (1720 cm^{-1}) and

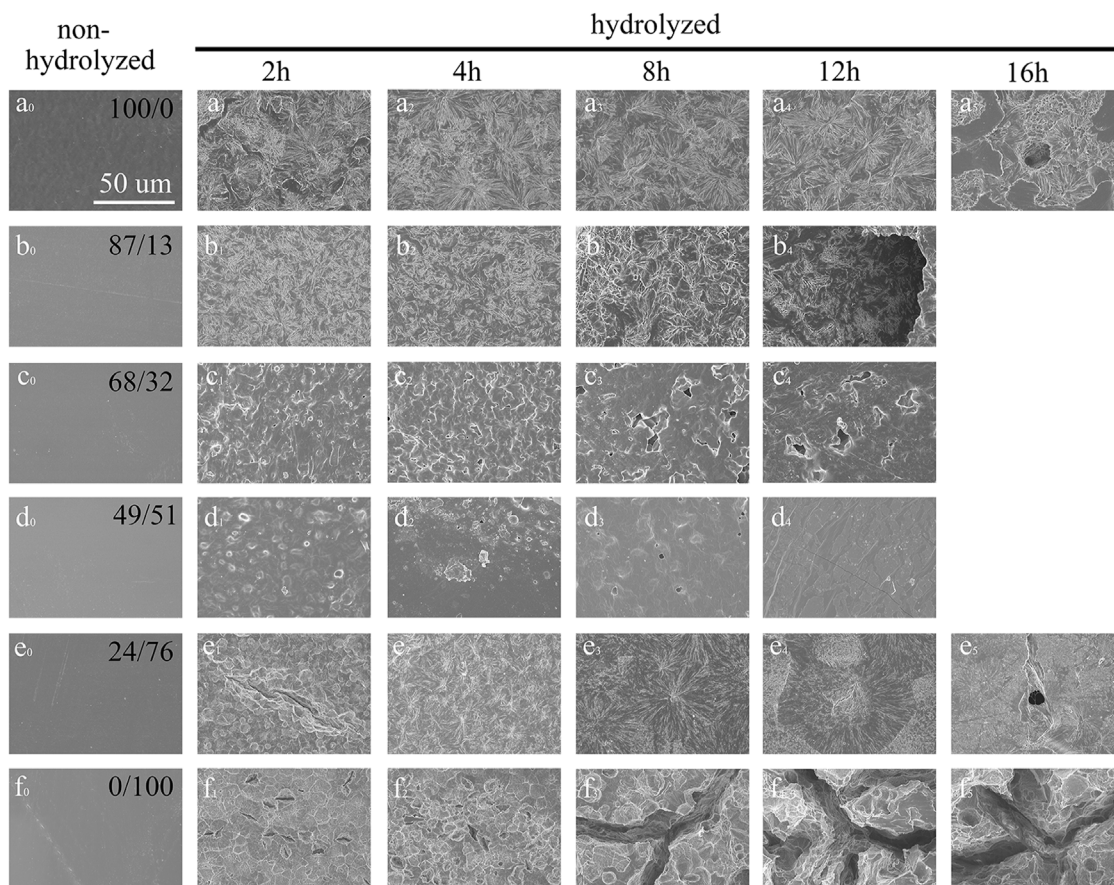


FIGURE 6 | SEM images of the polyester films after enzymatic hydrolysis with cutinase. **(A–F)**: PHS, P(HS-co-13ES), P(HS-co-32ES), P(HS-co-51ES), P(HS-co-76ES), and PES.

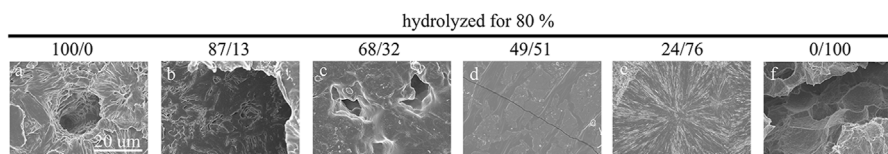


FIGURE 7 | SEM images of the polyester films after 80% of their masses were enzymatically hydrolyzed. **(A–F)**: PHS, P(HS-co-13ES), P(HS-co-32ES), P(HS-co-51ES), P(HS-co-76ES), and PES.

C–O ($1,150\text{ cm}^{-1}$) absorption peaks decreases with an increase in the hydrolysis time. The decrease in peak intensity is due to the pores that formed as the films degraded.

Figure 6 and **Figure 7** show the surface morphology of the polyester films after enzymatic hydrolysis. Before enzymatic hydrolysis, the polyester films had smooth surfaces (**Figures 6a₀–f₀**). The surface morphologies of neat PHS and PES films are rough and nonuniform after 2 h of incubation with the cutinase solution, and pits and cracks appear with an increase in the hydrolysis time as more of the ester bonds are cleaved. At the end stages of hydrolysis, the pits are deep and large (**Figures 6a₅/f₅**) due to the penetration of water into the amorphous regions of the films, which in turn increases

the rate of enzymatic hydrolysis (Azevedo et al., 2003). The results show that enzymatic hydrolysis occurs on the surface of the polyester films. The surface morphologies of P(HS-co-ES13) and P(HS-co-ES76) films are similar to those of the neat PHS and PES films, respectively. Meanwhile, the surface morphology of the P(HS-co-ES32) and P(HS-co-ES51) films did not change significantly after enzymatic hydrolysis. The surface of the P(HS-co-ES51) film remains relatively smooth after 12 h with only a few cracks due to incomplete enzymatic hydrolysis. These copolyesters are molten during the enzymatic hydrolysis experiments at 37°C and then recrystallized at room temperature for imaging, leading to formation of some cracks. **Figure 7** compares the surface

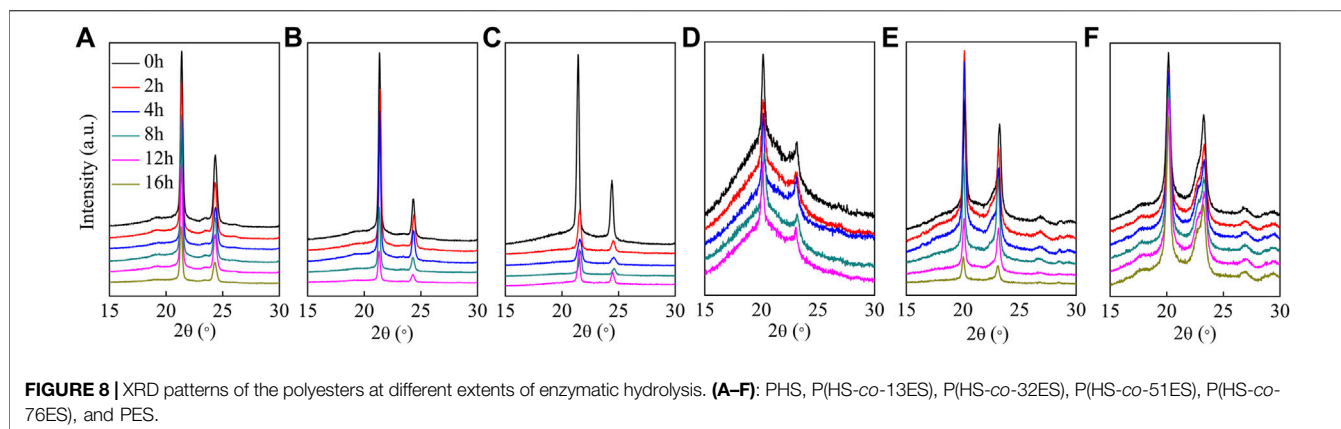


TABLE 2 | Thermal properties of the polyesters after enzymatic hydrolysis.

Polyester	Time (h)	T _m (°C)	X _c (%)	T _{5%} (°C)
PHS	0	59.9	50.9	321
	2	59.6	49.8	317
	4	55.9	50.1	315
	8	61.6	50.6	313
	12	56.2	47.6	303
	16	60.0	45.8	308
P(HS-co-ES13)	0	55.3	45.3	330
	2	51.9	43.8	321
	4	45.5	44.5	326
	8	50.1	42.2	327
	12	51.7	41.3	325
P(HS-co-ES32)	0	44.9	39.5	343
	2	46.6	38.8	318
	4	46.7	39.1	327
	8	43.9	37.6	323
	12	32.7	33.7	315
P(HS-co-ES51)	0	-	20.7	333
	2	-	20.1	328
	4	-	19.9	299
	8	-	18.9	318
	12	-	18.4	254
P(HS-co-ES76)	0	71.8	49.8	322
	2	69.7	48.2	397
	4	69.8	48.6	307
	8	70.0	49.5	309
	12	70.4	49.4	309
	16	-	48.2	309
PES	0	103.9	58.3	303
	2	102.2	57.8	302
	4	101.9	56.4	302
	8	102.1	56.2	301
	12	102.1	55.9	297
	16	102.6	56.6	293

morphologies of the copolyester films after 80% of their mass is lost, except for the image of the P(HS-co-ES51) film, where the degree of degradation was 50%. The water molecules easily penetrate the pits and cracks on the surface of the films, which leads to further corrosion and increases the rate of weight loss.

XRD patterns and the corresponding X_c of the hydrolyzed polyesters are presented in **Figure 8**; **Table 2**, respectively. As shown in **Figure 8A–F**, the positions of diffraction peaks did not change after enzymatic hydrolysis, indicating that the crystal structure did not change (Bai et al., 2018b); however, the degree of crystallinity varied with the copolyester chemical composition. The degree of crystallinity impacts the rate of enzymatic hydrolysis of the polyester (Bai et al., 2018a), where the materials with higher degrees of crystallinity have slower enzymatic hydrolysis rates (Seretoudi et al., 2002; Yasuniwa and Satou, 2002; Bikiaris et al., 2006). Although P(HS-co-ES51) has the lowest crystallinity (about 20.7%), the film was in a molten state during the hydrolysis experiments and did not completely hydrolyze at 37°C, suggesting that low degrees of crystallinity may also prevent the films from solidifying in the hydrolysis experiment conditions. Similarly, P(HS-co-ES32) eventually became molten during the long hydrolysis experiments, which causes the surface area to decrease and results in incomplete hydrolysis. Yet, P(HS-co-ES32) and P(HS-co-ES51) also have a greater hydrolysis rate in the earlier period. The degree of crystallinity of the prepared polyesters increases as P(HS-co-ES13) < P(HS-co-ES76) < PHS < PES, and the enzymatic hydrolysis rate follows the exact opposite trend, with P(HS-co-ES13) > P(HS-co-ES76) > PHS > PES, emphasizing that the polyester films with lower degrees of crystallinity degrade faster (Marten et al., 2003; Abou-Zeid et al., 2004; Zhang et al., 2021).

The cutinase used in this work was expressed with the gene from *Fusarium solani* and had excellent degradation performance as it was able to penetrate and hydrolyze the polyesters (Bai et al., 2018a). As the hydrolysis time increases, the area of the diffraction peaks in the XRD pattern measured of the hydrolyzed films has no obvious changes, but some of them decrease at the end of hydrolysis, indicating a decrease in X_c (**Table 2**). At the end of hydrolysis, the low molecular degradation products and the increased water absorption in the film decrease the degree of crystallinity (Sato et al., 2004).

The melting temperatures of polyester films also impact their rate of enzymatic hydrolysis (Bai et al., 2018a). **Table 2** lists the melting temperature of the polyesters before and after enzymatic hydrolysis determined from the first DSC heating curve. Because P(HS-co-ES32) and P(HS-co-ES51) became molten during the enzymatic hydrolysis process at 37°C, the total surface area of the films became smaller, which affected their enzymatic hydrolysis rate. The melting

TABLE 3 | Water contact angle, degree of swelling, and swelling ratio of the polyesters.

Polyester	WAC (°)	S _w (%)	S _r
PHS	94.7	1.071	1.005
P(HS-co-ES13)	93.3	1.195	1.004
P(HS-co-ES32)	88.6	0.715	1.005
P(HS-co-ES51)	89.3	0.265	1.002
P(HS-co-ES76)	94.3	0.129	1.002
PES	95.5	0.006	1.002

temperature of the P(HS-co-ES13) copolyester is lower than that of the neat PHS and PES, and as expected, the enzymatic hydrolysis rate of this film was faster than either of the neat polyester films. In addition, there is no significant difference in T_m before and after hydrolysis. Moreover, only P(HS-co-ES76) has a higher melting temperature than neat PHS, yet it hydrolyzes faster than neat PHS, indicating that there must be other factors that can influence the rate of enzymatic hydrolysis.

The thermal decomposition temperature ($T_{5\%}$) at an initial mass loss of 5% is listed in **Table 2** for the prepared polyesters. It is to be noted that the $T_{5\%}$ values of the P(HS-co-ES) copolymers are higher than those of either of the pure polymers. As the extent of the enzymatic hydrolysis increases, the thermal decomposition temperature decreases because more end groups form as the polymers degrade, which further facilitates the thermal decomposition of the polyesters (Bikiaris and Karayannidis, 1998). As the macromolecular chains degrade into small molecular oligomers and fragments, the number of carboxyl and hydroxyl end groups increases (Bikiaris and Karayannidis, 1999). Therefore, the thermal decomposition temperature of the polyester decreases, but this decrease is not significant, particular for P(HS-co-ES13), where the temperature decreases by less than 10°C.

The surface wettability of the polyester films was evaluated by measuring the water contact angle, and the results are listed in **Table 3**. The water contact angles of the P(HS-co-ES) copolyester films are smaller than those of PHS and PES, indicating that copolymers films are more hydrophilic than either of the neat PHS and PES films. In particular, the P(HS-co-ES32) and P(HS-co-ES51) copolyester films have lower water contact angles and are more hydrophilic, while the P(HS-co-ES13) and P(HS-co-ES76) copolyester films have higher water contact angles and were more hydrophobic. It should be noted that the wettability only reflects the hydrophilicity of the surface of the polyester films and is not directly related to the hydrophilicity of polyesters (Zeng et al., 2011). The experimental results show that the surface of the copolyester films was more wettable.

The swelling properties of the polyester films are related to the amount of water absorbed by the films to some extent (Lee et al., 2013). It can be seen from **Table 3** that the swelling ratio of the polyesters did not change after the films were degraded; however, the degree of swelling did change with the ES content in the copolyester

and is higher than that of pure PES. The largest degree of swelling was measured for the copolyester with an ES content of 13 mol%.

Based on the water contact angles, the hydrophilicity of polyesters follows P(HS-co-ES13) > P(HS-co-ES76) > PHS > PES, the same trend as the enzymatic hydrolysis rate. In other words, the most hydrophilic polymers have the fastest degradation. In summary, the main factors affecting the rate of enzymatic hydrolysis are hydrophilicity, melting temperature, and crystallinity, which can be tuned by adjusting the composition of the hydroxyl monomers in the copolymers.

CONCLUSION

In this work, a series of P(HS-co-ES) copolymers containing different HS/ES ratios were synthesized by adding HD/EG to improve the performance of the pure PHS and PES polyesters and expand their fields of application. The research results show that the mechanical properties of the P(HS-co-ES) copolymers improved compared to the pure polyesters. The crystal structures of the copolymers were similar to those of the corresponding pure polymer which was the majority monomer unit in the copolymer. The thermal decomposition temperatures of all polyesters were higher than 290°C and met the temperature requirements for industrial production. The enzymatic hydrolysis rates of the copolyester films using cutinase were faster than those of the pure polyesters. The physical and biodegradability properties of the polyesters could be tuned by adjusting the composition of the hydroxyl monomers in the copolymers, where polyesters that were more hydrophilic had lower melting temperatures, lower degrees of crystallinity, and biodegraded faster. Among the prepared copolymers, P(HS-co-ES13) was a soft but tough polymer with a high hydrolysis rate, while P(HS-co-ES76) was a partially brittle copolymer that also had a high hydrolysis rate. The tunable properties show that the copolymers with different compositions can be applied in different fields.

DATA AVAILABILITY STATEMENT

The raw data supporting the conclusion of this article will be made available by the authors, without undue reservation.

AUTHOR CONTRIBUTIONS

TS: conceptualization. ML: methodology and data curation. ML and JJ: formal analysis. ML and JJ: writing—original draft. TS: writing—review and editing. All authors contributed to manuscript revision and read and approved the submitted version.

REFERENCES

Abou-Zeid, D.-M., Müller, R.-J., and Deckwer, W.-D. (2004). Biodegradation of Aliphatic Homopolyesters and Aliphatic-Aromatic Copolyesters by Anaerobic Microorganisms. *Biomacromolecules* 5, 1687–1697. doi:10.1021/bm0499334

Azevedo, H. S., Gama, F. M., and Reis, R. L. (2003). *In Vitro* Assessment of the Enzymatic Degradation of Several Starch Based Biomaterials. *Biomacromolecules* 4, 1703–1712. doi:10.1021/bm0300397

Bai, Z., Liu, Y., Su, T., and Wang, Z. (2018a). Effect of Hydroxyl Monomers on the Enzymatic Degradation of Poly(ethylene Succinate), Poly(butylene Succinate), and Poly(hexylene Succinate). *Polymers* 10, 90. doi:10.3390/polym10010090

- Bai, Z., Shi, K., Su, T., and Wang, Z. (2018b). Correlation between the Chemical Structure and Enzymatic Hydrolysis of Poly(butylene Succinate), Poly(butylene Adipate), and Poly(butylene Suberate). *Polym. Degrad. Stabil.* 158, 111–118. doi:10.1016/j.polymdegradstab.2018.10.024
- Balart, R., Montanes, N., Dominici, F., Boronat, T., and Torres-Giner, S. (2020). Environmentally Friendly Polymers and Polymer Composites. *Materials* 13, 4892. doi:10.3390/ma13214892
- Bi, S., Tan, B., Soule, J. L., and Sobkowicz, M. J. (2018). Enzymatic Degradation of Poly (Butylene Succinate-Co-Hexamethylene Succinate). *Polym. Degrad. Stab.* 155, 9–14. doi:10.1016/j.polymdegradstab.2018.06.017
- Bikiaris, D. N., and Karayannidis, G. P. (1998). Calorimetric Study of Diepoxide Chain-Extended Poly(Ethylene Terephthalate). *J. Therm. Anal. Calorim.* 54, 721–729. doi:10.1023/a:1010127500694
- Bikiaris, D. N., and Karayannidis, G. P. (1999). Effect of Carboxylic End Groups on Thermooxidative Stability of PET and PBT. *Polym. Degrad. Stabil.* 63, 213–218. doi:10.1016/S0141-3910(98)00094-9
- Bikiaris, D. N., Papageorgiou, G. Z., and Achilias, D. S. (2006). Synthesis and Comparative Biodegradability Studies of Three Poly(alkylene Succinate)s. *Polym. Degrad. Stab.* 91, 31–43. doi:10.1016/j.polymdegradstab.2005.04.030
- Blanco, I., Ingrao, C., and Siracusa, V. (2020). Life-Cycle Assessment in the Polymeric Sector: A Comprehensive Review of Application Experiences on the Italian Scale. *Polymers* 12, 1212. doi:10.3390/polym12061212
- Castilla-Cortázar, I., Más-Estellés, J., Meseguer-Dueñas, J. M., Escobar Ivirico, J. L., Mari, B., and Vidaurre, A. (2012). Hydrolytic and Enzymatic Degradation of a Poly(ϵ -Caprolactone) Network. *Polym. Degrad. Stabil.* 97, 1241–1248. doi:10.1016/j.polymdegradstab.2012.05.038
- de Araújo Veloso, M. C. R., Scatolino, M. V., Gonçalves, M. M. B. P., Valle, M. L. A., de Paula Protásio, T., Mendes, L. M., et al. (2021). Sustainable Valorization of Recycled Low-Density Polyethylene and cocoa Biomass for Composite Production. *Environ. Sci. Pollut. R.* 28, 32810–32822. doi:10.1007/s11356-021-13061-y
- Gigli, M., Negroni, A., Zanolli, G., Lotti, N., Fava, F., and Munari, A. (2013). Environmentally Friendly PBS-Based Copolyesters Containing PEG-like Subunit: Effect of Block Length on Solid-State Properties and Enzymatic Degradation. *React. Funct. Polym.* 73, 764–771. doi:10.1016/j.reactfunctpolym.2013.03.007
- Hu, X., Gao, Z., Wang, Z., Su, T., Yang, L., and Li, P. (2016). Enzymatic Degradation of Poly(butylene Succinate) by Cutinase Cloned from *Fusarium Solani*. *Polym. Degrad. Stab.* 134, 211–219. doi:10.1016/j.polymdegradstab.2016.10.012
- Jing, J., Song, L., Su, T., and Wang, Z. (2021). Effects of Monomer Composition on Physical Properties and Enzymatic Hydrolyzability of Poly(butylene Succinate-Co-hexamethylene Succinate)s. *Polym. Eng. Sci.* 61, 379–387. doi:10.1002/pen.25581
- Karayannidis, G. P., Roupakias, C. P., Bikiaris, D. N., and Achilias, D. S. (2003). Study of Various Catalysts in the Synthesis of Poly(propylene Terephthalate) and Mathematical Modeling of the Esterification Reaction. *Polymer* 44, 931–942. doi:10.1016/S0032-3861(02)00875-3
- Kesavan, A., Rajakumar, T., Karunanidhi, M., and Ravi, A. (2021). Synthesis and Characterization of Random Copolymerization of Aliphatic Biodegradable Reunite D-Mannitol. *Mater. Today Proc.* doi:10.1016/j.matpr.2021.01.522
- Klug, H. P., and Alexander, L. E. (1974). *X-Ray Diffraction Procedures: For Polycrystalline and Amorphous Materials*. 2nd Edition. New York: John Wiley & Sons.
- Lee, J. M., Mohd Ishak, Z. A., Mat Taib, R., Law, T. T., and Ahmad Thirnazir, M. Z. (2013). Mechanical, Thermal and Water Absorption Properties of Kenaf-Fiber-Based Polypropylene and Poly(Butylene Succinate) Composites. *J. Polym. Environ.* 21, 293–302. doi:10.1007/s10924-012-0516-4
- Marten, E., Müller, R.-J., and Deckwer, W.-D. (2003). Studies on the Enzymatic Hydrolysis of Polyesters I. Low Molecular Mass Model Esters and Aliphatic Polyesters. *Polym. Degrad. Stabil.* 80, 485–501. doi:10.1016/S0141-3910(03)00032-6
- Nikolic, M. S., and Djonlagic, J. (2001). Synthesis and Characterization of Biodegradable Poly(butylene Succinate-Co-Butylene Adipate)s. *Polym. Degrad. Stabil.* 74, 263–270. doi:10.1016/S0141-3910(01)00156-2
- Pan, W., Bai, Z., Su, T., and Wang, Z. (2018). Enzymatic Degradation of Poly(butylene Succinate) with Different Molecular Weights by Cutinase. *Int. J. Biol. Macromol.* 111, 1040–1046. doi:10.1016/j.ijbiomac.2018.01.107
- Papageorgiou, G. Z., Tsanakis, V., Papageorgiou, D. G., Exarhopoulos, S., Papageorgiou, M., and Bikiaris, D. N. (2014). Evaluation of Polyesters from Renewable Resources as Alternatives to the Current Fossil-Based Polymers. Phase Transitions of Poly(butylene 2,5-Furan-Dicarboxylate). *Polymer* 55, 3846–3858. doi:10.1016/j.polymer.2014.06.025
- Polyák, P., Dohovits, E., Nagy, G. N., Vértessy, B. G., Vörös, G., and Pukánszky, B. (2018). Enzymatic Degradation of poly-[(R)-3-hydroxybutyrate]: Mechanism, Kinetics, Consequences. *Int. J. Biol. Macromol.* 112, 156–162. doi:10.1016/j.ijbiomac.2018.01.104
- Rizzarelli, P., Impallomeni, G., and Montaudo, G. (2004). Evidence for Selective Hydrolysis of Aliphatic Copolyesters Induced by Lipase Catalysis. *Biomacromolecules* 5, 433–444. doi:10.1021/bm034230s
- Sato, H., Dybal, J., Murakami, R., Noda, I., and Ozaki, Y. (2005). Infrared and Raman Spectroscopy and Quantum Chemistry Calculation Studies of C-H...O Hydrogen Bondings and thermal Behavior of Biodegradable Polyhydroxyalkanoate. *J. Mol. Struct.* 744–747, 35–46. doi:10.1016/j.molstruc.2004.10.069
- Sato, H., Murakami, R., Padermshoke, A., Hirose, F., Senda, K., Noda, I., et al. (2004). Infrared Spectroscopy Studies of CH...O Hydrogen Bondings and Thermal Behavior of Biodegradable Poly(hydroxyalkanoate). *Macromolecules* 37, 7203–7213. doi:10.1021/ma049117o
- Seretoudi, G., Bikiaris, D., and Panayiotou, C. (2002). Synthesis, Characterization and Biodegradability of Poly(ethylene Succinate)/poly(ϵ -Caprolactone) Block Copolymers. *Polymer* 43, 5405–5415. doi:10.1016/S0032-3861(02)00433-0
- Shi, K., Bai, Z., Su, T., and Wang, Z. (2019). Selective Enzymatic Degradation and Porous Morphology of Poly(butylene Succinate)/poly(lactic Acid) Blends. *Int. J. Biol. Macromol.* 126, 436–442. doi:10.1016/j.ijbiomac.2018.12.168
- Siracusa, V., and Blanco, I. (2020). Bio-Polyethylene (Bio-PE), Bio-Polypropylene (Bio-PP) and Bio-Poly(ethylene Terephthalate) (Bio-PET): Recent Developments in Bio-Based Polymers Analogous to Petroleum-Derived Ones for Packaging and Engineering Applications. *Polymers* 12, 1641. doi:10.3390/polym12081641
- Tan, B., Bi, S., Emery, K., and Sobkowicz, M. J. (2017). Bio-based Poly(butylene Succinate-Co-hexamethylene Succinate) Copolyesters with Tunable thermal and Mechanical Properties. *Eur. Polym. J.* 86, 162–172. doi:10.1016/j.eurpolymj.2016.11.017
- Yang, H., and Qiu, Z. (2013). Crystallization Kinetics and Morphology of Novel Biodegradable Poly(hexamethylene Succinate-Co-3 Mol % Ethylene Succinate) with Low and High Molecular Weights. *Ind. Eng. Chem. Res.* 52, 3537–3542. doi:10.1021/ie400107k
- Yasuniwa, M., and Satou, T. (2002). Multiple Melting Behavior of Poly(butylene Succinate). I. Thermal Analysis of Melt-Crystallized Samples. *J. Polym. Sci. B Polym. Phys.* 40, 2411–2420. doi:10.1002/polb.10298
- Zeng, J.-B., Jiao, L., Li, Y.-D., Srinivasan, M., Li, T., and Wang, Y.-Z. (2011). Bio-based Blends of Starch and Poly(butylene Succinate) with Improved Miscibility, Mechanical Properties, and Reduced Water Absorption. *Carbohydr. Polym.* 83, 762–768. doi:10.1016/j.carbpol.2010.08.051
- Zhang, K., Jiang, Z., and Qiu, Z. (2021). Effect of Different Lengths of Side Groups on the thermal, Crystallization and Mechanical Properties of Novel Biodegradable Poly(ethylene Succinate) Copolymers. *Polym. Degrad. Stab.* 187, 109542. doi:10.1016/j.polymdegradstab.2021.109542

Conflict of Interest: The authors declare that the research was conducted in the absence of any commercial or financial relationships that could be construed as a potential conflict of interest.

Publisher's Note: All claims expressed in this article are solely those of the authors and do not necessarily represent those of their affiliated organizations, or those of the publisher, the editors, and the reviewers. Any product that may be evaluated in this article, or any claim that may be made by its manufacturer, is not guaranteed or endorsed by the publisher.

Copyright © 2022 Li, Jing and Su. This is an open-access article distributed under the terms of the Creative Commons Attribution License (CC BY). The use, distribution or reproduction in other forums is permitted, provided the original author(s) and the copyright owner(s) are credited and that the original publication in this journal is cited, in accordance with accepted academic practice. No use, distribution or reproduction is permitted which does not comply with these terms.



OPEN ACCESS

EDITED BY
Zhangyong Wang,
Shenyang Agricultural University, China

REVIEWED BY
Antonis Mistriotis,
Agricultural University of Athens,
Greece
Paola Rizzarelli,
National Research Council (IPCB CNR),
Italy

*CORRESPONDENCE
Yigal Achmon,
yigal.achmon@gtiit.edu.cn

[†]These authors have contributed equally
to this work

[‡]PRESENT ADDRESS
Permanent Address,
Schulich Faculty of Chemistry,
Technion—Israel Institute of
Technology, Technion City, Israel

SPECIALTY SECTION
This article was submitted to Bioprocess
Engineering,
a section of the journal
Frontiers in Bioengineering and
Biotechnology

RECEIVED 18 April 2022
ACCEPTED 28 June 2022
PUBLISHED 08 August 2022

CITATION
Dar SU, Wu Z, Zhang L, Yu P, Qin Y,
Shen Y, Zou Y, Poh L, Eichen Y and
Achmon Y (2022). On the quest for
novel bio-degradable plastics for
agricultural field mulching.
Front. Bioeng. Biotechnol. 10:922974.
doi: 10.3389/fbioe.2022.922974

COPYRIGHT
© 2022 Dar, Wu, Zhang, Yu, Qin, Shen,
Zou, Poh, Eichen and Achmon. This is an
open-access article distributed under
the terms of the [Creative Commons
Attribution License \(CC BY\)](#). The use,
distribution or reproduction in other
forums is permitted, provided the
original author(s) and the copyright
owner(s) are credited and that the
original publication in this journal is
cited, in accordance with accepted
academic practice. No use, distribution
or reproduction is permitted which does
not comply with these terms.

On the quest for novel bio-degradable plastics for agricultural field mulching

Sami Ullah Dar ^{1,2†}, Zizhao Wu ^{1†}, Linyi Zhang ¹, Peirong Yu ¹,
Yiheng Qin ¹, Yezi Shen ¹, Yunfan Zou ¹, Leslie Poh ³, Yoav Eichen ^{2‡}
and Yigal Achmon ^{1,4,5*}

¹Biotechnology and Food Engineering, Guangdong Technion—Israel Institute of Technology, Shantou, China, ²Guangdong Technion Department of Chemistry—Israel Institute of Technology, Shantou, China, ³Polymer Physics Laboratory, Department of Chemical Engineering, Guangdong Technion—Israel Institute of Technology (GTIIT), Shantou, China, ⁴Faculty of Biotechnology and Food Engineering, Technion—Israel Institute of Technology, Haifa, Israel, ⁵Guangdong Provincial Key Laboratory of Materials and Technologies for Energy Conversion, Guangdong Technion—Israel Institute of Technology, Shantou, China

Plasticulture, the practice of using plastic materials in agricultural applications, consumes about 6.7 million tons of plastics every year, which is about 2% of the overall global annual plastics production. For different reasons, plastic material used for agriculture is difficult to recycle. Therefore, most of it is either buried in fertile soils, thereby significantly causing deterioration of their properties, or, at best case, end in landfills where its half-life is measured in decades and even centuries. Hence, developing biodegradable plastic materials that are suitable for agricultural applications is a vital and inevitable need for the global human society. In our labs, two types of potentially biodegradable plastic polymer films were prepared and characterized imidazolium in terms of their bio-degradability. In the first approach, polymers made of ionic liquid monomers were prepared using photo radical induced polymerization. The second approach relies on formation of polyethylene-like n-alkane disulfide polymers from 1,ω-di-thiols through thermally activated air oxidation. These two families of materials were tested for their biodegradability in soils by using a simulation system that combines a controlled environment chamber equipped with a respirometer and a proton-transfer-reaction time of flight mass spectrometer (PTR-TOF-MS) system. This system provides a time-dependent and comprehensive fingerprint of volatiles emitted in the degradation process. The results obtained thus far indicate that whereas the ionic-liquid based polymer does not show significant bio-degradability under the test conditions, the building block monomer, 1,10-n-decane dithiol, as well as its disulfide-based polymer, are bio-degradable. The latter reaching, under basic soil conditions and in room temperature, ~20% degradation within three months. These results suggest that by introduction of disulfide groups into the polyethylene backbone one may be able to render it biodegradable, thus considerably shortening its half-life in soils. Principal component analysis, PCA, of the data about the total volatiles produced during the degradation in soil indicates a distinctive volatile “fingerprint” of the disulfide-based bio-degradable products which comes from the volatile organic compounds portfolio as recorded by the PTR-TOF-MS. The biodegradation volatile

fingerprint of this kind of film was different from the “fingerprint” of the soil background which served as a control. These results can help us to better understand and design biodegradable films for agricultural mulching practices.

KEYWORDS

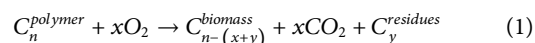
plastic biodegradation, soil respiration, microbial volatile organic compounds, PTR-ToF-MS (proton transfer reaction time-of-flight mass spectrometry), disulfide-based polymer binder

Introduction

Plastic waste is an increasing concern around the world. The use of plastics in agricultural practices such as mulching is on the rise as well (Huang et al., 2020). Plasticulture, i.e. agricultural practices that include the use of plastic materials, is essential for food security in most parts of the world. The usage of plastic polymers in agriculture is quite diverse, including for example: greenhouse covers, trailing, packaging, irrigation systems, silage, soil mulching and more (Briassoulis and Dejean, 2010; Zumstein et al., 2019; Zurier and Goddard, 2021). Although necessary, the use of plastics in agriculture can lead to wide environmental adverse effects, such as contamination of ground water, disturbance of the ecosystems of terrestrial and aquatic fauna and flora (Zhou et al., 2020), deterioration of soil properties of agricultural lands (for example their gas exchange and water retention capacity), spread of toxic microplastics particles (Sander, 2019; Huang et al., 2020; Zurier and Goddard, 2021) etc. Plastic mulching is probably the most abundant plasticulture practice. Agricultural plastic mulching is done for various reasons, including water preservation, crop protection, soil remediation, treatments against weeds and soilborne pathogens (such as solarization and fumigation (Achmon et al., 2017)) and other important practices used to increase the yields of crops. Mulching is estimated to cover an agricultural area of more than 128,500 km² around the world (Zhou et al., 2020) and China is the global leader in terms of plasticulture mulching practices (Huang et al., 2020). For these reasons, the need for biodegradable plastics for agricultural mulching is critical from the environmental point of view. Although it is an obvious need, not many commercial solutions are currently available and most of the agricultural mulching done today utilizes non-degradable plastic polymers, mainly polyethylene (PE), (Briassoulis et al., 2015; Ahmed et al., 2018; Zhang et al., 2019). Unlike the slow implementation of biodegradable plastic polymers in commercial agricultural mulching systems, research in this field receives increased attention and has a fast progress pace (Kyrikou and Briassoulis, 2007; Sander, 2019; Huang et al., 2020). There are several important characteristics that plastic mulching materials must possess along their entire service life in order to be widely applied in the field: 1) durability (mechanical,

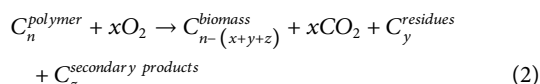
chemical, resistance to water and solvents, etc.), 2) mechanical flexibility (ability to be stretched over various shapes of field plots), 3) light weight, 4) modularity (can have variable thickness, color and gas permeability), 5) non-toxicity, and most important, 6) affordability (being inexpensive and easy to produce in very large quantities). The combination of these characteristics makes it hard to find alternative biodegradable plastic polymers to replace the current non-degradable ones. Moreover, it is challenging to define what can be considered as a biodegradable plastic in soil and what is only bio-available (a material that judging from its chemical formula looks biodegradable, but does not actually degrade in a relevant pace (Zumstein et al., 2019)). Some recent progress was done in this area by introducing the European Standard EN 17033: Plastics–Biodegradable mulch films (EN17033 Plastics, 2018). Additionally, most degradation processes are complex and are not sufficiently characterized, and hence are less understood from microbiological and chemical perspectives (Sander, 2019). Yet there are some examples of biodegradable mulching materials that are available, such as cellulose, starch, poly-b-hydroxybutyrate and alike (Kyrikou and Briassoulis, 2007; Sander, 2019). To date, most polymer soil biodegradability studies have been using standard methods such as respiration or polymer size reduction (Achmon et al., 2019) to assess the biodegradability rate. Some recent studies used ¹³C-labeled polymers to closely monitor the degradation of the carbon skeleton of the polymer (Thomas et al., 2021). The analysis of biodegradability is still a debatable issue and although standards are available and are being updated (EN17033 Plastics, 2018), there is still a lot of room for improvement. Generally, the biodegradability can be looked upon through the carbon conversion by Equation 1.

Equation 1:



Where C^{polymer} is the polymers' carbon backbone, C^{biomass} is the utilization of the carbon to build live biomass (mainly microbial) and C^{residues} represents the carbon remaining in polymer residues as long as biodegradation is not completed (Sander, 2019). However, a more precise equation is presented in Equation 2.

Equation 2:



Where $C^{\text{secondary products}}$ are additional secondary metabolites produced by those microbes that are not converting all of the polymer into biomass and emit secondary products back to the environment. In most of the studies on biodegradability of polymers the focus is on the CO_2 and C^{polymer} , and sometimes on C^{residues} , but rarely on $C^{\text{secondary products}}$. $C^{\text{secondary products}}$ can also be divided according to Equation 3.

Equation 3:

$$C_z^{\text{secondary products}} = C_a^{\text{non-volatile products}} + C_b^{\text{volatile products}} \quad (3)$$

Only few studies have looked at the $C^{\text{non-volatile products}}$ (Zumstein et al., 2019; Thomas et al., 2021) which are mainly soluble residues secreted by the microbial activity, and as far as the authors know, no study to date has looked at the $C^{\text{volatile products}}$ emanating by the polymer's biodegradation process in the soil.

In this study we tested two new synthetic materials as potential candidates to be used as biodegradable plastic polymers for agricultural mulching. We also report here a first insight into $C^{\text{volatile products}}$ (Volatile Organic Compounds (VOCs)) emitted during the biodegradation process of those two new types of polymers. This study is opening a hatch to a new way of looking at the complex mechanisms underlying the biodegradation of polymers in the soil through VOCs production during the process.

Materials and methods

Apparatus

Respirometry experiments were performed using a Micro-Oxymax Respirometer (Columbus Instruments, United States). Detectors of CO_2 Carbon Dioxide Sensor 0–10% CH_4 Methane Measuring (0–10%) and O_2 Paramagnetic Oxygen Sensor 0–100% - (Columbus Instruments, United States) where used to monitor the simulated process of the biodegradation of plastics in soil. Mass spectrometry was performed using a PTR-TOF-MS 1000 (Ionicon Analytik Ges.m.b.H., Innsbruck, Austria).

Materials

Ethyl bromoacetate, 1-vinyl imidazole, butylated hydroxyl toluene (BHT), 1,10-decanedithiol, sodium hydroxide (NaOH), phenylbis (2,4,6-triethylbenzoyl) phosphine oxide were

purchased from Sigma-Aldrich (Merck) and used as received. Microcrystalline cellulose was purchased from Alfa Aesar Co. and used as received. All solvents, such as ethyl acetate, methanol, THF and acetone, as well as other materials used in the present research were purchased from Shanghai Macklin Biochemical Co., and were of the highest purity available. All commercial materials were used as received unless specifically noted. Tryptic Soy Agar (TSA) was purchased from BD, MD, United States. Oxytetracycline-Glucose Yeast Extract (OGYE) Agar Base was purchased from Solarbio, Beijing, China. Oxytetracycline hydrochloride was purchased from Solarbio, Beijing China. *Bacillus cereus* (BC) Agar Base was purchased from OXOID, Basingstoke, United Kingdom. Eosin Methylene Blue Agar (EMBA) was purchased from HuanKai Microbial, Guangdong, China.

1-vinyl-3-(2-ethoxy-2-oxoethyl) imidazolium bromide

Ethyl bromoacetate (10.0 ml, 225 mmol) and 50.0 ml of ethyl acetate were added to a 100 ml round bottom flask equipped with a magnetic stirrer. 1-vinyl imidazole (8.17 ml, 90.2 mmol) containing 100 ppm butylated hydroxyl toluene (BHT) was added dropwise to the flask while stirring, and the mixture was left to stir for 24 h at room temperature. The precipitate was filtered and washed with three portions of ethyl acetate, then dried in a vacuum oven at 40°C for 24 h. The product, 1-vinyl-3-(2-ethoxy-2-oxoethyl) imidazolium bromide, in the form of an off-white solid, was obtained with an 81% yield.

Off white solid, M.P. = 95°C; 81% yield; 1H NMR (400 MHz, D_2O , δ): 9.10 (s, 1H, 2-Im), 7.80 (s, 1H, 4-Im), 7.57 (s, 1H, 5-Im), 7.11 (dd, J = 16.0, 8.0 Hz, 1H, N-CH = CH₂), 5.78 (dd, J = 16.0, 4.0 Hz, 1H, CH = CH₂), 5.42 (dd, J = 8.0, 8.0 Hz, 1H, CH = CH₂), 5.21 (s, 2H, -N⁺C-CH₂-C=O-), 4.23 (q, J = 6.0 Hz, 2H, CH₃-CH₂-O), 1.20 (t, J = 8.0 Hz, 3H, -CH₂-CH₃); ^{13}C NMR (400 MHz, D_2O , δ): 167.86, 135.95, 128.18, 124.23, 119.47, 110.30, 63.74, 50.35, 13.32; HRMS (MALDI-TOF) (ESI) m/z : [M-Br]⁺calc. for C₉H₁₃N₂O₂, 181.216; found, 181.052.

Poly-(1-vinyl-3-(2-ethoxy-2-oxoethyl) imidazolium bromide)

15 μ L of photoinitiator stock solution (0.3 g of phenylbis (2,4,6-triethylbenzoyl) phosphine oxide in 1 g of THF) was added to 1 g of a 1:1 w/v liquid mixture of 1-vinyl-3-(2-ethoxy-2-oxoethyl) imidazolium bromide and 1-vinyl imidazole. The combined solution was spread over glass slides and exposed to UV-VIS light to induce polymerization. The product is obtained in the form of a yellowish-brown film (Sevilia et al., 2022; Zertal et al., 2022).

Poly 1,10-disulfanyl-n-decane

1,10-decanedithiol (9.5 ml, 43.7 mmol) was added to a solution of NaOH (18 g, 450 mmol) in methanol (300 ml) using a 500 ml round bottom flask equipped with a compressed air inlet and an outlet. The reaction mixture was stirred vigorously for 5 days with the addition of 250 ml of methanol each day to compensate for evaporation. The crude, in the form of white color suspension with some lumps, was dried and washed with several portions of water until it became neutral, then with several portions of methanol and acetone, and then dried in a vacuum oven at 45 °C for 48 h. The product, in the form of a white solid, was obtained with a 54% yield (Tada et al., 2012).

White solid, 54% yield; ¹H NMR (400 MHz, CDCl₃, δ): 2.66–2.49 (t, q, J = 4 Hz, J = 8 Hz 8H, -H₂C-S-S-CH₂-), 1.60–1.67 (complex multiplet, 8H, -CH₂-CH₂-S-S-CH₂-CH₂-), 1.28–1.39 (complex multiplet, 24H, central alkyl chain); ¹³C NMR (400 MHz, CDCl₃, δ): 39.17, 34.03, 29.4–29.43, 28.36–28.52, 24.65.

Determination of inherent biodegradability

The biodegradability of polymer poly-(disulfanyl-n-decane) 1,10 decanedithiol (carbon content: 58.8%wt.) and of monomer 1,10-decane dithiol (carbon content: 58.2%wt.) in soil under basic conditions and unadjusted conditions was investigated in this preliminary experiment. The biodegradability of plastic materials was determined according to ISO 17556:2019 (ISO, 2019) by measuring the amounts of evolved CO₂. Soil samples were collected from the field experiment station of the GTIIT, in Shantou, Guangdong, China (23°31'4"N, 116°45'6"E). After collection, the soil was sieved to give particles smaller than 2 mm in size and obvious plant materials, stones and other inert materials were removed. The sieved soil was then air-dried under the sun for three days. In the test, a biodegradable reference material, microcrystalline cellulose (Alfa Aesar Co. Inc.), was used as a positive control. Samples were prepared by thoroughly mixing 60 g of dry soil with 0.6 g polymer/monomer/reference material. 24 g of distilled water were added to each sample to reach approximately 50% total water-holding capacity. To adjust the sample to the basic environment, 4.2 ml NaOH solution (1 M) was added to the samples at the beginning of the experiment. Throughout the experiment, samples' pH was maintained at 8.5–8.8 for basic groups and at 5.0–5.5 for unadjusted groups. Soil with only water addition served as the blank group of the test. The soil mixtures were placed inside 100 ml flasks which were connected to a Micro-Oxymax Respirometer (Columbus Instruments, United States). The system was set in aerobic mode and was capable of measuring CO₂, O₂ and CH₄ quantities (CO₂ Sensor 0–10% CH₄ Measuring (0–10%) and O₂ Paramagnetic Sensor

0–100% - Columbus Instruments, United States) with a cycle of approximately 4 h for each individual flask. All flasks were incubated in triplicates at 25°C. Every 10 days, water was added to keep the water content between 40 and 60%wt. of the total water-holding capacity and the soil was gently re-mixed.

The amount of CO₂ evolved was measured by the Micro-Oxymax Respirometer and the data was collected with the help of the Micro-Oxymax Windows software. Since the amount of CO₂ was recorded in volume units, the measured mass of CO₂ (m) was calculate by using the ideal gas law, Equation 4, and Equation 5.

Equation 4:

$$PV = nRT = \frac{m}{Mw}RT \quad (4)$$

Equation 5:

$$m = \frac{PVMw}{RT} \quad (5)$$

where V is the volume, P is the pressure in the respirometer (811 mmHg), R is the ideal gas constant, T is the system temperature (298°K), V is the measured volume of CO₂, and Mw is the molecular weight of CO₂ (44.01 g/mol).

In accordance with ISO 17556:2019, the percentage biodegradation (D_t) was calculated from Equation 6 and Equation 7:

Equation 6:

$$ThCO_2 = \frac{44}{12} \times M_T \times w_c \quad (6)$$

Equation 7:

$$D_t = \frac{\sum m_T - \sum m_B}{ThCO_2} \times 100 \quad (7)$$

where ThCO₂ is the theoretical amount of CO₂ that can be evolved by the test material, M_T is the mass of test material introduced into each flask, w_c is the carbon content of the test material determined from the chemical formula, Σm_T is the cumulative amount of CO₂ evolved in the flask containing test material and soil mixture, Σm_B is the cumulative amount of CO₂ evolved in the flask containing mere soil (blank). The test was done until 60% of the reference material, microcrystalline cellulose, was degraded given what can be named “inherent biodegradability” that indicates the potential of the materials to be bioavailable in a relatively short period of time.

PTR-TOF-MS analysis

Samples were prepared in 100 ml flasks as done for the biodegradability test at 25°C. An additional abiotic group was prepared by placing 0.9 g of plastics inside an empty flask. The flasks were capped with screw caps having two channels, one for aeration and one for injection into the apparatus. The headspace

composition of the samples was measured using a PTR-TOF 1000 (Ionicon Analytik Ges.m.b.H., Innsbruck, Austria) under the following working conditions: 630 V drift voltage, 2.30 mbar drift pressure, 6.5 sccm inlet flow, 80°C drift tube and inlet temperature. H_3O^+ was employed as the primary ion and the instrument was operated at an E/N ratio (E corresponds to the electric field strength and N to buffer gas number density within the drift tube) of 142 Td ($1 \text{ Td} = 10^{-17} \text{ Vcm}^2$). For each flask, more than 120 cycles (2 min each) were recorded, and a stable stage (generally 90 to 120 cycles) was used for the analysis. All the samples were measured once a day.

Microbial cultures of soil samples

A microbial test was done for microbial load in the tested samples. Four kinds of culture media were prepared for testing the microbial culture growth: Tryptic Soy Agar (TSA) (BD, MD, United States), Oxytetracycline-Glucose Yeast Extract (OGYE) Agar Base (Solarbio, Beijing, China) with the supplement of Oxytetracycline hydrochloride (Solarbio, Beijing China), *Bacillus cereus* (BC) Agar Base (OXOID, Basingstoke, United Kingdom) and Eosin Methylene Blue Agar (EMBA) (HuanKai Microbial, Guangdong, China). All media were prepared and sterilized according to their corresponding specifications. For each soil sample, 2 g of soil mixtures were transferred to 20 ml sterilized saline, followed by mixing using a vortex. After the dirt grains settled down, the supernatant (addressed as a 10^{-1} dilution) was collected and diluted to 10^{-2} . For each medium, 0.1 ml dilution was used for plating. TSA and EMBA were incubated at 37°C for 24 h, while OGYE and BC were incubated at 30°C for 24 h.

Data analysis

Statistical ANOVA tests were performed using the R 4.1.1 software (R Foundation for Statistical Computing, Vienna, Austria) to evaluate the differences in the CO_2 evolution rate between plastic/reference material degradation processes and their corresponding blanks. The PTR data were pre-processed and analyzed using PTR-MS Viewer 3.2 (Ionicon Analytik Ges.m.b.H., Innsbruck, Austria). Principal component analysis (PCA) was carried out using R 4.1.1, and 3D plots of the PTR spectra were generated using MATLAB R2021b (The MathWorks, Inc., Natick, MA, United States), based on the exported PTR data.

Results and discussion

Polymers

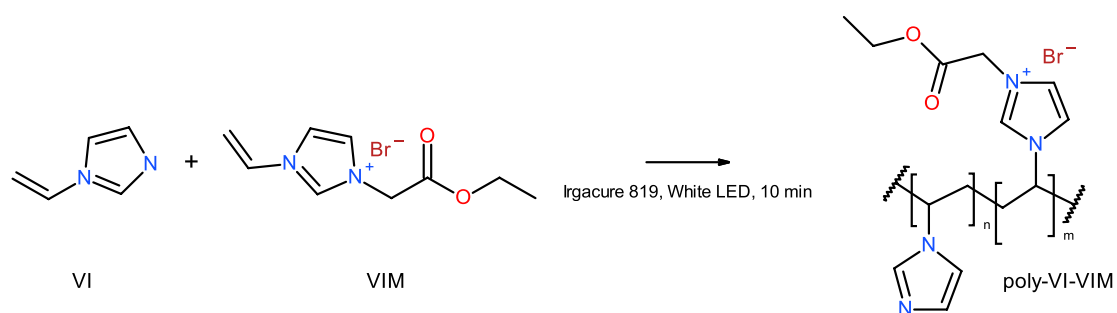
Two prototypes of polymer backbones were investigated, with the aim of developing novel biodegradable polymers,

based on their biodegradability properties. A first prototype, poly-VI-VIM, is composed of a mixture of 1-vinylimidazole (VI) and 1-vinyl-3-(2-ethoxy-2-oxoethyl) imidazolium bromide (VIM), and was prepared by photoinduced radical polymerization, according to Figure 1, where $n/m = 3.75$. A 1:1 wt. mixture of VI and VIM was prepared, then 0.0045 mg/ml of photo initiator (Irgacure 819) was added, and the mixture was well mixed, spreaded atop a glass plate and cured using a 100 W white LED. Curing was monitored by FT-IR, and irradiation proceeded until the complete disappearance of the vinyl absorption bands. The resulting films were used as prepared for the biodegradation experiments.

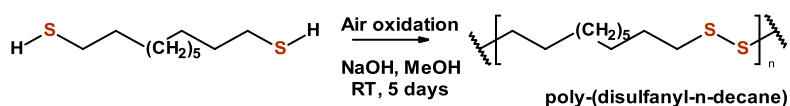
The second prototype material, poly-(disulfanyl-n-decane), was prepared in a single step from commercially available 1,10-decanedithiol through air oxidation under basic conditions, (Figure 2). 1,10-decanedithiol was dissolved in methanol containing NaOH and exposed to air flow for 5 days at room temperature. A white color thick melt was obtained, which was washed with several portions of distilled water until it became neutral, then washed with several portions of methanol and acetone, and then it was filtered and dried in a vacuum oven at 45°C for 48 h. The bright white powder, poly-(disulfanyl-n-decane), was used for the preparation of disk samples, $\Phi = 25 \text{ mm}$, thickness = 2 mm, through compression molding, done for 1 h at 125°C under 13 Mpa pressure between two smooth PTFE sheets.

Biodegradability of plastic polymers in the soil is usually measured by monitoring the emission of CO_2 during the process (Briassoulis et al., 2020; Huang et al., 2020; Zurier and Goddard, 2021). In this study the Micro-Oxymax respirometer system was used to monitor the CO_2 , O_2 and CH_4 evolution caused by the biodegradation of the two polymers poly-VI-VIM and poly-(disulfanyl-n-decane), in the soil (Figure 3).

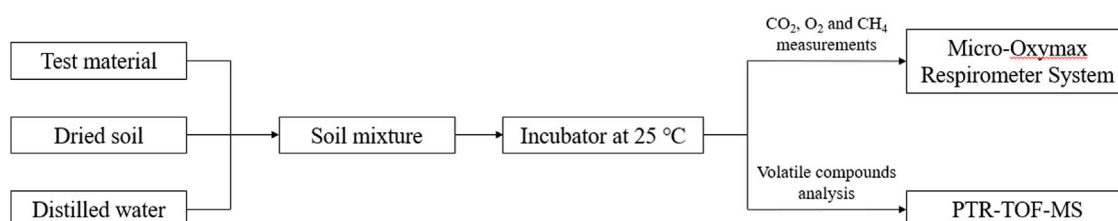
The system allowed a real-time and continuous measurement of the three relevant gases. The results showed that poly-VI-VIM exhibited very low biodegradability under the tested experimental conditions and it did not show any significant difference from the control soil system (data not shown). In contrast, poly-(disulfanyl-n-decane) showed significant biodegradability in the soil (Figures 4–6 and Table 1). A preliminary experiment was done to evaluate the optimal soil biodegradation conditions in terms of pH (Figure 4). In this experiment both poly-(disulfanyl-n-decane) and its monomer were tested for their bioavailability. The biodegradation assessment was done by monitoring the accumulation and evolution rate of CO_2 and O_2 respiration of the soil (Figure 4A,B,C,E). The accumulation and evolution rate of CH_4 was also monitored to see that no release of this potent greenhouse gas (GHG) takes place as part of the biodegradation process (Figure 4C,F). The results indicate a significantly more efficient degradation under basic conditions (pH~8.5) of the soil than under neutral conditions (pH~6) (Figure 4). The pH level is known to be an important factor that may have a significant

**FIGURE 1**

Synthesis of poly-VI-VIM copolymer, $n/m = 3.75$.

**FIGURE 2**

Air oxidation of 1,10-decanedithiol to poly-(disulfanyl-n-decane). Measuring the biodegradation of the polymers in the soil.

**FIGURE 3**

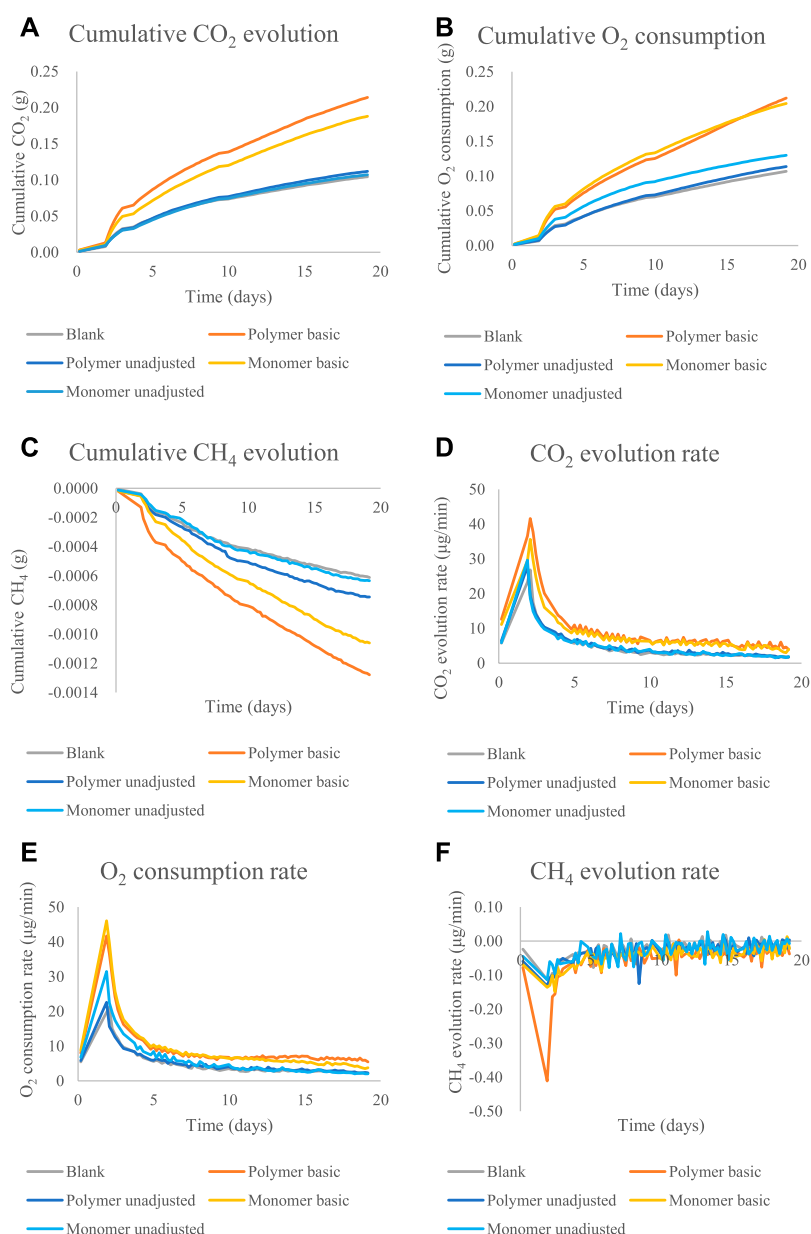
Flow chart of the biodegradability test and volatile compounds analysis. Test plastic (or reference material) and dried soil were mixed homogeneously with the supplement of distilled water. The soil mixture was incubated in a low temperature incubator with a constant temperature of 25 °C. The changes of CO₂, O₂ and CH₄ concentrations were measured by a Micro-Oxymax Respirometer System in real time and the volatile compounds were analyzed using a PTR-TOF-MS.

TABLE 1 CO₂ evolution rate of poly-(disulfanyl-n-decane).

Materials	Average rate (μg/min)	Maximal rate (μg/min)
poly-(disulfanyl-n-decane)	6.88 ± 0.197 ^b	39.13 ± 0.895 ^a
Crystalline cellulose (References material)	10.50 ± 0.280 ^a	25.61 ± 0.458 ^b
Blank	4.04 ± 0.152 ^c	25.27 ± 3.265 ^b

Values are means ± SD (n = 3).

*: The *p* value was obtained by an ANOVA, test with the blank at the same time span. Different letters indicate a significant difference between groups within each time section (α = 0.05).

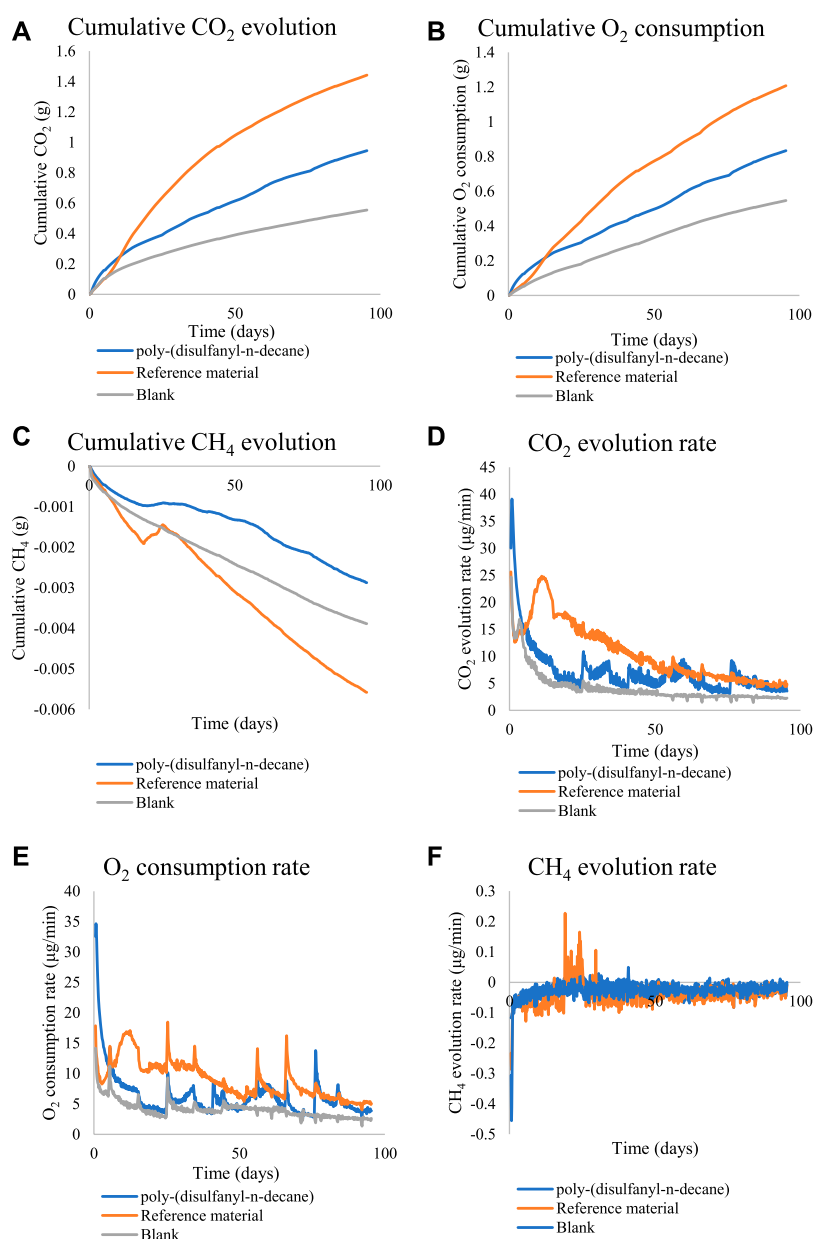
**FIGURE 4**

The cumulative amounts and rate of CO₂, O₂ and CH₄ emission for the biodegradability test of poly-(disulfanyl-n-decane) and monomer 1,10-decane dithiol under basic conditions (pH~8.5) and unadjusted conditions (pH~5.3): **(A)** the cumulative CO₂ evolution. **(B)** The cumulative O₂ consumption. **(C)** The cumulative CH₄ evolution. **(D)** The CO₂ evolution rate. **(E)** The O₂ consumption rate. **(F)** The CH₄ evolution rate.

impact on plastic biodegradation in the soil (Emadian et al., 2017; Fernandes et al., 2020; Liu et al., 2021). A recent study found that residues of plastic mulches have a lower negative impact on rice growth under basic conditions (pH 8.5) (Liu et al., 2021). In this study the “inherent” biodegradability was measured rather than a complete “ultimate biodegradability” which is a complete mineralization of the plastic polymer. The “inherent” biodegradability is a sufficient measurement to indicate how

much of the plastic polymer is available for a relatively short period of biodegradation.

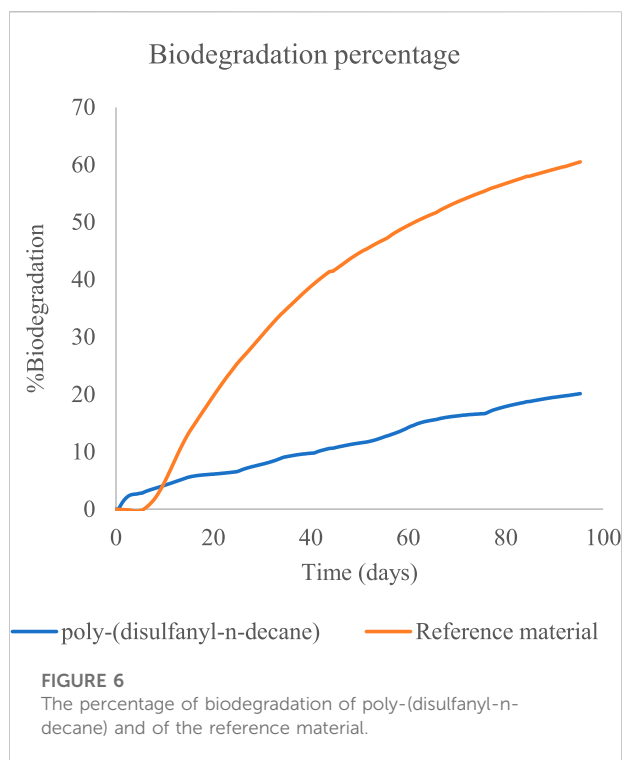
To get a better understanding of the biodegradation process of poly-(disulfanyl-n-decane) an additional study was performed under optimal pH conditions (pH ~8.5) and for a longer period (Figure 5). Poly-(disulfanyl-n-decane) showed significantly higher accumulation and evolution rate of CO₂ and O₂ respiration than those measured in the control soil respiration (Figure 5).

**FIGURE 5**

The cumulative amounts and rate of CO₂, O₂ and CH₄ for the biodegradability test of poly-(disulfanyl-n-decane). (A) The cumulative CO₂ evolution. (B) The cumulative O₂ consumption. (C) The cumulative CH₄ evolution. (D) The CO₂ evolution rate. (E) The O₂ consumption rate. (F) The CH₄ evolution rate.

Both CO₂ and O₂ respiration patterns were similar during the three months of the degradation in soil experiment. Around 0.8 and 0.4 g of CO₂ were produced during the three months from the reference material (cellulose microcrystalline) and the tested poly-(disulfanyl-n-decane) polymer respectively (after subtraction of the results from the soil control). A similar trend was observed for the oxygen consumption with close to 0.6 and 0.2 g of O₂ consumed during the three months more than the reference material (microcrystalline cellulose) and the tested poly-

(disulfanyl-n-decane) polymer respectively (after subtraction of the results from the soil control). It is worth noticing that oxygen consumption is a relative measure of the reduction of oxygen below the atmospheric levels (this is why the results are lower than the CO₂ production results). The known biodegrading reference material showed as expected the highest biodegradability and reached a 60% degradation in three months (Figure 6), while at the same time the tested poly-(disulfanyl-n-decane) polymer reached only 20% degradation. It is also interesting to note that



for an unknown reason the reference material had a certain “lag” phase in the degradation process which was different from the tested material. While at a first glance the observed degradation rate of poly-(disulfanyl-n-decane) seems slow, for many plasticulture applications, including mulching films, it is too fast. Mulching films are used under harsh conditions and their service life ranges from 1 month for short soil treatments to 6 months in some crop protection techniques (Kasirajan and Ngouajio, 2012; Achmon et al., 2018). Along this period of time, these polymer sheets are required to perform with no significant loss of their chemical and physical properties. In order to achieve this, the bio-degradation of the polymer should be by far slower than that of the reference material. The exact optimal degradation conditions test should be done in the specific needed field conditions in the future.

These results are encouraging as the biodegradability of poly-(disulfanyl-n-decane) suggests that it is bioavailable to the soil microbial population in the tested conditions. It was even shown that a significantly maximal rate of respiration was observed with poly-(disulfanyl-n-decane) than with the negative soil control as well as with the positive reference material (Table 1). As this study focuses on the potential of biodegradability rather than on looking at the complete mineralization of the polymer, the test was

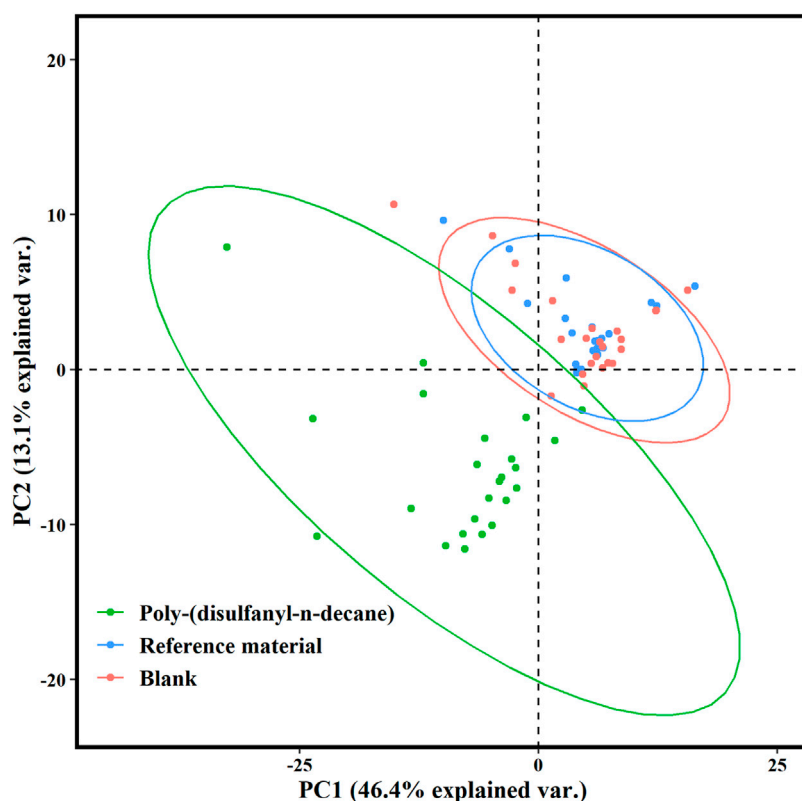
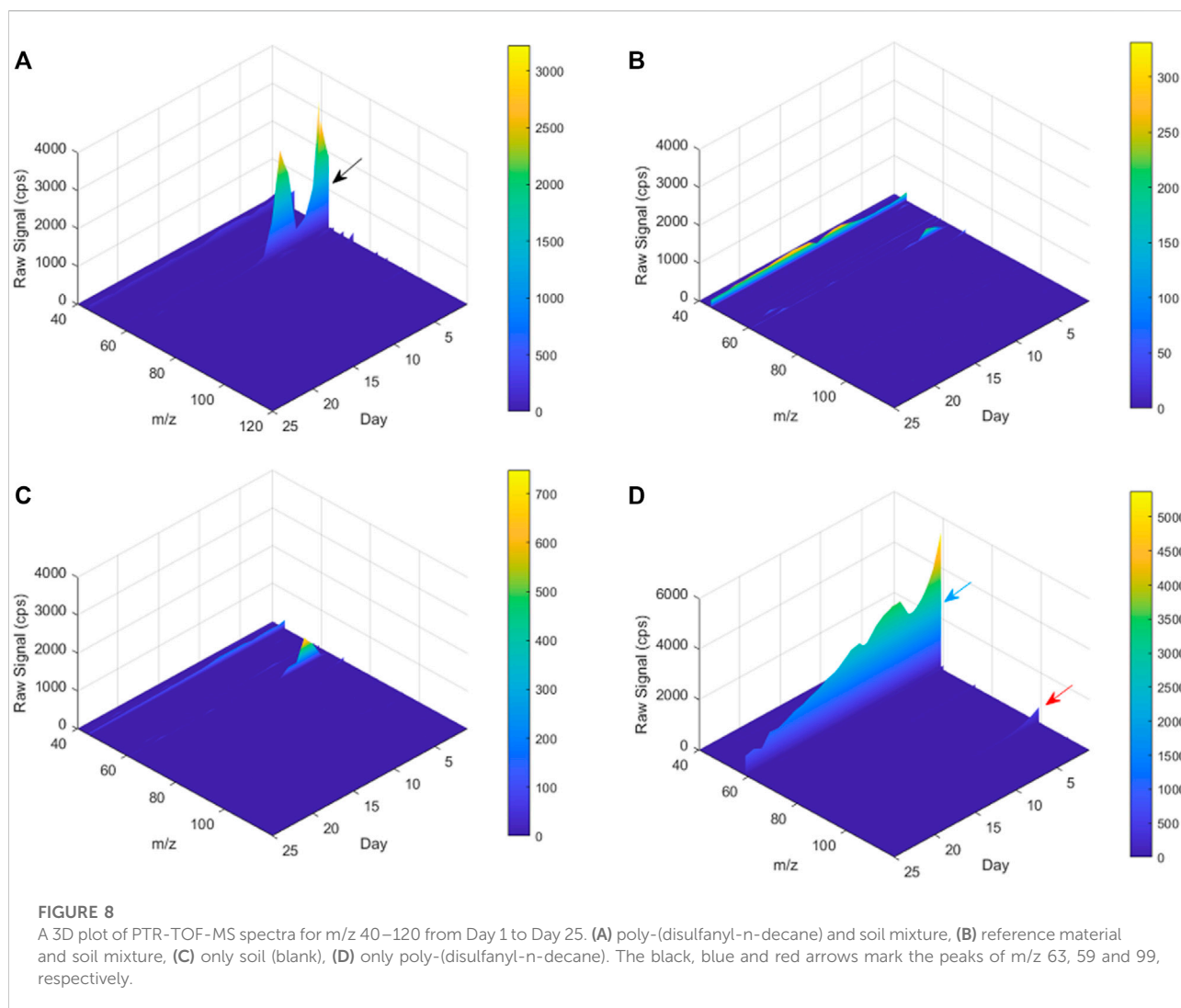


FIGURE 7

Score plot of the principal component analysis (PCA) for PTR-TOF-MS spectral data of the poly-(disulfanyl-n-decane) polymer, the reference material and the blank after 25 days. The first principal component (PC1) and the second principal component (PC2) described 46.4 and 13.1% of the sample variability, respectively.



conducted until 60% degradation of the reference material was reached (Briassoulis and Dejean, 2010). Additionally, all the tested polymers did not show any significant methane production (Figures 4, 5). Methane production from plastic degradation is attracting increasing attention as methane is a potent GHG and it was shown that plastic degradation may have an impact on the overall release of methane into the atmosphere (Royer et al., 2018). The fact that the tested polymer degraded in the soil without any significant production of methane is encouraging in terms of the environmental impact of the biodegradation in the soil of future mulching applications with such polymers.

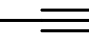
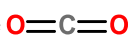
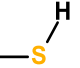
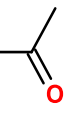
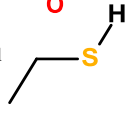
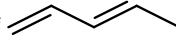
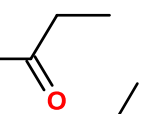
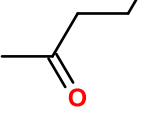
Volatiles profile of polymer biodegradation

Many studies about biodegradation of plastic polymers in soil have overlooked the characterization of non- CO_2 volatile

products that are being produced during the process. Previous studies recognized the risks of formation of carcinogenic and toxic VOC materials by plastic degradation (He et al., 2015; Kuchmenko et al., 2020). The present study is among the first to study the profile of VOCs emitted during the biodegradation of plastic polymers in the soil. $\text{C}_{\text{volatile products}}$ of the poly-(disulfanyl-*n*-decane) shows a distinct profile of volatiles that is markedly different from the reference material and from the control soil, as can be seen from the PCA plot (Figure 7). Additionally, by using the ability of the PTR-TOF-MS to constantly monitor VOCs emission during the entire biodegradation in soil processes, a plot of the time dependent VOCs emission was created (Figure 8). Interesting phenomena were observed in the production of VOCs over time during the biodegradation in soil process.

The tested poly-(disulfanyl-*n*-decane) polymer showed a high concentration of a molecule with an m/z ratio of 63 (Figure 8A) mainly in the initial first 15 days (this molecule is

TABLE 2 Tentative volatile compounds detected during the biodegradation of 1,10-decanedithiol polymer.

<i>m/z</i>	Ion formula	Parent formula	Tentative volatile compounds*
41 ^{a, b}	(C ₃ H ₄)H ⁺	C ₃ H ₄	Propyne 
45 ^{a, b}	(CO ₂)H ⁺	CO ₂	Carbon dioxide 
49 ^a	(CH ₄ S)H ⁺	CH ₄ S	Methanethiol 
59 ^b	(C ₃ H ₆ O)H ⁺	C ₃ H ₆ O	Acetone 
63 ^a	(C ₂ H ₆ S)H ⁺	C ₂ H ₆ S	Ethanethiol 
69 ^a	(C ₅ H ₈)H ⁺	C ₅ H ₈	Penta-1,3-diene 
73 ^{a, b}	(C ₄ H ₈ O)H ⁺	C ₄ H ₈ O	2-Butanone 
87 ^a	(C ₅ H ₁₀ O)H ⁺	C ₅ H ₁₀ O	2-Pentanone 

a: The ion intensity was relatively high in the soil mixture with poly-(disulfanyl-n-decane) polymer.

b: The ion intensity was relatively high in the control sample.

*: One tentative volatile compound was suggested according to the chemical formula.

probably ethanethiol), whereas the reference material showed significantly lower amounts of VOCs production during the tested period and also in the blank soil control (Figures 8B,C). When testing the polymer under basic conditions a high

emission with an *m/z* ratio of 59 was observed which might be an indicator for these conditions as it was not observed under natural conditions. The PTR-MS Viewer 3.2 program was used to assess the chemical composition of the VOCs, based on a library

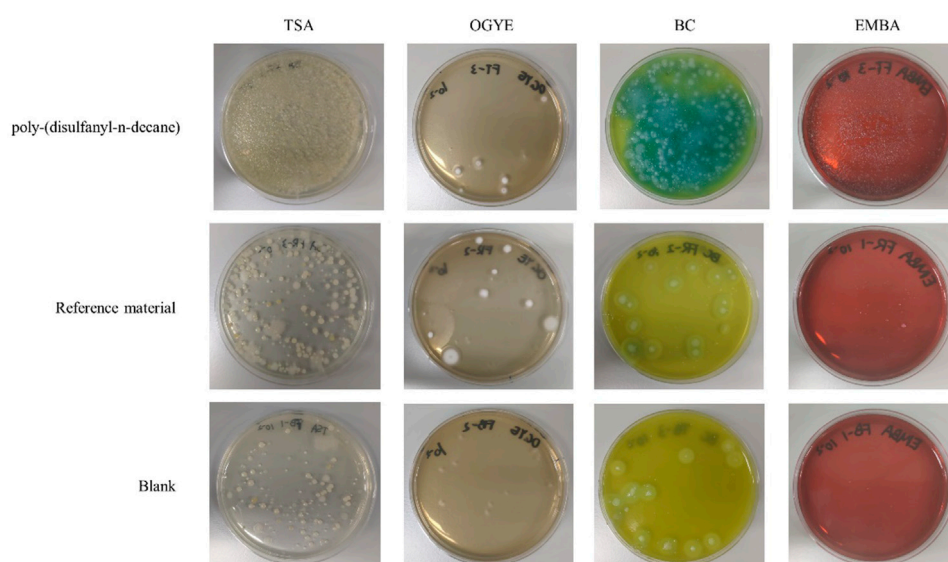


FIGURE 9

Plating of soil mixtures with a dilution of 10² in Tryptic Soy Agar (TSA), Oxytetracycline Glucose Yeast Extract (OGYE), *Bacillus cereus* Agar (BC) and Eosin Methylene Blue Agar (EMBA) in the end of the biodegradability test.

of recognized materials (Table 2). Among these recognized molecules, detailed in Table 2, those which could have a special interest are the ones that showed a significantly higher signal coming from the tested poly-(disulfanyl-n-decane) polymer. The major VOCs originating from poly-(disulfanyl-n-decane) polymer were methanethiol, ethanethiol, penta-1,3-diene and 2-pentanone. The presence of these molecules (especially the thiols) might be used as indicators for the biodegradability of poly-(disulfanyl-n-decane) in soil and, as shown in the 3D plot, was predominant at the beginning of the process (Figure 8A). Additional future studies may be able to correlate between the presence and amounts of these molecules and the rate of degradation, as well as to unveil the mechanism of the biodegradation process, in order to see how well the presence and amounts of these molecules can be used to assess the degradation pace of the specific polymer.

Culturable microbial profile of polymer biodegradation

Even though the soil microbial population responsible for the degradation of the polymer was not the focus of the current study, a general plating test was performed to see if any changes in this population can be observed (Figure 9). The results clearly indicate that the tested polymer had an impact on the soil microbial population expressed by higher numbers observed in the general count of microbes in the TSA plats. While no major differences were observed in the fungal population in the OGYE media, a distinctive difference was observed in both the *Bacillus cereus* agar and the gram-negative Eosin Methylene Blue Agar (EMBA) between the soil with the tested polymer and the positive and negative control soils (Figure 9). It should be noted that these are merely initial results that may suggest that a certain shift in the soil microbial population did occur and that a further study, including next generation DNA sequencing, should be carried out in order to better elucidate these changes.

Conclusions

The current study looked at two new plastic synthetic polymers which are prototype candidates for future biodegradable plastic mulching films. The initial results showed that one of the tested polymers, poly-(disulfanyl-n-decane), may be bio-available and degrade in the soil under standard conditions, especially under slightly basic soil conditions. Poly-(disulfanyl-n-decane) degrades at a rate of losing ~20% %wt. of the total polymer mass in three months, which might be too fast for mulching films that must retain their properties for periods of up to 6 months. It is important to note that the tests were done in laboratory conditions and

the materials were introduced into the soil which means that a longer period in field conditions should also be tested in the future. Poly-(disulfanyl-n-decane) is essentially a polyethylene into which disulfide bridges were inserted in order to allow biological entities, such as microbes, to break the undigestable long alkane chain into segments that are bioavailable and, as the present work shows, also biodegradable. As the results indicate that poly-(disulfanyl-n-decane) has high bioavailability, the next step will be to further dilute the disulfide bridges in the polyethylene skeleton, thereby creating polymers with mechanical and physical properties that are closer to those of ordinary polyethylene, while achieving at the same time also the desired biodegradability rate for mulching films.

A unique simulation system of biodegradation in field conditions allowed monitoring of the VOCs emitted by the degradation of the poly-(disulfanyl-n-decane) polymer. The system showed a specific volatile “fingerprint” containing methanethiol and ethanethiol which suggest degradation of the polymer through a combination of reduction of the disulfide bridges and cleavage of carbon-carbon bonds in positions $\alpha_{\text{carbon}}-\beta_{\text{carbon}}$ and $\beta_{\text{carbon}}-\chi_{\text{carbon}}$ relative to the sulfur atom. Monitoring of these materials might serve as markers for determining the rate of biodegradation of this polymer in the future. The microbial population of the soil appears to be impacted by the incorporation of the poly-(disulfanyl-n-decane) polymer into the soil. Future tests will be needed to further tailor this polymer for agricultural usage and to further understand its impact on the soil biological, chemical and physical properties as well as for looking at the fate of the degradation products in real agricultural systems.

Data availability statement

The raw data supporting the conclusions of this article will be made available by the authors, without undue reservation.

Author contributions

All authors listed have made a substantial, direct, and intellectual contribution to the work and approved it for publication.

Funding

This research was partially supported by Li Ka Shing Foundation (LKSF) Cross-Disciplinary Research Grant (#2020LKSG07D) and “Climbing Plan” project to be funded by the Guangdong Provincial Science and Technology Innovation Strategy Special Fund. The authors acknowledge the support of the Guangdong Provincial Key Laboratory of

Materials and Technologies for Energy Conversion. Supported by the 2021 Guangdong Special Fund for Science and Technology, Multi-effect valorization of tea waste by soil biosolarization and restoration of farmland soil ecosystem/土壤生物日晒对茶渣的多效循环利用及农田土壤生态系统的修复, (#STKJ2021128) and Special funds for higher education development of Guangdong Province.

Acknowledgments

The authors acknowledge the support of the Guangdong Provincial Key Laboratory of Materials and Technologies for Energy Conversion.

References

- Achmon, Y., Dowdy, F. R., Simmons, C. W., Zohar-Perez, C., Rabinovitz, Z., Nussinovitch, A., et al. (2019). Degradation and bioavailability of dried alginate hydrocolloid capsules in simulated soil system. *J. Appl. Polym. Sci.* 136, 48142. doi:10.1002/app.48142
- Achmon, Y., Fernández-Bayo, J. D., Hernandez, K., Mc Curry, D. G., Harrold, D. R., Su, J., et al. (2017). Weed seed inactivation in soil mesocosms via biosolarization with mature compost and tomato processing waste amendments. *Pest Manag. Sci.* 73, 862–873. doi:10.1002/ps.4354
- Achmon, Y., Sade, N., Wilhelmi, M., del, M. R., Fernández-Bayo, J. D., Harrold, D. R., et al. (2018). Effects of short-term biosolarization using mature compost and industrial tomato waste amendments on the generation and persistence of biocidal soil conditions and subsequent tomato growth. *J. Agric. Food Chem.* 66, 5451–5461. doi:10.1021/acs.jafc.8b00424
- Ahmed, T., Shahid, M., Azeem, F., Rasul, I., Shah, A. A., Noman, M., et al. (2018). Biodegradation of plastics: Current scenario and future prospects for environmental safety. *Environ. Sci. Pollut. Res.* 25, 7287–7298. doi:10.1007/s11356-018-1234-9
- Briassoulis, D., Babou, E., Hiskakis, M., and Kyrikou, I. (2015). Analysis of long-term degradation behaviour of polyethylene mulching films with pro-oxidants under real cultivation and soil burial conditions. *Environ. Sci. Pollut. Res.* 22, 2584–2598. doi:10.1007/s11356-014-3464-9
- Briassoulis, D., and Dejean, C. (2010). Critical review of norms and standards for biodegradable agricultural plastics part I. Biodegradation in soil. *J. Polym. Environ.* 18, 384–400. doi:10.1007/s10924-010-0168-1
- Briassoulis, D., Mistrionis, A., Mortier, N., and Tosin, M. (2020). A horizontal test method for biodegradation in soil of bio-based and conventional plastics and lubricants. *J. Clean. Prod.* 242, 118392. doi:10.1016/j.jclepro.2019.118392
- Emadian, S. M., Onay, T. T., and Demirel, B. (2017). Biodegradation of bioplastics in natural environments. *Waste Manag.* 59, 526–536. doi:10.1016/j.wasman.2016.10.006
- EN17033 Plastics (2018). EN17033 Plastics - biodegradable mulch films for use in agriculture and horticulture - requirements and test methods. Available at: <https://www.en-standard.eu/din-en-17033-plastics-biodegradable-mulch-films-for-use-in-agriculture-and-horticulture-requirements-and-test-methods>.
- Fernandes, M., Salvador, A., Alves, M. M., and Vicente, A. A. (2020). Factors affecting polyhydroxyalkanoates biodegradation in soil. *Polym. Degrad. Stab.* 182, 109408. doi:10.1016/j.polymdegradstab.2020.109408
- He, Z., Li, G., Chen, J., Huang, Y., An, T., Zhang, C., et al. (2015). Pollution characteristics and health risk assessment of volatile organic compounds emitted from different plastic solid waste recycling workshops. *Environ. Int.* 77, 85–94. doi:10.1016/j.envint.2015.01.004
- Huang, Y., Liu, Q., Jia, W., Yan, C., and Wang, J. (2020). Agricultural plastic mulching as a source of microplastics in the terrestrial environment. *Environ. Pollut.* 260, 114096. doi:10.1016/j.envpol.2020.114096
- ISO (2019). Plastics — determination of the ultimate aerobic biodegradability of plastic materials in soil by measuring the oxygen demand in a respirometer or the amount of carbon dioxide evolved. Available at: <https://www.iso.org/standard/74993.html>.26
- Kasirajan, S., and Ngouajio, M. (2012). Polyethylene and biodegradable mulches for agricultural applications: A review. *Agron. Sustain. Dev.* 32, 501–529. doi:10.1007/s13593-011-0068-3
- Kuchmenko, T., Umarmhanov, R., and Lvova, L. (2020). E-nose for the monitoring of plastics catalytic degradation through the released Volatile Organic Compounds (VOCs) detection. *Sensors Actuators B Chem.* 322, 128585. doi:10.1016/j.snb.2020.128585
- Kyrikou, I., and Briassoulis, D. (2007). Biodegradation of agricultural plastic films: A critical review. *J. Polym. Environ.* 15, 125–150. doi:10.1007/s10924-007-0053-8
- Liu, Y., Huang, Q., Hu, W., Qin, J., Zheng, Y., Wang, J., et al. (2021). Effects of plastic mulch film residues on soil-microbe-plant systems under different soil pH conditions. *Chemosphere* 267, 128901.
- Royer, S.-J., Ferrón, S., Wilson, S. T., and Karl, D. M. (2018). Production of methane and ethylene from plastic in the environment. *PLoS One* 13, e0200574. Available at: doi:10.1371/journal.pone.0200574
- Sander, M. (2019). Biodegradation of polymeric mulch films in agricultural soils: Concepts, knowledge gaps, and future research directions. *Environ. Sci. Technol.* 53, 2304–2315. doi:10.1021/acs.est.8b05208
- Sevilia, S., Parvari, G., Bernstein, J., Fridman, N., Grinstein, D., Gottlieb, L., et al. (2022). Imidazolium based energetic materials. *Chem. Select* 7, e202200322. doi:10.1002/slct.202200322
- Tada, Y., Yamamoto, T., Tezuka, Y., Kawamoto, T., and Mori, T. (2012). Effective synthesis and crystal structure of a 24-membered cyclic decanedisulfide dimer. *Chem. Letters* 41 (12), 1678–1680. doi:10.1246/cl.2012.1678
- Thomas, Z. M., Arno, S., Frederick, N. T., Rebekka, B., Dagmar, W., Michael, W., et al. (2021). Biodegradation of synthetic polymers in soils: Tracking carbon into CO₂ and microbial biomass. *Sci. Adv.* 4, eaas9024. doi:10.1126/sciadv.aas9024
- Zertal, Y., Yong, M., Levi, A., Sevilia, S., Tsoglin, A., Parvari, G., et al. (2022). Alkyl vinyl imidazolium ionic liquids as fuel-binders for photo-curable energetic propellants. *Adv. Funct. Mat.*. In press. doi:10.1021/acsapm.2c00499
- Zhang, H., Miles, C., Ghimire, S., Benedict, C., Zasada, I., DeVetter, L., et al. (2019). Polyethylene and biodegradable plastic mulches improve growth, yield, and weed management in floriculture red raspberry. *Sci. Hortic.* 250, 371–379. doi:10.1016/j.scienta.2019.02.067
- Zhou, B., Wang, J., Zhang, H., Shi, H., Fei, Y., Huang, S., et al. (2020). Microplastics in agricultural soils on the coastal plain of Hangzhou Bay, east China: Multiple sources other than plastic mulching film. *J. Hazard. Mat.* 388, 121814. doi:10.1016/j.jhazmat.2019.121814
- Zumstein, M. T., Narayan, R., Kohler, H.-P. E., McNeill, K., and Sander, M. (2019). *Dos and do nots when assessing the biodegradation of plastics*.
- Zurier, H. S., and Goddard, J. M. (2021). Biodegradation of microplastics in food and agriculture. *Curr. Opin. Food Sci.* 37, 37–44. doi:10.1016/j.cofs.2020.09.001

Conflict of interest

The authors declare that the research was conducted in the absence of any commercial or financial relationships that could be construed as a potential conflict of interest.

Publisher's note

All claims expressed in this article are solely those of the authors and do not necessarily represent those of their affiliated organizations, or those of the publisher, the editors and the reviewers. Any product that may be evaluated in this article, or claim that may be made by its manufacturer, is not guaranteed or endorsed by the publisher.



Biodegradation of Low-Density Polyethylene—LDPE by the Lepidopteran *Galleria Mellonella* Reusing Beekeeping Waste

Orlando Poma^{1,2*}, Betty Ricce^{1*}, Jeyson Beraún¹, Jackson Edgardo Perez Carpio¹, Hugo Fernandez¹ and Juan Soria³

¹Escuela Profesional de Ingeniería Ambiental, Facultad de Ingeniería y Arquitectura, Universidad Peruana Unión, Lima, Perú,

²Escuela Profesional de Ingeniería Ambiental, Facultad de Ingeniería y Arquitectura, Universidad Peruana Unión, Juliaca, Perú,

³Escuela UPG Ingeniería y Arquitectura, Escuela de Posgrado, Universidad Peruana Unión, Lima, Perú

OPEN ACCESS

Edited by:

Zhanyong Wang,
Shenyang Agricultural University,
China

Reviewed by:

Jingjing Zhao,
Liaoning Shihua University, China
Vinay Mohan Pathak,
University of Delhi, India

*Correspondence:

Betty Ricce
bettyricce@upeu.edu.pe
Orlando Poma
opoma@upeu.edu.pe

Specialty section:

This article was submitted to
Bioprocess Engineering,
a section of the journal
Frontiers in Bioengineering and
Biotechnology

Received: 07 April 2022

Accepted: 24 May 2022

Published: 09 September 2022

Citation:

Poma O, Ricce B, Beraún J,
Perez Carpio JE, Fernandez H and
Soria J (2022) Biodegradation of Low-
Density Polyethylene—LDPE by the
Lepidopteran *Galleria Mellonella*
Reusing Beekeeping Waste.
Front. Bioeng. Biotechnol. 10:915331.
doi: 10.3389/fbioe.2022.915331

Plastic pollution is one of the most serious environmental problems of this century because most plastics are single-use, and once their useful life is over, they become pollutants, since their decomposition takes approximately 100–400 years. The objective of this research is to evaluate the efficacy of low-density polyethylene (LDPE) biodegradation by *G. mellonella* in the district of Pangoa, Junín, Peru. For the development of the study, the *G. mellonella* was conditioned in three groups of beekeeping residues (beeswax, balanced diet, and wheat bran); after the conditioning stage, the biodegradation treatment was developed, which consisted of placing the *G. mellonella* in terrariums with the LDPE, the treatments were carried out at three different times (24, 36, and 48 h). To evaluate the efficacy of biodegradation, two analyses were taken into account: the Raman analysis of the low-density polyethylene samples and the weight reduction of the treated LDPE. The results of the Raman analysis indicated that the best treatment was the one applied with *G. mellonella* conditioned with beeswax, obtaining a wavelength intensity of 0.45 μ a., while the weight reduction of the LDPE indicated that the best results were given at 36 h and conditioned with beeswax with a reduction of 236.3 mg. In conclusion, the use of *G. mellonella* for the biodegradation of low-density polyethylene is effective when it is conditioned with beeswax and the treatment is carried out at 36 h.

Keywords: pollution, plastic, *Galleria mellonella*, LDPE, biodegradation

1 INTRODUCTION

Could anyone live without plastic in the 21st century? Well, no, since a large part of the objects we see and use is made of that material (Cáceres, 2017). It has become so ubiquitous that it is hard to believe that it has only been produced on an industrial scale since 1950 (Geyer et al., 2017).

According to the United Nations Environment Program, plastic pollution is one of the serious environmental problems of this century (Abaza, 2012). Estimates show that to date, 8,300 million metric tons of plastic (MT) have been produced, but about half was created in 2004; and of the total plastics produced, 30% is still in use; the rest (6,000 million MT) has become waste (9% recycled, 12% incinerated, and 79% in a landfill or thrown into the environment) (Geyer et al., 2017). With regard

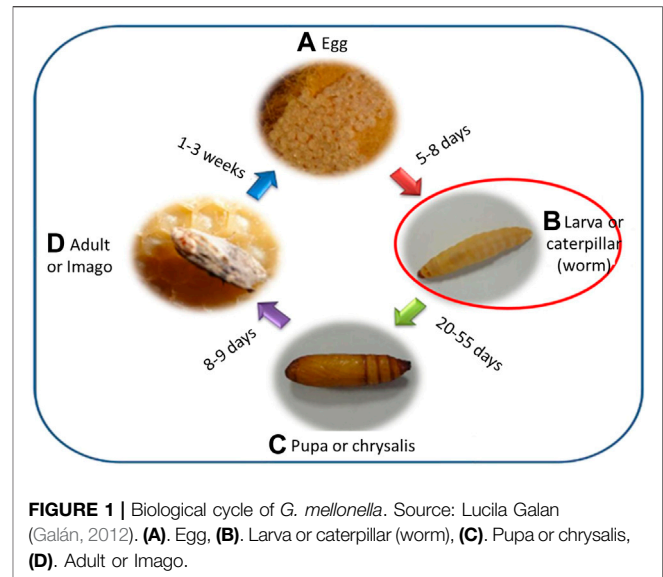
to plastic bags, 10 million bags are used in the world every minute and 5 billion a year, of which about 5–13 million tons are dumped into the ocean (Ellen MacArthur Foundation, 2016). With the appearance of the pandemic caused by COVID-19, its use has increased greatly (Flores, 2020).

In South America, plastic pollution has caused the formation of “plastic islands” in the North Pacific Ocean, and 80% of this waste comes from land sources (Elías, 2015), which is why it is vitally important to find adequate treatments and carry out good management of this type of waste (Urdaneta, 2014).

In the same way (Ministerio del Ambiente, 2014), 886 tons of plastic per day is generated in Lima and Callao (Ministerio del Ambiente, 2017). Currently, each citizen uses 30 kg of plastic per year and the total number of plastic bags is around 3,000 million, almost 6 thousand bags per minute (Ministerio del Ambiente, 2017); most of it is single-use and once its useful life is over, it becomes a pollutant, since its decomposition takes approximately 100–400 years (Bombelli et al., 2017). Since 2016, there have been environmental laws and comprehensive management plans to treat this type of waste, in which the ministries of the environment, health, and education; municipalities; and regional governments are involved (Ministerio del Ambiente, 2016a). Incidentally, in 2018, the law that regulates the use of plastic (Ministerio del Ambiente M, 2019) was enacted; however, due to the lack of control and inspection, the non-existence of control measures, and the absence of environmental education among citizens, not much has been achieved so far (Flores, 2020). On the other hand, the Ministry of Environment has lines of research that encourage this type of study in favor of the environment. This study is within this line of research: Component: Solid and Hazardous Waste; Thematic area: Treatment of solid and hazardous waste; Research line: Solid, organic, hazardous, and chemical waste treatment technologies (Ministerio del Ambiente, 2016b).

Low-density polyethylene (LDPE) is a plastic composed of olefin monomers, and it is polymerized at high pressure, highlighting its flexibility and chemical and dielectric resistance: undoubted characteristics that make it useful for the manufacture of bags and industrial packaging, among others items (Martin, 2012). Their great durability and slow biodegradation mean that these synthetic polymers can tolerate the ocean environment for years, decades, and even longer periods (Gutierrez, 2018). This causes marine animals to get trapped by the garbage; birds and other marine creatures consume plastic when they confuse it with their food; and this waste can act as a raft and move some species out of their area (Gutierrez, 2018). The plastic can be reduced in an ecological way with the help of soil bacteria and water availability, but it depends on the type of material that is made, for example, starch-based polymer is degraded by microbes and hydrolytic enzymes, and polymers to petroleum-based polyolefins, degraded through photodegradation (Pathak and Navneet, 2017).

The development of this study proposes an alternative treatment to plastic, as well as the reduction of the volume of plastic waste that arrives at the CEPAP (Pangoa District Sanitary Landfill) in order to increase the useful life of the transitory cells. The district of Pangoa, Satipo, Junín, has a population of 24,939



inhabitants in the urban area alone; the per capita generation of waste is 0.45 kg/person/day; and 4,113.6 tons of waste are generated per year, with plastic being the waste material with the second highest generation: 168.2 tons per year (Municipalidad Distrital de Pangoa, 2019).

That is why the objective of this research is to evaluate the efficiency of polyethylene biodegradation by treating plastic with *G. mellonella* larvae conditioned with three beekeeping residues (beeswax, balanced diet, and wheat bran) and subjected to three different times (24, 36, and 48 h).

2 MATERIALS AND METHODS

The study was carried out in the district of Pangoa, Junín, Peru (latitude: -11.4281 , longitude: -74.4881 , latitude: $11^{\circ}25'41''$ south, longitude: $74^{\circ}29'17''$ west), under laboratory conditions.

2.1 Materials and Equipment

The materials to be used for the packaging of the *G. mellonella* are the following:

- Balanced diet [to be prepared with wheat bran (150 gr), ground rice (70 gr), puppy biscuits (25 gr), honey (250 gr), and pollen (8 gr)].
- - Beeswax 3 kg
- - Wheat bran 3 kg
- - LDPE bag
- 2 packs of low-density polyethylene bags—PEBD (brand: Plásticos Alfa, material: low-density polyethylene, measurements: 86 mm × 19 mm, color: transparent, quantity: 50 units); each bag weighs 425.25 mg, and they were obtained from the local market.
- - Pieces of cardboard (to place the eggs).
- - Clamp (to remove the LDPE sample without altering or damaging it).

- - Latex gloves (to handle the sample without altering it).
- - Cooler
- - Digital multi-function electronic Scale
- - Thermo-hygrometer BOECO Germany
- - Photographic camera
- - Terrarium (glass box with measurements: 15 cm wide × 20 cm long × 10 cm high, covered with metal mesh and tulle fabric).
- One thousand larvae of *G. mellonella* (30 larvae for each treatment).

2.2 Conditioning of *G. Mellonella*

The work area was conditioned, and the wooden boxes for breeding were prepared. The *G. mellonella* was obtained from the company “Apícola Ayni S.A.C.” in the pupal and adult stage, and breeding was carried out in three groups with a different food for each group: A, balanced diet; B, beeswax; and C, wheat bran (Anwar et al., 2014). When *G. mellonella* reaches the larval stage, the stage in which it biodegrades LDPE (see **Figure 1**), the study begins.

2.3 Treatment

The low-density polyethylene-LDPE was previously analyzed in terms of weight and Raman spectroscopic effect to submit them to the treatments and control group. Surgical gloves and sterilized tweezers were used for handling and taking samples to avoid possible contamination of the sample. Then, it was subjected to treatment with *G. mellonella* obtained from the three groups mentioned (A, beeswax; B, balanced diet; and C, wheat bran), developing at three different times (24, 36, and 48 h) with three repetitions for each treatment (Montgomery and Wiley, 2004), and using 30 larvae for each treatment; the treatments were carried out by applying the larvae and adding 5 g of residue in each polyethylene treatment. Finally, the final weighing of the low-density polyethylene PEBD and the Raman spectroscopic effects of each of the treatments were carried out. For the latter, the services of the Mycology and Biotechnology Laboratory of the La Molina National Agrarian University were provided. It should be noted that among all the treatments, only 3 *G. mellonella* larvae died in the treatments: C1, 24 h; C3, 48 h; and A1, 48 h because they were at the beginning of the growth stage, the larval stage, and were just adapting to survival conditions. Polyethylene ingestion did not cause significant growth of *G. mellonella*.

2.4 Data Processing

The data obtained were processed for the publication of the results. The statistical design chosen for this study was the 32 factorial design since in this study we worked with 2 factors: A (beekeeping residue) and B (biodegradation time) and each factor had three levels: factor A (beeswax, balanced diet, and wheat bran) and factor B (24, 36, and 48 h); the product of the interaction of the factors with the levels, nine combinations of treatments, were obtained (Montgomery and Wiley, 2004). A normality test was performed by applying the Shapiro–Wilk test, verifying that a normal distribution was fulfilled, and the ANOVA parametric test was applied for the difference in means; these tests were carried out at a confidence level of 95%. The comparison of the degraded sample was carried out

by measuring the weight and the Raman effect of the low-density polyethylene before and after the treatment.

3 RESULTS

3.1 Weight Results of Low-Density Polyethylene

The analysis of the LDPE remnant was carried out due to the fact that readings of the stool samples of the larvae were not obtained; this remnant was evaluated in the vicinity of the holes made in the consumption of the LDPE of the larvae, and said evaluation was carried out in these points since Bombelli et al. (2017) mentioned that one of the beings responsible for the biodegradation of LDPE was the intestinal flora of *G. mellonella*.

Table 1 presents the results of the analysis of variance (ANOVA of 2 factors) applied to the data obtained from the weight reduction of the LDPE applied the treatment. The results of the statistical test indicated that at a confidence level of 95%, the beekeeping residue applied in the breeding of *G. mellonella* has a very marked effect on the weight reduction of the LDPE and that the treatment time also has a very marked effect on the weight reduction of the LDPE; in addition, it indicated that the interaction between the beekeeping residue applied in the breeding of the *G. mellonella* and the treatment time has great significance in the weight reduction of the LDPE.

In **Figure 2**, the interaction between the treatment time and the effect of the beekeeping residue applied in the breeding of *G. mellonella* can be seen. This graph indicates that for the larva conditioned with beeswax, the best time of treatment is 36 h, obtaining a greater average weight reduction of LDPE of 55.6% (263.3 mg); for the larva conditioned with the balanced diet and for the larva conditioned with wheat bran, the best treatment time is 48 h, obtaining an average LDPE weight reduction of 27.8% (118.1 mg) and 15.6% (66.2 mg), respectively.

In **Figure 3**, we can observe the weight reduction of the LDPE when subjected to the treatment; of the nine applied treatments, it is observed that the one with the greatest weight reduction is the treatment applied with the larva conditioned with beeswax at a treatment time of 36 h, with an average weight reduction result of LDPE of 55.6% (263.3 mg). In addition to this, it is observed that the second best result is obtained with the larva conditioned with beeswax at a treatment time of 48 h with an average LDPE weight reduction result of 40.0% (170.1 mg). These results indicate that the LDPE subjected to treatment with the larva conditioned with beeswax obtains better results compared to those conditioned with a balanced diet and wheat bran; in addition, the treatment of the larva conditioned with beeswax obtains better results with a treatment time of 36 h.

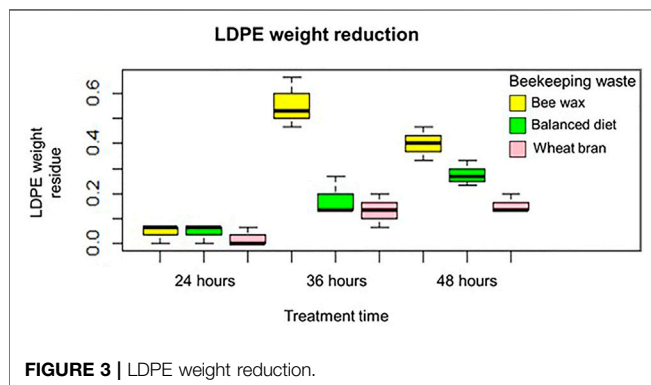
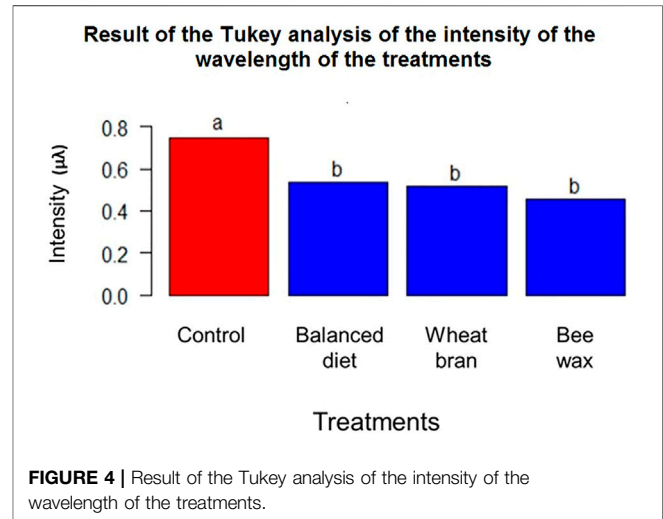
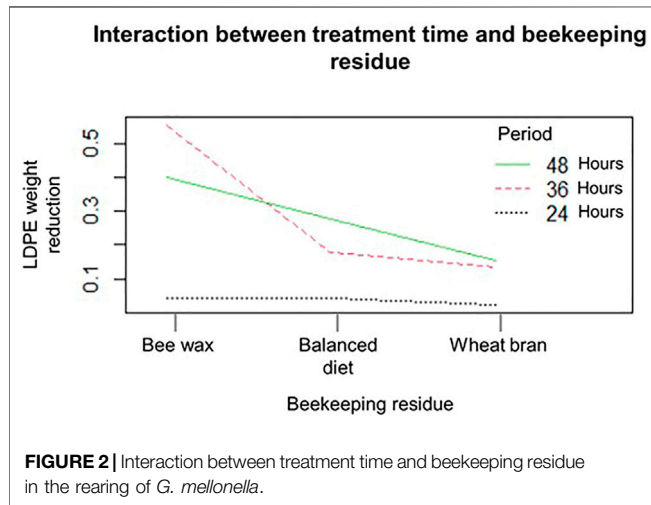
3.2 Low-Density Polyethylene Raman Analysis Result

3.2.1 Quantitative Analysis

Table 2 presents the results of the analysis of variance (ANOVA) applied to the data obtained from the wavelength intensity of the spectrum of the LDPE Raman analysis; the results of the statistical

TABLE 1 | Result of analysis of variance (ANOVA for 2 factors).

	Df	Sum sq	Mean sf	F value	p value
Beekeeping waste	2	0.2534	0.12671	33.84	7.98×10^{-7}
Treatment time	2	0.3645	0.18226	48.67	5.49×10^{-8}
Interaction between applied beekeeping residue and treatment time	4	0.1602	0.04004	10.69	0.000129
Residuals	18	0.0674	0.00374		

**TABLE 2** | Results of the analysis of variance (ANOVA) of the wavelength intensity of the Raman spectrum.

	Df	Sum sq	Mean sf	F value	p value
Beekeeping waste	3	0.4276	0.14253	5.068	0.00587
Treatment time	2	0.1707	0.08535	3.035	0.06305
Residuals	30	0.8438	0.02813		

test indicated that at a confidence level of 95%, the beekeeping residue applied in the breeding of *G. mellonella* has a very marked effect on the reduction of the intensity of the wavelength of the LDPE Raman spectrum and that the treatment time has no marked effect on the reduction of the wavelength intensity of the LDPE Raman spectrum.

In **Figure 4**, the results of the Tukey analysis of the wavelength intensity of the LDPE Raman spectrum highlighted with the beekeeping residues and with the treatment control are presented; the results of the statistical test indicated that at a confidence level of 95%, the wavelength intensity of the control is the only result that differs from the averages of beekeeping waste, thus indicating that there is a significance in the reduction of the wavelength intensity applying this treatment.

3.2.2 Qualitative Analysis

In **Figure 5**, the Raman spectrum of the control low-density polyethylene (LDPE) is shown, highlighting the most significant peaks, and **Table 3** details the functional group obtained in the peaks. The Raman bands of the spectrum for the crystal chain ($1,063$, $1,131$, $1,295$, and $1,418$ cm^{-1}) were taken, and these bands were used as a standard to compare the variations of the LDPE crystallinity (Kida et al., 2016).

The Raman spectra of the treatments carried out were compared with the control sample of the LDPE, and it was found that 74% of the treatments obtained a reduction in the intensity observed in the wavelength $1,063$ cm^{-1} ; 56% of the treatments, in the wavelength $1,131$ cm^{-1} ; 96% of the treatments, at the wavelength $1,295$ cm^{-1} ; and 100% of the treatments, at the wave number $1,418$ cm^{-1} . In this sense, the intensity reduction in these Raman bands indicated a decrease in the crystallinity of LDPE as a result of the treatment applied to the samples, in addition to a decrease in the functional groups C-H and CH₂. The breaking of the C-C bonds implies a level of degradation of the low-density polyethylene molecules—LDPE.

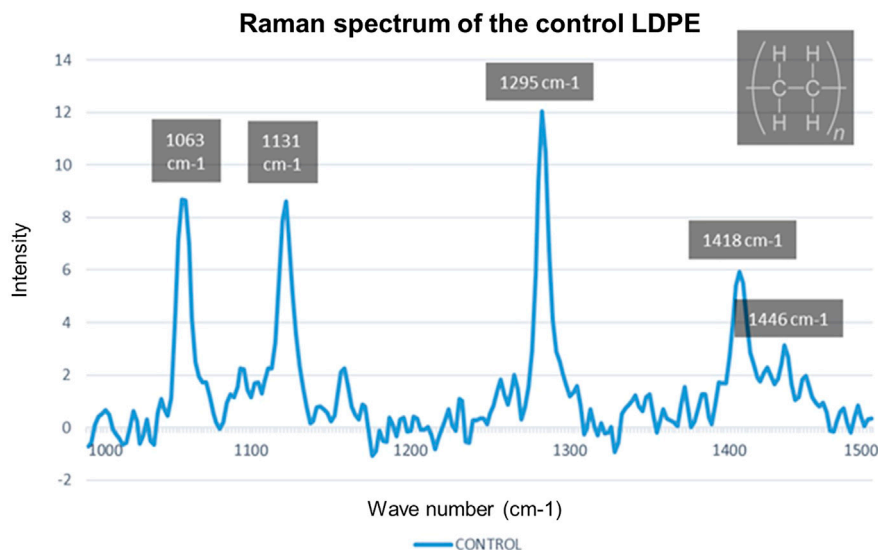


FIGURE 5 | Raman spectrum of the control LDPE.

TABLE 3 | Wave number and functional group [the values were assigned by comparing with the spectra reported by Kida et al. (2016)].

Wave number (cm ⁻¹)	Functional group
1,063	C-C
1,131	C-C
1,295	CH ₂
1,418	CH ₂
1,446	CH ₂

Therefore, there is a decrease in polyethylene as a contaminating factor due to its interaction with *G. mellonella*.

Figure 6 shows the Raman spectrum of the control LDPE and the A-36 h treatment since it is the treatment that obtained the best results.

3.3 Result of the Physical Change of the Low-Density Polyethylene

Figure 7 shows the differences between the control sample (Figure 7A) and the A1-36 h treatment of low-density polyethylene—LDPE (Figure 7B), showing a slight change in brightness and the appearance of some cracks; this was analyzed in 100% of the sample and with a level of 90 μm , a $\times 20$ Zeiss EC Epiplan objective (numerical aperture 0.4) with a white light LED for Köhler illumination was used; all micrographs were exported in TIF format with dimensions of $1,024 \times 653$ pixels; the activity that the *G. mellonella* larvae had on the LDPE was also observed with the naked eye (Figure 7C), an optical view made at the edges of the holes left by the *G. mellonella* larvae in the low-density polyethylene sample. LDPE (Figure 7D) was analyzed in the region “a” with a level of 23.36 μm .

4 DISCUSSION

The analysis of the LDPE remnant was carried out due to the fact that readings of the stool samples of the larvae were not obtained, this remnant was evaluated in the vicinity of the holes made in the consumption of the LDPE of the larvae, and the said evaluation was carried out in these points since Bombelli et al. (2017) mentioned that one of those items responsible for the biodegradation of LDPE is the intestinal flora of *G. mellonella*. In the present investigation, it was found that 30 larvae of the lepidoptera *G. mellonella* conditioned with “beeswax” biodegraded 263.3 mg (55.6%) of low-density polyethylene—LDPE—in 36 h at an average temperature of 25°C and a relative humidity average of 83%; it belongs to Treatment A1-36.

One of the ways to assess biodegradation efficiency is the amount of LDPE weight lost; in other words, how many milligrams of LDPE did *G. mellonella* consume? Bombelli et al. (2017) mention that 100 *G. mellonella* larvae are capable of biodegrading 92 mg of polyethylene in 12 h. Although we extended the time to 36 h, but applied only 30 larvae, we obtained a greater amount of biodegraded LDPE; in other words, 263.3 mg of biodegraded LDPE, which is higher, even if we double Bombelli’s 92 mg.

Alkassab et al. (2020), found that 10 larvae of *G. mellonella* degrade 0.0210 mg in 12 h at a temperature of 25°C. In our study, we obtained a degradation of 263.3 mg, and it is very high; this is because we increase the time and the number of larvae. However, we kept the same temperature of 25°C.

Márquez (Mandal and Vishwakarma 2016) showed that 480 *G. mellonella* larvae were conditioned at a temperature of 27°C and 70% relative humidity biodegraded 0.173 mg of polyethylene in 7 days. In this study, we see that the results are below the other results obtained in our study despite the fact

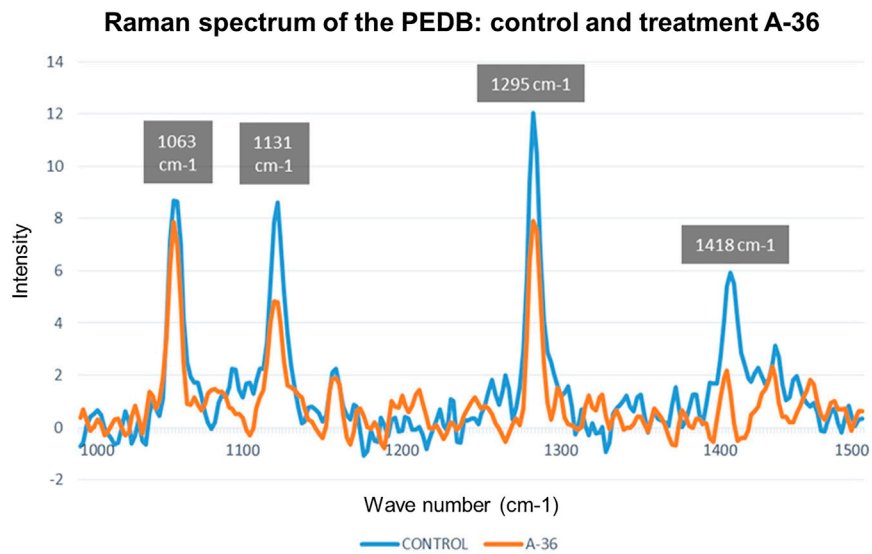


FIGURE 6 | Raman spectrum to contrast the difference between the LDPE control and the treatment A-36 h.

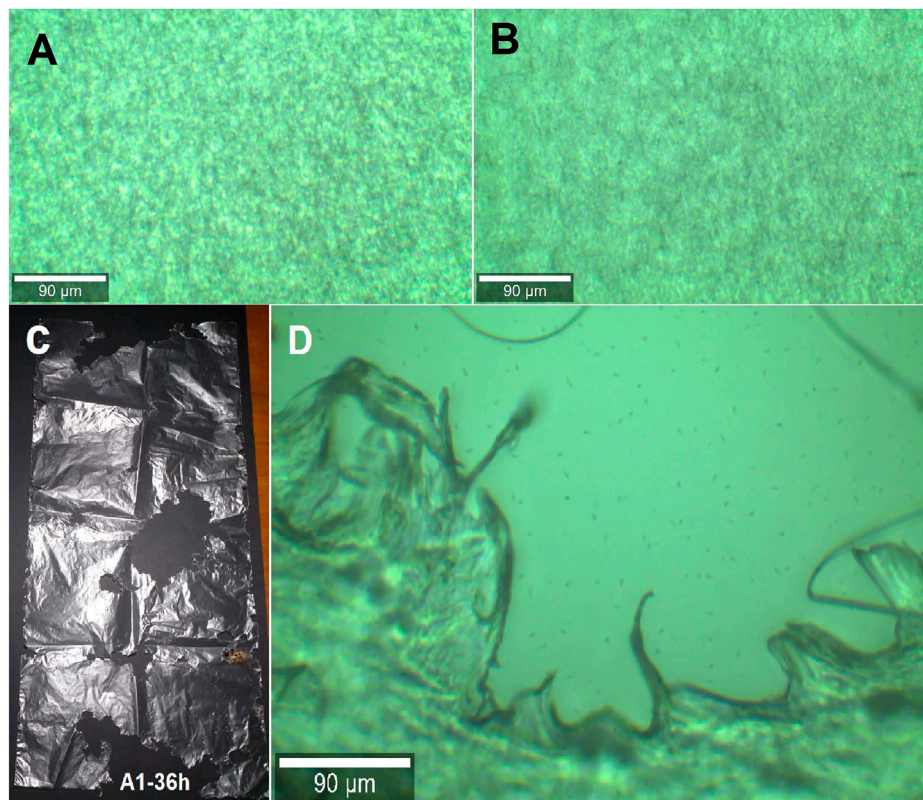


FIGURE 7 | Result of the physical change of the LDPE. In (A), the optical micrograph of the control sample is observed and in (B), the A1-36 h treatment; (C) shows the evidence of LDPE consumption of the A1-36 h treatment with a normal scale view, and (D) presents a light micrograph view of sample A1-36 h-a2.

that the treatment time was longer. Mandal and Vishwakarma (2016) mention that there is no relationship between relative humidity and larval growth. Yang (Yang et al., 2014)- Rivas

(Rivas, 2020) reported that the American *Periplaneta* cockroach, conditioned at a temperature of 35°C and 60% relative humidity, biodegrades 0.6 mg of plastic bag (LDPE) in 7 days, obtaining an

efficiency of 7.6%. This is very similar to *G. mellonella*, as both are active at night and like the same conditions of temperature and relative humidity.

Nevertheless, in our research, it was found that the larvae of *G. mellonella* biodegraded more low-density polyethylene at 36 h than at 48 h, due to the fact that at 36 h, a great concentration of the larvae was observed in the central part of the box (which has a reduced size of 10 cm × 20 cm) and they fed, very different from the activity at 48 h where the dispersion of the larvae was observed and they did not consume the LDPE in the same way, that is why Kwadha (Kwadha et al., 2017) mentions that the larvae feed more when they are together. On the other hand, the larvae that were at 36 h were more active and those that were at 48 h were not, since they were already beginning to pupate (Rodríguez, 2015).

Compared to these studies, it is shown that our research obtained better results of LDPE biodegradation in terms of weight loss, and taking into account the time, it was also relatively short. On the other hand, the temperature played an important role in the biodegradation of LDPE. Alkassab et al. (2020) worked with *G. mellonella* larvae at 25°C and 35°C, showing that the optimal temperature to carry out biodegradation is 25°C. Márquez (Mandal and Vishwakarma 2016) also worked with the same type of larvae at a temperature of 27°C. Rodríguez (Rodríguez, 2015) mentions that the larvae of *G. mellonella* have a normal development when they are at a temperature of 25°C and their lifetime ranges between 28 days. But if the temperature is too low, their activity becomes slow and their lifetime is prolonged; on the contrary, if the temperature is too high, their activity is accelerated and their lifetime is greatly shortened. For this reason, in our research, we work at a temperature of 25°C.

Regarding the feeding and conditioning of *G. mellonella*, we apply beeswax, a balanced diet, and wheat bran, since Salas (Salas, 2015) considers that the best diet to raise *G. mellonella* contains wheat bran, sugar, and honey. Rodríguez (Rodríguez, 2015) also includes in his diet: wheat bran, rice, croquettes of can, sugar honey, and honey; that is why we opted for these beekeeping residues as food to raise and condition *G. mellonella*. Márquez (Mandal and Vishwakarma 2016) found that treatments that include beeswax have a higher consumption of plastics; this is similar to our work, since the treatment with beeswax obtained better results because under natural conditions, these larvae feed on beeswax and your body is already used to it, you do not need to undergo an adaptation process that generates delayed development or slow activity (Kwadha et al., 2017). It should be noted that the contaminants do not show detectable impacts on beeswax (Alkassab et al., 2020). It should be noted that the contaminants do not show detectable impacts on beeswax (Alkassab et al., 2020), so the use of this residue to condition *G. mellonella* does not affect its growth. Moreover, it was observed that the growth of *G. mellonella* was not affected by the intake of low-density polyethylene-LDPE due to the fact that the composition and chemical structure of LDPE are very similar to those of beeswax (Bombelli et al., 2017).

Finally, Coreño (Coreño and Méndez, 2010) indicates that the crystallinity of polymers is a fundamental part of the solubility and permeability of said elements, that is to say, the reduction of

the crystallinity contributes to increasing the solubility and permeability; it also indicates that a reduction in crystallinity reduces the density of the polymer and therefore its resistance.

5 CONCLUSION

With the development of this research work, the following results are obtained:

- The comparison of the Raman spectra indicates that there is a reduction in the crystallinity of LDPE, finding that *G. mellonella* conditioned with beeswax obtains better results with an average wavelength intensity of 0.45 μ a.
- Beeswax is the residue of beekeeping conditioned with *G. mellonella*, and it obtains better results compared to the other applied treatments, which obtains an average weight reduction of 141.8 mg (33.3% reduction).
- The treatment developed at 36 h is the one that obtains the best results with an average weight reduction of low-density polyethylene of 122.9 mg (28.9% reduction).

In general, it is concluded that the most effective treatment is the one given with *G. mellonella* conditioned with beeswax and with a treatment time of 36 h, since the best results were obtained with an average weight reduction of low-density polyethylene of 236.3 mg (55.6% reduction) in addition to obtaining the best wavelength intensity of 0.45 μ a.

DATA AVAILABILITY STATEMENT

The original contributions presented in the study are included in the article/Supplementary Materials; further inquiries can be directed to the corresponding authors.

AUTHOR CONTRIBUTIONS

The contribution statement for each author is as follows: BR and JB: study design, data collection, and analysis; BR and JB: writing. JP, HF, and OP: statistical analysis and interpretation; HF and JS: Advice and review; OP, JP, HF, and JS: formal analysis. All co-authors contributed to the revision of the manuscript, and read and approved the submitted version.

FUNDING

The research was carried out with the researchers' own funds. Funding for open access charge: Universidad Peruana Unión (UPeU).

ACKNOWLEDGMENTS

We thank Universidad Peruana Unión—Faculty of Engineering and Architecture, especially our collaborator, Gina Tito.

Similarly, we thank the La Molina National Agrarian University—Mycology and Biotechnology Laboratory: Ilanít Samolski Klein and José Castañeda. Also, we thank the Environment Management—District Municipality of Pangoa; and the company “Apícola Ayni S.A.C.”

REFERENCES

- Abaza, H. (2012). Green Economy in Action: Articles and Excerpts that Illustrate Green Economy and Sustainable Development Efforts. [Internet] Available at: <http://www.facebook.com/hussein.m.abaza>.
- Alkassab, A. T., Thorbahn, D., Frommberger, M., Bischoff, G., and Pistorius, J. (2020). Effect of Contamination and Adulteration of Wax Foundations on the Brood Development of Honeybees. *Apidologie* 51 (4), 642–651. doi:10.1007/s13592-020-00749-2
- Anwar, A., Ansari, M., Al-Ghamdi, A., Mohamed, M., and Kaur, M. (2014). Effect of Larval Nutrition on the Development and Mortality of *Galleria mellonella* (Lepidoptera: Pyralidae). *Rev. Colomb. Entomol.* 40 (1), 49–54.
- Bombelli, P., Howe, C. J., and Bertocchini, F. (2017). Polyethylene Bio-Degradation by Caterpillars of the Wax Moth *Galleria mellonella*. *Curr. Biol.* 27 (8), R292–R293. doi:10.1016/j.cub.2017.02.060
- Cáceres, P. (2017). ¿Cuánto plástico hemos generado desde que se inventó y dónde ha ido a parar? *La Vanguard*. 2.
- Coreño, J., and Méndez, M. (2010). Relationship between structure and properties of polymers. *Educ. Quím. [Internet]* 21 (4), 291–299. Available at: [http://dx.doi.org/10.1016/S0187-893X\(18\)30098-3](http://dx.doi.org/10.1016/S0187-893X(18)30098-3)
- Eliás, R. (2015). Mar de plástico: Una revisión de plástico en el Mar. *Rev. Invest. y Desarro. Pesq.* [Internet]. [cited 2022 Feb 10];83–15. Available at: https://aquadocs.org/bitstream/handle/1834/10964/RevINIDEP27_83.pdf?sequence=1&isAllowed=y.
- Ellen MacArthur Foundation (2016). McKinsey. The New Plastics Economy_McKinsey. [Internet] Available at: <https://emf.thirdlight.com/link/u3k3oq221d37-h2ohow/@/preview/1?o>.
- Flores, P. (2020). “La problemática del consumo de plásticos durante la pandemia de la COVID-19,” in *South Sustain*, 1, e016. [Internet] Available at: <https://revistas.cientifica.edu.pe/index.php/southsustainability/article/view/733.2>.
- Galán, L. (2012). *Aislamiento e identificación de hongos entomopatógenos de las diferentes zonas citricolas de México*. Mexico: Universidad Autónoma de Nuevo León. [Internet]. Available at: <https://docplayer.es/64203404-Universidad-autonoma-de-nuevo-leon-facultad-de-ciencias-biologicas-instituto-de-biotecnologia.html>.
- Geyer, R., Jambeck, J. R., and Law, K. L. (2017). Production, Use, and Fate of All Plastics Ever Made. *Sci. Adv.* 3 (7), e1700782–9. doi:10.1126/sciadv.1700782
- Gutierrez, K. (2018). *Influencia de factores ambientales de crecimiento microbiano en la degradación de polietileno de baja densidad por la bacteria Pseudomonas aeruginosa en Huancayo*. Huancayo, Peru: Universidad Continental. Universidad Continental. [Internet] Available at: <file:///C:/Users/User/Downloads/fvm939e.pdf>.
- Kida, T., Hiejima, Y., and Nitta, K.-h. (2016). Raman Spectroscopic Study of High-Density Polyethylene during Tensile Deformation. *Int. J. Exp. Spectrosc. Tech.* 1 (1), 1–6. doi:10.35840/2631-505x/8501
- Kwadha, C. A., Ong’Amo, G. O., Ndegwa, P. N., Raina, S. K., and Fombong, A. T. (2017). The biology and control of the greater wax moth, *Galleria mellonella*. *Insects* 8 (2), 1–17.
- Mandal, S., and Vishwakarma, R. (2016). “Population Dynamics of Greater Wax Moth (*Galleria mellonella* L.) Infesting apis Mellifera L. Combs during Dearth Period,” in *Natl Environ. Assoc.* [Internet] IX(October):7. Available at: https://www.researchgate.net/profile/Santosh-Mandal/publication/319997757_POPULATION_DYNAMICS_OF_GREATER_WAX_MOTH_GALLERIA_MELLONELLA_L_INFESTING_APIS_MELLIFERA_L_COMBS_DURING_DEARTH_PERIOD/links/59c71e5aaca272c71bc2cdf6/POPULATION-DYNAMICS-OF-GREATER-WAX.
- Martin, K. (2012). *Bioprospección de la degradación del polietileno*. Bogotá, Colombia: Pontificia Universidad Javeriana. Pontificia Universidad Javeriana.
- Ministerio del Ambiente (2016). “Agenda de Investigación Ambiental al 2021,” in *Primera Ed. Dirección General de Investigación e Información Ambiental* (Lima: Biblioteca Nacional del Perú), 59.
- Ministerio del Ambiente (2017). Cifras del Mundo y el Perú. [Internet]. minam.gob.pe. Available at: <https://www.minam.gob.pe/menos-plastico-mas-vida/cifras-del-mundo-y-el-peru/>.
- Ministerio del Ambiente M (2019). *Reglamento de la Ley N° 30884, Ley que regula el plástico de un solo uso y los recipientes o envases descartables*. D.S. N° 006-2019-MINAM Lima. Peru: Diario Oficial El Peruano, 4–11.
- Ministerio del Ambiente (2016). *Plan Nacional De Gestión Integral de Residuos Sólidos*. Lima: Ministerio del Ambiente.
- Ministerio del Ambiente (2014). *Sexto Informe Nacional de Residuos Sólidos de la Gestión Municipal y No Municipal* 2013. Lima: Ministerio del Ambiente. [Internet] Available at: <http://redrrss.minam.gob.pe/material/20160328155703.pdf>.
- Montgomery, D. (2004). “Diseño y análisis de experimentos. 2° Edición,” in *Arizona: Editorial Limusa S.A. de C.V.*, Editor L. Wiley. Grupo Noriega Editores, 21, 692.
- Municipalidad Distrital de Pangoa (2019). *Estudio de caracterización de residuos sólidos 2019 de la Municipalidad Distrital de Pangoa*. Junín: Pangoa.
- Pathak, V. M., and Navneet (2017). Review on the Current Status of Polymer Degradation: a Microbial Approach. *Bioresour. Bioprocess.* 4. [Internet]. doi:10.1186/s40643-017-0145-9
- Rivas, J. (2020). Capacidad biodegradativa de la cucaracha Periplaneta americana (Linnaeus, 1758) sobre la bolsa plástica y el film.
- Rodriguez, L. (2015). Ciclo Biológico de *Galleria mellonella* Linnaeus (Lepidoptera: Pyralidae). Lima, Peru: Universidad Nacional Agraria La Molina
- Salas, M. (2015). *Efecto de dietas artificiales en la crianza de galleria mellonella L. (lepidoptera: pyralidae)* [Internet]. Trujillo, Peru: Universidad Nacional de Trujillo. Available at: <http://dspace.unitru.edu.pe/handle/UNITRU/4124>
- Urdaneta, S. (2014). *Manejo de residuos sólidos en América Latina y el Caribe*. Omnia Año. 20. [Internet] [cited 2022 Feb 10]. Available at: <https://www.redalyc.org/pdf/737/73737091009.pdf>.
- Yang, J., Yang, Y., Wu, W. M., Zhao, J., and Jiang, L. (2014). Evidence of polyethylene biodegradation by bacterial strains from the guts of plastic-eating waxworms. *Environ. Sci. Technol.* 48 (23), 13776–13784. doi:10.1186/s12957-021-02387-z

SUPPLEMENTARY MATERIAL

The Supplementary Material for this article can be found online at: <https://www.frontiersin.org/articles/10.3389/fbioe.2022.915331/full#supplementary-material>

Conflict of Interest: The authors declare that the research was conducted in the absence of any commercial or financial relationships that could be construed as a potential conflict of interest.

Publisher’s Note: All claims expressed in this article are solely those of the authors and do not necessarily represent those of their affiliated organizations, or those of the publisher, the editors, and the reviewers. Any product that may be evaluated in this article, or claim that may be made by its manufacturer, is not guaranteed or endorsed by the publisher.

Copyright © 2022 Poma, Ricce, Beraún, Perez Carpio, Fernandez and Soria. This is an open-access article distributed under the terms of the Creative Commons Attribution License (CC BY). The use, distribution or reproduction in other forums is permitted, provided the original author(s) and the copyright owner(s) are credited and that the original publication in this journal is cited, in accordance with accepted academic practice. No use, distribution or reproduction is permitted which does not comply with these terms.

Frontiers in Bioengineering and Biotechnology

Accelerates the development of therapies,
devices, and technologies to improve our lives

A multidisciplinary journal that accelerates the
development of biological therapies, devices,
processes and technologies to improve our lives
by bridging the gap between discoveries and their
application.

Discover the latest Research Topics

[See more →](#)

Frontiers

Avenue du Tribunal-Fédéral 34
1005 Lausanne, Switzerland
frontiersin.org

Contact us

+41 (0)21 510 17 00
frontiersin.org/about/contact



Frontiers in
Bioengineering
and Biotechnology

